UNIVERSITÀ DEGLI STUDI DI SALERNO

UNIVERSITÀ DEGLI STUDI DI SALERNO

Dipartimento di Farmacia

PhD Program

in **Drug Discovery and Development**

XXXIV Cycle — Academic Year 2021/2022

PhD Thesis in

Development and application of omics technologies for the monitoring of personalized therapeutic protocols

Candidate

Fabrizio Merciai

Supervisor

Prof. *Pietro Campiglia*

PhD Program Coordinator: Prof. Dr. *Gianluca Sbardella*

“If you change the way you look at things,

the things you look at change”

Max Planck

Index

Chapter I

Chapter II

Chapter III

Chapter IV

Chapter V

Chapter VII

Chapter VIII

Figure Captions

Chapter II

Chapter III

Chapter IV

Chapter V

Chapter VI

Chapter VII

Table Captions

Chapter II

Chapter III

Chapter IV

Chapter V

Chapter VI

Chapter VII

CHAPTER I

Research project presentation: Development and application of omics technologies for the monitoring of personalized therapeutic protocols

1. Introduction

The application of "omics sciences" is shifting the pharmaceutical and medical approach to a novel paradigm: the "personalized medicine" [1]. Understanding the molecular pathways activated by a physio-pathological stimulus, such as a disease, a drug, or a specific diet, gives the opportunity to make an early diagnosis, to monitor the course of the disease and to choose the best therapeutic treatment to enhance the efficacy and reduce the side effects. This is made possible, for example, by metabolomics, which being at the bottom of the "Omics cascade" [2], provides the most "up-to-date" and detailed image of what is happening, rather than offering a prediction of what could happen. Metabolites represent both the downstream product of the genome and the upstream influence from the environment. Therefore, the study of metabolites and metabolism, allows scientists to gain insight into gene–environment interactions. Metabolomics not only enables the identification of disease biomarkers in the form of endogenous metabolites (gene-derived metabolites) and exogenous metabolites (environmentally derived metabolites), but it is also capable to provide rational and precise insights into the fundamental causes of disease [3].

Metabolomics is, indeed, defined as the quali-quantitative analysis of the molecules present in a biological system in response to a genetic or a morbid stimulus. The metabolome includes a large variety of molecules with small molecular weight, < 1.5 KDa, such as: amino acids, lipids, vitamins, organic acids and drugs [4]. The alterations of their molecular pathways, observed by the detection of perturbations in concentrations or in the flux of these metabolites, and the interpretation of the obtained data through a bio-informatics approach, allows a global vision of the metabolite's variations and permit to determine the differences and the relationship between variables and samples.

Among the countless metabolites there is a constant growth of interest in lipids. In fact, in addition to being involved in the onset of numerous chronic diseases [5,6], they also play a key role in the development of genetic [7,8] or viral diseases [9]. Nowadays, lipidomics, indeed, represents one of the emerging fields of biomedical research [10]. This branch of metabolomics investigates and analyses lipids and their interaction partners in a biological system [11].

Metabolomics employs cutting-edge analytical chemistry techniques and advanced computational methods to characterize complex biochemical mixtures. The diversity of applications of metabolomics derives from the fact that it can be used to analyse a wide range of biological specimens, such as tissues [12], biofluids [13] and gases, such as breath [14]. Unlike genomics, transcriptomics, or proteomics, in which a single instrument is often sufficient to perform the necessary measurements, metabolomics analysis cannot be performed on a single analytical platform. Over the last 15 years different technologies have emerged as the workhorses in metabolomics: nuclear magnetic resonance (NMR) spectroscopy, gas chromatography mass spectrometry (GC-MS) and liquid chromatography MS (LC-MS) [15]. Each technique provides broad coverage of many classes of organic compounds and has strengths and weakness.

Metabolomics strategies can be divided into untargeted and targeted approaches, each with their own advantages and limitations. Untargeted approaches are focused on the analysis of all the detectable metabolites in a sample, including unknowns. By contrast, targeted methods are based on the measurement of defined groups of metabolites of interest [16].

Mass spectrometry, often in hyphenation with ultra-high performance liquid chromatography (UHPLC), represent nowadays the golden standard for both metabolomic and lipidomic analysis. Untargeted methods usually rely on the employment of high-resolution mass spectrometry, that is capable to deliver crucial information for the identification of known and unknown metabolites/lipids.

Specifically, hybrid instruments such as quadrupole/QTOF and quadrupole/orbital ion trap dominate the field in untargeted metabolomics and lipidomics studies by their intrinsic advantages in mass accuracy, resolution, dynamic range, acquisition rate, and sensitivity [17]. For MS/MS stages, different fragmentation strategies are available, such as collision induced dissociation (CID) [18], Higher-energy C-trap dissociation (HCD) [19], and ultra-violet photo dissociation (UVDP) [20]. Classic data-dependent acquisition (DDA) acquisition methods still dominate the field but, recently, data-independent strategies (DIA), such as Sequential Window Acquisition of All Theoretical Mass Spectra (SWATH) [21], or all ion fragmentation (AIF) [22], have shown improved coverage for low-abundance precursor ions and retrospective analysis by dedicated software.

Targeted approaches, in contrast, are dominated by the employment of triple quadrupole (QqQ) or quadrupole ion trap (Q-Trap) instruments routinely operating via selected reaction monitoring (SRM) and/or multiple reaction monitoring (MRM). Modern systems are capable to monitor hundreds of transitions in a single run, and hence, with the availability of selected

standards, these approaches are the choice for absolute quantitative analysis also of trace metabolites, by sensitivity in the attomole range [23].

Processing metabolomics/lipidomics data is a very critical step in the overall workflow. These data can reach rapidly Terabytes and need powerful hardware to process such an overwhelming amount of data. LC–MS data processing pipelines include multiple stages, such as: filtering, feature detection, peak alignment, and data normalization. The final output comprises extracted m/z values, their retention times, and corresponding intensity for all detected peaks [24]. Several commercial and open-source data processing tools are currently available, such as: Compound Discoverer, Metaboscape, MassHunter, XCMS, MZmine 2, MS-DIAL. Metabolite annotation is still the bottleneck in the processing workflow, but numerous steps have been performed to harmonize metabolite annotation in metabolomics and lipidomics, such as the efforts from metabolomics and lipidomics standard initiative [25,26].

In this regard, my PhD project is focused on the elucidation of the molecular changes related to disease development and/or to a specific nutraceutical supplement employment. For this purpose, two complementary metabolomics approaches, targeted and untargeted [27], are necessary and the research activity aims to develop high sensitivity and resolution analytical methods.

In the first phase of my PhD project, the research activity focused on the investigation of a possible correlation between the blood levels of sphingolipids and hypertension. This still represents one of the main risk factors for mortality and CVDs [28].

In detail, a targeted lipidomic pilot-study (33 subjects) was performed to establish a potential correlation between sortilin (Sort), a glycoprotein related to vascular and metabolic disorders [29], and the plasma levels of sphingosine-1-phosphate (S1P), ceramide C16, ceramide C18, ceramide C24:1. Our results were further confirmed and validated in a large-scale study. The

prospective cohort enrolled 289 patients, equally distributed into: normotensive, controlled hypertensives, and uncontrolled hypertensives. Furthermore, an untargeted lipidome plasma profiling was carried out through a direct infusion high resolution mass spectrometry strategy. So, this approach gave us both the possibility to have a preliminary look at the investigative power of the FT-ICR-MS platform and to highlight possible further altered sphingolipids in the context of hypertension (**Chapter II**).

Hypertension, atherosclerosis and dyslipidaemia are comorbid disease often found in combination. Natural compounds are gaining more and more importance as adjuvants of drug therapies and in the field of prevention [30]. In this regard, have been investigated the metabolic changes exerted by SP6, a novel decameric peptide released during a simulated gastrointestinal digestion of *Spirulina Platensis*, in the modulation of atherosclerosis progression model in HFD ApoE$^{-/-}$ mice with DI-FT-ICR-MS, which provided very high mass accuracy in the identification of the investigated molecules (**Chapter III**).

In the field of lipidomics there is a continuous necessity to improve the quality of lipid profiling, to detect the greatest possible number of lipid perturbations related to a pathological state or a regime diet. In this regard, ion mobility, in addition to an LC-MS system, acts as a powerful analytical technique. This innovative approach allows to separate isomers, achieve better signal to noise and increases the confidence of lipid annotation [31]. In this regard, nano liquid chromatography coupled to trapped ion mobility mass spectrometer (TIMS) was employed to clarify a possible involvement of the endocannabinoid pathways in the AP-4 deficiency syndrome, a severe childhood hereditary paraplegia, and to have a preliminary look to other possible lipid alterations (**Chapter IV**).

Liquid chromatography – mass spectrometry (LC-MS) based lipidomics is almost exclusively performed with analytical flow rates due to its throughput and robust operation. However, higher flow rates and larger column diameters lower the electrospray efficiency and hence sensitivity [32]. To increase throughput and robustness of nanoflow separations, the Evosep One LC system, a novel nano-LC platform widely used in proteomics field [33,34,35], has been adapted to lipidomics challenges and its performance, once hyphenated to a trapped ion mobility spectrometry, was evaluated (**Chapter V**).

Given the great impact that Covid has had and still has, both in Italy and in the rest of the world [36], the TIMS approach has been coupled to ultra high-performance liquid chromatography with the aim to uncover lipid changes in plasma Covid-19 patients and to elucidate possible biomarkers of severity and mortality (**Chapter VI**).

1.1. References

[1] Eckhart A.D., Beebe K., Milburn M. Metabolomics as a key integrator for "omic" advancement of personalized medicine and future therapies. *Clin Transl Sci*. **2012**. 5 (3): 285-288.

[2] Preidis G.A., Hotez P.J. The newest "omics"--metagenomics and metabolomics--enter the battle against the neglected tropical diseases. *PLoS Negl Trop Dis*. **2015**. 9 (2): 1-12.

[3] Wishart D. Emerging applications of metabolomics in drug discovery and precision medicine. *Nat Rev Drug Discov*. **2016**. 15: 473–484.

[4] Dettmer K., Aronov P.A., Hammock B.D. Metabolic profiles of cancer cells. *Nat Rev Cancer*. **2006**. 4: 551-561.

[5] Ferro C.J., Mark P.B., Kanbay M., Sarafidis P., Heine G.H., Rossignol P., Massy Z.A., Mallamaci F., Valdivielso J.M., Malyszko J., Verhaar M.C., Ekart R., Vanholder R., London G., Ortiz A., Zoccali C. Lipid management in patients with chronic kidney disease. *Nat Rev Nephrol*. **2018**. 14: 727–749.

[6] Vlahos R. Lipids in Chronic Obstructive Pulmonary Disease: A Target for Future Therapy?. *Am J Respir Cell Mol Biol*. **2020**. 62 (3): 273–274.

[7] Murphy E.J., Schapiro M.B., Rapoport S.I., Shetty H.U. Phospholipid composition and levels are altered in down syndrome brain. *Brain Res*. **2000**. 867 (1-2): 9-18.

[8] Block R.C., Dorsey E.R., Beck C.A., Brenna J.T., Shoulson I. Altered cholesterol and fatty acid metabolism in Huntington disease. *J Clin Lipidol*. **2010**. 4 (1): 17-23.

[9] Monson E.A., Trenerry A.M., Laws J.L., Mackenzie J.M., Helbig K.J. Lipid droplets and lipid mediators in viral infection and immunity. *FEMS Microbiol. Rev.* **2021**. 45 (4): 1-20.

[10] Orešič M., Hänninen V.A., Vidal-Puig A. Lipidomics: as a new window to biomedical frontiers. *Trends Biotechnol*. **2008**. 26 (12): 647-652.

[11] Watson A.D. Lipidomics: a global approach to lipid analysis in biological systems. *J Lipid Res*. **2006**. 47: 2101-2111.

[12] Neumann E.K., Migas L.G., Allen J.L., Caprioli R.M., Van de Plas R., Spraggins J.M. Spatial Metabolomics of the Human Kidney using MALDI Trapped Ion Mobility Imaging Mass Spectrometry. *Anal. Chem.* **2020**. 92 (19): 13084-13091.

[13] Zhang A., Sun H., Wang P., Han Y., Wang X. Recent and potential developments of biofluid analyses in metabolomics. *J. Proteomics*. **2012**. 75 (4): 1079-88.

[14] Grassin-Delyle S., Roquencourt C., Moine P., Saffroy G., Carn S., Heming N., Fleuriet J., Salvator H., Naline E., Couderc L.J., Devillier P., Thévenot E.A., Annane D for the Garches COVID-19 Collaborative Group RECORDS Collaborators and Exhalomics® Collaborators. Metabolomics of exhaled breath in critically ill COVID-19 patients: A pilot study. *EBioMedicine*. **2021**. 63: 103154.

[15] Azad R.K., Shulaev V. Metabolomics technology and bioinformatics for precision medicine. *Brief Bioinform*. **2019.** 20 (6): 1957-1971.

[16] Cajka T., Fiehn O. Toward Merging Untargeted and Targeted Methods in Mass Spectrometry-Based Metabolomics and Lipidomics. *Anal. Chem*. **2016**. 88 (1): 524–545.

[17] Dettmer K., Aronov P.A., Hammock B.D. Mass spectrometry-based metabolomics. *Mass Spectrom Rev*. **2007**. 26 (1): 51-78.

[18] Li P., Hoffmann W.D., Jackson G.P. Multistage mass spectrometry of phospholipids using collision-induced dissociation (CID) and metastable atom-activated dissociation (MAD). *Int. J. Mass*. **2016**. 403: 1-7.

[19] Hsu F.F. Electrospray ionization with higher-energy collision dissociation tandem mass spectrometry toward characterization of ceramides as $[M + Li]^+$ ions: Mechanisms of fragmentation and structural identification. *Anal Chim Acta*. **2021**. 1142: 221-234.

[20] Brodbelt J.S., Morrison L.J., Santos I. Ultraviolet Photodissociation Mass Spectrometry for Analysis of Biological Molecules. *Chem Rev*. **2020**. 120 (7): 3328-3380.

[21] Drotleff B., Illison J., Schlotterbeck J., Lukowski R., Lämmerhofer M., Comprehensive lipidomics of mouse plasma using class-specific surrogate calibrants and SWATH acquisition for large-scale lipid quantification in untargeted analysis. *Anal. Chim. Acta*. **2019**. 1086: 90-102.

[22] Ventura G., Bianco M., Calvano C.D., Losito I., Cataldi T.R.I. HILIC-ESI-FTMS with All Ion Fragmentation (AIF) Scans as a Tool for Fast Lipidome Investigations. *Molecules*. **2020.** 25 (10): 2310.

[23] Takeda H., Izumi Y., Takahashi M., Paxton T., Tamura S., Koike T., Yu Y., Kato N., Nagase K., Shiomi M., Bamba T. Widely-targeted quantitative lipidomics method by supercritical fluid chromatography triple quadrupole mass spectrometry. *J Lipid Res*. **2018** 59 (7): 1283-1293.

[24] Boccard J., Veuthey J.L., Rudaz S. Knowledge discovery in metabolomics: an overview of MS data handling. *J Sep Sci*. **2010**. 33 (3): 290-304.

[25] Sumner L.W., Amberg A., Barrett D., Beale M.H., Beger R., Daykin C.A., Fan T.W., Fiehn O., Goodacre R., Griffin J.L., Hankemeier T., Hardy N., Harnly J., Higashi R., Kopka J., Lane A.N., Lindon J.C., Marriott P., Nicholls A.W., Reily M.D., Thaden J.J., Viant M.R. Proposed minimum reporting standards for chemical analysis. *Metabolomics*. **2007**. 3, 211–221.

[26] Köfeler H.C., Eichmann T.O., Ahrends R., Bowden J.A., Danne-Rasche N., Dennis E.A., Fedorova M., Griffiths W.J., Han X., Hartler J., Holčapek M., Jirásko R., Koelmel J.P., Ejsing C.S., Liebisch G., Ni Z., O'Donnell V.B., Quehenberger O., Schwudke D., Shevchenko A., Wakelam M.J.O., Wenk M.R., Wolrab D., Ekroos K. Quality control requirements for the correct annotation of lipidomics data. *Nat. Commun*. **2021**. 12: 4771.

[27] Ribbenstedt A., Ziarrusta H., Benskin, J. P. Development, characterization and comparisons of targeted and non-targeted metabolomics methods. *PloS one*. **2018**. 13 (11): 1-18.

[28] Kokubo Y., Iwashima Y. Higher Blood Pressure as a Risk Factor for Diseases Other Than Stroke and Ischemic Heart Disease. *Hypertension*. **2015**. 66 (2): 254-259.

[29] Goettsch C., Kjolby M., Aikawa E. Sortilin and Its Multiple Roles in Cardiovascular and Metabolic Diseases. *Arterioscler Thromb Vasc Biol*. **2018**. 38 (1): 19-25.

[30] Lin S.R., Chang C.H., Hsu C.F., Tsai M.J., Cheng H., Leong M.K., Sung P.J., Chen J.C., Weng C.F. Natural compounds as potential adjuvants to cancer therapy: Preclinical evidence. *Br J Pharmacol*. **2020**. 177 (6): 1409-1423.

[31] Zhang X., Quinn K., Cruickshank-Quinn C., Reisdorph R., Reisdorph N. The application of ion mobility mass spectrometry to metabolomics. *Curr Opin Chem Biol*. **2018**. 42: 60-66.

[32] Schmidt A., Karas M., Dülcks T. Effect of Different Solution Flow Rates on Analyte Ion Signals in Nano-ESI MS, or: When Does ESI Turn into Nano-ESI?. *J Am Soc Mass Spectrom*. **2003**. 14: 492–500.

[33] Krieger J.R., Wybenga-Groot L.E., Tong J., Bache N., Tsao M.S., Moran M.F. Evosep One Enables Robust Deep Proteome Coverage Using Tandem Mass Tags while Significantly Reducing Instrument Time. *J Proteome Res*. **2019**.18 (5): 2346-2353.

[34] Bache N., Geyer P.E., Bekker-Jensen D.B., Hoerning O., Falkenby L., Treit P.V., Doll S., Paron I., Müller J.B., Meier F., Olsen J.V., Vorm O., Mann M. A Novel LC System Embeds Analytes in Pre-formed Gradients for Rapid, Ultra-robust Proteomics. *Mol Cell Proteomics*. **2018**. 17 (11): 2284-2296.

[35] Brunner A.D., Thielert M., Vasilopoulou C.G., Ammar C., Coscia F., Mund A., Hoerning O.B., Bache N., Apalategui A., Lubeck M., Raether O., Park M.A., Richter S., Fischer D.S., Theis F.J., Meier F., Mann M. Ultra-High Sensitivity Mass Spectrometry Quantifies Single-Cell Proteome Changes upon Perturbation. *BioRxiv*. ***2020***.

[36] Wang C., Wang Z., Wang G., Yiu-Nam Lau J., Zhang K., Li W. COVID-19 in early 2021: current status and looking forward. *Sig Transduct Target Ther*. **2021**. 6 (1): 114.

.

CHAPTER II

Targeting the ASMase/S1P pathway protects from sortilin-evoked vascular damage in hypertension

Abstract

Hypertension is characterized by endothelial dysfunction and vascular remodeling. Sortilin has been positively correlated with vascular disorders in humans. No study has yet evaluated the possible effect of sortilin on vascular function. Previous studies showed that it promotes activation of acid sphingomyelinase (ASMase), a key enzyme in sphingolipids (SPs) metabolism. And since lipids, and especially SPs have been implicated in vascular tone and function, in this contribution we investigated the differences in sphingosine-1-phosphate (S1P) and ceramides plasma levels of hypertensive patients belonging to two different cohorts and we investigated a possible correlation with sortilin.

Here we demonstrate that sortilin-mediated ASMase activation induces aberrant S1P levels and suggest the potential of these molecules as novel biomarkers for the prediction of high blood pressure.

2.1. Introduction

High blood pressure is an important risk factor for many cardiovascular diseases (CVDs) that makes hypertension one of the major worldwide causes of death [1]. Although the precise cause-effect relationship is controversial, many studies have proposed that endothelial dysfunction may contribute to emergence of hypertension [2]. Over the past years, there has been

increasing evidence placing ROS as a downstream signaling of bioactive sphingolipids in vascular tissue [3]. Sphingolipids are involved in the regulation of both vascular growth and vascular tone. Among several of them, most studies place emphasis on the cardiovascular effect of sphingosine-1-phosphate (S1P) and ceramides, reporting the correlation between their aberrant expression and CVD risk factors, including hypertension [4,5,6]. The mechanism linking hypertension and sphingolipids is still unknown. Acid sphingomyelinase (ASMase) is a crucial enzyme involved in sphingolipids biosynthesis producing bioactive ceramide which is then converted into other sphingolipids [7,8]. Previous mechanistic studies reported that sortilin (sort), a member of the vacuolar protein sorting 10 (VPS10P) family of receptors, triggers translocation and activation of ASMase inducing an increase of NADPH oxidase activity in coronary endothelial cells [9,10]. Moreover, a growing body of evidence has shown that elevated plasma sortilin levels in human correlated positively with vascular and metabolic disorders [11]. Furthermore, several evidence suggests that sortilin may contribute to the pathogenesis of cardiovascular diseases independently of its role in lipid metabolism [12,13,14] pointing to the existence of alternative mechanisms of action and highlighting the role of sortilin in the pathogenesis of cardiovascular disease.

Our hypothesis is that sortilin may modulate sphingolipids levels acting through ASMase enzyme, thereby leading to vascular oxidative stress and endothelial dysfunction.

To test this concept, we measured SPs levels (S1P, Ceramide C16, Ceramide C18, Ceramide C24:1) both in human umbilical vein endothelial cells (HUVECs) incubated with sortilin and in plasma samples from two different cohorts.

Sphingolipid's quantification was carried out by multiple reaction monitoring (MRM) mass spectrometry coupled to ultra-high performance liquid chromatography (UHPLC) method,

which allowed great sensitivity and reproducibility [15]. Furthermore, a soft extraction protocol, avoiding any hydrolysis step, was employed to avoid SP's structural alterations and to not lose sphingoid base phosphate compound [16].

In this study, we have provided evidence that sortilin acts as a modulator of bioactive sphingolipids. The demonstration that sortilin levels are higher in uncontrolled hypertensive patients and correlated with S1P levels could constitute useful new biomarkers for hypertension diagnosis from the early stages of vascular disease.

2.2. Aim of the work

The study aimed to investigate the role of sortilin in the hypertension disease and its involvement in the sphingolipids metabolism. This work expected to clarify sphingosine-1-phosphate and ceramide behavior in the context of high blood pressure in order to point out potentially new biomarkers.

2.3. Results

2.3.1. UHPLC-MRM validation

The LC-MS/MS method employed a 15 cm column with C18 stationary phase and core-shell particulate that allowed to obtain a good compromise between peak symmetry and total analysis time (**supporting information figure S1.1**).

The analytical method was validated in terms of linearity, limits of detection (LOD), limits of quantification (LOQ) and precision considering intra-day and inter-day variability. The coefficient of variation (CV %) values for each analyte, relative to both the retention time and the peak area, are shown in **table 2.1**. Linear regression equation and coefficient correlation (R^2) were used to evaluate the linearity of the results. LOD and LOQ were calculated as follows

$$\text{LOD} = 3.3 * \frac{\sigma}{s} \quad \text{(Eq. 1)}$$

$$\text{LOQ} = 10 * \frac{\sigma}{S} \quad \text{(Eq. 2)}$$

where σ is the standard deviation of the response and S is the slope coefficient of the calibration curves.

Table 2.1. *RP-UHPLC-QqQ quantitative parameters.*

Sphingolipids	Range (ng/mL)	R^2	LOD (ng/mL)	LOQ (ng/mL)	CV% Intra-day	CV% Inter-day	CV% Rt
S1P	50-0.1	0.9977	0.01	0.05	1.62	1.81	0.05
C16 Ceramide	100-0.1	0.9999	0.05	0.18	1.33	3..32	0.44
C18 Ceramide	200-1.0	0.9992	0.06	0.21	1.07	4.26	0.41
C24:1 Ceramide	200-0.5	0.9991	0.06	0.20	1.72	2.04	0.38

S1P: Sphingosine-1-phosphate; **R^2:** coefficient of correlation; **CV % Intra-day:** 5 injections in a row; **CV % Inter-day:** Day 1: 5 injections in row, Day 2: 5 injections in row; **Rt:** retention time.

2.3.2. Preliminary sphingolipids analysis on cell lines and human plasma

The analytical extraction protocol was optimized starting from the lipid extracts of human umbilical vein endothelial cells (HUVECs). Changes in SP's levels in HUVECs treated with sortilin (2.5 ng/mL × 1 hour) were measured. The results showed an increase in S1P and ceramide C16 levels in cells incubated with sort, while no significant changes in ceramide C18 and C24:1 were observed (**figure 2.1**).

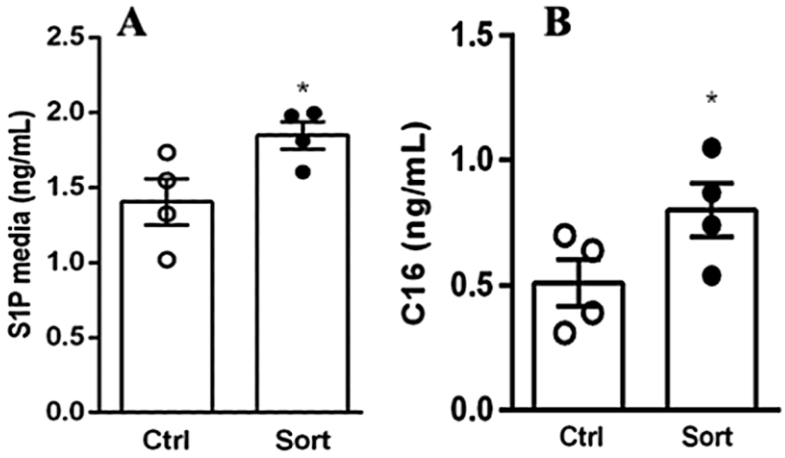

Figure 2.1. *LC-MS/MS quantification of S1P (**A**) ceramide C16 (**B**) levels in HUVECs treated with vehicle (Ctrl) or sortilin (sort), results are expressed as mean ± SD (* p value <0.05).*

To translate our experimental findings, we first investigated plasma sortilin and SPs concentrations in hypertensive patients belonging to the Campania Salute Network. Characteristics of study population are presented in **table 2.2.**

Table 2.2. *Clinical characteristics of hypertensive patients from the Campania Salute Study.*

Parameter	Normotensive (N=9)	Hypertensive (N=24)
	Clinical characteristics	
Age, y	70 ± 7	69 ± 7
Sex, M/F	4/5	11/13
SBP (mmHg)	121 ± 1.9	143.6 ± 15.7
DBP (mmHg)	78 ± 5.1	89.56 ± 12.5
Body weight (Kg)	72 ± 12.5	76.36 ± 11.9
TC (mg/dL)	168.5 ± 12.1	212.8 ± 47.4
HDL (mg/dL)	50.2 ± 4.1	55.25 ± 10.9
TG (mg/dL)	106.8 ± 3.3	130.5 ± 60.4
Glucose (mg/dL)	90.2 ± 3.9	96.46 ± 12.1
Creatinine (mg/dL)	0.86 ± 0.2	0.9 ± 0.2
	Medication (%)	
β-blockers	0	5 (20)
ARBs	0	12 (48)
ACE-inhibitor	0	8 (32)
Diuretics	0	11 (44)
CCB	0	9 (36)

Data are reported as mean ± SD. SBP and DBP indicate respectively systolic and diastolic blood pressure; TC, total cholesterol; HDL, high density lipoproteins; TG, triglycerides; ARBs, angiotensin II receptor blockers; CCB, amlodipine/olmesartan medoxomil.

Interestingly, plasma levels of sortilin were substantially increased in hypertensive patients when compared to normotensive individuals (**figure 2.2 C**), thus supporting the relevance of sortilin for endothelial dysfunction in patients with arterial hypertension. We next investigated whether our cohort of hypertensive subjects showed aberrant SP's expression. Quantification by liquid chromatography-tandem mass spectrometry (LC-MS/MS) revealed a significant increase in sphingosine-1-phosphate and ceramide C16 levels in patients with an elevated BP (blood pressure) when compared to the normotensive counterpart (**figure 2.2 A, B**). These findings prompted us to investigate a potential association with sortilin levels. Notably, we found a significant correlation between plasma sort and S1P in hypertensive group (**figure 2.2 D)**, but

no correlation between sort and ceramide C16, supporting that the pathophysiological mechanism identified in our experimental model and based on sort and S1P may contribute to altered BP in humans.

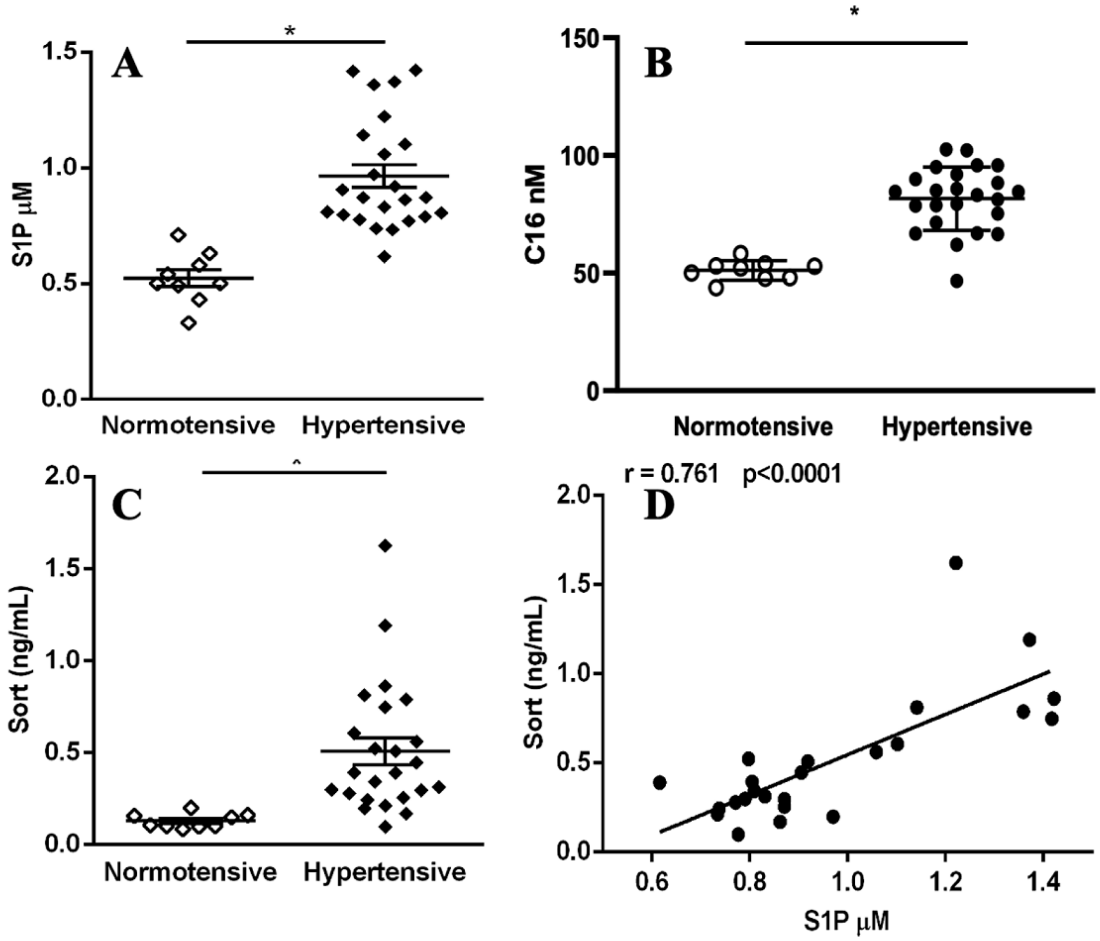

Figure 2.2. *LC-MS/MS quantification of plasma S1P (**A**) and ceramide C16 (**B**) levels in humans with or without hypertension. (**C**) Quantification of sortilin's plasma level (normotensive subjects, N=9; hypertensives subjects, N=24). Results are expressed as mean ± SD. Unpaired Student's t-test was used (* p value <0.05). (**D**) Pearson's correlation coefficient analysis between sortilin and S1P plasma levels in hypertensive subjects.*

2.3.3. Prospective cohort study

To strengthen and confirm the translational relevance of our findings, we then extended our studies to measure plasma levels of sortilin and sphingolipids in a large population-based cohort of the Moli-Sani study (https://www.moli-sani.org/). This cohort consisted of hypertensive patients taking antihypertensive medication who were stratified into controlled hypertensive, uncontrolled hypertensives and normotensive control subjects. The clinical and biochemical characteristics are summarized in **table 2.3**.

Table 2.3. *Clinical characteristics of hypertensive and normotensive individuals from the Moli-Sani Study.*

	Hypertensives		Normotensives	p-value
Parameter	**Controlled (N=91)**	**Uncontrolled (N=90)**	**(N=89)**	
Clinical characteristics				
Age, years	61.4 ± 9.7	60.1 ± 9.8	60.2 ± 9.3	0.56
Sex, M/F	43/48	40/50	43/46	0.865
SBP (mmHg)	129.9 ± 7.7 [a]	167.6 ± 17.6 [a,b]	121.9 ± 5.8	<0.001
DBP (mmHg)	78.1 ± 6.3 [c]	96.2 ± 6.2 [a,b]	73.6±5.4	<0.001
TC (mg/dL)	218.3 ± 37.4	221.9 ± 36.1	221.3 ± 39.5	0.65
HDL (mg/dL)	56.7 ± 13.7	57.3 ± 13.3	61.3 ± 17.6	0.17
TG (mg/dL)	122.7 ± 55.0	128.8 ± 53.8	119.2 ± 65.9	0.07
Glucose (mg/dL)	97.2 ± 10.9	97.7 ± 11.1	94.8 ± 11.4	0.13
Creatinine (mg/dL)	0.8 ± 0.2	0.9 ± 0.3	0.8 ± 0.1	0.11
WBC (10^3/μL)	6.0 ± 1.4	6.2 ± 1.4	6.0 ± 2.2	0.15
RBC (10^3/μL)	4.9 ± 0.4	5.0 ± 0.5	4.8 ± 0.7	0.11
Hgb (g/dL)	14.5 ± 1.3	14.7 ± 1.5	14.4 ± 1.3	0.48
Htc (%)	43.1 ± 3.6	43.6 ± 3.9	42.9 ± 3.8	0.67
MCV (fl)	88.8 ± 5.2	88.0 ± 6.0	89.8 ± 6.7	0.07
MCH (pg)	29.8 ± 2.1	29.7 ± 2.5	30.1 ± 2.6	0.39
MCHC (g/dl)	33.6 ± 1.1	33.7 ± 1.1	33.5 ± 1.1	0.40
RDW (%)	12.8 ± 0.7	13.0 ± 1.4	12.8 ± 0.9	0.72
PLT (10^3/μL)	251.2 ± 62.6	257.9 ± 62.7	251.1 ± 61.1	0.80
Medication (%)				
β-blockers	18 (20)	22 (20)	0	
ARBs	44 (48.8)	35 (38.4)	0	
ACE-inhibitors	26 (28.8)	36 (39.5)	0	
Diuretics	40 (44.4)	35 (38.4)	0	
CCBs	11 (12.2)	15 (16.4)	0	
Statins	0	0	0	
VKAs	0	0	0	
Other anticoagulants	0	0	0	

SBP, systolic blood pressure; DBP, diastolic blood pressure; TC, total cholesterol; HDL, high density lipoprotein; TG, triglycerides; WBC, with blood cells; RBC, red blood cells; Hgb, hemoglobin; Htc, Hematocrit; MCV, mean cell volume; MCH, mean corpuscular hemoglobin; MCHC, mean corpuscular hemoglobin concentration; RDW, red cell distribution width; PLT, platelets; ARBs, Angiotensin II receptor blockers; CCBs, Calcium channel blockers; VKAs, Vitamin K antagonists. *P*-value based on One-way ANOVA for continuous variables and Chi-Square test for categorical variables. a, $p<0.001$ *vs.* normotensives; b, $p<0.001$ *vs.* controlled hypertensives; c, $p=0.008$ *vs.* normotensives.

The three groups were strictly matched with respect to age, gender and laboratory characteristics, but differed significantly in terms of blood pressure levels. Plasma sortilin and S1P levels were markedly elevated in the entire hypertensive population as compared to healthy controls, and the increase was even more pronounced in hypertensive patients with uncontrolled BP than in controlled hypertensive and normotensive counterparts (**figure 2.3. A, B**). The LC-MS/MS didn't reveal a dysregulation in ceramide C16 levels, thus confirming the lack of linearity observed between the human plasma levels of sortilin and this sphingolipid in patients of Campania Salute Network.

Furthermore, we confirmed even in the Moli-Sani study a significant positive correlation between circulating sortilin and S1P levels in the entire hypertensive population ($r= 0.465$, $p<0.0001$; **figure 3 C**).

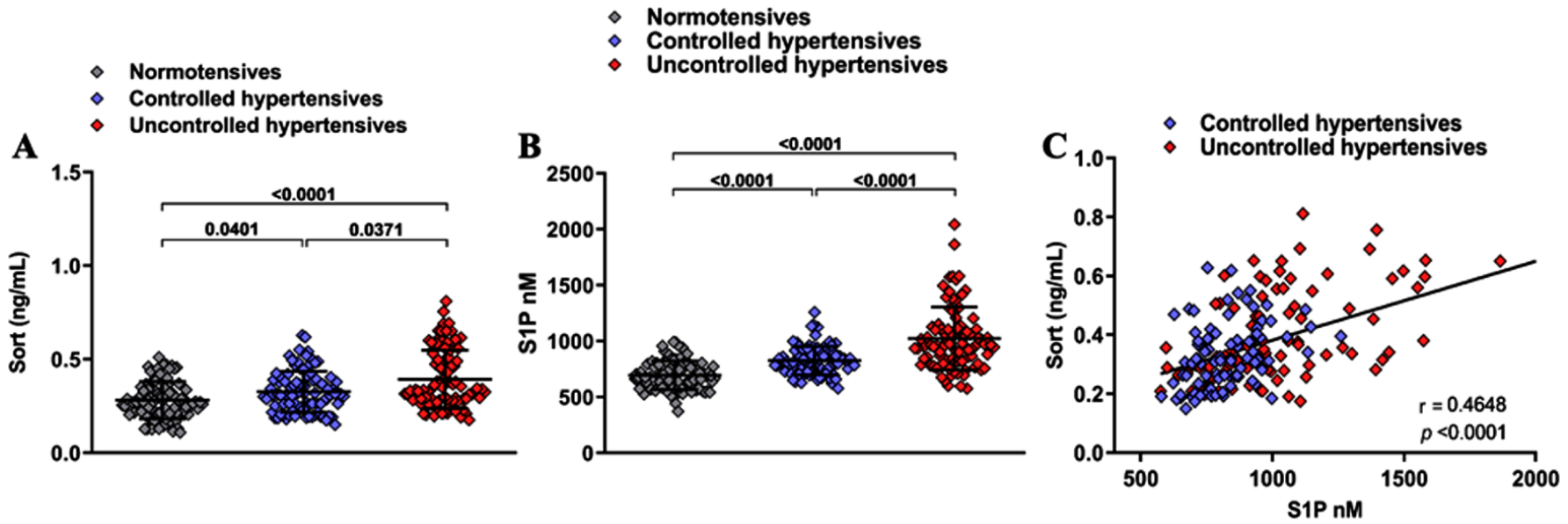

Figure 2.3. *Plasma sortilin levels (**A**), assessed by ELISA assay, and LC-MS/MS quantification of plasma S1P levels (**B**) in normotensives, controlled and uncontrolled hypertensives from the Moli-Sani Study; (N=81 normotensives, N=91 controlled hypertensives, N=90 uncontrolled hypertensives). Results are expressed as mean* ± SD. *Non-parametric Kruskal-Wallis test with Dunn's correction was used. (**C**) Pearsons's correlation coefficient between sortilin and S1P plasma levels in the entire hypertensives population*

2.3.4. Sortilin induces dysfunction by altering sphingolipid metabolism

Acid sphingomyelinase (ASMase) is a lipid hydrolase that cleaves sphingomyelin to produce ceramide and bioactive sphingolipids. Previous studies have shown that sortilin is required for ASMase activation to induce ceramide-derived lipid rafts (LRs) clustering [9,17]. Along with this line and clinical studies reporting the correlation between higher sortilin levels and cardiovascular disease and considering the elevated plasma concentrations of sortilin and sphingosine-1-phospohate in hypertensives, we hypothesized that sortilin itself could promote the activation of ASMase in endothelial cells thereby leading to the impairment of endothelium-dependent vasodilation in mesenteric arteries. Confirming our hypothesis, we observed a higher ASMase activity in hypertensive subjects of both the investigated patients group and, similarly to sortilin and S1P levels, its activity was more pronounced in uncontrolled hypertensive subjects (**figure 2.4. A, B**).

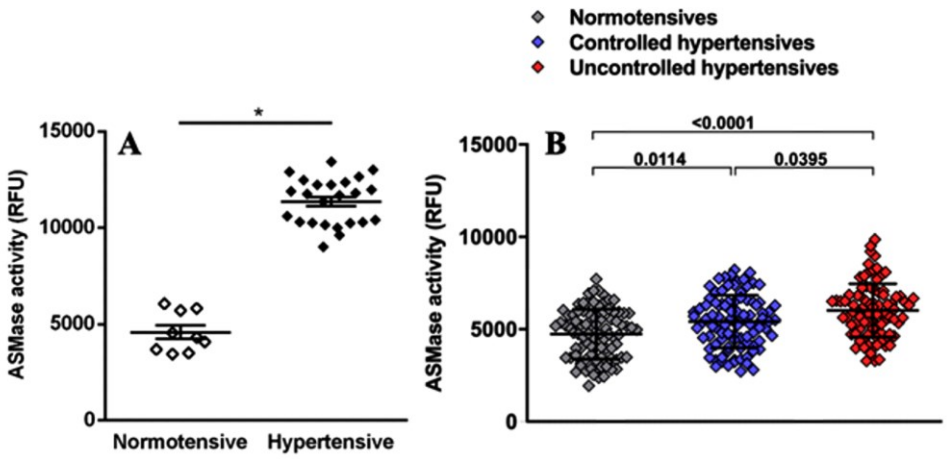

Figure 2.4. *Plasma levels of ASMase activity in (**A**) Campania Salute Network and (**B**) Moli-Sani study. Unpaired T-test (**A**) and Non-parametric Kruskal-Wallis test with Dunn's correction (**B**) were used. Results are expressed as mean* ± SD *(* p value <0.05).*

2.3.5. Confirmatory analysis on HUVECs

In efforts to prove once more that in hypertension the metabolism of sphingolipids is shifted in favor of S1P and to exclude in this regard not only the involvement of ceramide C16, but also of potential other ceramides, we performed a new experiment on HUVECs increasing the number of samples and enlarging the monitored ceramides (**supporting information figure S1.2**) through a novel computational tool that allows to build in silico MRM transitions of target lipids, named LipidCreator [18]. Remarkably, quantification of sphingolipid levels in sortilin-treated endothelial cells showed a consistent decrease in intracellular ceramide content, including cer-C16, cer-C18, cer-C22, cer-C24 and cer-C24:1 that was paralleled by increased extracellular S1P levels (**figure 2.5**). No differences for cer-C14 and cer-C20. This indicates that

sortilin drives the activation of the ASMase pathway, leading to an altered rheostat in favour of S1P at the expense of ceramide.

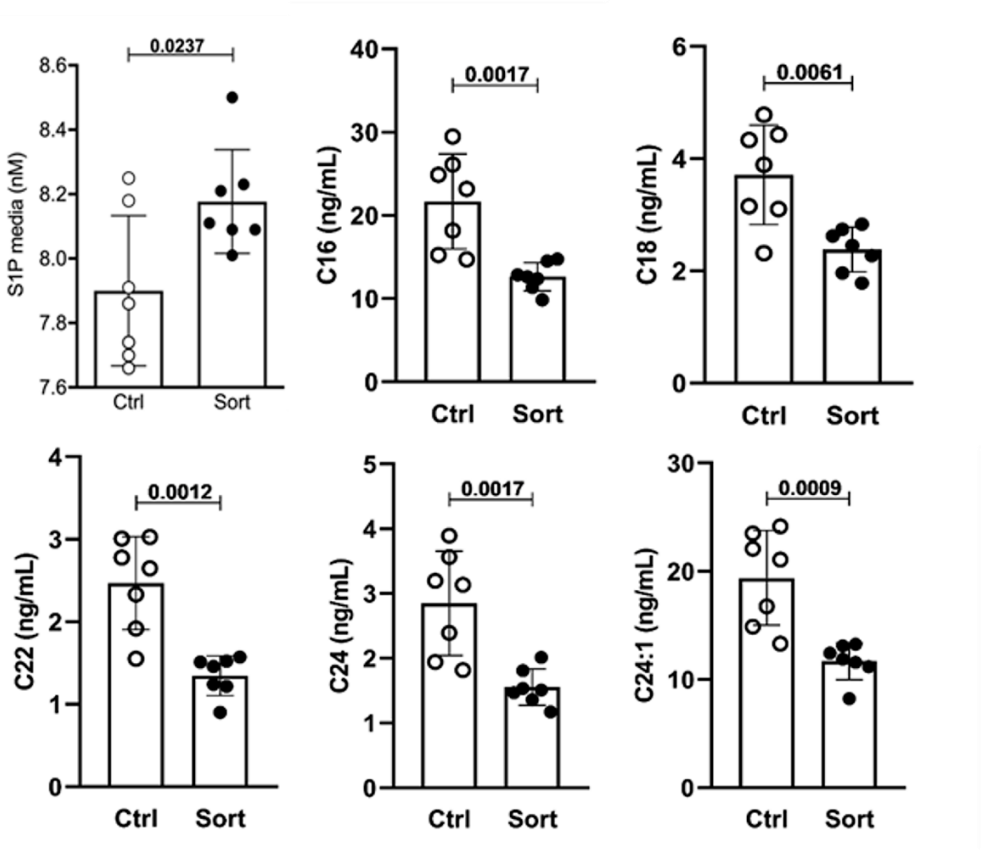

Figure 2.5. *Individual sphingolipid species measured by LC-MS/MS in HUVECs treated with vehicle (ctrl) or sortilin for 1 hr, (N=7). Results are expressed as mean ± SD. Unpaired two-tailed Student's t-test was used.*

Moreover, to evaluate other potential changes in SP's levels, we performed a fast untargeted analysis by a DI-FT-ICR platform (**supplementary information S7.1.1**) that showed dysregulation in some deoxy-ceramides levels, but no significant changes in the putative annotated ceramides. The employed analytical method could be useful as backup strategy to draw potential biochemical connections to other SP's alterations.

2.4. Discussion

In the present study, we provide evidence that sortilin could be involved in the onset of hypertension. Our data showed that sortilin promotes arterial hypertension via a sphingolipid-dependent mechanism. To an accurate SPs quantification several analytical methods and extraction protocols were considered and, at the end, we employed a reverse-phase chromatography (RP) and a not common solvent mixture for the extraction protocol. RP chromatography represents one of the most used methods for the sphingolipidome analysis [19,20], but despite that, the separation of these molecules is challenging and characterized by several hindrances. The most notable one is the difference in polarity and hydrophobicity between ceramides and sphingosine-1-phosphate. Furthermore, S1P contains an aliphatic chain with 18 carbon atoms and a hydrophilic group with a residue of phosphoric acid [21] which gives the molecule amphipathic properties. These features, during the separation on C18 column, give a notable peak asymmetry, which manifests itself with a pronounced tailing effect [22] deriving from secondary interactions with the stationary phase. In opposite, ceramides are strongly retained on reverse phase columns and therefore they may require long gradients for their elution. The employment of a C18 Kinetex EVO^{TM} column provided good results in the separation of the molecules of interest. Indeed, this stationary phase is characterized by a weak positive charge at acid pH which determined a repulsion effect resulting in a reduction, although not complete, of S1P's peak tailing. The core shell technology also allowed to use a high mobile phase flow without losing efficiency during more than 900 analyzes (each sample was acquired three times in order to achieve a better quantification), and to develop a LC method with a fast runtime that enabled the complete elution of ceramides in less than 10 minutes with perfectly symmetrical peaks.

Although the Bligh & Dyer and Folch [23,24] extractions protocols are considered to be milestones in lipidomics works, these showed bad recoveries in the extraction of polar sphingolipids. Indeed sphingosine 1-phosphate, due to its amphipathic characteristics, tends to distribute itself in the aqueous phase affecting its extraction. The extracting solvents mixture (IPA/EtOAc 15/85 v/v) let us possible to obtain a correct distribution in the biphasic system of both ceramides and S1P and also to avoid the breaking of O-acyl bonds of SPs structure [16].

Although previous studies have shown that S1P exerts vasculoprotective effects [25,26], our data provide evidence that in response to sortilin and ASMase activation S1P could play a leading role in the development of hypertension.

In the pilot study, we found that circulating sortilin and S1P levels were elevated in hypertensive individuals with elevated BP, thus supporting the hypothesis of their involvement in the pathogenesis or sequelae of hypertension. These findings were further evaluated in a second cohort of patients without additional comorbidities and stratified by blood pressure level. Even more thrilling, the results emerging from hypertensive stratification revealed that plasma sort and S1P concentrations were higher in hypertensive patients with uncontrolled blood pressure than in controlled hypertensives and the normotensives counterpart.

Moreover, our findings may add new aspects to the pathophysiology of the sphingolipid pathway, revealing the mechanism by which an alternative signalling pathway involving ASMase drives to a dysregulated sphingolipids signalling leading to the deregulation of cardiovascular functions. Thus, although SPs are essential regulators of cardiovascular homeostasis, our results could offer a plausible explanation for the altered sphingolipids levels observed in CVDs [27,28]. In agreement with the results obtained in HUVECs, demonstrating how sphingolipid metabolism is altered in favour of S1P at the expense of ceramides, our data in humans suggest

that sortilin and its mediators may represent new biomarkers for the prediction of high blood pressure. This hypothesis is also coherently supported by the positive correlations found in our cohorts of hypertensive patients between plasma levels of sortilin and S1P.

2.5. Limitations

Our study is based on a set of homogeneous group of patients in terms of ethnicity and geography. Our selection criteria may not rule out the possible influence of other endothelial stressors as could be revealed in a population at higher risk of CVDs. Indeed, elevated circulating levels of sortilin were previously observed in statin-naive subjects with coronary artery disease who underwent bypass surgery. At this time, we can only speculate that the presence of more cardiovascular risk factors can further increase the circulating level of sortilin and S1P, whose could be potentially used as an early biomarker for organ damage. Although our results highlight evidence of elevated levels of S1P, sortilin and ASMase, these need to be confirmed in multi-centre and prospective follow-up studies.

2.6. Materials and Methods

2.6.1. Cell culture and treatment

Commercially available human umbilical vein endothelial cells (HUVECs) were obtained from ATCC. HUVECs were cultured in Vascular Cell Basal Medium and supplemented with Endothelial cell growth kit before experiments were performed. Cells were maintained at 37 °C and 5% CO_2 in a humidified incubator. Before experiments, HUVECs were seeded in 24 well plate, 60 mm or 100 mm dishes and grown until 80% confluency. Next, cells were pre-treated with K145 (Sigma-Aldrich, #SML1003) 1.5 μM for 1 hour; (2R, 3S, 4E)-N-methyl-5-(4′-pentylphenyl)-2-aminopent-4-ene-1,3-diol (SK1-I) 5 μM (Enzo, #BML-EI411) for 1 hour; W146 100nM (Sigma-Aldrich, #W1020) for 30 minutes; 1-Chloro-1-(4-chlorophenylhydrazono)]-

3,3-dimethyl2-butanone] (TY-52156) 5 μM for 30 minutes; ML171 (Tocris #4653) 1.5 μM for 30 minutes or GSK2795039 (MCE # HY-18950) for 30 minutes and incubated with sortilin (2.5 ng/mL, 1 hr) or vehicle (medium). All the experiments were performed at least in triplicate and repeated at least twice.

2.6.2. Human subjects

2.6.2.1. Campania Salute Network

24 patients with hypertension (defined as DBP ≥90 mmHg and SBP ≥140 mmHg or on the basis of use of anti-hypertensive medication) and 9 healthy donor control subjects belonging to the Campania Salute Network Registry, were studied. Campania Salute is an open registry collecting information from a network of general practitioners and community hospitals networked with the Hypertension Center of Federico II University Hospital, Naples. The database generation of the Campania Salute Network was approved by the Federico II University Hospital Ethic Committee.

All patients had no history of previous cardiovascular diseases, symptomatic heart failure, ischemic heart disease, atrial fibrillation, stroke or cognitive dysfunction.

2.6.2.2. Moli-Sani Study

We collected a total of 289 plasma samples from the biodata bank of the Moli-Sani Study, a prospective cohort study established in 2005 to 2010 with an enrollment of 24.325 men and women (≥35 years of age) randomly recruited from the general population of Molise, a southern Mediterranean region in Italy [29].

Data are accessible upon written request to the Moli-Sani Study PI, Prof. Licia Iacoviello. 19 hemolyzed samples were excluded from our analysis. A total of 270 patients were stratified in normotensives (N=89), and in controlled (N=91) or uncontrolled hypertensive subjects

(N=90), strictly matched and with no previous history of cardiovascular diseases. Hypertension was defined as controlled (SBP was <140 and DBP <90 mmHg with treatment), and uncontrolled (SBP was ≥140 and DBP ≥90 mmHg with treatment).

All patients included in this study were not on statin therapy, which is known to influence the circulating sortilin level [30].

2.6.3. Reagents

Plasma levels of sortilin were measured using ELISA Kit (Elabscience; #E-EL-H5414) following the manufacturer's protocol. Acidic sphingomyelinase activity was determined in human plasma samples by Acidic Sphingomyelinase Assay Kit (Abcam, #ab190554).

2.6.4. Sphingolipid extraction

All solvent and additives were LCMS grade and purchased from Sigma-Aldrich (Milan, Italy). Standard of S1P, Ceramides C16, C18, C24:1 and deuterated Ceramide mix were purchased by Avanti Polar Lipids (Alabaster, AL, U.S.A). For the extraction of sphingolipids, human plasma (20 µL) were diluted to 400 µL with Milli-Q water, following samples were extracted by addition of 400 µL of isopropanol/ethyl acetate 15/85 (v/v), vortexed for 20 sec and centrifuged for 5 minutes at 14580 rpm. The upper organic phase was collected, while the aqueous phase was acidified with 20 µL of formic acid and re-extracted with 400 µL of fresh isopropanol/ethyl acetate 15/85 (v/v %). The obtained solution was vortexed and centrifuged. The supernatants were pooled and dried under a gentle stream of nitrogen.

For sphingolipid extraction, culture medium (500 µL) or cell lysate were diluted with 1 mL isopropanol/ethyl acetate 15/85 (v/v %), 3 microliters of the internal standard were added and processed as described above.

Samples were re-solubilized with 150 µL of Methanol, 1 mM $HCOONH_4$ plus 0.2% HCOOH (v/v %) prior to UHPLC-MS/MS analysis.

2.6.5. UHPLC-MS/MS conditions

Sphingolipid's quantification was carried out with a Shimadzu Nexera (Shimadzu, Milan, Italy) coupled online to a triple quadrupole LCMS 8050 (Shimadzu, Kyoto, Japan) by an ESI source. The separation was performed on a Kinetex EVO^{TM} C18 150 mm x 2.1 mm, 2.6 µm 100Å (Phenomenex, Bologna, Italy), at a flow rate of 0.5 mL/min, employing as mobile phase A) ACN/H_2O: 60/40 10 mM $HCOONH_4$ plus 0.1% HCOOH (v/v%), and B) Isopropanol/ACN 90/10 plus 0.1% HCOOH (v/v%) with the following gradient: 0 min, 5% B, 0-2.50 min, 50% B, 2.51-7 min 50-99% B, isocratic for 2.50 min. Returning to 5% in 4 min. 5 microliters were injected. Column oven was set at 55° C. The ESI was operated in positive ionization. MS source parameters were: Interface temperature 300°C, Desolvation line temperature 250°C, Heat Block temperature 400°C; nebulizing gas (N^2), drying gas (N^2), and heating gas (Air) were set respectively to 3, 10, 10 L/min. MS/MS analysis of sphingolipids were performed in multiple reaction monitoring (MRM). The SRM transitions of non-available ceramides were in silico optimized using the Lipid Creator tool (https://skyline.ms/skyts/home/software/Skyline/tools/details.view?name=LipidCreator) in the freely available Skyline open source.

For quantifying C14 Ceramide was employed the following transition: 510.4881>264.2686 (quantifier ion), collision energy (CE) -19.9; 510.4881>282.2791 (qualifier ion), CE -19.9; 510.4881>492.4775 (qualifier ion), CE -19.9. Dwell time 5msec. For quantifying C16 Ceramide was employed the following transitions: 538.20>264.30 (quantifier ion), Q1 pre bias -28.0 V, CE -27.0, Q3 pre bias -28.0 V; 538.5194>252.2686 (qualifier ion), CE -21.0. Dwell time 5msec. For quantifying C16 Ceramide-d7 was employed the following transitions:

545.50>271.40 (quantifier ion), Q1 pre bias -30.0 V, CE -26.0, Q3 pre bias -18.0 V; 545.50>82.20 (qualifier ion), Q1 pre bias -30.0, CE -55.0, Q3 pre bias -12.0 V; 545.50>527.60 (qualifier ion), Q1 pre bias -30.0, CE -13.0, Q3 pre bias -24.0 V. Dwell time 10msec. For quantifying C18 Ceramide was employed the following transitions: 566.50>264.30 (quantifier ion), Q1 pre bias -32.0 V, CE -32.0, Q3 pre bias -17.0 V; 566.50>548.50 (qualifier ion), Q1 pre bias -32.0, CE -15.0, Q3 pre bias -26.0 V. Dwell time 5msec. For quantifying C18 Ceramide-d7 was employed the following transitions: 573.60>271.40 (quantifier ion), Q1 pre bias -32.0 V, CE -30.0, Q3 pre bias -29.0 V; 573.60>259.30 (qualifier ion), Q1 pre bias -32.0, CE -32.0, Q3 pre bias -26.0 V; 573.60>555.60 (qualifier ion), Q1 pre bias -32.0, CE -30.0, Q3 pre bias -29.0 V. Dwell time 10msec. For quantifying C20 Ceramide was employed the following transition: 594.5820>264.2686 (quantifier ion), CE -23.3; 594.5820>252.2686 (qualifier ion), CE -23.3; 594.5820>282.2791 (qualifier ion), CE -23.3. Dwell time 5msec. For quantifying C22 Ceramide was employed the following transition: 622.6133>264.2686 (quantifier ion), CE -24.4; 622.6133>252.2686 (qualifier ion), CE -24.4; 622.6133>282.2791 (qualifier ion), CE -24.4. Dwell time 5msec. For quantifying C24:1 Ceramide was employed the following transitions: 648.50>264.30 (quantifier ion), Q1 pre bias -20.0 V, CE -29.0, Q3 pre bias -27.0 V; 648.50>630.50 (qualifier ion), Q1 pre bias -36.0, CE -16.0, Q3 pre bias -30.0; 648.6289>252.2686, CE -25.4. Dwell time 5msec. For quantifying C24:1 Ceramide-d7 was employed the following transitions: 655.70>271.40 (quantifier ion), Q1 pre bias -20.0 V, CE -31.0, Q3 pre bias -27.0 V; 655.70>289.35 (qualifier ion), Q1 pre bias -20.0, CE -33.0, Q3 pre bias -13.0 V; 655.70.60>637.65 (qualifier ion), Q1 pre bias -20.0, CE -15.0, Q3 pre bias -22.0 V. Dwell time 10msec. For quantifying C24:0 Ceramide was employed the following transition: 650.6446>264.2686 (quantifier ion), CE -25.5; 650.6446>252.2686 (qualifier ion), CE -25.5;

650.6446>282.2791 (qualifier ion), CE -25.5. Dwell time 5msec. For quantifying C24:0 Ceramide-d7 was employed the following transitions: 657.60>271.40 (quantifier ion), Q1 pre bias -20.0 V, CE -30.0, Q3 pre bias -17.0 V; 657.60>289.35 (qualifier ion), Q1 pre bias -20.0, CE -32.0, Q3 pre bias -30.0 V; 657.60.60>639.60 (qualifier ion), Q1 pre bias -20.0, CE -30.0, Q3 pre bias -17.0 V. Dwell time 10msec. For quantifying Sphingosine 1-Phospate was employed the following transitions: 380.10>264.40 (quantifier ion), Q1 pre bias -21.0 V, CE -16.0, Q3 pre bias -18.0. Dwell time 100msec.

For human plasma samples and preliminary HUVECs quantification the instrumental calibration was performed through the external standard method, and a calibration line for each sphingolipid was generated. For sphingosine 1-phosphate the stock solution was prepared in 0.3 M NaOH solution, then diluted with ethanol, and the calibration curve was obtained in a concentration range between 50 - 0.1 ng mL^{-1}, with seven concentration levels and triplicate injection of each level were run. The linear regression was used to generate the calibration line with values of $R^2 = 0.9977$ ($y = 0.0001x + 0.8626$). For ceramide C16 the stock solution was prepared in EtOH and the calibration curve was obtained in a concentration range between 100 - 0.1 ng mL^{-1}, with seven concentration levels and triplicate injection of each level were run. The linear regression was used to generate the calibration line with R^2 values = 0.99996 ($y= 0.00001x - 0.67955$). For the ceramide C18 the stock solution was prepared in EtOH and the calibration curve was obtained in a concentration range between 200 - 1 ng mL^{-1}, with seven concentration levels and triplicate injection of each level were run. The linear regression was used to generate the calibration line with values of $R^2 = 0.99918$ ($y= 0.00001x + 1.28477$). For the ceramide C24:1 the stock solution was prepared in EtOH and the calibration curve was obtained in a concentration range between 200 – 0.5 ng mL^{-1}, with seven concentration levels

and triplicate injection of each level were run. The linear regression was used to generate the calibration line with values of $R^2 = 0.99908$ ($y = 0.00001x + 1.71977$). For confirmatory HUVECs analysis the instrumental calibration was performed through the internal standard method and 3 µl of deuterated ceramide mix were added to the sample prior to extract them. The following calibration curves were built, with ten levels and triplicate injection of each level. Ceramide C16/Ceramide C16-d7: $y= 0.3291x + 0.0217$, $R^2= 0.9995$; Ceramide C18/Ceramide C18-d7: $y= 0.9352x + 0.0141$, $R^2= 0.9999$; Ceramide C24:1/Ceramide C24:1d7: $y= 1.3122x + 0.0304$, $R^2= 0.9995$.

2.6.6. Statistics

Results are expressed as mean ± SD. Two-sided unpaired Student's *t*-test was performed for comparisons between two independent groups and non-parametric Kruskal-Wallis test (with Dunn's multiple comparison) was used for comparisons of multiple means. Pearson's correlation analysis was used to measure the degree of correlation between two variables. Statistical analysis was performed with GraphPad Prism software (version 8.0, GraphPad Software, San Diego, CA).

2.6.7. Study approval

All human data was collected in accordance with the Declaration of Helsinki and with local Ethics Committee approval. We included individuals from two prospective Italian studies, The Campania Salute Network Study (University of Naples Federico II; permit number: 16/14) and the Moli-Sani Study (Catholic University of Rome, Italy; permit number: P99, A.931/03-138-04/C.E./2004). Written informed consent was obtained from all included participants.

2.7. Conclusion

Despite the efficacy of current drug treatment, the difficulty in achieving the optimal BP levels by a large percentage of hypertensive patients reveals the importance to develop new preventive approaches. Taken together, our results have unmasked a novel molecular mechanism underpinning the role of sortilin in the sphingolipid dysregulation. Higher circulating sortilin and S1P levels could constitute useful biomarkers for hypertension diagnosis from the early stage of vascular disease.

2.8. References

[1] Murakami Y., Hozawa A., Okamura T., Ueshima H. Evidence for Cardiovascular Prevention From Observational Cohorts in Japan Research Group (EPOCH-JAPAN). Relation of blood pressure and all-cause mortality in 180,000 Japanese participants: pooled analysis of 13 cohort studies. *Hypertension*. **2008**. 51 (6): 1483-91.

[2] Carretero O.A., Oparil S. Essential hypertension. Part I: definition and etiology. *Circulation*. **2000**. 101 (3): 329-35.

[3] Dumitru C.A., Zhang Y., Li X., Gulbins E. Ceramide: a novel player in reactive oxygen species-induced signaling? *Antioxid Redox Signal*. **2007**. 9 (9): 1535-40.

[4] Fyrst H., Saba J. An update on sphingosine-1-phosphate and other sphingolipid mediators. *Nat Chem Biol.* **2010**. 6: 489–497.

[5] Borodzicz S., Czarzasta K., Kuch M., Cudnoch-Jedrzejewska A. Sphingolipids in cardiovascular diseases and metabolic disorders. *Lipids Health Dis*. **2015**. 14: 55.

[6] Spijkers L.J., van den Akker R.F., Janssen B.J., Debets J.J., De Mey J.G., Stroes E.S., van den Born B.J., Wijesinghe D.S., Chalfant C.E., MacAleese L., Eijkel G.B., Heeren R.M., Alewijnse A.E., Peters S.L. Hypertension is associated with marked alterations in sphingolipid biology: a potential role for ceramide. *PLoS One*. **2011**. 6 (7): e21817.

[7] Airola M.V., Hannun Y.A. Sphingolipid metabolism and neutral sphingomyelinases. *Handb Exp Pharmacol*. **2013**. 215: 57-76.

[8] Henry B., Ziobro R., Becker K.A., Kolesnick R., Gulbins E. Acid sphingomyelinase. *Handb Exp Pharmacol*. **2013**. 215: 77-88.

[9] Bao J.X., Jin S., Zhang F., Wang Z.C., Li N., Li P.L. Activation of membrane NADPH oxidase associated with lysosome-targeted acid sphingomyelinase in coronary endothelial cells. *Antioxid Redox Signal*. **2010**. 12 (6): 703-12.

[10] Yang L., Jin G.H., Zhou J.Y. The Role of Ceramide in the Pathogenesis of Alcoholic Liver Disease. *Alcohol*. **2016**. 51 (3): 251-7.

[11] Goettsch C., Kjolby M., Aikawa E. Sortilin and Its Multiple Roles in Cardiovascular and Metabolic Diseases. *Arterioscler Thromb Vasc Biol*. **2018**. 38 (1): 19-25.

[12] Mortensen M.B., Kjolby M., Gunnersen S., Larsen J.V., Palmfeldt J., Falk E., Nykjaer A., Bentzon J.F. Targeting sortilin in immune cells reduces proinflammatory cytokines and atherosclerosis. *J Clin Invest*. **2014**. 124 (12): 5317-22.

[13] Goettsch C., Hutcheson J.D., Aikawa M., Iwata H., Pham T., Nykjaer A., Kjolby M., Rogers M., Michel T., Shibasaki M., Hagita S., Kramann R., Rader D.J., Libby P., Singh S.A., Aikawa E. Sortilin mediates vascular calcification via its recruitment into extracellular vesicles. *J Clin Invest*. **2016**. 126 (4): 1323-36.

[14] Goettsch C, Iwata H, Hutcheson JD, O'Donnell CJ, Chapurlat R, Cook NR, Aikawa M, Szulc P, Aikawa E. Serum Sortilin Associates With Aortic Calcification and Cardiovascular Risk in Men. Arterioscler Thromb Vasc Biol. **2017**. 37 (5):1005-1011.

[15] Takeda H., Izumi Y., Takahashi M., Paxton T., Tamura S., Koike T., Yu Y., Kato N., Nagase K., Shiomi M., Bamba T. Widely-targeted quantitative lipidomics method by super-critical fluid chromatography triple quadrupole mass spectrometry. *J Lipid Res*. **2018**. 59 (7): 1283-1293.

[16] Bielawski J., Szulc Z.M., Hannun Y.A., Bielawska A. Simultaneous quantitative analysis of bioactive sphingolipids by high-performance liquid chromatography-tandem mass spectrometry. *Methods*. **2006**. 39 (2): 82-91.

[17] Jin S., Yi F., Zhang F., Poklis J.L., Li P.L. Lysosomal targeting and trafficking of acid sphingomyelinase to lipid raft platforms in coronary endothelial cells. *Arterioscler Thromb Vasc Biol.* **2008**. 28 (11): 2056-62.

[18] Peng B., Kopczynski D., Pratt B.S., Ejsing C.S., Burla B., Hermansson M., Benke P.I., Tan S.H., Chan M.Y., Torta F., Schwudke D., Meckelmann S.W., Coman C., Schmitz O.J., MacLean B., Manke M.C., Borst O., Wenk M.R., Hoffmann N., Ahrends R. LipidCreator workbench to probe the lipidomic landscape. *Nat Commun*. **2020**. 11 (1): 2057.

[19] Merrill A.H. Jr, Sullards M.C., Allegood J.C., Kelly S., Wang E. Sphingolipidomics: high-throughput, structure-specific, and quantitative analysis of sphingolipids by liquid chromatography tandem mass spectrometry. *Methods*. **2005**. 36 (2): 207-24.

[20] Haynes C.A., Allegood J.C., Park H., Sullards M.C. Sphingolipidomics: methods for the comprehensive analysis of sphingolipids. *J Chromatogr B Analyt Technol Biomed Life Sci*. **2009**. 877 (26): 2696-2708.

[21] Rosen H., Stevens R.C., Hanson M., Roberts E., Oldstone M.B. Sphingosine-1-phosphate and its receptors: structure, signaling, and influence. *Annu Rev Biochem*. **2013**. 82: 637-62.

[22] B Gowda S.G., Ikeda K., Arita, M. Facile determination of sphingolipids under alkali condition using metal-free column by LC-MS/MS. *Anal Bioanal Chem.* **2018**. 410: 4793–4803.

[23] Folch J., Lees M., Sloane Stanley G.H. A simple method for the isolation and purification of total lipides from animal tissues. *J Biol Chem*. **1957**. 226 (1): 497-509.

[24] Bligh E.G., Dyer W.J. A rapid method of total lipid extraction and purification. *Can J Biochem Physiol*. **1959**. 37 (8): 911-7.

[25] Tölle M., Pawlak A., Schuchardt M., Kawamura A., Tietge U.J., Lorkowski S., Keul P., Assmann G., Chun J., Levkau B., van der Giet M., Nofer J.R. HDL-associated lysosphingolipids inhibit NAD(P)H oxidase-dependent monocyte chemoattractant protein-1 production. *Arterioscler Thromb Vasc Biol*. **2008**. 28 (8): 1542-8.

[26] Cantalupo A., Gargiulo A., Dautaj E., Liu C., Zhang Y., Hla T., Di Lorenzo A. S1PR1 (Sphingosine-1-Phosphate Receptor 1) Signaling Regulates Blood Flow and Pressure. *Hypertension*. **2017**. 70 (2): 426-434.

[27] Deutschman D.H., Carstens J.S., Klepper R.L., Smith W.S., Page M.T., Young T.R., Gleason L.A., Nakajima N., Sabbadini R.A. Predicting obstructive coronary artery disease with serum sphingosine-1-phosphate. *Am Heart J*. **2003**. 146 (1): 62-8.

[28] Sattler K., Lehmann I., Gräler M., Bröcker-Preuss M., Erbel R., Heusch G., Levkau B. HDL-bound sphingosine 1-phosphate (S1P) predicts the severity of coronary artery atherosclerosis. *Cell Physiol Biochem*. **2014**. 34 (1): 172-84.

[29] Di Castelnuovo A., Costanzo S., Persichillo M., Olivieri M., de Curtis A., Zito F., Donati M.B., de Gaetano G., Iacoviello L. MOLI-SANI Project Investigators. Distribution of short and lifetime risks for cardiovascular disease in Italians. *Eur J Prev Cardiol*. **2012**. 19 (4): 723-30.

[30] Nozue T., Hattori H., Kujiraoka T., Iwasaki T., Michishita I. Effects of Statin Therapy on Plasma Proprotein Convertase Subtilisin/kexin Type 9 and Sortilin Levels in Stati-Naïve Patients with Coronary Artery Disease. *J Atheroscler Thromb.* **2016**. 23 (7): 848-56.

CHAPTER III

Analysis of the metabolic switch induced by the spirulina peptide SP6 in high fat diet ApoE$^{-/-}$ mice model: A direct infusion FT-ICR-MS based approach

Abstract

Atherosclerosis, dyslipidemia and hypertension are comorbid diseases often found in combination. Among different pharmacological approaches the employment of natural multifunctional peptides is an attractive option as side therapy. Mass spectrometry-based metabolomics provide valuable information on metabolic changes and can be useful to elucidate peptide pharmacodynamics. In this work we performed a preliminary investigation on the potential effect of a recently characterized *Spirulina platensis* peptide (SP6: GIVAGDVTPI) on the modulation of metabolism in a high fat diet ApoE$^{-/-}$ mice atherosclerotic model. A direct infusion Fourier transform ion cyclotron resonance mass spectrometry (DI-FT-ICR-MS) approach was used to elucidate polar and non-polar metabolites extracted by mice plasma following four weeks SP6 treatment. The method delivered fast analysis time, repeatability, high mass accuracy and resolution for unambiguous molecular formula assignment. Multivariate statistical analysis (PLS-DA) highlighted a clear class separation, revealing the alteration of numerous metabolites levels belonging to different classes. Sphingolipids, glycerophospholipids, TCA cycle intermediates, and amino acids, which are key players in the atherosclerotic process and progression, were upregulated in saline alone HFD ApoE$^{-/-}$ group, while were sensibly decreased after treatment

with SP6 peptide. These results could open the way to further, large-scale, investigation of SP6 peptide effects in the regulation of atherosclerotic disease development and progression and show the potential of DI-FT- ICR as fast analytical tool to take snapshots of metabolic changes before moving to targeted MS-based approaches.

3.1. Introduction

In the landscape of metabolic disorders, hypertension and dyslipidemia are comorbid pathologic conditions often found in combination, that are also associated to the development of endothelial disfunction. Several evidences demonstrate that long-term high-fat diet (HFD) induces hypertension, and impair NO release [1]. Moreover, clinical studies showed that hypertension it is not only a well-known cardiovascular risk, but can contribute to the atherosclerosis development, and could play a strictly connected role in the exacerbation of this process, partially due to the synergy between elevated blood pressure and other atherogenic stimuli, inducing oxidative stress on the arterial vessels [2]. In fact, an increase of reactive oxidative species (ROS) generation, results in higher oxidation rate of low-density lipoprotein (LDL) in atherosclerotic lesions [3]. The employment of natural compounds has experienced a boost in the last years as possible adjuvant or side approaches to pharmacological therapy for the prevention and treatment of multifactorial cardiovascular disorders. Bioactive compounds, especially those of plant or marine origin, have been recognized of several healthy properties, through their involvement in different biochemical pathways, and have found widespread adoption in novel products, such as nutraceuticals and functional foods [4]. Besides phytochemicals, bioactive peptides have garnered attention as novel therapeutic molecules. Peptides are usually encrypted in the sequence of respective proteins, and released after proteolysis events, which can occur *in vivo* or *in vitro*, and exploit their activity [5]. The interest towards natural peptides is related to several aspects, in fact they show low or absent side effects, are easily metabolized by

endogenous enzymes, and can display very high specificity for their biological targets. Bioactive peptides from food and other natural matrices have shown therapeutic application against different and closely related pathologies such as diabetes, hypertension and dyslipidemia, which define the metabolic syndrome [6]. Microalgae have emerged as a rich source of peptides with different properties, and, in particular, for the prevention of cardiovascular disease [7]. In this regard, we recently characterized a novel decameric peptide from the gastro-intestinal digest of *Spirulina platensis*, named SP6 (GIVAGDVTPI, allophycocyanin alpha-chain, f: 95–104), which showed very potent in vivo anti-hypertensive activity by exerting endothelium-dependent vasodilation via a PI3K (phosphoinositide-3-kinase)/AKT (serine/threonine kinase Akt) pathway, converging on nitric oxide (NO) release [8]. Bioactive peptides from natural sources are often labelled as "multifunctional", due to combined effects such as hypotensive and hypocholesterolemic, as showed by milk, soybean and lupin protein derived peptides [9]. Food derived tripeptides Val-Pro-Pro and Ile-Pro- Pro have shown anti-obesity properties [10] while vasodilating dipeptides were reported to reduce atherosclerotic lesions in ApoE models [11]. For the comprehension of the complex interconnected metabolic mechanisms in physio pathological conditions, mass spectrometry-based metabolomics has emerged as leading method to monitor multiple metabolite classes and is highly suited to highlight molecular changes associated to drug treatments or in disease progression and outcome [12]. The high complexity of metabolic profiling, and the presence of metabolites with different chemistry, polarity and concentration range, requires high resolving power, mass accuracy and wide dynamic range. In this regard, high resolution mass spectrometry (HRMS) in direct infusion (DI) and/or coupled to ultra-high performance liquid chromatography (UHPLC-HRMS) is now the work-horse of metabolomics and lipidomics [13]. In particular, Fourier transform ion cyclotron mass spectrometry (FT-ICR-MS) offers ultra-high resolution and mass accuracy, together with the

ability to measure isotopic fine structure (ISF), leading to unambiguous identification of molecular formulas; DI-FT-ICR, in direct infusion mode is a powerful tool for rapid phenotyping studies [14]. In this study we applied a fast and accurate direct infusion nano-electrospray Fourier transform ion cyclotron mass spectrometry (DI-FT-ICR) approach to reveal in vivo metabolic changes exerted by the spirulina peptide SP6 in the modulation of atherosclerosis progression in HFD ApoE$^{-/-}$ mice model. The analysis of plasma polar and non-polar metabolites following four weeks treatment with SP6 could open valuable insight of the molecular mechanisms modulated in the atherosclerotic process, paving the way to further investigation for its employment in interconnected cardiovascular diseases.

3.2. Aim of the work

Natural peptides have emerged as an attractive option for the treatment of cardiovascular diseases. For this purpose, the potential anti-atherosclerotic effects of a novel peptide from *Spirulina Platensis* (SP6) in a high fat diet ApoE$^{-/-}$ mice model was evaluated through a metabolomics approach. The work also aimed to test the applicability of high-resolution mass spectrometry operating in direct infusion as a tool for a fast, accurate and reliable metabolomic analysis.

3.3. Results

3.3.1. SP6 treatment in HFD ApoE$^{-/-}$ mice reduces aorta monocytes/macrophages infiltration without affecting hemodynamic parameters

During all six weeks of SP6 gavage administration we monitored the peptide possible action on systolic and diastolic blood pressure and heart rate. As shown in **figure 3.1**, the monitoring of all three cardiovascular parameters measured revealed that chronic treatment with a dosage of 5 mg/kg/day for 42 days did not significantly change blood pressure (**figure 3.1. A, B**) and heart rate (**figure 3.1. C**) compared to control animals treated with saline alone. Interestingly,

the weight of the animals progressively increases with the weeks of high-fat diet (**figure 3.1. D**), in line with what has already been reported in the literature, thus confirming the metabolic effect of HFD. Furthermore, we have stained mice aortic arch with the important muscular marker of vascular re-organization, alpha-smooth muscle actin (α-SMA), and with monocytes/macrophages marker CD68 to evaluate the possible impact of SP6 treatment on this phenomenon (**figure 3.1. E, F**). Interestingly, while the mean-area-quantification of α-SMA did not show significant differences between saline and SP6 group, the area quantification of CD68 signal highlights an important reduction of the red positive area, thus suggesting a potential beneficial effect of SP6 on the mechanisms that regulates the monocytes/macrophages vessels accumulation.

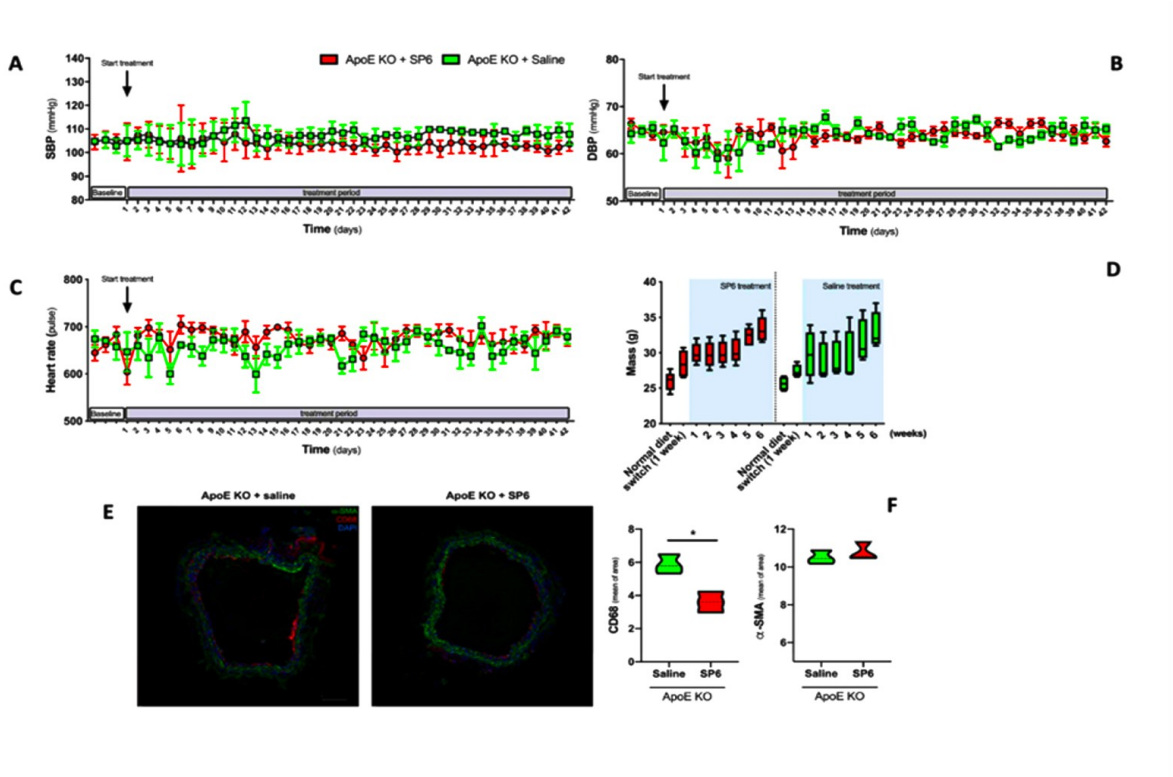

Figure 3.1. *Daily measurement of systolic (**A**), diastolic blood pressure (**B**) and heart rate (**C**) in mice treated with saline or SP6 for 4 weeks. (**D**) Bar graph reporting weekly measurement of mice body weight in both mice groups. (**E**) Representative immunofluorescence staining of aortic arches from treated ApoE knockout mice, using the monocyte/macrophage marker CD68 and the smooth muscle cell marker αSMA; (**F**) Mean area quantification of red (CD68) and green signals (αSMA) performed using RGB measurement in ImageJ.*

3.2.2. DI-FT-ICR MS analysis

The DI-FT-ICR method used an automated nanoelectrospray (nESI) direct infusion system and the whole analysis took roughly 1.50 min per sample comprising sample draw, analysis time and tip change. FT-ICR spectra of polar and lipid extracts, with both ionizations, are reported in **figure 3.2 A**. Mass accuracy values were on average 0.10 and 0.22 for polar metabolites and lipids respectively, which reflect the extreme mass accuracy of FT-ICR measurement, that, together with high resolution and isotopic fine structure (ISF) ability, leads to unambiguous molecular formula assignment, also for compound with several heteroatoms, such as the metabolite indoxyl sulphate, whose signal enlargement, simulated isotope pattern and molecular formula are depicted in **figure 3.2 B**, resulting in a very low mass error (0.08 ppm) and a calculated resolution of 290.757. In this study QC samples were prepared and employed to monitor the repeatability of the DI-FT-ICR workflow and were run randomly during the batch. In this regard, the coefficient of variation (CV %) relative to peak intensity was comprised between 0.11 and 10.95 % for polar extract sample (relative to the m/z range 100–750), and between 0.59 and 11.19 % for lipid extract sample (relative to the m/z range 150–885) indicating an acceptable repeatability for both metabolite classes (**supporting information table S2.1**). Furthermore, a satisfactory clustering of QC samples can be appreciated from PCA scores plot (**supporting information figure S2.2**) of both metabolite and lipids datasets, indicating that the quality of data was acceptable for the next steps of the study.

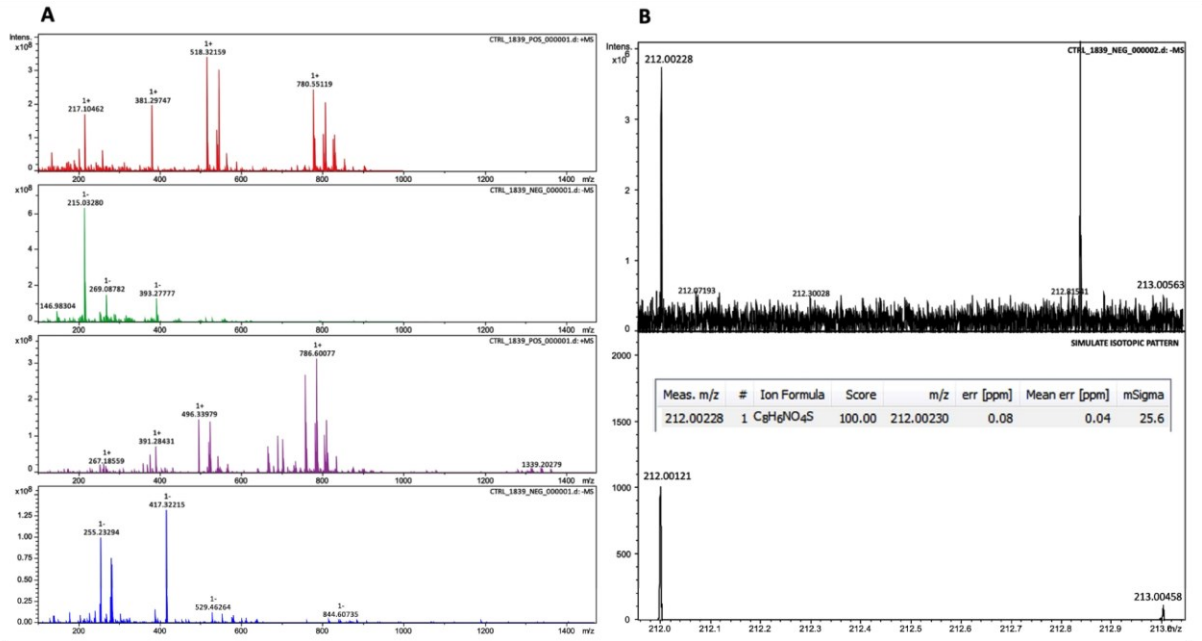

Figure 3.2. *DI-FT-ICR spectra of polar (red, ESI$^+$, green ESI$^-$) and lipids (violet ESI$^+$, blue ESI$^-$) samples (**A**); Spectra enlargement showing the signal of metabolite indoxyl sulphate ($C_8H_7NO_4S$, HMDB0000806) and its simulated isotope pattern with molecular formula assignment (bottom, **B**).*

3.3.3. Multivariate data analysis of plasma samples

Data preprocessing was based on sample filter to remove peaks that were not present in at least 80 % of a single group, maximum deviation for mass accuracy was set to 1 ppm for DI-FT-ICR annotation and molecular formula generation, **supporting information table S2.1** reports the whole bucket table features after filtering, for lipids and metabolites in both ionization modes. The Volcano plot representation of significant metabolites (FC > 1 or < -1, $p < 0.05$) of saline and SP6 treated peptides is reported in **supporting information figure S2.3**. PLS-DA was used to investigate the metabolic changes in high fat diet ApoE$^{-/-}$ mice after the treatment with SP6 peptide with respect to those who received saline alone. **Figure 3.3 A, D** shows the results of PLS-DA model for plasma polar and lipids extracts, as can be appreciated, the two groups are clearly separated. In particular for polar sample the first component explains 24.5 %

of the variance, while the second explains 23.9 %, instead, for lipid sample, values were 17.9 % and 8.8 % respectively, with class discrimination parameters R^2: 0.98, 0.99, Q^2: 0.95, 0.92, for polar (**figure 3.3 B**) and lipid sample respectively (**figure 3.3 E**), which indicate a robust multivariate model. Metabolites that contributed to the clustering and discrimination were extracted based on the variable importance of projection (VIP), which were generated after PLS-DA processing. The first 15 metabolites with highest VIP scoring of both polar and lipid extracts, are reported in **figure 3.3 C, F.**

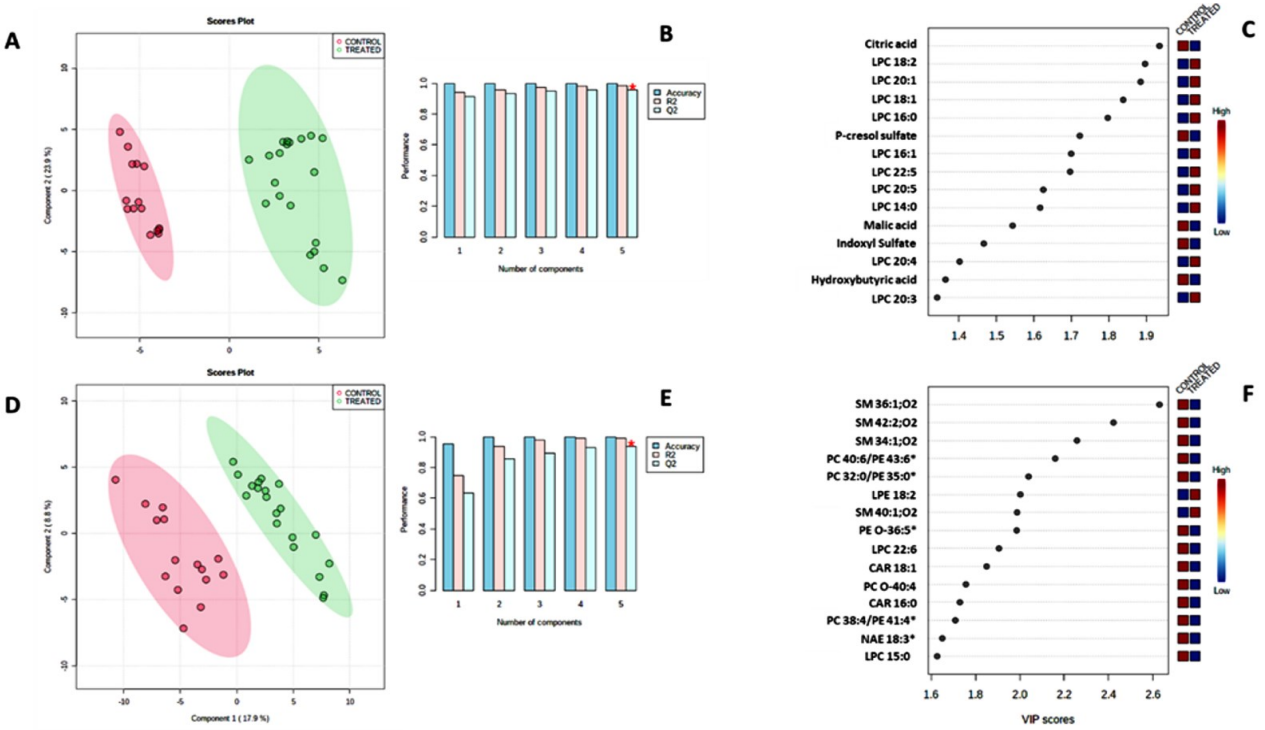

Figure 3.3. *Comparative analysis of polar (**A**) and lipid (**D**) plasma extracts of HFD ApoE$^{-/-}$ mice treated with saline alone (red circle) and those treated with spirulina peptide SP6 (green circle) expressed as PLS-DA score plot, with respective cross validation values (**B**, **E**), R^2 and Q^2 indicate prediction accuracy and model robustness, respectively. The first 15 variables important in projection (VIP) identified by the corresponding PLS-DA were reported (**C**, **F**).*

3.3.4. Annotation of statistically relevant metabolites

Table 3.1 reports the putative annotation of metabolites with VIP score >1.2 and $p < 0.05$ showed in **figure 3.3 C, F,** which were considered to be most influential for the separation between saline group and those which received SP6 peptide administration. Despite DI- FT-ICR delivers ultra-high mass accuracy, this data alone often cannot differentiate the large amount of isomers occurring in biological samples, and thus additional information, such as MS/MS fragmentation pattern comparison against a reference spectra, is mandatory for reliable metabolite annotations [15]. For this reason, we performed in parallel two UHPLC-HRMS/MS distinct methods for lipids and polar metabolites; in particular all statistically relevant metabolites annotated by DI-FT-ICR method were checked by fragmentation pattern and comparison with reference MS/MS spectra, accurate mass, isotope pattern and retention time, obtained on the Q-Exactive platform. In the largest part it was possible to support the annotation of several compounds, such as acyl or alkyl lysophosphatidylcholines [16], differentiate sphingomyelins (SM) between ceramide phosphorylethanolamines (PE-Cer) with the former that are characterized by diagnostic ions at 184 and 264 m/z [17] while the latter (that were not detected) by the neutral loss of 141 m/z [18], or further enforce the annotation of polar metabolites. Clearly, for lipids assignment of double bond position and precise isomer annotation requires a more detailed analysis. HCD MS/MS spectra of some relevant metabolites are reported in **figure 3.4 A-D** and in **supporting information figure S2.4**. Where MS/MS data were not available, such as for the four metabolites labelled with asterisk in **table 3.1**, they were tentatively assigned to chemical classes and reported with MSI level 3. Noteworthy UHPLC-HRMS/MS confirmed also the statistical trend observed for DI-FT-ICR method (**supporting information figure S2.5**).

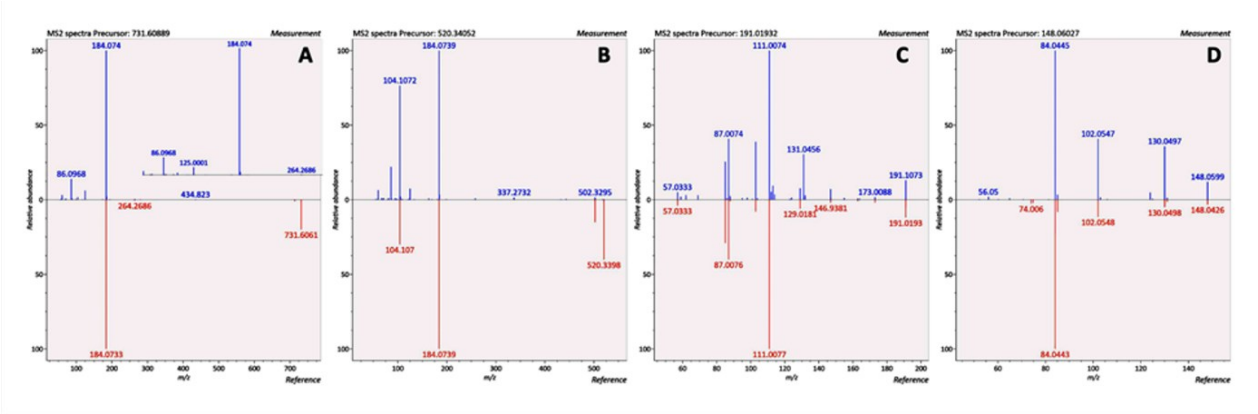

Figure 3.4. *HCDMS/MS spectra of relevant metabolites obtained by UHPLC-HRMS/MS methods, **A**: SM 36:1;O2; **B**: LPC 18:2; **C**: Citric acid; **D**: Indoxyl sulphate. MS/MS spectra of other metabolites reported in **table 3.1** are showed in **supporting information figure S2.4**.*

.

Table 3.1. *List of statistical relevant annotated metabolites derived from PLS-DA analysis. Metabolites labelled with asterisk indicate compounds which MS/MS spectra were unavailable and/or where molecular formula was shared among different metabolites, these were generally assigned to a class of compounds. Detailed MS/MS spectra of relevant metabolites are reported in* ***figure 3.4*** *and* ***supporting information figure S2.4****, complete UHPLC-HRMS/MS data are reported in* ***supporting information table S2.1****.*

m/z	Ion type/Adduct	Name	MSI level	Molecular Formula	Biochemical Class/Sub class	VIP value	p.value
103.04007	$[M-H]^-$	Hydroxybutyric acid	2	$C_4H_8O_3$	Alpha hydroxy acids and derivatives	1.36	3.30^{E-15}
133.01424	$[M-H]^-$	Malic acid	2	$C_4H_6O_5$	Beta hydroxy acids and derivatives	1.53	5.20^{E-12}
187.00704	$[M-H]^-$	p-Cresol sulfate	2	$C_7H_8O_4S$	Arylsulfates	1.70	4.70^{E-07}
191.01970	$[M-H]^-$	Citric acid	2	$C_6H_8O_7$	Tricarboxylic acids and derivatives	1.91	3.00^{E-06}
212.00228	$[M-H]^-$	Indoxyl sulfate	2	$C_8H_7NO_4S$	Arylsulfates	1.45	1.10^{E-05}
322.27413	$[M+H]^+$	NAE 18:3*	3	$C_{20}H_{35}NO_2$	Fatty amides*	1.43	1.15^{E-02}
400.34224	$[M+H]^+$	CAR 16:0	2	$C_{23}H_{45}NO_4$	Fatty acyl carnitines	1.53	6.65^{E-03}
426.35789	$[M+H]^+$	CAR 18:1	2	$C_{25}H_{47}NO_4$	Fatty acyl carnitines	1.55	1.70^{E-04}
478.29294	$[M+H]^+$	LPE 18:2	2	$C_{23}H_{44}NO_7P$	Glycerophosphoethanolamines	1.67	3.30^{E-05}
482.32422	$[M+H]^+$	LPC 15:0	2	$C_{23}H_{48}NO_7P$	Glycerophosphocholines	1.44	1.23^{E-02}
490.29033	$[M+Na]^+$	LPC 14:0	2	$C_{22}H_{46}NO_7P$	Glycerophosphocholines	1.60	8.90^{E-04}

516.30599	$[M+Na]^+$	LPC 16:1	2	$C_{24}H_{48}NO_7P$	Glycerophosphocholines	1.68	1.80^{E-03}
518.32162	$[M+Na]^+$	LPC 16:0	2	$C_{24}H_{50}NO_7P$	Glycerophosphocholines	1.78	2.10^{E-03}
542.32164	$[M+Na]^+$	LPC 18:2	2	$C_{26}H_{50}NO_7P$	Glycerophosphocholines	1.87	3.60^{E-03}
544.33724	$[M+Na]^+$	LPC 18:1	2	$C_{26}H_{52}NO_7P$	Glycerophosphocholines	1.81	4.70^{E-03}
564.30598	$[M+Na]^+$	LPC 20:5	2	$C_{28}H_{48}NO_7P$	Glycerophosphocholines	1.60	1.00^{E-02}
566.32163	$[M+Na]^+$	LPC 20:4	2	$C_{28}H_{50}NO_7P$	Glycerophosphocholines	1.40	6.90^{E-12}
568.33711	$[M+Na]^+$	LPC 20:3	2	$C_{28}H_{52}NO_7P$	Glycerophosphocholines	1.33	1.80^{E-02}
568.34000	$[M+H]^+$	LPC 22:6	2	$C_{30}H_{50}NO_7P$	Glycerophosphocholines	1.59	1.20^{E-04}
572.36859	$[M+Na]^+$	LPC 20:1	2	$C_{28}H_{56}NO_7P$	Glycerophosphocholines	1.86	1.80^{E-02}
592.33726	$[M+Na]^+$	LPC 22:5	2	$C_{30}H_{52}NO_7P$	Glycerophosphocholines	1.68	2.30^{E-02}
703.57504	$[M+H]^+$	SM 34:1;O2	2	$C_{39}H_{79}N_2O_6P$	Sphingomyelins	2.00	2.90^{E-06}
724.52789	$[M+H]^+$	PE O-36:5*	3	$C_{41}H_{74}NO_7P$	Glycerophosphoethanolamines*	1.80	2.50^{E-05}
731.60637	$[M+H]^+$	SM 36:1;O2	2	$C_{41}H_{83}N_2O_6P$	Sphingomyelins	2.22	8.70^{E-11}
734.56966	$[M+H]^+$	PC 32:0/PE 35:0*	3	$C_{40}H_{80}NO_8P$	Glycerophospholipids*	1.85	1.80^{E-06}
787.66893	$[M+H]^+$	SM 40:1;O2	2	$C_{45}H_{91}N_2O_6P$	Sphingomyelins	1.69	3.10^{E-05}
810.60095	$[M+H]^+$	PC 38:4/PE 41:4*	3	$C_{46}H_{84}NO_8P$	Glycerophospholipids*	1.50	6.65^{E-03}
813.68478	$[M+H]^+$	SM 42:2;O2	2	$C_{47}H_{93}N_2O_6P$	Sphingomyelins	2.12	2.50^{E-09}

824.65303	$[M+H]^+$	PC O-40:4	2	$C_{48}H_{90}NO_7P$	Glycerophosphocholines	1.60	1.40^{E-04}
834.60101	$[M+H]^+$	PC 40:6/PE 43:6*	3	$C_{48}H_{84}NO_8P$	Glycerophospholipids*	1.90	7.50^{E-07}

3.3.5. Plasma metabolic differences between HFD ApoE$^{-/-}$ and SP6 treated mice

Different metabolite classes were found dysregulated, and in particular hydroxyl and tricarboxylic-organic acids, amino acids, lysophosphatidylcholines, sphingomylelins, and other glycerophospholipids. To visualize and identify the metabolic pathways influenced by the SP6 peptide administration, the HMDB identities of significant altered metabolites ($p < 0.05$) were imported in the pathway analysis tool of Metaboanalyst 4.0 to construct the metabolic maps which are reported in **figure 3.5 A, B**. Among the pathways that showed significant perturbations were sphingolipids and glycerophospolipids metabolism, fatty acid biosynthesis, tricarboxylic acid cycle (TCA), and glutamate/glutamine metabolism.

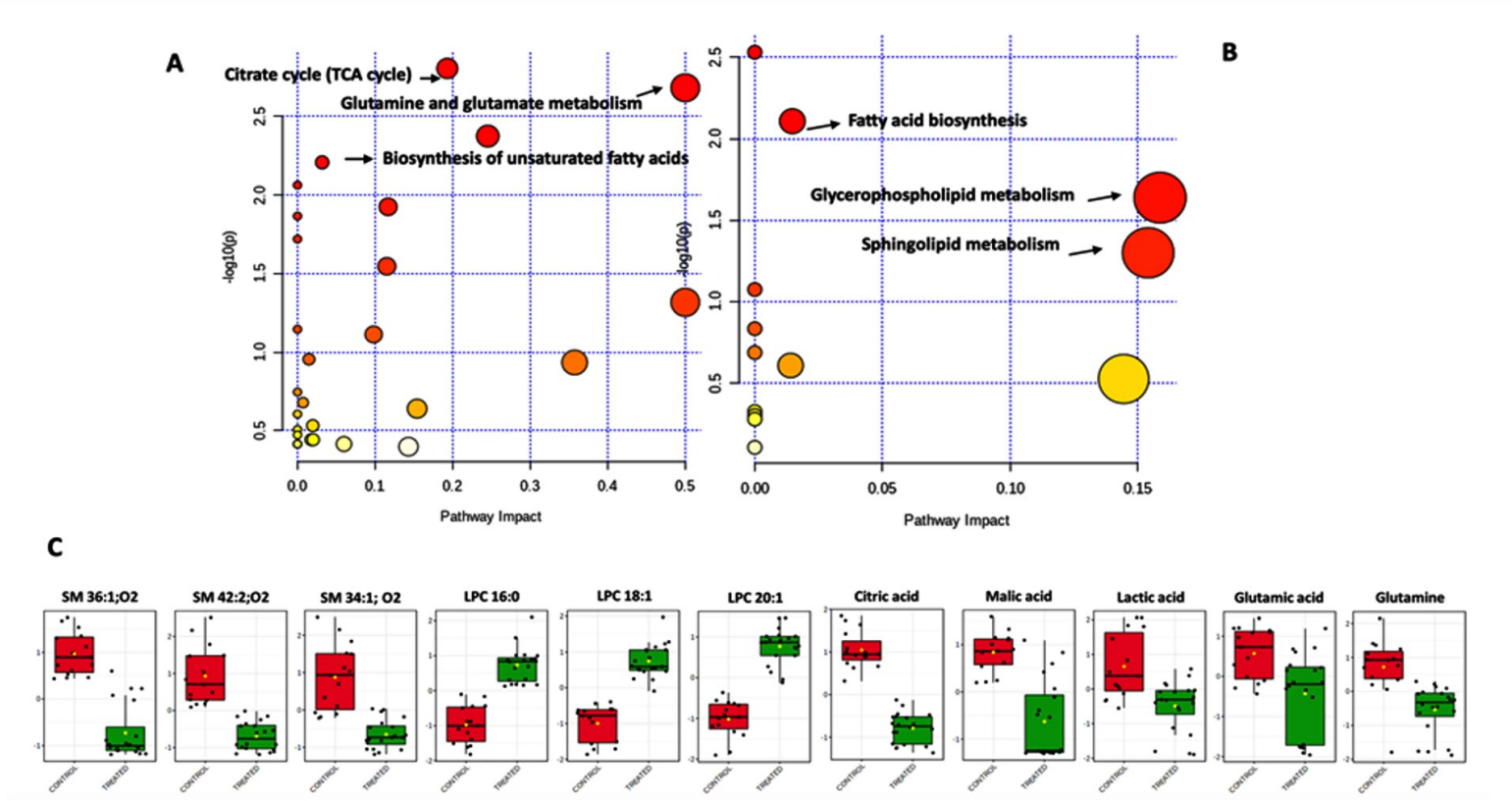

Figure 3.5. *Pathway analysis of metabolic (**A**) and lipidomic (**B**) routes influenced by the administration of SP6 peptide in HFD ApoE$^{-/-}$ mice model. Pathway analysis was performed on all significantly altered metabolites ($p < 0.05$) between the two groups. Whisker box plots (red color: saline only group, green color: SP6 treated group) relative to sphingomyelins, lysoPCs, tricarboxylic acids, amino acids (**C**)*

3.3.6. Dysregulated lipids and metabolites

As can be appreciated from the box-plots in **figure 3.5 C**, several sphingomyelins (SM) were increased in saline HFD ApoE$^{-/-}$ group, and, in this class, in particular: 34:1, 36:1, 42:2; these results are in accordance with several HFD ApoE$^{-/-}$ models [19,20]. Plasma levels of numerous Lysophospatydylcholines (LysoPCs) were reduced in saline group (LysoPCs: 14:0, 15:0, 16:0, 16:1, 18:1, 18:2, 19:0, 22:5, **figure 3.5 C**) which is in agreement with previous lipidomic analyses in HFD obese mice models [21].

TCA cycle related metabolites citric, malic and lactic acid levels were higher in the saline ApoE$^{-/-}$ group (**figure 3.5 C**). Glutamate and glutamine levels were upregulated in the saline group, while they were both decreased in SP6 group. Both p-cresol and indoxyl sulphate levels were higher in ApoE$^{-/-}$ saline alone group, while reduced in SP6 (**figure 3.5 C, supporting information figure S2.6**).

3.4. Discussion

In a previous paper [8] we characterized a novel allophycocyanin derived peptide, named SP6, that at the dose of 10 mg/kg of SP6 reduced systolic blood pressure in an experimental model of arterial hypertension. Considering the important hemodynamic effect evoked by acute high-dosage treatment with SP6, here we chronically treated HFD ApoE knockout mice with a lower-dosage (5 mg/kg) of SP6, which, while is not sufficient to modulate blood pressure, is still associated with a significantly improved vascular function in mesenteric arteries [8].

The adopted dosage of the peptide, indeed, did not induce substantial changes of blood pressure or heart rate values, however it allowed to appreciate a potential anti-atherosclerotic activity as evidenced by the reduction of the area underlying the CD68. It is well-known that one of the first processes that acts as key factor of the atherosclerotic event, is represented by the recruitment of monocytes/macrophages to the vessels wall, which favors the lipid accumulation

and inflammation [22], despite this, the complex molecular mechanisms involved in plaque progression still remain obscure [23].

Based on these results, to elucidate the possible modulation of molecular pathways by SP6 and translate into useful information for pharmacodynamic comprehension, we moved to evaluate the metabolomic changes by an untargeted DI-FT-ICR-MS platform. The total runtime was considerably lower than UHPLC-HRMS/MS methods (RPLC: 19 min, HILIC: 16 min, **supporting information figure S2.1**), moreover, since no single chromatographic method is able to resolve both lipids and polar metabolites, usually RPLC and HILIC or capillary electrophoresis (CE) are used in combination [24], which can result in an exponential increase of the overall analysis time.

The pathway analysis revealed a broad range of lipids and metabolites potentially affected by the administration of SP6. Sphingolipid's metabolism resulted as one of the most perturbated. Indeed, both *in vitro* and *in vivo* studies have demonstrated the links between SM and atherosclerosis, in fact, the inhibition of SM synthesis prevents the development of atherosclerotic lesions, and reduces atherosclerotic plaque area [25], moreover SM 34:1 and SM 42:2 have been positively correlated to mortality in vascular and metabolic diseases [26]. Interestingly, after the four weeks treatment with peptide SP6, the levels of all the corresponding sphingomyelins were decreased. Notably these were among the lipids with the highest statistical influence (VIP $\geq$ 2). Regarding glycerophospholipids, several metabolites were differently modulated in the saline alone HFD ApoE$^{-/-}$ group, in accordance with previous relevant findings on induced HFD obese mice models [27,28]. Decreased LysoPCs levels have been also found in inflammatory status and their composition can play potential protective role in cardiovascular diseases (CVDs), in particular LysoPCs 16:0, 18:0 and 18:2 have been negatively associated with CVDs

mortality [26]. Opposite to saline group, the trend of the listed LysoPCs was increased in SP6 treated group, and these metabolites were among the main contributors to class separation.

TCA cycle, the terminal of fat oxidation, is dysregulated in diet induced obesity and diabetic models, and results in inflammation process and oxidative stress [29]. We found reduced TCA metabolites levels in SP6 treated group. Similar results were obtained in rabbit atherosclerotic models, where the increased levels of TCA intermediates translate into enhanced aerobic fatty acid oxidation and anaerobic pathways for ATP production in macrophage-rich atherosclerotic arteries [30].

Among amino acids, glutamate and glutamine have been often recognized as markers of atherosclerosis development and CVD risk. L-glutamate alteration has been associated to proatherogenic effects, through an increased triglycerides accumulation in macrophages [31], whereas glutamine has been linked with clinical evidence of atherosclerosis, since it has been associated with higher risk for both plaque development and increased intima–media thickness [32]. Among other altered metabolites, particularly interesting are the two uremic toxins, indoxyl sulphate and p-cresol sulphate were decreased in SP6 group. In fact, these two metabolites have been associated to several diseases such as endothelial disfunction, atherosclerosis and hypertension and have been found upregulated in plasma and urine of obesity models [33].

Overall, the metabolic profile carried out by DI-FT-ICR points out a significant change of several metabolites after four-week treatment with SP6 peptide, resulting in the modulation of key markers of atherosclerosis and dyslipidemia, and the crosstalk with multiple molecular pathways. Clearly, being this a pilot study, the obtained findings should be considered in the context of study limitations, such as a small sample size, and the need of further histological and biochemical investigations, such as correlation with lipoproteins, triglycerides and cholesterol levels, as well as analysis of other vessels for plaque evaluation and immunological

studies. Nevertheless, these results show a distinct significant metabolic response induced by SP6 treatment, that, besides its hypotensive and vasodilating potential at higher doses, could be a promising alternative for adjuvant or preventive therapies in atherosclerosis at lower dosage. The analytical approach used allows to take a rapid and accurate "snapshot" of both polar and non-polar metabolite changes in very short time, and overcomes the limitation of LC-MS methods, such as longer analysis time and drift of retention times. DI-FT-ICR could be easily adapted for larger sample numbers, which will employ other animal models, diet conditions and comparison with drugs employed in cardiovascular diseases, which are necessary to explore the pharmacodynamics of SP6 peptide, before moving to UHPLC-HRMS/MS methods for confirmation of metabolite annotation or targeted LC-MS/MS approaches for quantification purposes.

3.5. Materials and methods

3.5.1. Animal experiments

The data that support the findings of this study are available from the corresponding authors on reasonable request. Synthesis and purification of SP6 peptide is described in detail in **supporting information S7.2.1.** All animal studies were performed in accordance with approved protocols by the IRCCS Neuromed Animal Care Review Board and by the Istituto Superiore di Sanità and were conducted according to EU Directive 2010/63/EU for animal experiments. ApoE$^{-/-}$ mice (Charles River Laboratories, Sant'Angelo Lodigiano, Italy) were born at the expected mendelian ratios, developed normally, and were maintained in a ventilated environment. All animals were randomly divided into the control group treated with saline solution and group treated with peptide SP6 (5 mg/Kg) by daily gavage administration. Mice were fed up to 10 weeks with normal rodent chow (4.5 % fat; Ralston Purina Co.), and subsequently switched to the Western diet-high fat diet (HFD) (Complete feed for Rodents Purified Diet 60 % ENERGY

FROM FATS – Mucedola) at 11 weeks for 1 week. Subsequently, in the next week they have been treated by gavage with saline solution (N = 4) or with SP6 (N = 5) daily for 4 weeks.

3.5.2. Mice monitoring and sample collection

All mice have been subjected to constant monitoring of systolic, diastolic blood pressure and heart rate during all observation period by non-invasive tail-cuff method using the BP-2000 instrument (Visitech systems, Apex, NC, U.S.A) as previously described [8]. Moreover, mice were weighed throughout the observation period using electronic veterinary weighing scale (Soehnle Industrial Solu- tions, Backnang, Germany).

At the end of treatment (4th week), blood was collected from the heart through cardiac puncture of isoflurane-anesthetized mice in heparinized tube, and rapidly centrifuged at 2200 rpm for 15 min to obtain plasma samples.

3.5.3. Immunofluorescence analysis

Immunofluorescence analyses of aortic arch from ApoE$^{-/-}$ mice treated with saline solution or SP6 for 4 weeks were performed on snap-frozen segment in OCT embedding medium. Frozen sections (10 µm) were treated with blocking solution (2% donkey serum, 1.5 % BSA, 0.5 % fish gelatin) for 45 min and immunostained overnight at 4°C in blocking solution with antibodies anti– αSMA (1:200, abcam) and with anti-CD68+ (1:200; abcam) and revealed with appropriate secondary antibodies (Rhodamine-Red anti-mouse IgG; Jackson ImmunoResearch; Alexa Fluor 488 anti-sheep IgG; Molecular Probes, Invitrogen). Nuclei were counterstained with DAPI. The images were acquired using a fluorescence THUNDER Imaging Systems (Leica, Buccinasco, Milan, Italy) microscope.

3.5.4. Sample preparation

Polar metabolites and lipids were extracted following the Matyash protocol with slight modifications [34]. Briefly 20 µL of plasma were thawed on ice and 225 µL of ice cold MeOH were

added, samples were vortexed for 10 s, subsequently 750 µL of cold MTBE were added and the solution was mixed in a thermomixer® (Eppendorf) for 6 min at 4°C. Subsequently 188 µL of H_2O were added and samples were vortexed for 20 and finally centrifuged at 14680 rpm, for 5 min at 4°C for phase separation. The two phases were recovered separately and dried under nitrogen. The non-polar extract was solubilized in 400 µL of 5 mM CH_3COONH_4 MeOH/DCM 90/10 (v/v), while the polar extract was solubilized in 200 µL of 1:1 ACN/H_2O 0.1 % HCOOH (v/v). A pooled quality control (QC) sample was prepared for both polar and non-polar analysis. This was achieved by pooling an aliquot of plasma from each sample until the same volume used for extraction and subsequently extracted as described above. Unless otherwise described, all solvents and additives were LCMS grade and purchased by Merck (Darmstadt, Germany).

3.5.5. DI-FT-ICR analysis

Analyses were performed in direct infusion nano-electrospray by an automated multisample chip-based nESI sample ionization platform TriVersa NanoMate (Advion BioSciences Ltd, Ithaca NY, U.S.A), which was operated with the following parameters: gas pressure (nitrogen) was 0.3 psi, spray voltage 1.45 kV, sample volume was 5 µL, sample plate temperature was set to 10°C, 5 µm nominal internal diameter nozzle chip was used. Data were acquired on a SolariX XR 7 T (Bruker Daltonics, Bremen, Germany). The instrument was tuned with a standard solution of sodium trifluoracetate (NaTFA). Mass Spectra were recorded in broadband mode in the range 150–1500 m/z for lipids, whereas 90−800 m/z was used for polar metabolites, with an ion accumulation of 10 ms, 32 scans were acquired using 2 million data points (2 M), with a resolution of 150.000 at m/z 400. Drying gas (nitrogen) was set at 2 mL/min, with a drying temperature of 150°C. Funnel amplitude was set to 90 V (polar metabolites) or 100 V (lipids), transfer was set at 0.6 MHz, and TOF 0.7 s. Both positive and negative ESI ionization were

employed in separate run. Five replicates of each injection were carried out. The instrument was controlled by Bruker FTMS Control (Bruker).

3.5.6. UHPLC-HRMS/MS analysis

Two UHPLC-HRMS/MS methods (reversed phase and hydrophilic interaction liquid chromatography) were employed to enforce DI-FT-ICR results and avoid metabolite misannotation. Analyses were performed on a Thermo Ultimate RS 3000 coupled online to a Q-Exactive hybrid quadrupole Orbitrap mass spectrometer (Thermo Fisher Scientific, Bremen, Germany) equipped with a heated electrospray ionization probe (HESI II). For Lipid analysis the separation was performed with an Acquity UPLC CSH C18 column (100 × 2.1 mm; 1.7 µm) protected with a VanGuard CSH precolumn (5 × 2.1 mm; 1.7 µm) (Waters, Milford, MA, U.S.A). The column temperature was set at 55 ◦C, a flow-rate of 0.4 mL/min was used, mobile phase consisted of (A): ACN/H_2O with 10 mM $HCOONH_4$ and 0.1 % HCOOH 60:40 (v/v) and (B): IPA/ACN with 0.1 % HCOOH 90:10 (v/v). The following gradient has been used: 0 min, 40 % B, 2 min, 43 % B, 2.10 min, 50 % B, 10 min, 60 % B, 12 min, 75 % B, 13 min, 99 % B hold for 2 min, returning to 40 % in 0.1 min. The separation of polar metabolites was performed in HILIC mode, with an Acquity BEH Amide (100 × 2.1 mm; 1.7 µm) protected with a VanGuard amide precolumn (5 × 2.1 mm; 1.7 µm) (Waters). The column temperature was set at 40 ◦C, and the flow-rate was 0.350 mL/min. The mobile phase was (A): 0.1 % HCOOH in H_2O (v/v) and (B): 0.1 % HCOOH in ACN (v/v). The following gradient was employed: 0 min, 99 % B, 1 min, 99 % B, 10.50 min, 20 % B, 11 min, 20 % B, returning to 99 % in 0.1 min, 2 µL were injected in both RP and HILIC. Full MS (Lipids: 300−1500 m/z, polar metabolites: 50−800 m/z) and data-dependent MS/MS were performed at a resolution of 35.000 and 15.000 FWHM respectively, a fixed normalized collision energy (NCE) value of 30 was used. Both ESI^+ and ESI^- were used, in separate run. Source parameters: Sheath gas pressure, 45 arbitrary units;

auxiliary gas flow, 15 arbitrary units; spray voltage, +/-3.5 kV; capillary temperature, 280 °C; auxiliary gas heater temperature, 350 °C. Three replicate of each sample were performed, QC were randomly inserted in the batch to monitor system stability over time.

3.5.7. Data processing

DI-FT-ICR data analysis was performed with Metaboscape (v. 5.0, Bruker). The first step is the creation of a matrix (bucket table) using the T-ReX 2D algorithm. The T-Rex 2D algorithm for feature extraction from FT-ICR single spectra extracts m/z / intensity pairs (peaks) from acquired raw data and subjects them to deisotoping in order to create features consisting of isotope patterns. Subsequently, spectra alignment, filtering, normalization were performed. The spectra were processed in positive mode using H^+ as the primary ion, Na^+ and NH_4^+ as a potential adducts, while in negative mode H^- was set as the primary ion and Cl^- as a potential adduct. For metabolite annotation, assignment of the molecular formula was performed for the detected features using Smart FormulaTM (SF), isotopic fine structure (ISF) and data recalibration. The bucket table was annotated with a list of metabolites and lipids obtained respectively from the HMDB (https://hmdb.ca/) and LIPIDMAPS database (www. lipidmaps.org). Annotation was performed with 0.2 ppm (narrow) or 1 ppm (wide) mass tolerance and a mSigma value below 200, molecular formulas were manually inspected taking into account the most probable adduct form. For UHPLC-HRMS processing Thermo RAW. data files were converted to ABF format using Reifycs Abf (Analysis Base File) converter, subesequently data alignement and metabolite annotation were performed by MS-DIAL software (v. 4.16, http://prime.psc.riken.jp/compms/msdial/ main.html). Detailed parameters for peak picking, alignment and annotation are reported in **supporting information S7.2.2**. Metabolites were putatively annotated on level 2 Metabolomics Standard Initiative (MSI level 2) with accurate mass/isotopic fine structure or spectral similarity, for some case where isomeric overlap

occurred and/or in absence of reference MS/MS spectra, metabolites were annotated on level 3 and thus assigned to a biochemical class [35].

3.5.8. Statistical analysis

Statistical analysis of systolic, diastolic blood pressure and heart rate was performed using two-way ANOVA followed by Bonferroni's multiple comparisons test. Two-way ANOVA followed by Sidak's multiple comparisons test was used for weight comparison. Unpaired t-test was used for α-SMA and CD68 comparisons between groups. For DI-FT-ICR-MS and UHPLC-HRMS/MS univariate and multivariate statistical analysis were conducted with normalized and pareto-scaled HRMS data using MetaboAnalyst (v. 4.0, http://www.metaboanalyst.ca/), data from both ionization polarities were treated simultaneously. The normalized variables obtained from data processing were visualized in a Volcano Plot to show which variables present a stronger combination of fold change (FC) and statistical significance (p-value) from a Student t-test, features with fold change >1, <-1 and p value ≤0.05 were considered statistically significant. Principal component analysis (PCA) and partial least square discriminant analysis (PLS-DA) was used to visualize discrimination among the two groups, the validity and robustness of the PLS-DA model was evaluated using the coefficient R^2 (model-fit) and the coefficient Q^2 (predictive ability), respectively, using the 5-fold internal cross-validation method. The loading plot was used to identify significant metabolites responsible for maximum separation in the PLS-DA score plot, and these metabolites were ranked according to their variable influence on projection (VIP) scores. Metabolic pathways and Whisker box plot were created and visualized using Metaboanalyst.

3.6. Conclusions

In this study, a fast and accurate direct infusion FT-ICR based metabolic profiling was applied for the preliminary evaluation of the effect of the novel spirulina peptide SP6 in a model

of atherosclerosis, namely high fat diet ApoE$^{-/-}$. DI-FT-ICR analysis with a short analysis time of 1.50 min per sample delivered high mass accuracy and resolution, together with good repeatability. The statistical analysis allowed to elucidate a significant modulation of different metabolic routes caused by the administration of SP6 peptide, comprising key metabolites which are involved in atherosclerotic plaque progression and development. These preliminary results encourage to extend the investigation of the possible employment of SP6 peptide in the prevention and treatment of multifactorial cardiovascular diseases.

3.7. References

[1] Roberts C.K., Vaziri N.D., Wang X.Q., Barnard R.J. Enhanced NO inactivation and hypertension induced by a high-fat, refined-carbohydrate diet. *Hypertension*. **2000**, 36: 423–429.

[2] Alexander R.W. Hypertension and the pathogenesis of atherosclerosis. *Hypertension*. **1995**, 25: 155–161.

[3] Azumi H., Inoue N., Ohashi Y., Terashima M., Mori T., Fujita H., Awano K., Kobayashi K., Maeda K., Hata K., Shinke T., Kobayashi S., Hirata K., Kawashima S., Itabe H., Hayashi Y., Imajoh-Ohmi S., Itoh H., Yokoyama M. Superoxide generation in directional coronary atherectomy specimens of patients with angina pectoris: important role of NAD(P)H oxidase. *Arterioscler. Thromb. Vasc. Biol.* **2002**, 22: 1838–1844.

[4] Huang W.Y., Davidge S.T., Wu J. Bioactive natural constituents from food sources-potential use in hypertension prevention and treatment. *Crit. Rev. Food Sci. Nutr*. **2013**, 53: 615–630.

[5] Pepe G., Sommella E., Ventre G., Scala M.C., Adesso S., Ostacolo C., Marzocco S., Novellino E., Campiglia P. Antioxidant peptides released from gastrointestinal digestion of "Stracchino" soft cheese: characterization, in vitro intestinal protection and bioavailability. J. *Funct. Foods.* **2016**. 26: 494–505.

[6] Alberti K.G., Zimmet P., Shaw J. IDF Epidemiology Task Force Consensus Group, the metabolic syndrome–a new worldwide definition. *Lancet*. **2005**. 366: 1059–1062.

[7] Sommella E., Conte G.M., Salviati E., Pepe G., Bertamino A., Ostacolo C., Sansone F., Del Prete F., Aquino R.P., Campiglia P. Fast profiling of natural pigments in different Spirulina (Arthrospira platensis) dietary supplements by DI-FT-ICR and evaluation of their antioxidant potential by pre-column DPPH-UHPLC assay. *Molecules.* **2018**. 23, 1152.

[8] Carrizzo A., Conte G.M., Sommella E., Damato A., Ambrosio M., Sala M., Scala M.C., Aquino R.P., De Lucia M., Madonna M., Sansone F., Ostacolo C., Capunzo M., Migliarino S., Sciarretta S., Frati G., Campiglia P., Vecchione C. A novel potent decameric peptide of Spirulina platensis reduces blood pressure levels through a PI3K/AKT/eNOS-dependent mechanism. *Hypertension*. **2019**. 73: 449–457.

[9] Lammi C., Aiello G., Boschin G., Arnoldi A. Multifunctional peptides for the prevention of cardiovascular disease: A newconcept in the area of bioactive food-derived peptides, *J. Func. Foods*. **2019**. 55: 135–145.

[10] Chakrabarti S., Wu J.P. Milk-derived tripeptides IPP (Ile-Pro-Pro) and VPP (Val-Pro-Pro) promote adipocyte differentiation and inhibit inflammation in 3T3-F442A cells. *PLoS One.* **2015**. 10: 0117492.

[11] Matsui T., Sato M., Tanaka M., Yamada Y., Watanabe S., Fujimoto Y., Imaizumi K., Matsumoto K. Vasodilating dipeptide Trp-His can prevent atherosclerosis in apo E-deficient mice. *Br. J. Nutr*. **2010**. 103: 309–313.

[12] Beger R.D., Dunn W., Schmidt M.A., Gross S.S., Kirwan J.A., Cascante M., Brennan L., Wishart D.S., Oresic M., Hankemeier T., Broadhurst D.I., Lane A.N., Suhre K., Kastenmüller G., Sumner S.J., Thiele I., Fiehn O., Kaddurah-Daouk R., for "Precision Medicine and Pharmacometabolomics Task Group"-Metabolomics Society Initiative., Metabolomics enables precision medicine: "A White Paper, Community Perspective", *Metabolomics*. **2016**, 12: 149.

[13] Cajka T., Fiehn O. Toward Merging Untargeted and Targeted Methods in Mass Spectrometry-Based Metabolomics and Lipidomics. *Anal. Chem*. **2016**. 88: 524–545.

[14] Brown S.C., Kruppa G., Dasseu J.L. Metabolomics applications of FT-ICR mass spectrometry. *Mass Spectrom. Rev*. **2005**. 24: 223–231.

[15] Gil-de-la-Fuente A., Godzien J., Saugar S., Garcia-Carmona R., Badran H., Wishart D.S., Barbas C., Otero A. CEU mass mediator 3.0: a metabolite annotation tool. *J. Proteome Res.* **2019**. 18: 797–802.

[16] Khaselev N., Murphy R.C. Electrospray ionization mass spectrometry of lysoglycerophosphocholine lipid subclasses. J. *Am. Soc. Mass. Spectrum*. **2000**. 11: 283–291.

[17] Godzien J., Ciborowski M., PazMartínez-Alcazar M., Samczuk P., Kretowski A., Barbas C. Rapid and reliable identification of phospholipids for untargeted metabolomics with LC−ESI−QTOF−MS/MS. *J. Proteome Res*. **2015**. 14: 3204–3216.

[18] Masood M.A., Yuan C., Acharya J.K., Veenstra T.D., Blonder J. Quantitation of ceramide phosphorylethanolamines containing saturated and unsaturated sphingoid base cores. *Anal. Biochem*. **2010**. 400: 259–269.

[19] Chen Y., Wen S., Jiang M., Zhu Y., Ding L., Shi H., Dong P., Yang J., Yang Y. Atherosclerotic dyslipidemia revealed by plasma lipidomics on ApoE$^{-/-}$ mice fed a high-fat diet. *Atherosclerosis*. **2017**. 262: 78–86.

[20] Dang V.T., Huang A., Zhong L.H., Shi Y., Werstuck G.H. Comprehensive Plasma Metabolomic Analyses of Atherosclerotic Progression Reveal Alterations in Glycerophospholipid and Sphingolipid Metabolism in Apolipoprotein E-deficient Mice. *Sci. Rep*. **2016**. 6: 35037.

[21] Barber M.N., Risis S., Yang C., Meikle P.J., Staples M., Febbraio M.A., Bruce C.R. Plasma Lysophosphatidylcholine Levels Are Reduced in Obesity and Type 2 Diabetes. *PLoS One.* **2012**. 7: 41456.

[22] Moore K., Sheedy F., Fisher E. Macrophages in atherosclerosis: a dynamic balance. *Nat. Rev. Immunol*. **2013**. 13: 709–721.

[23] Moore K.J., Tabas I. Macrophages in the pathogenesis of atherosclerosis. *Cell.* **2011**. 145: 341–355.

[24] González-Riano C., Dudzik D., Garcia A., Gil-de-la-Fuente A., Gradilla A., J Godzien., López-Gonzálvez Á., Rey-Stolle F., Rojo D., Ruperez F.J., Saiz J., Barbas C. Recent developments along the analytical process for metabolomics workflows. *Anal. Chem*. **2020**. 92: 203–226.

[25] Park T.S., Panek R.L., Bak Mueller S., Hanselman J.C., Rosebury W.S., Robertson A.W., Kindt E.K., Homan R., Karathanasis S.K., Rekhter M.D. Inhibition of sphingomyelin synthesis reduces atherogenesis in apolipoprotein E-knockout mice. *Circulation*. **2004**. 110: 3465–3471.

[26] Sigruener A., Kleber M.E., Heimerl S., Liebisch G., Schmitz G., Maerz W. Glycerophospholipid and Sphingolipid Species and Mortality: The Ludwigshafen Risk and Cardiovascular Health (LURIC) Study. *PLoS One*. **2014**. 9: 85724.

[27] Kim H.J., Kim J.H., Noh S., Hur H.J., Sung M.J., Hwang J.-T., Park J.H., Yang H.J., Kim M.S., Kwon D.Y., Yoon S.H. Metabolomic analysis of Livers and Serum from High-Fat Diet Induced Obese Mice. *J. Prot. Res.* **2011**. 10: 722–731.

[28] Eisinger K., Liebisch G., Schmitz G., Aslanidis C., Krautbauer S., Buechler C. Lipidomic Analysis of Serum from High Fat Diet Induced Obese Mice. *Int. J. Mol. Sci*. **2014**. 15: 2991–3002.

[29] Satapati S., Sunny N.E., Kucejova B., Fu X., Teng He T., Méndez-Lucas A., Shelton J.M., Perales J.C., Browning J.D., Burgess S.C. Elevated TCA cycle function in the pathology of diet-induced hepatic insulin resistance and fatty liver. *J. Lipid Res*. **2012**. 53: 1080–1092.

[30] Yamashita A., Zhao Y., Matsuura Y., Yamasaki K., Moriguchi-Goto S., Sugita C., Iwakiri T., Okuyama N., Koshimoto C., Kawai K., Tamaki N., Zhao S., Kuge Y., Asada Y.

Increased metabolite levels of Glycolysis and pentose phosphate pathway in rabbit atherosclerotic arteries and hypoxic macrophage. *PLoS One*. **2014**. 9: e86426.

[31] Roma O., Grajeda-Iglesiasa C., Najjara M., Abu-Saleh N., Volkova N., Esther Dar D., Hayek T., Aviram M. Atherogenicity of amino acids in the lipid-laden macrophage model system in vitro and in atherosclerotic mice: a key role for triglyceride metabolism. J. *Nutr. Biochem*. **2017**. 45: 24–38.

[32] Würtz P., Raiko J.R., Magnussen C.G., Soininen P., Kangas A.J., Tynkkynen T., Thomson R., Laatikainen R., Savolainen M.J., Laurikka J., Kuukasjärvi P., Tarkka M., Karhunen P.J., Jula A., Viikari J.S., Kähönen M., Lehtimäki T., Juonala M., Ala-Korpela M., Raitakari O.T. High-throughput quantification of circulating metabolites improves prediction of subclinical atherosclerosis. *Eur. Heart J.* **2012**. 33: 2307–2316.

[33] Taki K., Tsuruta Y., Niwa T. Indoxyl Sulfate and Atherosclerotic Risk Factors in Hemodialysis Patients. *Am. J. Nephrol*. **2007**. 27: 30–35.

[34] Matyash V., Liebisch G., Kurzchalia T.V., Shevchenko A., Schwudke D.J. Lipid Extraction by Methyl-Tert-Butyl Ether for High-Throughput Lipidomics. *J. Lipid Res.* **2008**. 49: 1137–1146.

[35] Sumner L.W., A. Amberg A., Barrett D., Beale M.H., Beger R., Daykin C.A., Fan T.W.M., Fiehn O., Goodacre R., Griffin J.L., Hankemeier T., Hardy N., Harnly J., Higashi R., Kopka J., Lane A.N., Lindon J.C., Marriott P., Nicholls A.W., Reily M.D., Thaden J.J., Viant M.R. Proposed minimum reporting standards for chemical analysis Chemical Analysis Working Group (CAWG) metabolomics standards initiative (MSI). *Metabolomics*. **2007**. 3: 211–221.

CHAPTER IV

Dysregulated endocannabinoid pathway and its role in AP-4 deficiency syndrome

Abstract

Adaptor protein (AP-4) is implicated in intracellular vesicle trafficking of cargo proteins. AP-4 is an heterotetrametric complex and alterations in one of the four subunits cause a severe form of childhood hereditary spastic paraplegia, named AP-4 deficiency syndrome. This is a neurodegenerative disease characterized by intellectual disability, spasticity and axonal growth defects. Spatial proteomic studies highlighted that the diacylglycerol lipase beta (DAGLB) was a possible candidate as a novel AP-4 cargo protein. DAGLB plays a key role in the generation of the 2-arachidonoylglycerol (2-AG), an endocannabinoid responsible of the correct axonal growth. An untargeted lipidomics approach to monitor endocannabinoid levels in brain of AP-4 deficient mice and to elucidate any further dysregulated lipid subclasses was applied. Our study revealed a reduction of 2-AG abundance in *Ap4e1* mice supporting the hypothesis of DAGLB as a novel AP-4 cargo protein.

4.1. Introduction

Hereditary spastic paraplegias (HSP) are a group of diversified neurodegenerative disorders. They are classified, according to the phenotype and to the involved altered genes, into “pure HSPs” or “complex HSPs” [1].

The "pure forms" are characterized by neurologic impairment limited to progressive lower extremely spastic weakness and urinary disfunctions. Patients affected by "complex HSPs" suffer of additional symptoms, such as: intellectual disability, dementia, ataxia and extrapyramidal signs. HSPs can be manifested due to mutations in more than 40 genes [2]. In this context, mutations in one of the four genes encoding the subunits (*AP4B1, AP4E1, AP4M1*, *AP4S1*) cause a severe and rare neurodegenerative disorder, defined as AP-4 deficiency syndrome [3]. AP-4 belongs to the family of adaptor proteins, and it localizes at trans-Golgi network, where it is involved in trafficking of cargo proteins [4]. Alterations in the subunits of the heterotetrametric complex AP-4 lead to an autosomal-recessive pathology with the onset of symptomatology in childhood, distinguished by spastic tetraplegia, intellectual disability, foot deformities, seizures. In addition, brain imaging show thinning of *corpum callosum*, delayed myelinization and ventriculomegaly [5]. Furthermore, in knockout mice for the gene *Ap4e1* have been documented defective axons [6] and a dysregulated autophagy [7].

The role and functions of AP-4 are still poorly clarified due to its scarce abundance [8] and, consequently, the physio-pathogenesis of the related disease is not yet well defined. Davies et al [9], through a spatial proteomic method called dynamic organellar map, recently identified, in AP-4 deficient cells, ATG9A as a novel AP-4 cargo protein responsible for the dysregulated autophagy. Then, with a more sensitive exploratory analysis of the obtained data, an additional hit, named DAGLB (diacylglycerol lipase-beta), has been proposed as a potential novel cargo protein of AP-4 vesicles. DAGLB is a key enzyme for generation of 2-arachidonoylglycerol (2-AG) [10], the most abundant endocannabinoid in brain [11]. In developing neurons, an unknown pathway targets DAGLB to the distal axon, where 2-AG is required to promote axonal growth and guidance [12,13].

Considering the low levels of endocannabinoids in biological samples, liquid chromatography coupled to mass spectrometers has become the method of choice for monitoring their potential dysregulation in neurodegenerative disease [14]. Here, to prove AP-4's involvement in DAGLB transport, a nano liquid chromatography ion mobility mass spectrometry (nLC x IMS) strategy was employed to monitor the brain levels of 2-AG, arachidonic acid (AA), and stearoyl-sn-arachidanoyl-glycerol (SAG) and to investigate other possible lipidome perturbations in *Ap4e1* deficient mice.

4.2. Aim of the work

The study aimed to investigate and confirm the possible involvment of AP-4 complex in the transport of the Diacylglycerol lipase-beta. To this end, in a context of an untargeted lipidomic profiling, the brain levels of three endocannabinoids in *Ap4e1* knock-out and wild-type mice were monitored.

4.3. Results

4.3.1. Analytical method

The lipidomic profiling was performed employing a platform based on nano-LC-TIMS-qTOF instrument, working with PASEF (parallel accumulation serial fragmentation) technology to increase the number of selected precursors for MS/MS fragmentation. The adopted system let us to increase the confidence of each annotated compound, considering that every lipid is extracted from four-dimensional data space (retention time, ion-mobility, m/z, MS/MS). The study was conducted with a quality control (QC) strategy to assess system stability and repeatability. QCs were analyzed at the beginning, in the middle and at the end the batch. The reported lipids had coefficient of variation (CV %) among QCs lower than 35%, as can be appreciated from their great clustering in the PLS-DA score plot (**figure 4.1 A**). Furthermore, the final 585 lipids (**supporting information table S3.1**) were present at least in the in 75% of analyzed

subgroups (Wild-type, WT; *Ap4e1* knock-out, KO). The identified lipids belong to 24 different lipid subclasses, emphasizing the broad coverage of the entire lipid profile (**figure 4.1 B**): Fatty Acid (FA), Diradylglycerols (DG), Triradylglycerols (TG), Phosphatidylcholines (PC), Phosphatidylethanolamines (PE), Phosphatidylglycerols (PG), Phosphatidylinositols (PI), Phosphatidylserines (PS), Lysophosphatidylcholines (LPC), Ceramides (Cer), Neutral glycosphingolipids (HexCer), Sphingomyelins (SM), Cholesteryl esters (CE), Fatty Acid (FA), Lysophosphatidylethanolamines (LPE), Lysophosphatidylinositols (LPI), Lysophosphatidylglycerols (LPG), Lysophosphatidylserines (LPS), Ether-linked phosphatidylcholines (PC-O), Ether-linked phosphatidylethanolamines (PE-O), Ether-linked phosphatidilglycerols (PG-O), Sulfatides (SHexCer), Oxidized sulfatides (ShexCer-O), Bismonoacylglycerophosphate (BMP).

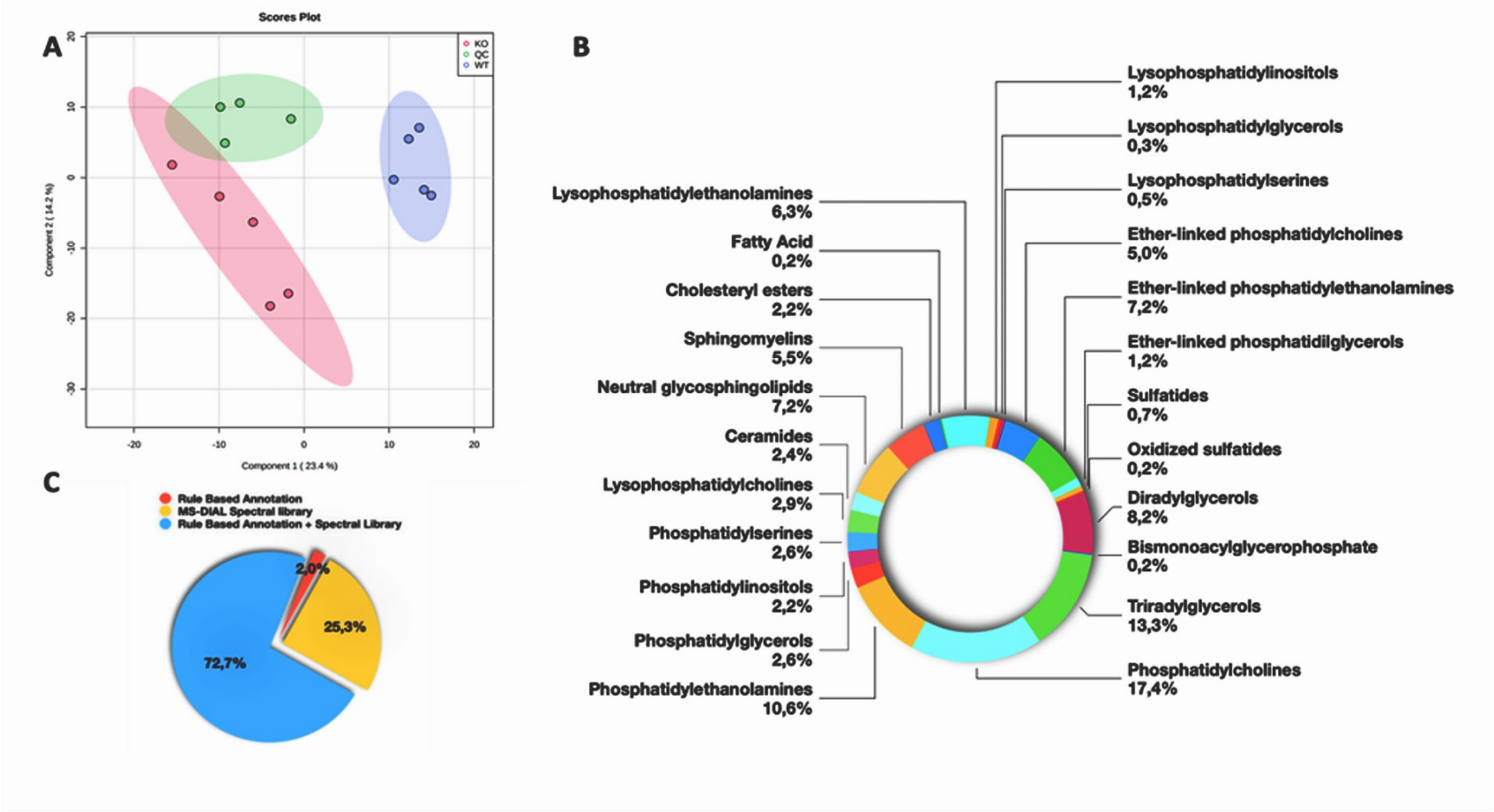

Figure 4.1. *(**A**) PLS-DA score plot showing discrimination among Ap4e1 knock-out group (red), wild-type animals (blue) and quality controls (green); (**B**) Subclass classification of the putative identified compounds in the brain lipidome extract; (**C**) Distribution of identified lipids between employed spectral libraries.*

Noteworthy, almost the 73 % of the identified lipids were annotated by both the libraries that we employed (**figure 4.1 C**). Data analysis showed high accuracy and precision (**figure 4.2**).

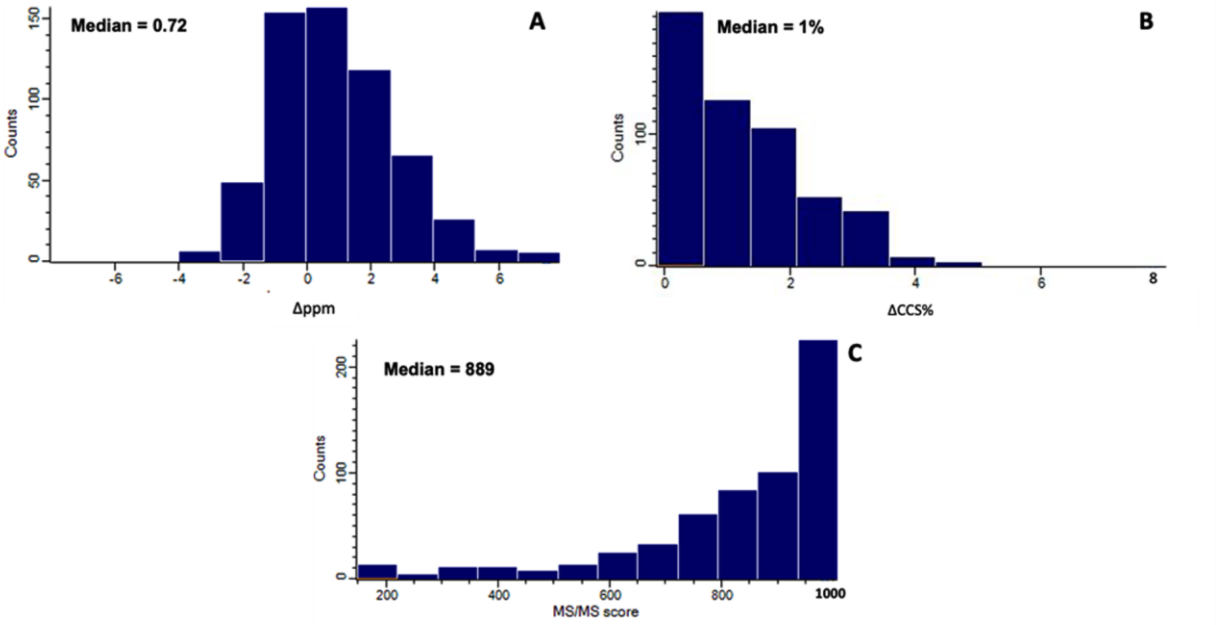

Figure 4.2. *Frequency distribution of ppm error (**A**), ΔCCS error (**B**) and MS/MS score (**C**) of the identified lipids. Median values are reported.*

4.3.2. Endocannabinoid pathway analysis

To evaluate the involvement of the AP-4 complex in the transport of DAGLB we used a RP-LC-TIMS approach to monitor the brain levels of 2-AG, AA, and their precursor SAG. To this end, we employed a deuterated compound (2-AG-d8, SAG-d8, AA-d8) for each endocannabinoid under study. The internal standards were spiked to the tissues prior to homogenization allowing in this way to correct the results for any sample losses and to further facilitate their

identification. The analysis revealed an approximately 30% reduction in 2-AG and 20% reduction in AA in the AP-4-deficient mice (**figure 4.3**), but no significant difference in the levels of 1-stearoyl-2- arachidonoyl-sn-glycerol.

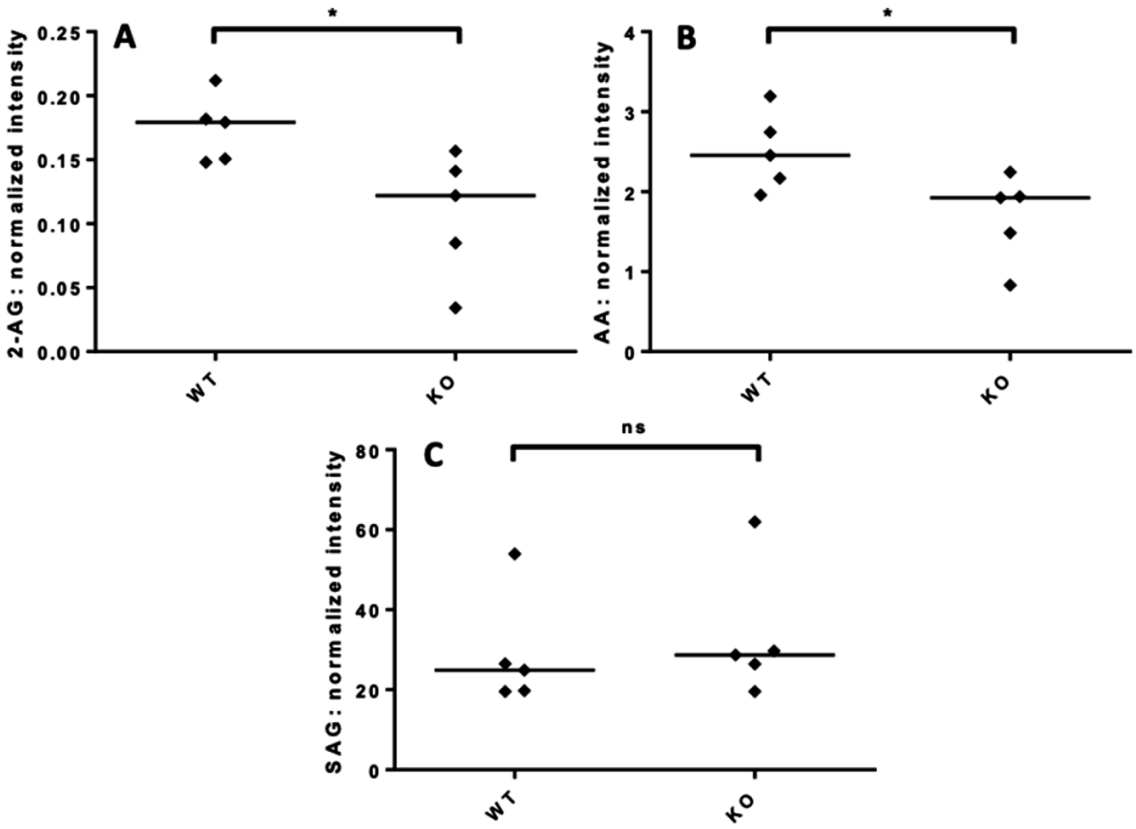

Figure 4.3. *Relative quantification of (**A**) 2-AG, (**B**) AA and (**C**) SAG, from WT and KO mouse brains (5 animals per group; horizontal bar indicates median). Data were subjected to a two-tailed Mann-Whitney U-test: *$p \leq 0.05$; ns $p > 0.05$.*

4.3.3. Brain lipidome profiling

As shown in **figure 4.4** the principal component analysis built on lipids showed a clear separation between the two groups, the first and the second component explain, respectively, the 35.8% and the 14.4% of the variance.

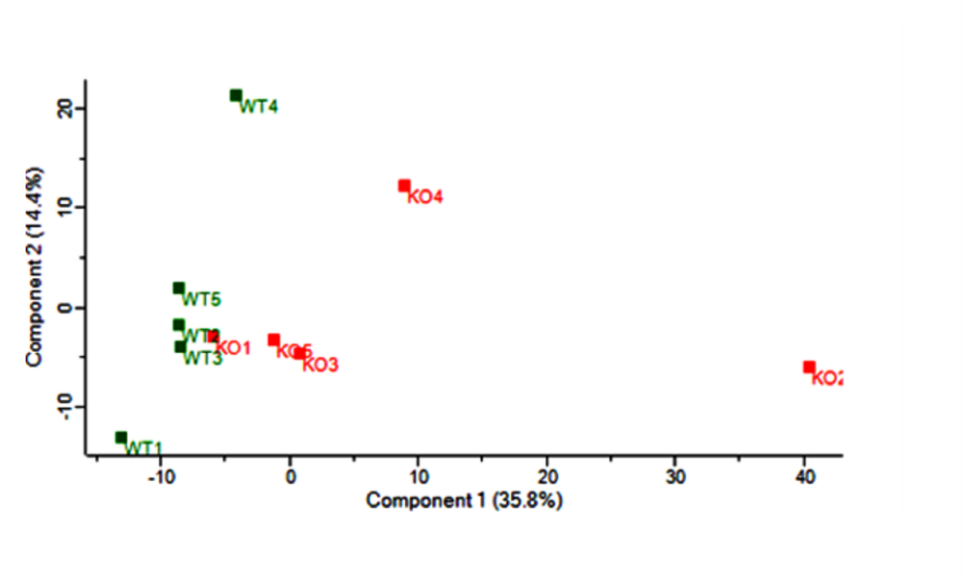

Figure 4.4. *PCA 2D score plots built on lipids showing the discrimination between WT (green) and KO (red).*

The statistical analysis revealed 96 lipids with a *p*-value <0.05 (**supporting information figure S4.1**, **supporting information table S3.2**). Subsequently, three different methods (Variable importance in projections; VIP, Significant analysis of metabolomics; SAM, and volcano plot) were employed to reduce the number of significant dysregulated lipids in the comparison between *Ap4e1* knock-out and wild-type mice and to put in evidence the most affected lipid subclasses. The molecules statistically significant and in common among the statistical tests are summarized in **table 4.1**. Hexosylceramide's metabolism was the most perturbated, with a 43.0 % decrease in KO group, while cholesteryl ester subclass was the only increased (39.4 %) in the AP-4 deficient mice (**figure 4.5**).

Table 4.1. *Significant lipids according to the statistical tests adopted.*

Compound	Lipid main class	VIP Score	raw pvalue (Volcano Plot)	dvalue (SAM)
BMP 42:10	Glycerophosphoglycerol	2.0598	0.00017214	6.5846
DG 41:1	Diradylglycerol	2.0862	$9.3214\ e^{-05}$	7.1916
DG 42:1	Diradylglycerol	2.0916	$8.1252\ e^{-05}$	7.3331
DG O-36:6	Diradylglycerol	1.7968	0.0053023	3.7913
HexCer 18:1;2O/20:0	Neutral glycophingolipid	1.8282	0.0040284	3.9859
HexCer 18:1;2O/22:0	Neutral glycophingolipid	1.8136	0.0045893	3.8931
HexCer 18:1;2O/24:0	Neutral glycophingolipid	1.9263	0.0014421	4.7517
HexCer 18:1;2O/24:0;O	Neutral glycophingolipid	1.7721	0.0064878	3.6507
HexCer 18:1;2O/25:0;O	Neutral glycophingolipid	1.7759	0.0062974	3.6713
HexCer 18:1;2O/26:0	Neutral glycophingolipid	2.0282	0.00032057	6.0079
HexCer 18:1;2O/38:2;O	Neutral glycophingolipid	1.7544	0.0074481	3.5556
HexCer 20:2;2O/26:0;O	Neutral glycophingolipid	1.9848	0.00065606	5.3871
LPC 24:0	Glycerophosphocoline	1.8399	0.0036173	4.0632
LPC 24:1	Glycerophosphocoline	1.7916	0.0055402	3.7605
PG 34:2/BMP 34:2*	Glycerophosphoglycerol	1.7423	0.0081596	3.4932
PG 39:5 /BMP 39:5*	Glycerophosphoglycerol	1.8221	0.0042597	3.946
PG 40:7 /BMP 40:7*	Glycerophosphoglycerol	1.7606	0.0071026	3.5882
SM 38:1	Phosphosphingolipid	1.9007	0.0019427	4.5228

*Not resolved identification

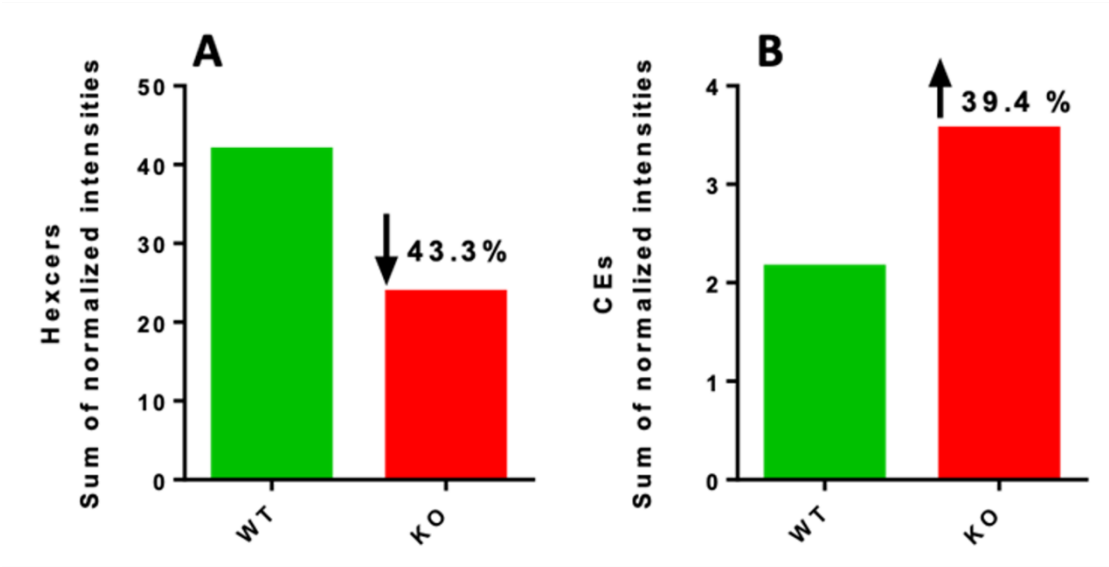

Figure 4.5. *Summed signal intensities for monitored sphingolipids (**A**) and cholesteryl esters (**B**), (WT, green; KO, red).*

Statistically significant lipids responsible for maximum separation between groups in PLS-DA were extracted through VIP scores (**figure 4.6 C, supporting information table S3.3**). The built model showed good quality of class discrimination parameters R^2= 0.99931, Q^2= 0.68967 and the analysis revealed 76 lipids with a VIP score greater than 1.5. Volcano plots were performed with fold change (FC) 2 and p-value of <0.01 (**figure 4.6 A, supporting information table S3.5)**. The results highlighted 3 up-regulated (2 cholesteryl esters and 1 phosphatidylcholines) and 18 down-regulated lipids (3 diradylglycerols, 4 glycerophosphoglycerols, 8 neutral glycosphingolipids, 1 phosphosphingolipid and 2 phosphatidylcholines) in the knock-out group when compared to WT animals. Then, in order to reinforce the obtained data, SAM analysis with a restrictive false discovery rate (FDR) of 0.047 was conducted, revealing 45 lipids all down regulated in KO subgroup (**figure 4.6 B, supporting information table S3.6)**.

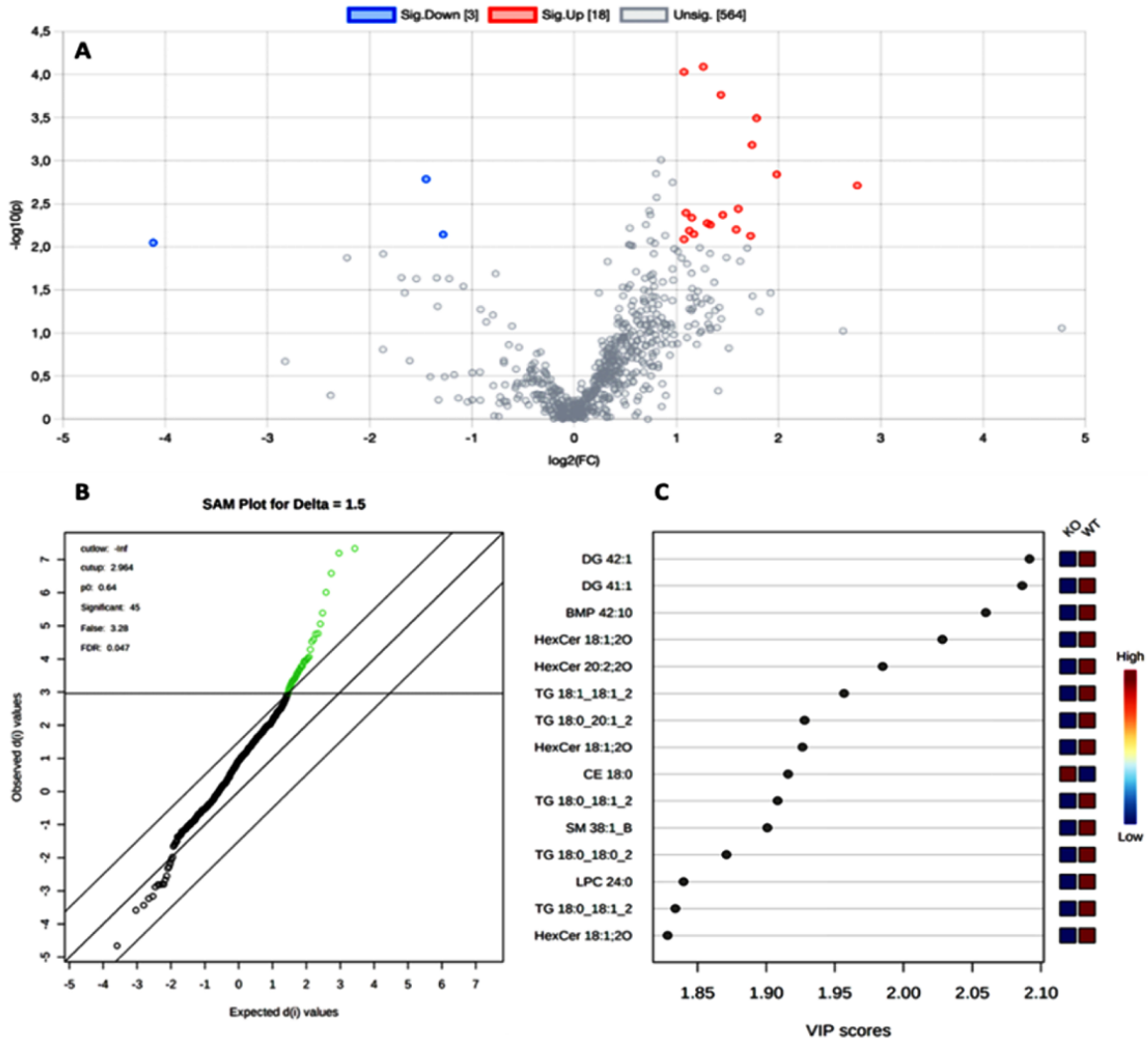

Figure 4.6. *(**A**) Volcano plot of final dataset. The data for all lipids are shown as log2 fold change versus the -log10 of pvalue. Blue dots, red dots and grey dots indicate, respectively, down-regulated, up-regulated and statistically not significant lipids in the direction comparison (WT/KO); (**B**) SAM plot graph indicating statistically significant lipids with green dots; (**C**) VIP scores plot displays the best 15 lipids identified by PLS-DA. The colored boxed on the right indicate the relative abundance in the group.*

Furthermore, we also observed a reduction (**supplementary figure S3.2**) in the *Ap4e1* knock-out brain levels of most of the lipids containing the arachidonic acid chain in their structure, except for LPC 20:4 and DG 20:4_20:4.

4.4. Discussion

DAGLB is a key enzyme for generation of the endocannabinoid 2-AG, which is an important signalling lipid in the central nervous system. The major pathway for 2-AG biosynthesis is hydrolysis of diacylglycerol (DAG) at the *sn1* position by DAG lipase [12]. DAGLs are required for diverse aspects of brain function, including axonal growth during development, neurogenesis in the adult brain and retrograde synaptic signalling [15]. These functions require not only temporal control of DAGL expression, but also tight regulation of DAGL subcellular localisation. Downstream of DAGL activity, 2-AG is hydrolysed by monoacylglycerol lipase (MGLL) to produce arachidonic acid [16]. Thus, DAGL activity controls the levels of both 2-AG and AA, and both lipids decrease in parallel in the brains of *Ap4e1* knockout mice. Based on this model of the 2-AG pathway, we hypothesised that the missorting of DAGLB in AP-4 deficiency may lead to impaired DAGL activity, and hence to reduce levels of 2-AG and AA in the brain. To test this hypothesis, in this study we used a lipidomic approach as a tool to reveal dysregulated lipid classes and to compare endocannabinoids levels in brains of wild-type and *Ap4e1* knock-out mice. In confirmation of our hypothesis the mass spectrometry analysis revealed a reduction in 2-AG and AA brain levels in the AP-4-deficient mice, but no significant difference in the level of the major substrate of DAGLB, SAG [17]. Thus, our data support that DAGLB missorting in AP-4-deficient neurons leads to impaired DAGL activity and dysregulated endocannabinoid signalling.

Furthermore, analysis of sphingolipids showed an overall decrease in the levels of hexosylceramides in AP-4 deficient mice. Alteration of sphingolipids pathway have been associated

with hereditary spastic paraplegias phenotype [18]. Noteworthy, a decreased level of hexcers have been positively correlated with a reduced axonal growth and the inability of neurons to form axonal branches [19]. The untargeted approach also revealed an overall increase of cholesteryl esters, lipids involved in the transport and storage of cholesterol. Alterations in CEs have been documented in many neurological disorders, such as: Huntington disease, multiple sclerosis [20,21] and in brain lesions that involves the breakdown of myelin [22].

Integrations of omics sciences, such as lipidomics and proteomics, is confirmed as a priceless survey instrument to broaden the knowledge of the complex mechanism that are among the causes of serious diseases, such as HSPs, and thus to propose possible new pharmacological hits and targets.

4.5. Methods and material

4.5.1. Animal model

All animal procedures were conducted at the University of Cambridge, Cambridge Institute for Medical Research, in accordance with the UK Animals (Scientific Procedures) Act of 1986 and under the authority of the project licence PPL7008339 held by Prof. Margaret Robinson. *Ap4e1* knockout mice (C57Bl/6N-Ap4e1[tm1b{KOMP}Wtsi]), generated using the knockout-first tm1b allele system [23], were obtained via the European Mouse Mutant Archive (EMMA; strain EM:09451) from Helmholtz Zentrum München Deutsches Forschungszentrum für Gesundheit und Umwelt (GmbH). The brain samples used in this study were taken at 6 months (range 178-197 days). The WT group consisted of 4 females and 1 male; the KO group consisted of 3 females and 2 males.

4.5.2. Lipid extraction

Brains used for lipid analyses were removed from animals and placed immediately into ice-cold PBS, before being snap frozen in liquid nitrogen. Frozen brain samples were then stored

at -80°C, until the time of lipid extraction. Lipids were extracted with a generic methanol-chloroform-based protocol. Brains from five wild-type (WT) and five *Ap4e1* knockout (KO) mice were weighed and quickly transferred (within seconds and without thawing) to a homogenizer containing 16 mL of cold Chloroform:Methanol:Water ($CHCl_3$:MeOH:H_2O, 2:1:1 v:v:v) doped with the following internal standards: 2-Arachidonoyl-Glycerol-d8 (2-AG-d8), 1-Stearoyl-2-Arachidonoyl-sn-Glycerol-d8 (SAG-d8), Arachidonic Acid-d8 (AA-d8), all purchased from Cayman Chemical (USA), C17 Ceramide (d18:1/17:0) and a mixture of deuterated internal standards (Splash Lipidomix®) purchased from Avanti Polar Lipids (Alabaster, AL, U.S.A). Brain homogenates were then vortexed and centrifuged at 2000 rpm, at 4 °C, for 5 min in order to separate the organic fraction. The bottom phase (organic) was collected and the upper phase was re-extracted with 4 mL $CHCl_3$ containing 40 µL formic acid and centrifuged as described above. The bottom phase (organic) was collected again and both organic phases were combined, vortexed and 250 µL were dried. Finally, dried extracts were resuspended in 250 µL 1-butanol:iso-propanol:water (BuOH-IPA-H_2O, 8:23:69 v:v:v) and directly measured.

4.5.3. Lipid measurements by nanoLC-timsTOF Pro mass spectrometry

For measurements of lipids by liquid chromatography coupled to mass spectrometry (LC-MS), a setup of nanoLC chromatography coupled with ion mobility mass spectrometry was used, as described by Vasilopoulou et al [24]. Briefly, an Easy-nLC 1200 (Thermo Fisher Scientific) ultra-high pressure nanoflow chromatography system was used to separate lipids on an in-house reversed-phase column (20 cm × 75 µm i.d.) with a pulled emitter tip, packed with 1.9 µm C18 material (Dr. Maisch, Ammerbuch-Entringen, Germany). The column compartment was heated to 60 °C, the mobile phases A and B were acetonitrile:water (ACN/H_2O 60:40 v:v) and isopropanol:acetonitrile (IPA/ACN 90:10 v:v), both buffered with 0.1% formic acid and 10 mM ammonium formate. The mobile flow was set to 400 nL min^{-1} and lipids were separeted

with the following gradient: 0 – 3 min, 1-30 %B; 3 – 4 min, 30-51 %B; 4 – 9 min, 51-61 %B; 9 – 14 min, 61-71 %B; 14 – 19 min, 71-99 %B; 19 – 24 min, isocratic at 99 %B; 24 – 25 min, returnig to 1 %B and finally 3 min to re-equilibrate the column. The global LC runtime was 40 min, including time for refilling LC pumps and sample loading. The nanoLC was coupled to a hybrid trapped ion mobility-quadrupole time-of-flight mass spectrometer (timsTOF Pro, Bruker Daltonics, Bremen, Germany) via a modified nanoelectrospray ion source (Captive Spray, Bruker Daltonics). Electrosprayed ions enter the first vacuum stage where they are deflected by 90° and accumulated in the front part of a dual TIMS analyser. The instrument was operated with the PASEF method activated in both positive and negative ionization modes. The analysis were acquired in the following m/z and ion-mobility range: 50-1550 m/z and 0.60-1.95 Vs/cm^2, respectively. The accumulation and the ramp time were both set to 100ms. Precursors were fragmented with an ion-mobility dependent collision energy, which increased from 25 to 45 eV in the positive mode and from 35 to 55 eV in negative mode. One full TIMS-MS scan and three PASEF MS/MS scans were performed with an acquisition cycle of 0.4 s. The TIMS ion charge control (ICC) was set to 7.5 Mio. Both the TOF and the TIMS dimensions were calibrated linearly using four selected ions from the Agilent ESI LC/MS tuning mix [m/z, 1/K0: (322.0481, 0.7318 Vs cm^{-2}), (622.0289, 0.9848 Vs cm^{-2}), (922.0097, 1.1895 Vs cm^{-2}), (1221,9906, 1.3820 Vs cm^{-2})] in positive mode and [m/z, 1/K0: (666.01879, 1.0371 Vs cm^{-2}), (965.9996, 1.2255 Vs cm^{-2}), (1265.9809, 1.3785 Vs cm^{-2})] in negative mode. Each sample was injected in triplicate (injection volume 1 µL in positive and 2 µL in negative mode), in a randomized order, while blanks were scheduled after the triplicate injection of each sample. A quality control (QC) strategy was employed to monitor instrument performance.

4.6.4. Lipid data analysis

Processing and analysis of the raw files was performed with MetaboScape 2021 version (Bruker Daltonics, Germany), which contains a feature finding algorithm (T-ReX 4D). This latter automatically extracts data from the four-dimensional space (m/z, retention time, ion mobility and intensity) and assigns MS/MS spectra to them. Precursor ion masses were recalibrated with the lock masses m/z 622.028960 (positive mode) and m/z 666.019887 (negative mode) while the ion mobility dimension was recalibrated using the Tuning Mix ions, as above. Feature detection was performed using an intensity threshold of 3000 counts in positive mode and 1000 counts in the negative mode. The minimum number of data points in the 4D TIMS space was set to 100, or 50 when using recursive feature extraction. Lipid annotation was performed with both a rule-based annotation and the LipidBlast spectral library of MS DIAL (http://prime.psc.riken.jp/compms/msdial/main.html), setting the following parameters: tolerance: narrow 2 ppm, wide 10 ppm; mSigma: narrow 30, wide 250, MS/MS score: narrow 800, wide 150. CCS%: narrow 2, wide 5. The successive adduct ions were searched in positive mode: $[M+H]^+$, $[M+Na]^+$, and $[M+NH_4]^+$; instead in negative mode: $[M–H]^–$, $[M+Cl]^–$, $[M+HCOO]^–$. All the annotated lipids were manually investigated and filtered according to: peak shape, MS/MS spectrum, linearity of Retention time VS Total carbons number and m/z VS CCS values within lipid subclass and total double bonds number. Considering the MS/MS spectra information on the fatty acyl-chain composition, we reported lipids using the following nomenclature: a short name, e.g., DG 34:0, or a long name, e.g., DG 18:1_18:1. Structural isomers are labeled as A or B.

4.6.5. Lipid statistical analysis

The raw values of lipid species of 2-AG, SAG and AA were normalized based on the intensity of the corresponding internal standard and the wet tissue weight. Finally, mean values from

the triplicate injections were used for statistical analysis. Statistical analyses were performed in GraphPad Prism version 8.4.1 for Windows. Data were analyzed using a two-tailed Mann-Whitney *U*-test. Before performing statistical analysis for the untargeted lipidomic considerations, all the lipids with a coefficient of variation (CV %) greater than 35 % among QC and missing more than 75 % in real samples were discarded. Each lipid was normalized based on the intensity of the internal standard belonging to the same lipid subclass and the obtained dataset was log-tranformed and auto-scaled. Statistical analysis was performed with Metaboanalyst 5.0 (https://www.metaboanalyst.ca) and Perseus (v1.6.0.8). Both unsupervised principal component analysis (PCA) and supervised partial least squares discriminant analysis (PLS-DA) were employed to visualize discrimination in the acquired dataset. Variable importance in projection (VIP) scores, based on PLS-DA results, Significance analysis of Metabolomics (SAM), giving a delta value of 1.5, and univariate Volcano plots analysis were used to identify lipids responsible for the maximum separation of the groups.

4.6. Conclusions

In conclusion, we have identified an important role for AP-4 in transport of DAGLB providing a missing link in understanding the spatial regulation of endocannabinoid signalling. Our findings open up a new direction for the pathomechanisms of AP-4 deficiency syndrome: aberrant spatial control of 2-AG synthesis leading to developmental defects in axon formation. We suggest that the diverse neurological symptoms of AP-4-deficient patients may be in part caused by compound effects of impaired 2-AG production due to DAGLB missorting.

4.7. References

[1] Roubertie A., Hieu N., Roux C.J., Leboucq N., Manes G., Charif M., Echenne B., Goizet C., Guissart C., Meyer P., Marelli C., Rivier F., Burglen L., Horvath R., Hamel C.P., Lenaers G. AP4 deficiency: A novel form of neurodegeneration with brain iron accumulation? *Neurol Genet*. **2018**. 4 (1): e217.

[2] Kara E., Tucci A., Manzoni C., Lynch D.S., Elpidorou M., Bettencourt C., Chelban V., Manole A., Hamed S.A., Haridy N.A., Federoff M., Preza E., Hughes D., Pittman A., Jaunmuktane Z., Brandner S., Xiromerisiou G., Wiethoff S., Schottlaender L., Proukakis C., Morris H., Warner T., Bhatia K.P., Korlipara L.V., Singleton A.B., Hardy J., Wood N.W., Lewis P.A., Houlden H. Genetic and phenotypic characterization of complex hereditary spastic paraplegia. *Brain*. **2016**. 139 (Pt 7): 1904-18.

[3] Abou Jamra R., Philippe O., Raas-Rothschild A., Eck S.H., Graf E., Buchert R., Borck G., Ekici A., Brockschmidt F.F., Nöthen M.M., Munnich A., Strom T.M., Reis A., Colleaux L. Adaptor protein complex 4 deficiency causes severe autosomal-recessive intellectual disability, progressive spastic paraplegia, shy character, and short stature. *Am J Hum Genet***. 2011.** *88* (6): 788–795.

[4] Abdollahpour H., Alawi M., Kortüm F., Beckstette M., Seemanova E., Komárek V., Rosenberger G., Kutsche K. An AP4B1 frameshift mutation in siblings with intellectual disability and spastic tetraplegia further delineates the AP-4 deficiency syndrome. *Eur J Hum Genet*. **2015**. 23 (2): 256-9.

[5] Ebrahimi-Fakhari D., Behne R., Davies A.K., Hirst J. AP-4-Associated Hereditary Spastic Paraplegia. **2018**. In: Adam M.P., Ardinger H.H., Pagon R.A., Wallace S.E., Bean L.J.H, Gripp K.W., Mirzaa G.M., Amemiya A., editors. GeneReviews® [Internet]. Seattle (WA): University of Washington, Seattle; 1993–2021.

[6] De Pace R., Skirzewski M., Damme M., Mattera R., Mercurio J., Foster A.M., Cuitino L., Jarnik M., Hoffmann V., Morris H.D., Han T.U., Mancini G., Buonanno A., Bonifacino, J.S. Altered distribution of ATG9A and accumulation of axonal aggregates in neurons from a mouse model of AP-4 deficiency syndrome. *PLoS Genet*. **2018**.*14* (4): e1007363.

[7] Matsuda S., Miura E., Matsuda K., Kakegawa W., Kohda K., Watanabe M., Yuzaki M. Accumulation of AMPA receptors in autophagosomes in neuronal axons lacking adaptor protein AP-4. *Neuron*. **2008**. 57 (5): 730-45.

[8] Itzhak D.N., Tyanova S., Cox J., Borner G.H. Global, quantitative and dynamic mapping of protein subcellular localization. *Elife*. **2016.** 5: e16950.

[9] Davies A.K., Itzhak D.N., Edgar J.R., Archuleta T.L., Hirst J., Jackson L.P., Robinson M.S., Borner G.H.H. AP-4 vesicles contribute to spatial control of autophagy via RUSC-dependent peripheral delivery of ATG9A. *Nat Commun*. **2018**. 9 (1): 3958.

[10] Hsu K.L., Tsuboi K., Adibekian A., Pugh H., Masuda K., Cravatt B.F. DAGLβ inhibition perturbs a lipid network involved in macrophage inflammatory responses. *Nat Chem Biol*. **2012**. 8 (12): 999-1007.

[11] Shonesy B.C., Bluett R.J., Ramikie T.S., Báldi R., Hermanson D.J., Kingsley P.J., Marnett L.J., Winder D.G., Colbran R.J., Patel S. Genetic disruption of 2-arachidonoylglycerol synthesis reveals a key role for endocannabinoid signaling in anxiety modulation. *Cell Rep*. **2014.** 9 (5): 1644-1653.

[12] Bisogno T., Howell F., Williams G., Minassi A., Cascio M.G., Ligresti A., Matias I., Schiano-Moriello A., Paul P., Williams E.J., Gangadharan U., Hobbs C., Di Marzo V., Doherty P. Cloning of the first sn1-DAG lipases points to the spatial and temporal regulation of endocannabinoid signaling in the brain. *J Cell Biol*. **2003**. 163 (3): 463-8.

[13] Williams E.J., Walsh F.S., Doherty P. The FGF receptor uses the endocannabinoid signaling system to couple to an axonal growth response. *J Cell Biol*. **2003**. 160 (4): 481-6.

[14] Marchioni C., de Souza I.D., Acquaro V.R. Junior, de Souza Crippa J.A., Tumas V., Queiroz M.E.C. Recent advances in LC-MS/MS methods to determine endocannabinoids in biological samples: Application in neurodegenerative diseases. *Anal Chim Acta*. **2018**. 1044: 12-28.

[15] Oudin M.J., Gajendra S., Williams G., Hobbs C., Lalli G., DohertyP. Endocannabinoids Regulate the Migration of Subventricular Zone-Derived Neuroblasts in the Postnatal Brain. *J Neurosci*. **2011**. 31 (11): 4000-4011.

[16] Dinh T.P., Carpenter D., Leslie F.M., Freund T.F., Katona I., Sensi S.L., Kathuria S., Piomelli D. Brain monoglyceride lipase participating in endocannabinoid inactivation. *Proc Natl Acad Sci U S A*. **2002.** 99 (16): 10819-24.

[17] Ogasawara D., Deng H., Viader A., Baggelaar M.P., Breman A., den Dulk H., van den Nieuwendijk A.M., Soethoudt M., van der Wel T., Zhou J., Overkleeft H.S., Sanchez-Alavez M., Mori S., Nguyen W., Conti B., Liu X., Chen Y., Liu Q.S., Cravatt B.F., van der Stelt M. Rapid and profound rewiring of brain lipid signaling networks by acute diacylglycerol lipase inhibition. *Proc Natl Acad Sci U S A*. **2016**. 113 (1): 26-33.

[18] Darios F., Mochel F., Stevanin G. Lipids in the Physiopathology of Hereditary Spastic Paraplegias. *Front Neurosci*. **2020**. 14: 74.

[19] Schwarz A., Rapaport E., Hirschberg K., Futerman A.H. A regulatory role for sphingolipid in neuronal growth: inhibition of sphingolipid synthesis and degradation have opposite effects on axonal branching. *J Biol Chem*. **1995**. 270: 10990–8.

[20] Phillips G.R., Hancock S.E., Brown S.H.J., Jenner A.M., Kreilaus F., Newell K.A, Mitchell T.W. Cholesteryl ester levels are elevated in the caudate and putamen of Huntington's disease patients. *Sci Rep.* **2020.** 10 (1): 20314.

[21] Pitkänen A.S.L., Halonen T.O., Kilpeläinen H.O., Riekkinen P. J. Cholesterol esterase activity in cerebrospinal fluid of multiple sclerosis patients. *J. Neurol. Sci*. **1986.** 74: 45–53.

[22] Kim J.H., Ee S.M., Jittiwat J., Ong E.S., Farooqui A.A., Jenner A.M., Ong W.Y. Increased expression of acyl-coenzyme A: cholesterol acyltransferase-1 and elevated cholesteryl esters in the hippocampus after excitotoxic injury. *Neuroscience*. **2011**. 185: 125-34.

[23] Karnes W.C., Rosen B., West A.P., Koutsourakis M., Bushell W., Iyer V., Mujica A.O., Thomas M., Harrow J., Cox T., Jackson D., Severin J., Biggs P., Fu J., Nefedov M., De Jong P.J., Stewart A. F., Bradley A. A conditional knockout resource for the genome-wide study of mouse gene function. *Nature*. **2011.** *474* (7351): 337–344.

[24] Vasilopoulou C.G., Sulek K., Brunner A.D., Meitei N.S., Schweiger-Hufnagel U., Meyer S.W., Barsch A., Mann M., Meier F. Trapped ion mobility spectrometry and PASEF enable in-depth lipidomics from minimal sample amounts. *Nat. Commun*. **2020.** *11* (1): 1–11.

CHAPTER V

Pre-formed gradients for high-throughput and robust nanoflow lipidomics with trapped ion mobility and PASEF

Abstract

Lipidomics is gaining more and more space in the biomedical research. In recent years liquid chromatography-mass spectrometry has become one of the essential analytical techniques for clinical studies. To achieve a high sensitivity in order to monitor lipid species present in low abundance in biological samples, nano LC chromatography coupled with ESI ionization represents one of the most valid approaches. However, in the lipidomics landscape nano chromatography is still challenging. Here we adapted a new concept of nano liquid chromatography, namely Evosep One, to lipidomics. Its characteristic is a pre-formed gradient strategy that guarantees robustness with high flow rate (1 µL/min), if compared to nano-LC, and high-throughput with acquisition of more than 40 samples per day and most important while maintaining the nanoflow sensitivity when starting from minimum material (1 µL) of plasma. Analysis of standard compounds as well as complex plasma lipid extracts demonstrated excellent chromatographic performance with narrow peak widths across the major lipid classes and high run-to-run-reproducibility. And more important, lipids with Evosep One are bounded in a C18 solid phase material that can extend their stability over 27 hours preventing sample degradation, a challenge often faced in the lipid extracts when kept in liquid form in the typical LC's

autosampler. Injecting samples from disposable trap columns also offers faster turnaround times as compared with conventional nanoflow LC.

5.1. Introduction

Lipids play a pivotal role in the life of every organism. Indeed, they are involved in the most common life processes, such as: energy storage, molecular signalling and structural functions [1]. Given their broad spectrum of functions, lipid dysregulations have been positively correlated to many types of diseases, such as cancers, cardiovascular disorders, neurological disturbs, neurodegenerative pathologies and metabolic syndromes [2,3,4,5,6]. Identifying the highest number of lipids or providing a measure of their concentration in the studied biological systems represents one of the main goals of biomedical research in the lipidomics field. Lipid profiling is extremely challenging due to the high complexity and heterogeneity of lipid species and their investigations are usually carried out through mass spectrometry (MS) methods. There are two MS approaches that are widely used, direct infusion (DI) or liquid chromatography (LC) coupled to MS [7]. DI-MS is a high-throughput technique, which allows the profiling of a high number of samples in a short time and generates data with a reduced complexity if compared to the LC-MS platforms [8]. However, DI-MS can suffer from a poor ionization of lipid classes and of molecules in general low abundant in biological samples [9], and even more critical, at least for lipidomics, it is unable to separate isomeric or isobaric species [10]. Therefore, in many studies the choice falls on the use of LC-MS methods. There are two main strategies widely employed. HILIC (hydrophilic interaction liquid chromatography) columns separate lipids according to the polar head group, while reverse phase chromatography (RP) allows to separate the single lipids by exploiting the interactions established between the stationary phase and the fatty acids building lipids [11,12]. Furthermore, LC-MS based lipidomics is almost exclusively performed with analytical flow rates due to its throughput and robust operation. Using micro,

narrow or analytical bore LC columns [13,14] is preferred to nano-LC columns systems as they are less subject to leaks, peak broadening and emitters clogging due to the presence of salts that are usually added to lipidomics mobile phases [15]. However, higher flow rates and larger column diameters lower the electrospray efficiency and hence sensitivity. Moving to a nano-electrospray ionization (nESI) system reduces drastically the sample consumption, solvents cost and increases the efficiency [16]. To increase throughput and robustness of nanoflow separations, the Evosep One LC system elutes samples from disposable trap columns and embeds the analytes in a pre-formed gradient, which is then pushed through the separation column with a single high-pressure pump [17]. Here, we adapted this system to the specific challenges of lipidomics and evaluated its performance in combination with trapped ion mobility spectrometry (TIMS) and deep MS/MS analysis in single runs by parallel accumulation – serial fragmentation (PASEF) [18].

5.2. Aim of the work

In the present study we aimed to develop and establish an innovative nano-LC system for untargeted lipidomic analysis. This work is settled to offer a valid alternative to the classic nano-liquid chromatography systems able to overcome the most common lipidomics challenges and to provide a high-throughput and sensitive platform for biomedical research in the lipidomics landscape.

5.3. Results

5.3.1. Evosep One Method Validation

The core of the Evosep One system is based on four low-pressure pumps (A, B, C, D), a single high-pressure pump (HP), a storage loop and disposable trap columns, namely Evotips (**supplementary figure S4.1**). Lipids extracts, once loaded on the Evotips, are eluted with a gradient generated by pumps A and B; the latter is subsequently diluted by the mobile flow

pumped by C and D. At this point, this off-set gradient, containing the analytes, is stored inside a storage loop (ID 100 µm, 30 µL) and then pushed into the column by a single high-pressure pump facilitating peak focusing and thus symmetric and sharp peaks. The chromatographic separation is carried out on a C18 column with the following geometry: 8 cm × 150 µm ID × 1.5 µm. We started from a classical nano-LC method of 30 min with 12 minutes of overhead time until to get a final method that allowed the complete elution of all the lipid classes present in a plasma sample in 28 minutes at a flow rate of 1 µL/min with 3 minutes of overhead time. Base peak chromatograms (BPCs) of plasma lipid extract in both the ionization modes are shown in **figure 5.1** and **figure 5.2**.

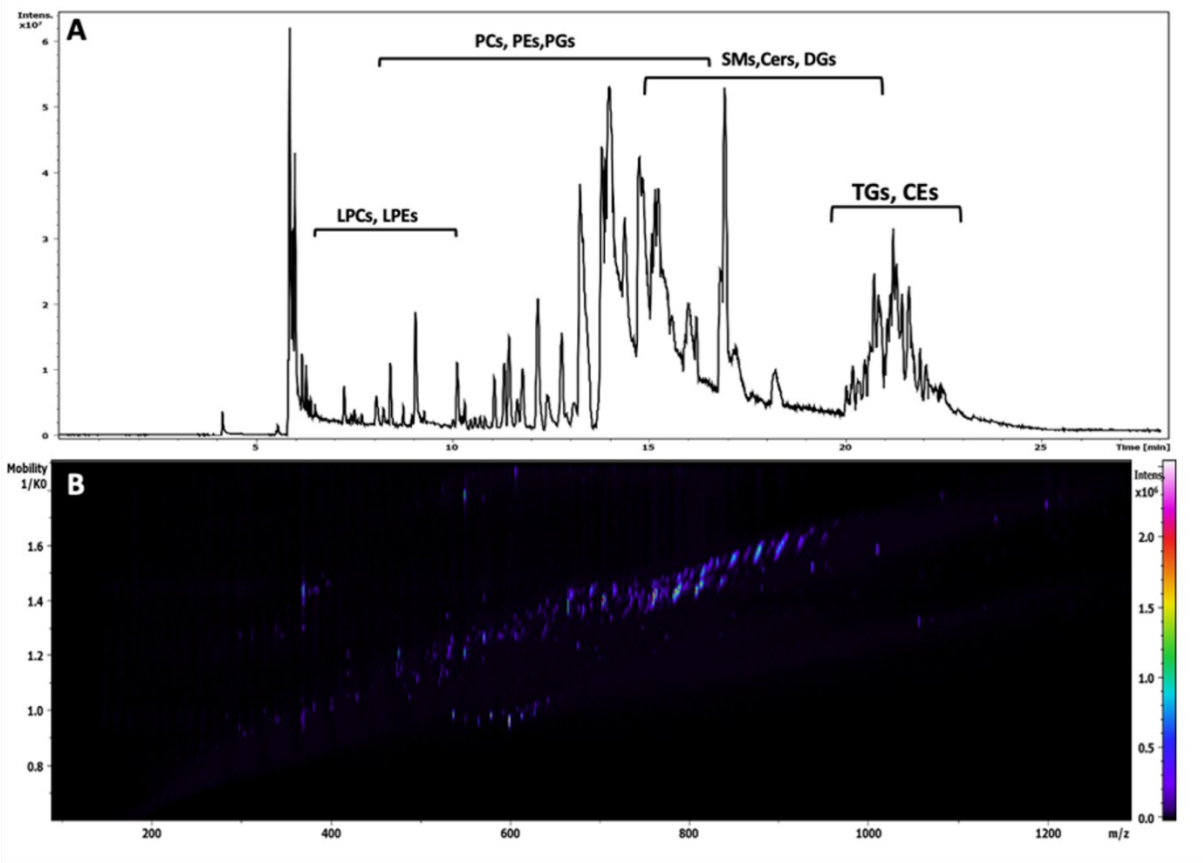

Figure 5.1. *BPC (**A**) and heatmap of mobility space (**B**) of plasma lipid extract acquired in positive mode (LPCs: Lysophophatidylcholines, LPEs: Lysophosphatidylethanolamines, PCs: Phosphatidyl-cholines, PEs: Phosphatidylethanolamines, PGs: Phosphatidylglycerols, SMs: Sphingomyelins, Cers: Ceramides, DGs: Diacylglycerols, TGs: Triacylglycerols, CEs: Cholesteryl esters).*

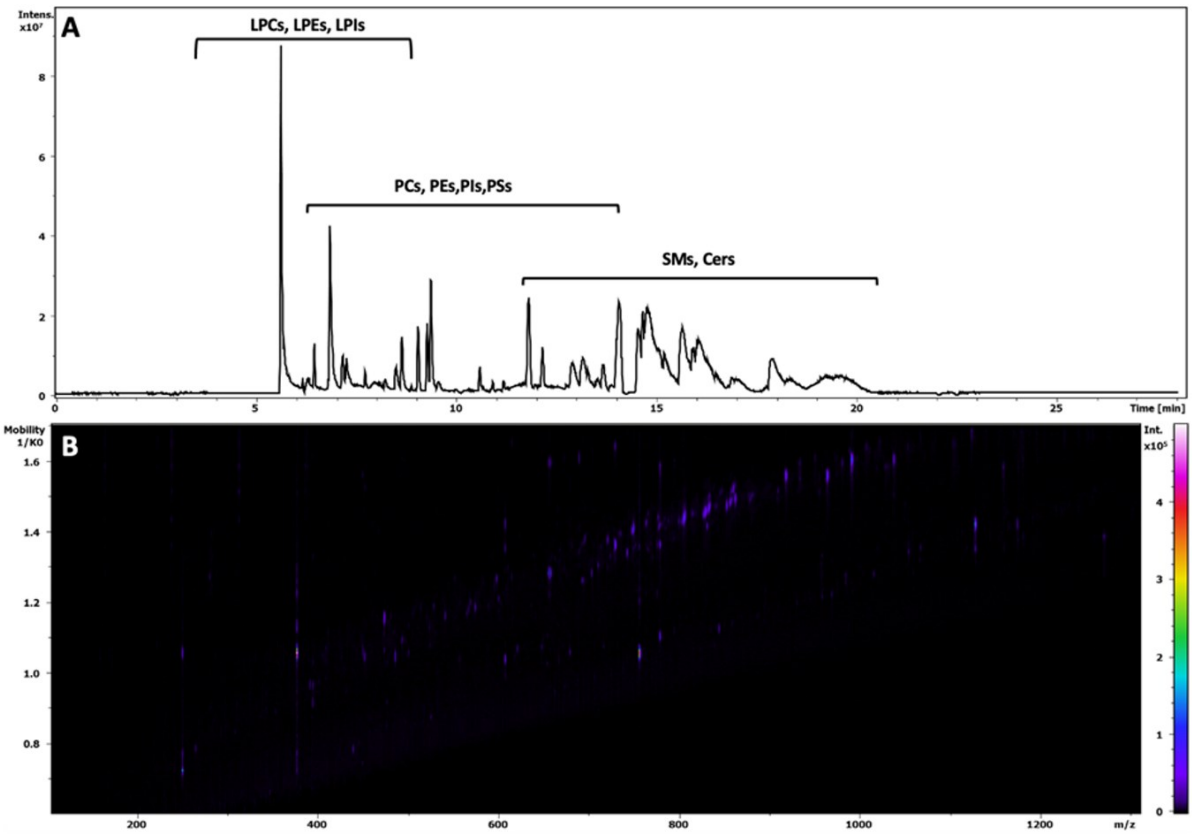

Figure 5.2. *BPC (**A**) and heatmap of mobility space (**B**) of plasma lipid extract acquired in negative mode (LPCs: Lysophophatidylcholines, LPEs: Lysophosphatidylethanolamines, LPIs: Lysophosphatydilinositols, PCs: Phosphatidylcholines, PEs: Phosphatidylethanolamines, PIs: Phosphatidylinositols, PSs: Phosphatidylserines, SMs: Sphingomyelins, Cers: Ceramides).*

The chromatographic performance was evaluated by using a mixture of deuterated standards which showed peak capacity value equal to 66.85 (**supplementary figure S4.2**) with very high run-to-run retention time and cross collision reproducibility across replicate injections for 27 hours (**figure 5.3**).

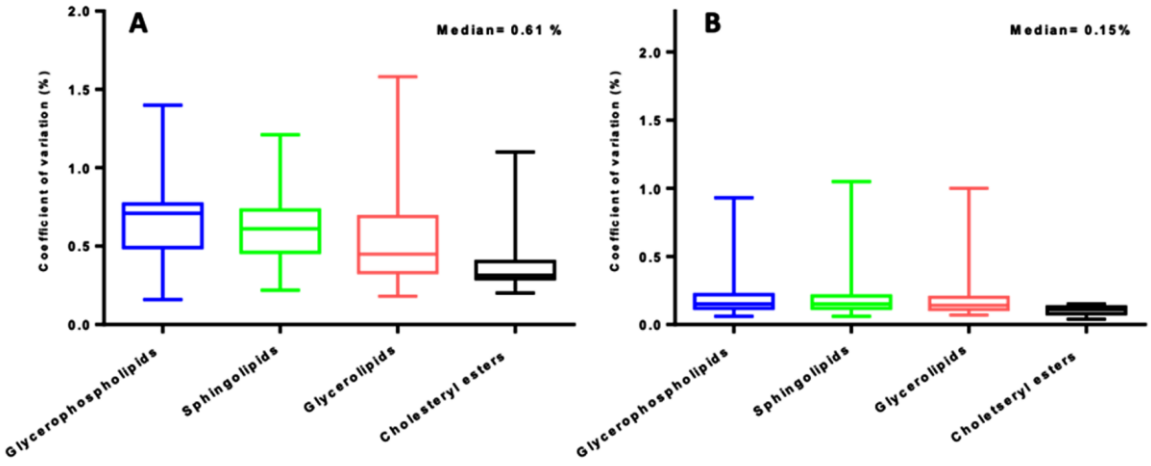

Figure 5.3. *Retention time (**A**) and cross collisional section values (**B**) variation of lipid subclasses over 27 h experiment. Median values are reported.*

Thus, the Evosep One-TIMS-qTOF technology allowed, after strict filtering parameters (referring to retention time, peak shape, MS and MS/MS spectra, CCS values, carry over effect, incidence of missing values) the identification of 435 unique lipids from starting material of 1 µL plasma and by injecting 0.04 µL of plasma lipid extract into the column. The number of identified lipids covers a total of 15 lipid subclasses. A comparative analysis between Evosep One and the conventional nano-LC system led to the identification of only 11 lipids less in the Evosep One, as shown in the **figure 5.4 A**, but with a consistent gain in time (**figure 5.4 B**).

Furthermore, data analysis showed high accuracy (90.6 % of the lipids had an error less than ± 2 ppm) and highly confident identification with a median MS/MS score of 772.5 by using both the rule based approach (Bruker) and LipidBlast spectral library from MS-DIAL, as shown in the **figure 5.4 C, D.**

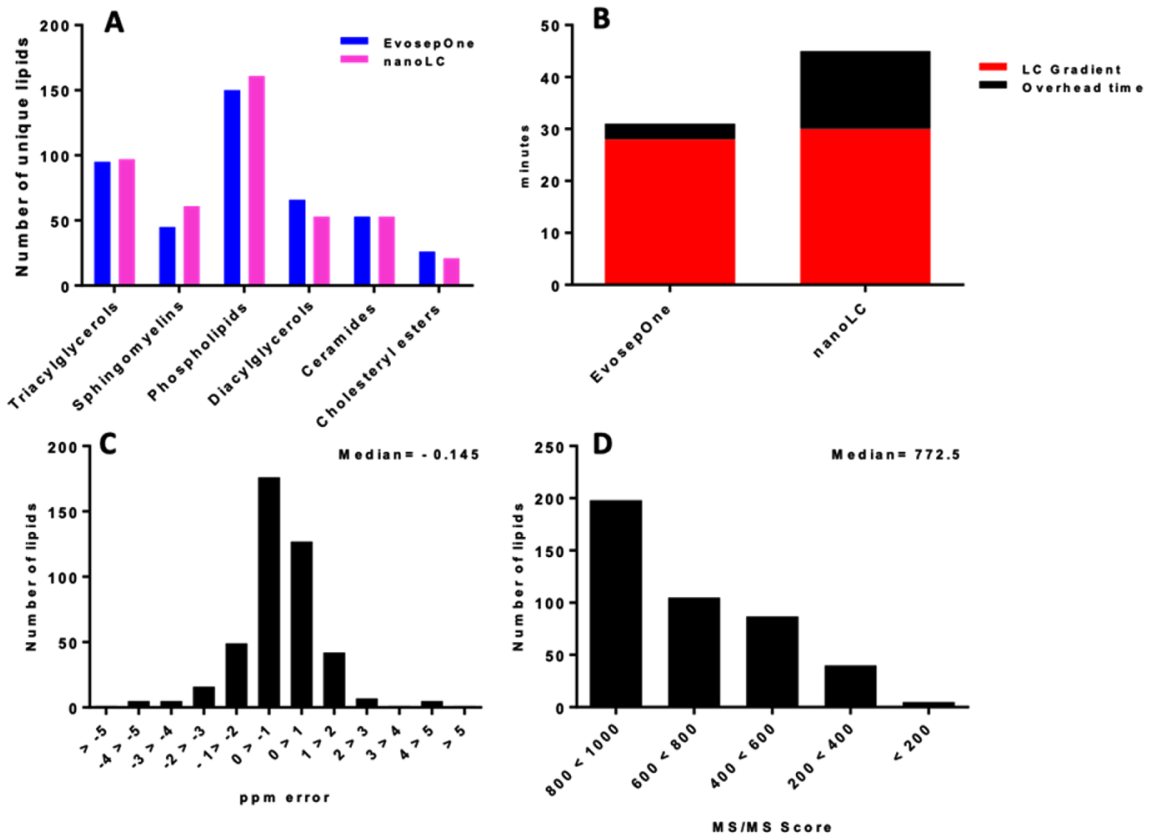

Figure 5.4. *(**A**) Comparison of unique identified lipids and (**B**) total acquisition time between Evosep One (blue) and nanoLC (pink) system. Frequency distribution of ppm error (**C**) and MS/MS score (**D**) of 435 lipids annotated with Evosep One.*

5.3.2. Evotips loading protocol

In order to develop the methodology, it was first of all necessary to optimize an adequate lipidomics Evotips activation protocol, since these tip-shaped trap columns contain a C18 stationary phase disk which needs to be properly handled and activated before coming in contact with the lipid extract. Evotips activation protocols is described in **table 5.1**. All the reported steps are repeated twice. At the end, 40 µL of water are added on top of the tips to prevent Evotips from drying out. This workflow, developed after testing several buffers and

experimental conditions, made possible to achieve a fair compromise between artifacts, often faced in lipidomic field, and binding capacity of the lipid extract to the C18 disk contained into the tip.

Table 5.1. *Lipidomics Evotips sample loading protocol.*

Evotips C18 disk pore size: 100 A
WASH tips with 20 µL of isopropanol plus 0.1 % formic acid (v/v)
CONDITION tips soaking them in isopropanol
EQUILIBRATE tips with 20 µL of water plus 0.1 % formic acid (v/v)
LOAD 20 µL of lipids extract using 1200 g centrifugal force
WET with 40 µL of water plus 0.1 % formic acid (v/v)

Furthermore, to test the binding capacity of the C18 disks and of the optimized loading protocol we injected different concentration of the mixture of the labeled lipids. The result confirmed an excellent linear (R^2=0.99) increase to signal intensity (**figure 5.5**).

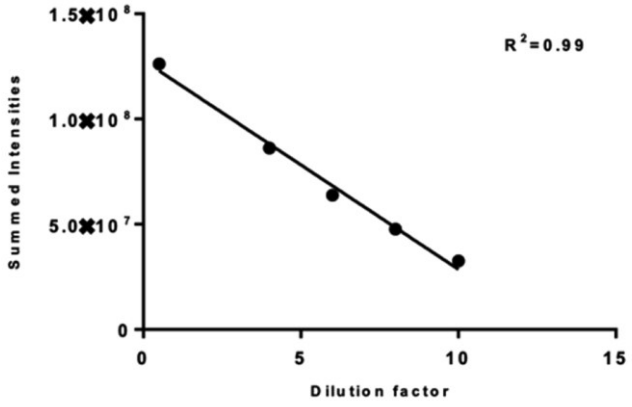

Figure 5.5. *Linear correlation between signal intensity and decreasing amount of deuterated standard mix.*

5.3.3. Sample stability and carry-over effect

Our results indicate that loading minimal (0.04 µL) sample amounts in the Evotips was very reproducible and greatly facilitated by binding the lipids to the Evotip solid phase material before injection, while keeping samples stable over extended periods of time at room temperature. During the course of a 27-hour experiment the sample remained stable as shown from the BPCs (**figure 5.6**). Additional evidences for that are demonstrated from the total intensity of unique annotated lipids over 27 h that had fold change ranging from 0.94 to 1.17 (**supplemental figure S4.3**). Coherently, high values of correlation were obtained plotting lipids intensities at "time 0 h versus 8 h" and "time 0 h versus 24 h" (**figure 5.7**).

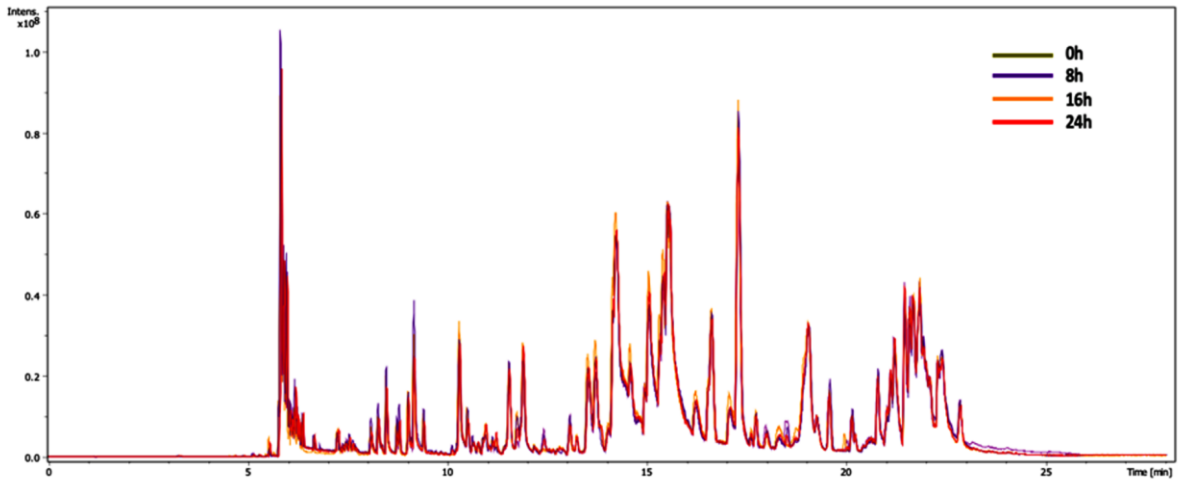

Figure 5.6. *Overlapped base peak chromatograms (BPC) of plasma sample extract acquired at different time points (Time 0, green; 8 h, purple; 16 h, yellow; 24 h, red).*

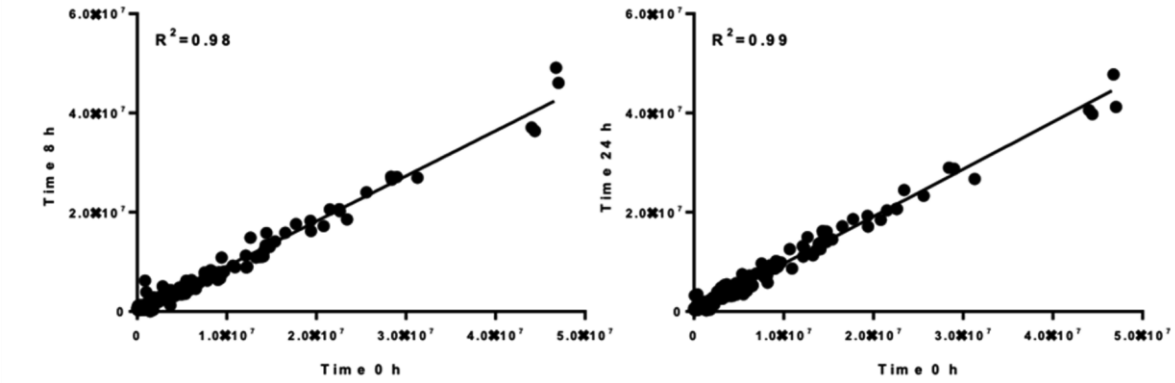

Figure 5.7. *Pearson's coefficient of correlation between a plasma sample acquired at time 0 versus one acquired after 8 h (left) and 24 h (right).*

Subsequently, in order to clarify whether there may be a degradation of a certain lipid class, we investigated their behavior over time per class. The results, once again, did not show substantial alterations to the intensity of both internal standards (**supplementary figure S4.4**) or endogenous lipids (**figure 5.8 A, B**), with a fold change ranging from 0.97 to 1.05 and from 0.93 to 0.99 for positive and negative ionization, respectively.

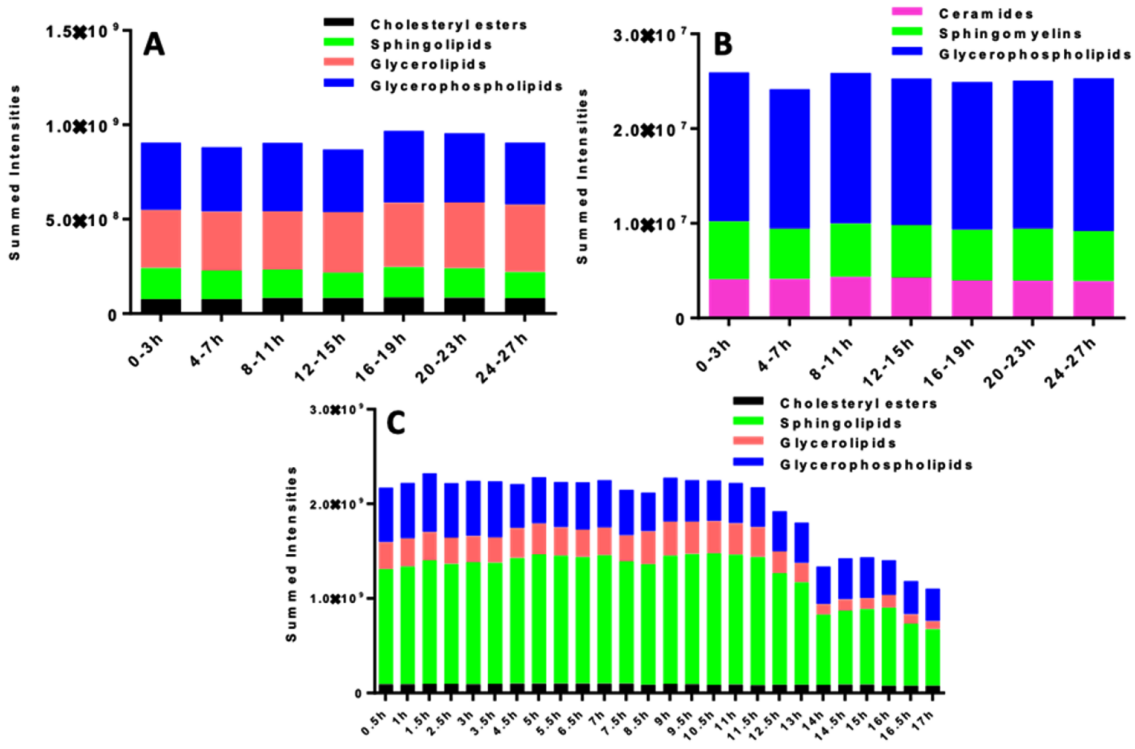

Figure 5.8. *Summed intensities variations over 27 h experiment of lipid subclasses in positive (**A**) and negative (**B**) mode acquired with Evosep One system and a classic nLC system (**C**) operating in ESI$^{(+)}$.*

As next step, we compared these findings with the results coming from the equivalent experiment carried out with a classic nano-LC system, equipped with a refrigerated (+ 4°C) autosampler. The data revealed a clear degradation (**figure 5.8 C**) of the solubilized lipid extract stored in the autosampler starting from the thirteenth hour, and on, from the moment when the sample was dissolved and prepared for the LC-MS injection.

Disposable trap-column injecting technology combined with appropriate and extensive wash condition demonstrated a sample-to-sample carryover for the most abundant molecules of every lipid class less than 2% (**figure 5.9 A, B; supplementary figure S4.5**). Remarkably, the

carryover of one plasma injection remained to the same level after five and nine consecutive plasma injections (**figure 5.9 C**).

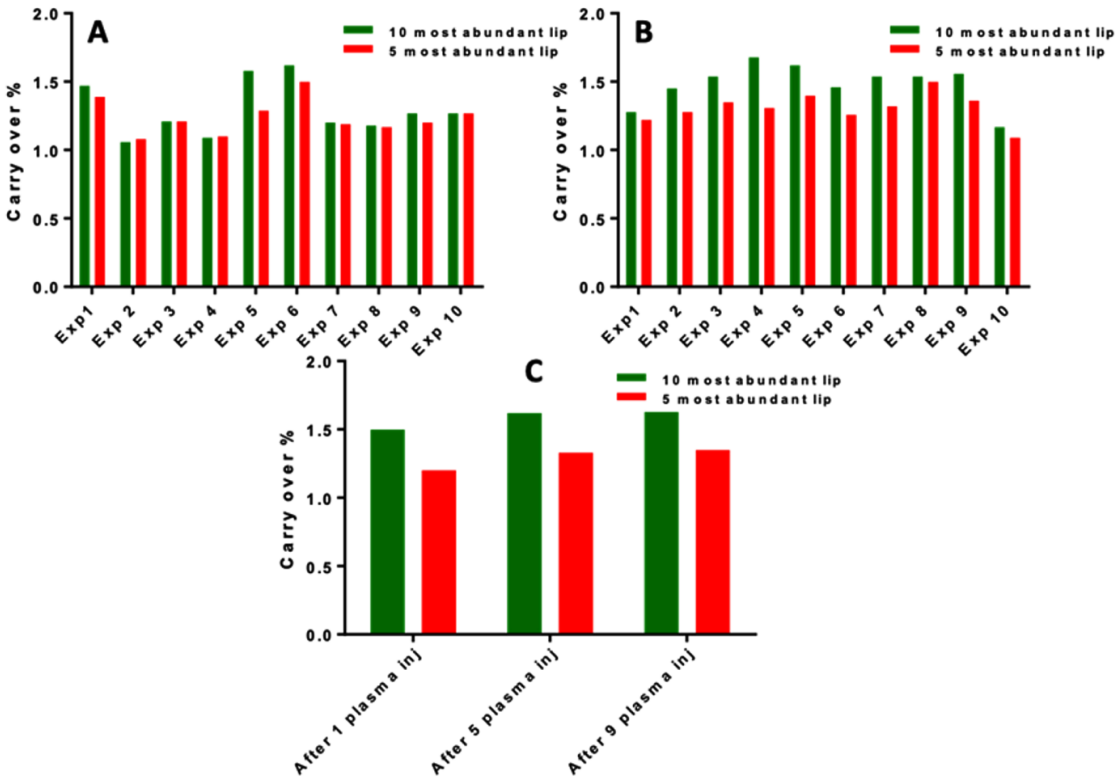

Figure 5.9. *Sample-to-sample carry over in positive (**A**) and negative (**B**) mode; system carryover after multiple replicates of plasma lipid extract in positive mode (**C**). The summed intensities of 5 (red) and 10 (green) most abundant lipids per each lipid class are used for carry-over considerations.*

5.3.4. Trapped ion mobility spectrometry (TIMS) advantages

The PASEF technology offers the opportunity to reduce analysis time without compromising sensitivity and thus lipid coverage. Indeed, working with an additional dimension of separation, TIMS is able to manage a possible increase in the number of co-eluted lipids. This is the case of PC O-32:4 and PE 36:2, which as evident from the EICs completely coelute at 15.02

min. Instead, although these two lipids differ by only 0.036 Da, they are nicely separated in the mobility dimension (**figure 5.10 A, B**).

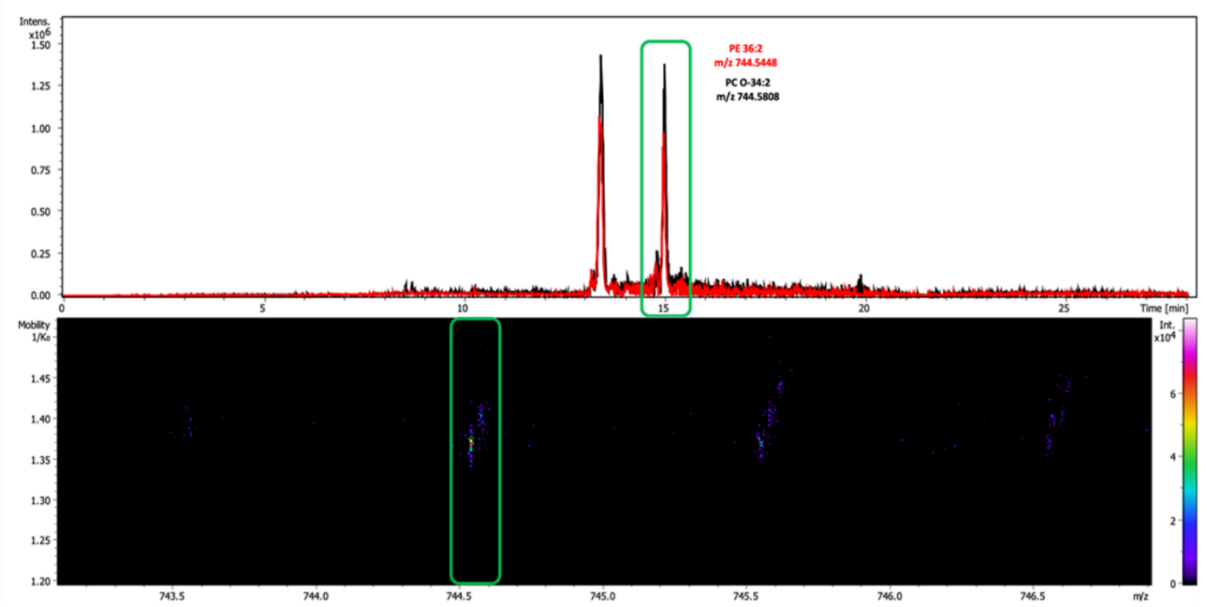

Figure 5.10. *The upper panel shows EIC traces of PC O-34:2 (black) and PE 36:2 (red) while lower panel shows their separation in the mobility dimension.*

Indeed, it is possible to observe two peaks, through the EIMs (extracted ion mobilograms), completely resolved at the base line thanks to different mobility values that translate in different cross collision section values. This results in distinct and clear fragmentation spectra which increase the degree of confidence of the identifications process. In detail, we can observe the typical neutral loss of 141 Da for phosphoethanolamines and the head group fragment at 184 m/z for phosphocholines (**figure 5.11**).

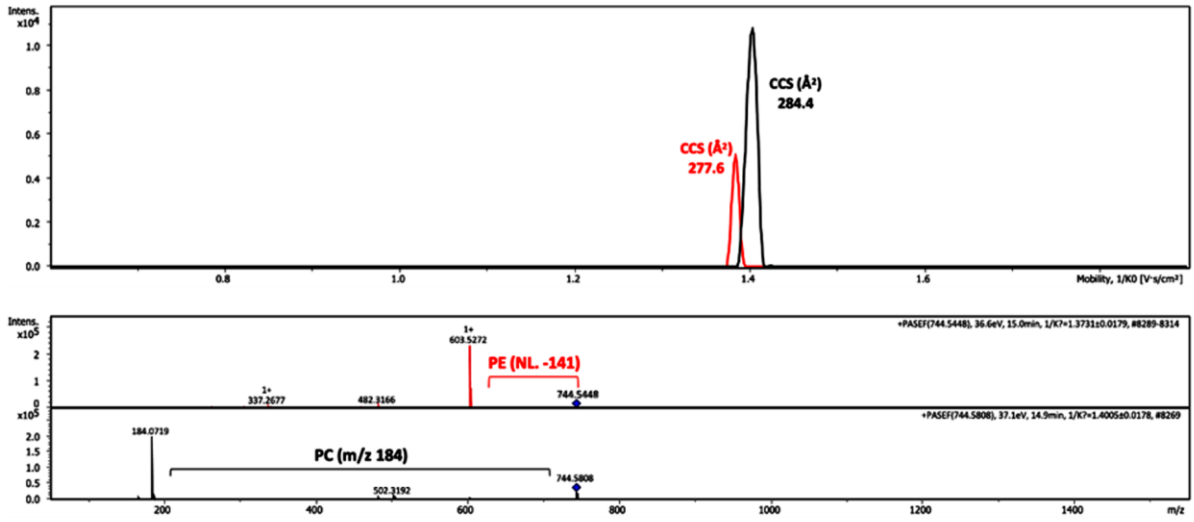

Figure 5.11. *The panel above shows the EIMs of PC O-34:2 (black) and PE 36:2 (red). The panel below shows their respectively (PC O-34:2, black; PE 36:2, red) clear MS/MS spectra.*

5.4. Discussion

Our main focus was to develop and establish an innovative LC methodology starting from minimal sample amount of biological sample and apply a lipidomics innovative workflow able to generate dataset that could be, subsequently, integrated and interpretated in the context of biological network [19,20]. Starting from 1 µL of human plasma, lipids were extracted based on MeOH/MTBE protocol. Crude extracts were then injected with the Evosep One system and eluted with a 28 min gradient. The high nano-flow performance was evaluated coupling it to TimsTOF Pro that operated in both ionization mode. Focusing on the conventional lipidomics nano-chromatography we observed that we were facing two main limitations. First, the equilibration, loading and washing steps in the classic nano-LC are time consuming [21] and so significantly increase the analysis time per sample. Secondly, in lipidomics, it is commonly faced difficulty to keep the samples stables over times in terms of ion intensity and detected molecules, due to the high volatile solvents necessary to dissolve lipids' extract. Indeed, we observe

a 35.1 % decrease in the total intensity coming from the annotated lipids after 14 h of waiting time in the autosampler, while this reduction becomes even higher (45.2 %) after 17 hours. Since our objective was the application in clinical studies, we tried to improve these limitations by turning into a novel LC concept never used, to date, in lipidomics.

The novel LC system is called Evosep One and has mainly been designed for proteomic clinical use [22]. Thus, we tested and adapted it for typical lipidomics buffers [23] and high back-pressure levels. In more details, at first the sample is loaded to a disposable tip with a trap C18 stationary phase, namely Evotip, and positioned in a box on the tray of the autosampler. The manipulator with its ceramic needle picks up the Evotip from the box, that stays at room temperature, and positions it for the injection in line with the solvent flow path. At this point, two low pressure pumps (A and B) form a primary gradient that flows through the Evotip and elutes the analytes of interest. In order to lower the organic content of this gradient, such the analytes are initially retained on the analytical column, an offset gradient with the embedded analytes is formed by using pumps C and D. Then, analytes are moved into the storage loop and the system switches the loop in line with the high-pressure pump where the main gradient has been already formed and stored. Finally, the HP pump pushes the sample and gradient toward the analytical column. It has to be emphasized, as well described by Bache et al [17], that Evosep platform is based on two separate sub-systems. A low-pressure system (15- 30 bar) formed by pumps A, B, C, D and a high-pressure system based on the HP pump and they are in communication only through the storage loop. Considering that all the steps which lead to the formation of the gradient are carried out at low pressures, this novel LC concept ensures higher robustness and a lower risk of leaks if compared to the classical nano-LCs. Furthermore, with the developed technology the Evosep One system can reduce the overhead time to less than 5 minutes between injections increasing the number of potentially samples analyzed per day.

To evaluate Evosep One in lipidomics we considered the following aspect: chromatographic performance, retention time behavior of lipids classes, reproducibility of retention times, sample stability, carry over effect and finally a comparison of the number of the identified lipids between nano-LC and Evosep One system. In that way, in this study we designed an experiment loading lipid extract on 27 Evotips that upon activation were sequentially acquired for a time period of 27 hours with a flow rate of 1 µl/min applied to 8 cm RP column and hyphenated to Timstof-Pro, where PASEF method was activated. Starting from BPCs of our plasma runs we observed that the behavior of each lipid class follows the expected elution sequence and retention time range as indicated from other studies [24,25], remarkable lipids present nice forms and sharp peaks with a nice peak capacity. Since we observed high efficiency, an important indicator to evaluate the current setup is the retention time reproducibility. This is already known to be very good in proteomic experiment [17], however the different chemistry of the molecules together with the fact that we are using mixed solvent in our buffers that are high volatile create the need to evaluate the retention time reproducibility. We achieve prior to alignment, a median coefficient of variation retention time of 0.61 % over the 27 h experiment. An additional aspect that we evaluated is the stability of the sample across time when lipids are bound to the solid phase material at a room temperature. The 27 hours dataset has been split into 7 small subsets where each subset comprises 3 hours injection and, in that way, consecutive time period from 0 to 3 hours, 3 to 6 hours and so on, have been defined. The total intensity of unique lipids within each time period has been investigated. It is remarkable that the summed intensities are high comparable across the 27 h experiment for both the ionization modes. As a next step, in order to discard the hypothesis that a potential degradation of a lipid category might be compensated by an increase of another lipid class, we investigated the total intensity of each distinct lipid category. It is noteworthy that the intensities within each category are highly reproducible

across the 7 subsets and at the same time comparable with the initial time point. These findings strongly indicate that samples remain stable when bounded to the solid phase material and cold conditions are not necessary to keep them alive upon these binding. Additionally, we examinated the capability of both the developed Evotip sample loading protocol and nano-LC system to handle the carry-over effect, that is well known to affect all the HPLC or nano-LC in lipidomics such as in proteomics [9,26]. In this regard, we performed additional experiments evaluating the 5 and 10 most abundant lipids per each lipid class not only in the common sequence plasma/blank, but also considering the carry-over after replicates of plasma injections. Alternating plasma to blanks runs we obtained average carry-over values of 1.24 % and 1.30 % for, respectively, 5 and 10 most abundant lipids. Interestingly, the carry-over values for the 5 and 10 most intense lipids slightly increase to 1.63 % and 1.35 % after nine replicates. Together these results suggest that Evosep One system is able to increase the number of real biological samples acquired in one day without compromising either quality of quantification or accuracy in lipids measurements. Finally, an important comparison to take into account is the number of identified lipids in human plasma between the two LC systems. Both setups achieved similar total number of unique identified lipids and the 83 % of them were common between the two platforms. Evaluating further the number of identified lipids per lipid categoric we observed a decrease (26 %) in the sphingolipids while at the same diacylglycerols were increased (20 %).

Another major challenge in lipidomics is the large number of isobaric or near-isobaric species [27]. TIMS alleviates this problem by separating co-eluting lipids as a function of their collisional cross section, which is particularly advantageous for short gradients. Moreover, switching the quadrupole isolation windows rapidly within a single TIMS scan in PASEF mode [28] characterizes the vast majority of detected isotope patterns via MS/MS.

5.5. Materials and method

5.5.1. Chemicals and reagents

LC–MS-grade Water (H_2O) acetonitrile (ACN), methanol (CH_3OH), ethanol (EtOH), MTBE metyl-tert-butyl-ether (MTBE), isopropanol (IPA), 1-butanol (BuOH), additives formic acid (HCOOH) and ammonium formate ($HCOONH_4$) were all purchased from Sigma-Aldrich (St. Louis, MO). 15:0-18:1-d7-PC, 18:1-d7 Lyso PC, 18:1-d7 Lyso PE, 15:0-18:1-d7-PE, 18:1 SM (d18:1/18:1)-d9, 15:0-18:1-d7 DG, 15:0-18:1-d7-15:0 TG, 18:1 Chol (D7) ester, 15:0-18:1-d7-PI, 15:0-18:1-d7-PG and C18 Ceramide d17:1/18:0 were purchased by Avanti Polar Lipids (Alabaster, AL, U.S.A).

5.5.2. Lipid extraction

Lipids were extracted following Matyash [29] protocol with slight modifications. Briefly, 1 µL of plasma NIST SRM 1950 (Sigma Aldrich) was thawed on ice and added to 200 µL of iced MeOH containing an internal standard mixture, vortexed and additionated with 800 µL of MTBE. The obtained solution was incubated for 6 min at 4 °C and, after the addition of 200 µL of H_2O, centrifuged for 10 minutes at 4°C and 10000 g. The upper layer was carefully collected and evaporated with a speed-vacuum (Eppendorf, Hamburg, Germany). Lipids extracts were dissolved in 500 µL of BuOH/IPA/ H_2O (8/23/69 v/v) and 20 µL loaded on Evotips as described in paragraph 5.3.2.

5.5.3. nLC—MS/MS analysis

LC-MS instrumentation consisted of an Evosep One (Evosep Byosistem) coupled to Tims-TOF Pro (Bruker Daltonics, Bremen, Germany) via a modified nano-electrospray ion source (Captive Spray, Bruker Daltonics). Lipids were separated on a Pepsep C18 column 8 cm × 150 µm ID ×1.5µm with a column oven temperature of 65°C. Mobile phases were: A) ACN/H_2O 5/95 (v/v) and B) IPA/ACN 90/10 (v/v) both buffered with 10 mM $HCOONH_4$ + 0.1% HCOOH. The employed gradient is illustrated in **figure 5.12**.

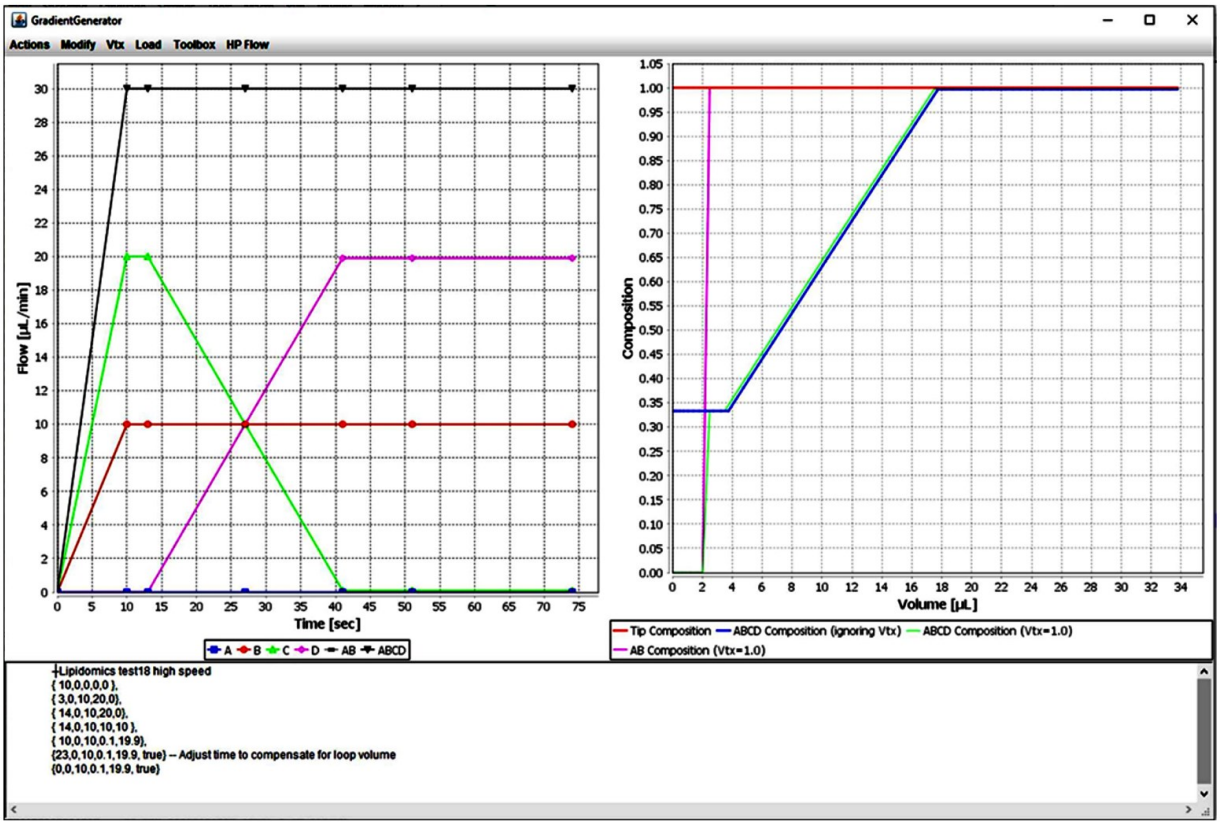

Figure 5.12. *LC gradient composition.*

For nano chromatography comparison [18] an Easy-nLC 1200 (Thermo Fisher Scientific) with an in-house reverse phase column (20 cm × 75 µm i.d.) with a pulled emitter tip, packed with 1.9 µm C18 material was used (Dr. Maisch, Ammerbuch-Entringen, Germany); mobile phases were: A) ACN/H_2O 60/40 (v/v) and B) IPA/ACN 90/10 both buffered with 10 mM $HCOONH_4$ + 0.1 % HCOOH. The column oven was set at 65°C, the injection volume was 1 µL for positive mode and 2 µL for negative mode. The following gradient was employed: 1 to 30% within 3 min, then to 51% within 4 min, and then every 5 min to 61, 71 and 99%, where it was kept for 5 min and 3 minutes at 1% for column re-equilibration. Both LCs instruments were coupled to a TimsTOF Pro working in both positive and negative mode and with parallel accumulation serial fragmentation (PASEF) on. Lipids were acquired in the range 50/1550 m/z

and the mobility was scanned from 0.6 to 1.95 Vs/cm^2. Precursors for data dependent acquisition were fragmented with an ion mobility dependent collision ranging from 25 to 45 eV and from 35 to 55 eV, respectively, for positive and negative mode. Ion charge control was set to 7.5 Mio. Method consists of one TIMS/MS scan and three PASEF MS/MS scan with an acquisition cycle of 0.4 s. Instrument was calibrated using the following ions from Agilent ESI LC/MS Tuning MIX [m/z, 1/K_0: (322.0481, 0.7318 Vs cm^{-2}), (622.0289, 0.9848 Vs cm^{-2}), (922.0097, 1.1895 Vs cm^{-2}), (1221,9906, 1.3820 Vs cm^{-2})] in positive mode and [m/z, 1/K_0: (666.01879, 1.0371 Vs cm^{-2}), (965.9996, 1.2255 Vs cm^{-2}), (1265.9809, 1.3785 Vs cm^{-2})] in negative mode.

5.5.4. Data processing

Raw files were analyzed with Metaboscape 2021 (Bruker Daltonics) with a 4D algorithm (T-Rex 4D) that automatically extracts features from 4D space (retention time, m/z, intensity and ion mobility).

The mass was online recalibrated with lock masses m/z 622.028960 (positive mode) and m/z 666.019887 (negative mode) and the ion mobility dimension was recalibrated using the ions of the tuning mix as above. Feature detection was performed using an intensity threshold of 3000 counts in positive mode and 1000 counts in the negative mode, with at least 100 data point in the 4D TIMS space, or 50 when using recursive feature extraction. Lipids were annotated with both a Rule based approach (Bruker) and a LipidBlast spectral library from MS-DIAL (http://prime.psc.riken.jp/compms/msdial/main.html) setting the following parameters: $[M+H]^+$, $[M+Na]^+$, $[M+K]^+$, $[M+H-H_2O]^+$ and $[M+NH_4]^+$ ions in positive mode, while $[M–H]^–$, $[M+Cl]^–$, $[M+ HCOO]^–$ and $[M-H_2O]^–$ for the negative. The initially annotated lipids were filtered based on the retention time, the mass accuracy, the observed adduct, the mobility value and the ms/ms fragmentation profile following the guidelines reported by Lipidomic

Standard initiative (LSI) (https://lipidomics-standards-initiative.org/guidelines/lipid-species-identification/general-rules), and following theoretical carbon number (TCN) rule and correlation between m/z and CCS values. Lipids were reported with a short or long name according to the information coming from the MS/MS spectra. Note that sn1/sn2/sn3 chain assignments, positions of the double bonds, as well as cis/trans isomers are not evident from our data and therefore not annotated.

5.5.5. Method validation

Instrument repeatability was evaluated monitoring retention times, intensities and cross collision section values of both endogenous lipids and deuterated internal standards over 27 h. Plasma lipid extracts, once loaded on the Evotips, were placed on the sample tray (room temperature) and acquired one after one, blanks were inserted in the batch and regularly injected. Carry over effect was determined by injecting sequences of plasma – blank runs, or plasma replicates (3 and 9) followed by blank run. Peak capacity was evaluated with the following equation according to Neue equation [30].

$$n_c = 1 + \frac{t_g}{w_{awg}}$$

Where t_g is the gradient run, w_{awg} is the average peak width.

5.6. Conclusions

In conclusion, we have established a nanoflow TIMS-PASEF workflow that enables a highly sensitive, comprehensive and in-depth analysis of lipidome starting from minimal sample amounts (1µl blood plasma and 0.04 µl of lipid extract injected). Since we have observed that nano-LC troubles could represent limitations in lipidomics workflow, we have introduced an adapted and novel LC system in this work that merges the convenience and the robustness and of high flow system with the sensitivity of the nanoflow. So far, our results point out the Evosep

One as a high-throughput and reproducibility system for lipidomics, while the greatest advantage is that sample bounded on Evotips stay stable at room temperature for long time. This concept has the potential to provide a highly sensitive platform for clinical applications.

5.7 References

[1] Yang K, Han X. Lipidomics: Techniques, Applications, and Outcomes Related to Biomedical Sciences. *Trends Biochem Sci*. **2016**. 41 (11): 954-969.

[2] Perttula K., Schiffman C., Edmands W.M.B, Petrick L., Grigoryan H., Cai X., Gunter M.J., Naccarati A., Polidoro S., Dudoit S., Vineis P., Rappaport S.M. Untargeted lipidomic features associated with colorectal cancer in a prospective cohort. *BMC Cancer*. **2018**. 18 (1): 996.

[3] Barchuk M., Dutour A., Ancel P., Svilar L., Miksztowicz V., Lopez G., Rubio M., Schreier L., Nogueira J.P., Valéro R., Béliard S., Martin J.C., Berg G., Gaborit B. Untargeted Lipidomics Reveals a Specific Enrichment in Plasmalogens in Epicardial Adipose Tissue and a Specific Signature in Coronary Artery Disease. *Arterioscler Thromb Vasc Biol*. **2020**. 40 (4): 986-1000.

[4] Zhang X., Liu W., Zan J., Wu C., Tan W. Untargeted lipidomics reveals progression of early Alzheimer's disease in APP/PS1 transgenic mice. *Sci Rep*. **2020**. 10 (1): 14509.

[5] Kim W.S., Jary E., Pickford R., He Y., Ahmed R.M., Piguet O., Hodges J.R., Halliday G.M. Lipidomics Analysis of Behavioral Variant Frontotemporal Dementia: A Scope for Biomarker Development. *Front Neurol*. **2018**. 28 (9):104.

[6] Monnerie, S., Comte, B., Ziegler, D., Morais J.A., Pujos-Guillot E., Gaudreau P. Metabolomic and Lipidomic Signatures of Metabolic Syndrome and its Physiological Components in Adults: A Systematic Review. *Sci Rep.* **2020**. 10: 669.

[7] Xu T., Hu C., Xuan Q., Xu G. Recent advances in analytical strategies for mass spectrometry-based lipidomics. *Anal Chim Acta*. **2020**. 1137: 156-169.

[8] Southam A.D., Weber R.J., Engel J., Jones M.R., Viant M.R. A complete workflow for high-resolution spectral-stitching nanoelectrospray direct-infusion mass-spectrometry-based metabolomics and lipidomics. *Nat Protoc*. **2016**. 12 (2): 310–328.

[9] Züllig T., Köfeler H.C. High resolution mass spectrometry in lipidomics. *Mass Spectrom. Rev.* **2021**. 40: 162-176.

[10] Levy A.J., Oranzi N.R., Ahmadireskety A., Kemperman R.H.J., Wei M.S., Yost R.A. Recent progress in metabolomics using ion mobility-mass spectrometry. *TrAC - Trends Anal. Chem.* **2019**. 116: 274-281.

[11] Lange, M., Fedorova, M. Evaluation of lipid quantification accuracy using HILIC and RPLC MS on the example of NIST® SRM® 1950 metabolites in human plasma. *Anal Bioanal Chem.* **2020**. 412: 3573–3584.

[12] Lange, M., Ni, Z., Criscuolo, A., Fedorova M. Liquid Chromatography Techniques in Lipidomics Research. *Chromatographia.* **2019**. 82: 77–100.

[13] Cajka T., Fiehn O. Toward Merging Untargeted and Targeted Methods in Mass Spectrometry-Based Metabolomics and Lipidomics. *Anal. Chem.* **2016**. 88, 1: 524–545.

[14] Avela H.F., Heli Sirén H. Advances in analytical tools and current statistical methods used in ultra-high-performance liquid chromatography-mass spectrometry of glycero-, glycerophospho- and sphingolipids. *Int. J. Mass Spectrom.* **2020**. 457: 116408.

[15] Danne-Rasche N., Coman C., Ahrends R. Nano-LC/NSI MS Refines Lipidomics by Enhancing Lipid Coverage, Measurement Sensitivity, and Linear Dynamic Range. *Anal. Chem.* **2018**, 90: 8093–8101.

[16] Karas M., Bahr U., Dülcks T. Nano-electrospray ionization mass spectrometry: addressing analytical problems beyond routine. *Fresenius J Anal Chem*. **2000**. 366 (6-7): 669-76.

[17] Bache N., Geyer P.E., Bekker-Jensen D.B., Hoerning O., Falkenby L., Treit P.V., Doll S., Paron I., Müller J.B., Meier F., Olsen J.V., Vorm O., Mann M. A Novel LC System Embeds Analytes in Pre-formed Gradients for Rapid, Ultra-robust Proteomics. *Mol Cell Proteomics*. **2018**. 17 (11): 2284-2296.

[18] Vasilopoulou C.G., Sulek K., Brunner A.D., Meitei N.S., Schweiger-Hufnagel U., Meyer S.W., Barsch A., Mann M., Meier F. Trapped ion mobility spectrometry and PASEF enable in-depth lipidomics from minimal sample amounts. *Nat Commun*. **2020**. 11 (1): 331.

[19] Müller J.B., Geyer P.E., Colaço A.R., Treit P.V., Strauss M.T., Oroshi M., Doll S., Virreira Winter S., Bader J.M., Köhler N., Theis F., Santos A., Mann M. The proteome landscape of the kingdoms of life. *Nature.* **2020**. 582: 592–596.

[20] Santos A., Colaço A.R., Nielsen A.B., Niu L., Geyer P.E., Coscia F., Albrechtsen N.J.W., Mundt F., Jensen L.J., Mann M. Clinical Knowledge Graph Integrates Proteomics Data into Clinical Decision-Making. **2020**. *bioRxiv*.

[21] Bian Y., Zheng R., Bayer F.P., Wong C., Chang Y.C., Meng C., Zolg D.P., Reinecke M., Zecha J., Wiechmann S., Heinzlmeir S., Scherr J., Hemmer B., Baynham M., Gingras A., Boychenko O., Kuster B. Robust, reproducible and quantitative analysis of thousands of proteomes by micro-flow LC–MS/MS. *Nat Commun*. **2020**. 11: 157.

[22] Krieger J.R., Wybenga-Groot L.E., Tong J., Bache N., Tsao M.S., Moran M.F. Evosep One Enables Robust Deep Proteome Coverage Using Tandem Mass Tags while Significantly Reducing Instrument Time. *J Proteome Res*. **2019**.18 (5): 2346-2353.

[23] Cajka T., Fiehn O. Increasing lipidomic coverage by selecting optimal mobile-phase modifiers in LC–MS of blood plasma. *Metabolomics*. **2016**. 12 (2): 34.

[24] Fauland A., Köfeler H., Trötzmüller M., Knopf A., Hartler J., Eberl A., Chitraju C., Lankmayr E., Spener, F. A comprehensive method for lipid profiling by liquid chromatography-ion cyclotron resonance mass spectrometry. *J Lip Res*. **2011**. 52 (12): 2314–2322.

[25] Ovčačíková M., Lísa M., Cífková E., Holčapek M. Retention behavior of lipids in reversed-phase ultrahigh-performance liquid chromatography-electrospray ionization mass spectrometry. *J Chromatogr A.* **2016**. 1450: 76-85.

[26] Mitulović G., Stingl C., Steinmacher I., Hudecz O., Hutchins J.R., Peters J.M., Mechtler K. Preventing carryover of peptides and proteins in nano LC-MS separations. *Anal Chem*. **2009**. 81 (14): 5955-60.

[27] Berthias F., Poad B.L.J., Thurman, H.A., Bowman A.P., Blanksby S.J., Shvartsburg A.A. Disentangling Lipid Isomers by High-Resolution Differential Ion Mobility Spectrometry/Ozone-Induced Dissociation of Metalated Species. *J. Am. Soc. Mass Spectrom.* **2021**, 32 (12): 2827–2836.

[28] Meier F., Brunner A.D., Koch S., Koch H., Lubeck M., Krause M., Goedecke N., Decker J., Kosinski T., Park M.A., Bache N., Hoerning O., Cox J., Räther O., Mann M. Online Parallel Accumulation-Serial Fragmentation (PASEF) with a Novel Trapped Ion Mobility Mass Spectrometer. *Mol Cell Proteomics*. **2018**. 17 (12): 2534-2545.

[29] Matyash V., Liebisch G., Kurzchalia T. V., Shevchenko A., Schwudke, D. Lipid extraction by methyl- tert -butyl ether for high-throughput lipidomics. *J. Lipid Res*. **2008**. 49: 1137–1146.

[30] Neue U.D. Theory of peak capacity in gradient elution. J. *Chromatogr. A.* **2005**. 1079 (12): 153-161.

CHAPTER VI

Untargeted Lipidomics Analysis Reveals Specific Lipid Profiles in Hospitalized Covid-19 patients predictive for Severity and Mortality Outcome

Abstract

Covid-19 infection evokes various systemic alterations that push patients not only towards severe acute respiratory syndrome, but causes an important metabolic dysregulation with following multi-organ alteration and potentially poor outcome. To discover novel potential biomarkers able to predict disease's severity and patient's outcome, we applied untargeted lipidomics, by an ultra-high performance liquid chromatography-trapped ion mobility mass spectrometry platform (UHPLC-TIMS), on blood samples collected at hospital admission in an Italian cohort of Covid-19 patients (45 mild, 54 severe, 21 controls). In a subset of patients, we also collected a second blood sample in correspondence of clinical phenotype modification (longitudinal population). Plasma lipid profiles revealed that LPCs, LPC-Os and PC-O levels were significantly modified in Covid-19 patients with respect to controls and able to discern between mild and severe clinical phenotype. A machine learning model was built by using the entire lipidomics dataset, yielding 70% accuracy for severity. Furthermore, using a panel of six lipids, comparable results were obtained, predicting severity (AUC= 0.777, CI: 0.639-0.904) and outcome (AUC= 0.789, CI: 0.658-0.910) considering death as final endpoint. Finally, re-

building the model with 25 longitudinal (t1) samples, this resulted in 21 patients correctly classified. In conclusion, our study introduces a novel panel of lipid markers that could be used to monitor the possible trajectory of Covid-19 patients at hospital admission in faster, targeted approaches.

6.1. Introduction

The current pandemic caused by severe acute respiratory syndrome coronavirus 2 (SARS-CoV-2) is still delivering an enormous impact on health management globally. Indeed, the scarce vaccination practice in countries with weaker health and economic systems makes Covid-19 still a relevant health and social problem worldwide [1]. While roughly 80% of Covid-19 patients show only mild symptoms, conditions can rapidly evolve to severe phenotype. The pathophysiology of Covid-19 is indeed highly complex; beyond immune changes, metabolism emerged as a critical regulator that is tightly bound to the host response and involved in the disease's progression [2]. Some patients with Covid-19 undergo an altered metabolic state, known as “phenoconversion”, predictive of multi-organ alteration and poor outcome. Specifically, clinical deterioration in patients with Covid-19 involves multiple pathways, including chemotaxis and interleukin production, but also endothelial dysfunction, the complement system, and immunothrombosis. Indeed, unfavorable outcome in hospitalized Covid-19 patients has been previously associated with changes in concentrations of IL-6, IL-8, IL-10, soluble Receptor for Advanced Glycation End Products (sRAGE), vascular cell adhesion molecule 1 (VCAM-1) and Pentraxin-3 [3]. Moreover, also lipids play various critical biological functions in cellular barriers, signal transduction, material transport, energy storage, cell differentiation, and apoptosis. SARS-CoV-2 can induce characteristic molecular changes detected in patients’

sera using proteomic and metabolomic technologies [4,5], which also correlates with modification of the inflammatory profile of the COVID19 patients [6].

Therefore, omics sciences, such as metabolomics and lipidomics, can be instrumental in identifying predictive biomarkers of severity and progression, monitoring the metabolic status of individuals during the time and thus applied to evaluate the metabolic host response to SARS-CoV-2 infection.

In this regard, lipids cover a crucial role in numerous metabolic processes, such as energy management and storage, act as structure and membrane components, and are essential players in cell signaling. They have also been found deeply dysregulated in other viral infections, like Ebola virus disease (EVD) [4,7,8,9]. Lipids are essential also in the life cycle of SARS-CoV-2, which is an envelope virus surrounded by a lipid bilayer, furthermore, following infection, host immune cells like macrophages show a change in lipid metabolism upon activation, which is tightly connected to the immune response to pathogens [10]. Initial studies have in fact evidenced that eicosanoids dysregulation, as well as lower serum HDL levels are connected with disease severity and mortality rate [11,12]. Therefore lipidomics, with its potential to identify and quantify several lipid subclasses in a single analysis [13] can be a useful tool for a better comprehension of Covid-19 physiopathology and identification of novel therapeutic strategies.

In this regard, targeted [6,14] and untargeted mass spectrometry-based lipidomics studies [15,16] have been carried out on different Covid-19 cohorts. All these studies, even if heterogeneous and carried out with different technologies, evidenced a profound dysregulation in plasma lipidome of Covid-19 patients, such as increased sphingomyelins (SM) and reduced diacylglycerol (DG) levels [9], increased ceramides (Cer) and triglycerides (TG) [8], and generally decreasing glycerophospholipids [16] even with conflicting results [8,9]. Overall, lipid biomarkers mirror the

severity statuses, but their effective predictive potential has not been clearly identified. Thus, we hypothesize that metabolic changes in Covid-19 patients are earlier than clinical changes and, therefore, potentially exploitable for early prognostic assessment. In this study, to uncover the lipid changes in the plasma of Covid-19 patients, we applied an untargeted lipidomics approach, by ultra-high-performance liquid chromatography coupled with trapped ion mobility mass spectrometry (UHPLC-TIMS-MS), in an Italian cohort of hospitalized Covid-19 patients. We highlight a profound alteration of different lipid subclasses, particularly a significant and progressive decrease of glycerophospholipids, already at the time of admission, and explored the potential capability of a specific lipid subset to predict Covid-19 patients' outcome.

6.2. Aim of the work

The work aimed to investigate the possible lipid alterations in the plasma of patients with a different severity degree of SARS-CoV-2 through a statistical approach and the development of a machine learning model. The study intended to identify a restricted pool of lipids that if measured at the time of hospitalization it may be able not only to provide information about the current condition of the patient, but also the possible outcome of subjects positive to Covid-19.

6.3. Results

6.3.1. Untargeted lipidomics analysis of Covid-19 plasma samples

Untargeted lipidomics analyses were conducted with an RP-UHPLC-TIMS/MS strategy summarized in **figure 6.1**. System repeatability was assessed by a pooled QC strategy, which closely clustered as can be observed from PCA score plot (**supporting information figure S5.1**), while lipid annotations were performed following the lipidomic standard initiative guidelines (**supporting information figure S5.2**) (https://lipidomics-standards-initiative.org/). In detail our initial workflow started from 994 annotations which were subjected to several filters:

mass accuracy (Δppm: max 5.0 ppm), collision section error values (ΔCCS: max 5 %), peak shape, most probable adduct form, MS/MS spectral similarity score, RT and CCS values linearity, carryover, and CV < 35 % in QCs. As a result, retention time reproducibility resulted in a median CV value of 0.42 %, prior to the RT alignment, while average MS/MS score, Δppm and ΔCCS were respectively: 914.60 MS/MS score, 0.60 Δppm, 1.30% ΔCCS (**supporting information figure S5.2**). After further manual curation, 348 unique lipids belonging to 16 subclasses (**supporting information figure S5.3**) were annotated with high confidence (**supporting information table S5.1**). Notably, 91.67 % of the annotations were in common between rule based and spectral library approaches, moreover the implementation of trapped ion mobility ensured further confidence in lipid annotation, by comparison of experimental CCS values with those reported in libraries.

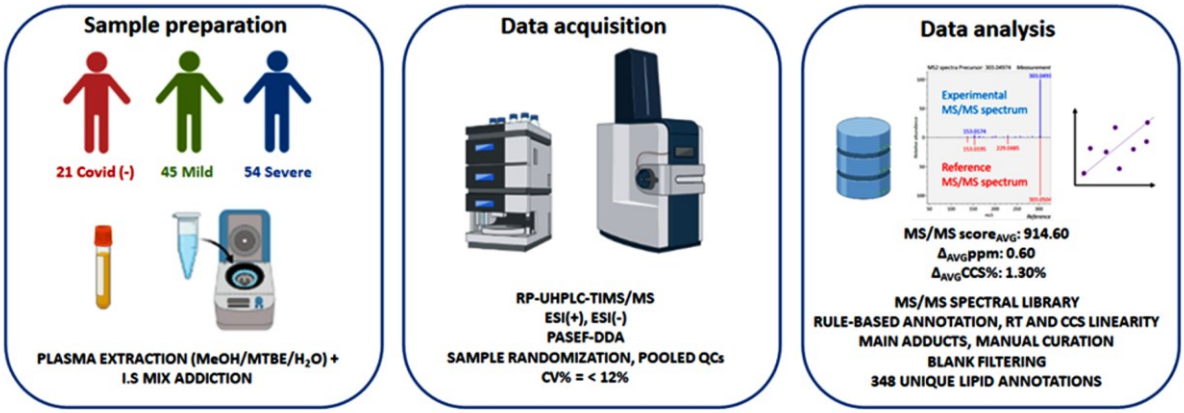

Figure 6.*1.* *Workflow of the untargeted lipidomics approach: 120 plasma samples were extracted and analyzed by RP-UHPLC-TIMS/MS, repeatability was assessed by a pooled QC strategy, lipid annotation was performed by spectral library comparison, rule-based annotation, retention time and cross collisional section linearity.*

6.3.2. Clinical features of Covid-19 patients

In our cohort, no significant differences in baseline characteristics were identified at admission between mild and severe patients. We found a slight prevalence of female patients with no difference of age between mild and severe phenotype. For all the comorbidities analyzed we did not detect a significant difference between the two groups. Furthermore, we subdivided Mild and Severe groups into “survivors” and “non-survivors” considering death as final endpoint. The demographic and comorbidities information are summarized in **table 6.1**. In the Mild group no demographic and prevalence comorbidities differences were found between “survivors" and “non-survivors” except for valvular disease and peripheral arterial disease (PAD), (1 patient in “non-survivor” group). The same observation was for the Severe group except for the presence of PAD (1 patient in the “survivor” group). Data are reported in **tables 6.2** and **6.3**.

Table 6.1. *Clinical characteristics of Covid-19 patients subdivided by phenotype at admission; CAD: coronary artery diseases; HF: heart failure; PAD: peripheral artery disease; CKD: chronic kidney disease; COPD: Chronic obstructive pulmonary disease.*

	COVID (+)		
	Mild (45)	**Severe (54)**	**p value**
Sex	F 23 (51.1%) M 22 (48.9%)	F 38 (70.4%) M 16 (29.6%)	0.05
Age	67.91 ± 17.22	67.85 ± 11.62	0.984
CAD	7 (15.6%)	12 (22.2%)	0.475
HF	4 (8.9%)	2 (3.7%)	0.068
Obesity	4 (8.9%)	12 (22.2%)	0.905
Atrial Fibrillation	6 (13.3%)	5 (9.3%)	0.124
Valvular disease	1 (2.2%)	2 (3.7%)	0.863
PAD	1 (2.2%)	1 (1.9%)	0.490
Dyslipidemia	6 (13.3%)	8 (14.8%)	0.280
Diabetes mellitus	14 (31.1%)	17 (31.5%)	0.119
Arterial hypertension	26 (57.8%)	32 (59.3%)	0.093
CKD	7 (15.6%)	7 (13.0%)	0.513
Smoking	3 (6.7%)	7 (13.0%)	0.597
COPD	10 (22.2%)	9 (13.7%)	0.062
Autoimmune Disease	1 (2.2%)	4 (7.4%)	0.738

Table 6.2. *Subdivision of Covid-19 Mild patients by outcome in "survivors" and "non-survivors"; CAD: coronary artery diseases; HF: heart failure; PAD: peripheral artery disease; CKD: chronic kidney disease; COPD: Chronic obstructive pulmonary disease.*

	Mild "survivors" (37)	**Mild "not survivors" (8)**	**p value**
Sex	F 19 (51%) M 18 (49%)	F 3 (37.5%) M 5 (62.5%)	0.489
Age	65.24 ± 17.33	80.25 ± 10.37	0.024
CAD	5 (13.5%)	2 (25.0%)	0.307
HF	3 (8.1%)	1 (12.5%)	0.637
Obesity	4 (10.8%)	-	0.317
Atrial Fibrillation	4 (10.8%)	2 (25.0%)	0.355
Valvular disease	-	1 (12.5%)	0.040
PAD	-	1 (12.5%)	0.008
Dyslipidemia	4 (10.8%)	2 (25.0%)	0.201
Diabetes mellitus	12 (32.4%)	2 (25.0%)	0.835
Arterial hypertension	22 (59.5%)	4 (50.0%)	0.364
CKD	4 (10.8%)	3 (37.5%)	0.195
Smoking	1 (2.7%)	2 (25.0%)	0.006
COPD	6 (16.2%)	4 (50.0%)	0.014
Autoimmune disease	1 (2.7%)	2 (25.0%)	0.700

Table 6.3. *Subdivision of Covid-19 Severe patients by outcome in "survivors" and "non-survivors"; CAD: coronary artery diseases; HF: heart failure; PAD: peripheral artery disease; CKD: chronic kidney disease; COPD: Chronic obstructive pulmonary disease.*

	Severe "survivors" (20)	Severe "not survivors" (34)	p value
Sex	F 6 (30%) M 14 (70%)	F 10 (29%) M 24 (71%)	0.964
Age	65.00 ± 14.40	69.53 ± 9.47	0.169
CAD	5 (25.0%)	7 (20.6%)	0.673
HF	1 (5.0%)	1 (2.9%)	0.684
Obesity	6 (30.0%)	6 (17.6%)	0.196
Atrial Fibrillation	1 (5.0%)	4 (11.8%)	0.416
Valvular disease	1 (5.0%)	1 (2.9%)	0.662
PAD	1 (5.0%)	-	0.187
Dyslipidemia	5 (25.0%)	3 (8.8%)	0.108
Diabetes mellitus	4 (20.0%)	13 (38.2%)	0.277
Arterial hypertension	12 (60.0%)	20 (58.8%)	1.000
CKD	3 (15.0%)	4 (11.8%)	0.480
Smoking	6 (30.0%)	1 (2.9%)	0.090
COPD	3 (15.0%)	6 (17.6%)	0.776
Autoimmune disease	1 (5.0%)	3 (8.8%)	0.642

6.3.3. Differential lipidomic signature discerns between Covid-19 phenotypes

For lipidomic analysis, exploratory analysis was performed by unsupervised principal component analysis (PCA) which showed that the first 24 components explained the 95% of total variance (**supporting information figure S5.1**). To visualize classes separation supervised partial least square discriminant analysis (PLS-DA) was used. As shown in **figure 6.2 A,B** PLS-DA score plots clearly differentiated the healthy controls Covid-19 (−) from Covid-19 (+) patients, while in the context of Covid-19 group, the PLS-DA score could still discriminate between mild and severe phenotypes. The lipid features that contributed to the class separation and discrimination between the three groups were reported according to their variable of

importance in projection (VIP) scores, extracted by PLS-DA. The 15 highest scoring VIP lipids (VIP score ≥ 1.8) are shown in **figure 6.2 C**. Interestingly 9/15 lipids were lysophosphatidylcholines, in particular: six LPCs (LPC 20:1, LPC 18:0, LPC 20:2, LPC 17:0, LPC 16:0, LPC 18:1) three ether-linked LPCs (LPC O-16:0, LPC O-18:1, LPC O-16:1), two ether-linked phosphatidylcholines (PC O-34:3, isomers), whose levels were all lower in Covid-19 patients. The remaining four lipids were TGs (TG 18:1_18:2_22:6, TG 18:1_18:1_22:6, TG 16:0_18:1_22:5, TG 16:0_20:4_22:6) which, inversely, display upregulation in COVID-19 patients. We next performed univariate comparison on the internal standard normalized, log transformed and auto scaled dataset. A total of 191 out of 348 lipids were found significantly modulated ($p < 0.01$, FDR: 0.01%, complete results are reported in **supporting information table S5.2**) across the different classes. Noteworthy, ANOVA and significance analysis of metabolomics (SAM, **supporting information table S5.3**) shared six metabolites which were top listed as significant in all compared conditions namely: LPC 20:1, LPC O-16:0, LPC O-18:1, LPC 18:0, PC O-34:3 and LPC O-16:1. The heatmap, based on the top 50 lipid features (**figure 6.2 D**, p-value < 0.001), evidences the lipidome signature that discriminates the Covid (-) and the two different severity status. In particular, a progressive decrease of LPCs, LPC-Os, PC-Os and PCs, together with HexCers (HexCer 18:1;2O/22:0, HexCer 18:1;2O/24:0) and SMs (SM 39:1, SM 30:1, SM 42:1) can be observed from mild to severe status. Contrariwise, severe status is characterized by an increase in overall TGs, PEs (PE 18:0_22:6, PE 16:0_22:6, PE 16:0_18:1, PE 18:2_16:0, PE 16:1_22:5, PE 16:0_20:4) Cer (Cer 18:1;2O/24:1) and DG (DG 18:1_20:4) levels

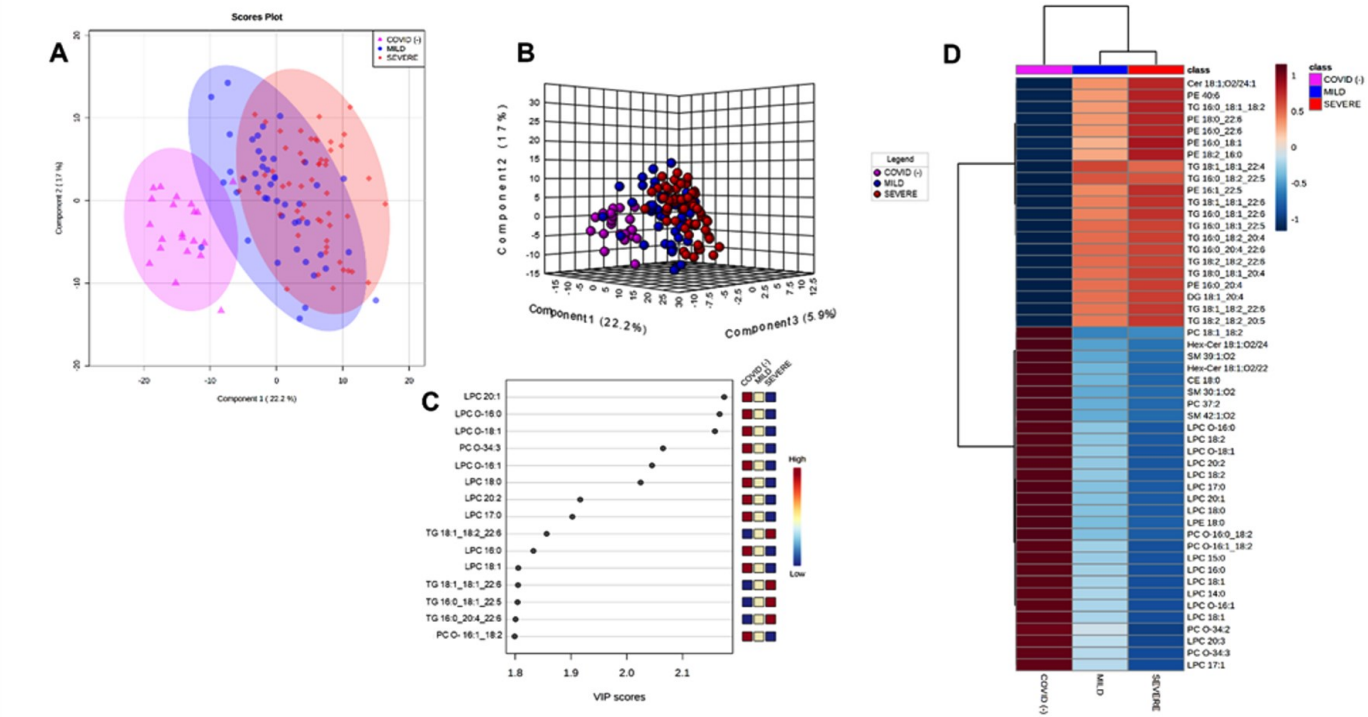

Figure 6.2. *2D (**A**) and 3D (**B**) PLS-DA model score plot showing the discrimination of different classes: Covid (−): red, Mild: green, Severe: blue. (**C**) The 15 highest scoring variables importance in projection (VIP) lipids are shown. The number of VIPs was established by setting the VIP-score ≥ 1.8 as a cutoff value. The colored boxes on the right indicate the relative amount of the corresponding lipid compound in each group. (**D**) Heatmap reporting the top 50 lipid compounds based on the univariate statistical analysis (ANOVA, p-value < 0.001, FDR < 0.01 %), the colors reflect the normalized lipid concentration.*

6.3.4. Lipidome signature predicts Covid-19 severity and outcome

The different lipid patterns between the control and Covid-19 group and, in particular, their progression along the phenotypes (from mild to severe) suggests that the lipidome signature measured at hospital admission could reflect the progression of disease and outcome. Therefore, to unveil the predictive potential of the discovered lipidome signature, we built a Random Forest (RF) machine learning (ML) model. The entire dataset was randomly divided into a training set, which was used to optimize and train the model, and a test set, to evaluate the model performance, which was assessed by area under curve (AUC) values of Receiver Operating Characteristic (ROC) curve. The model was trained on the complete annotated lipidome dataset (348 lipid features), by using repeated random subsampling cross validation (CV) (repeats = 100), the significance of the model's fit was computed using a permutation test with n=1000 obtaining a p-value of 0.005. The model reached AUC values of 0.751 (95% CI: 0.599-0.887) for severity and 0.815 (95% CI: 0.662-0.944) for outcome respectively; the ROC curves are reported in **figure 6.3 A, B**.

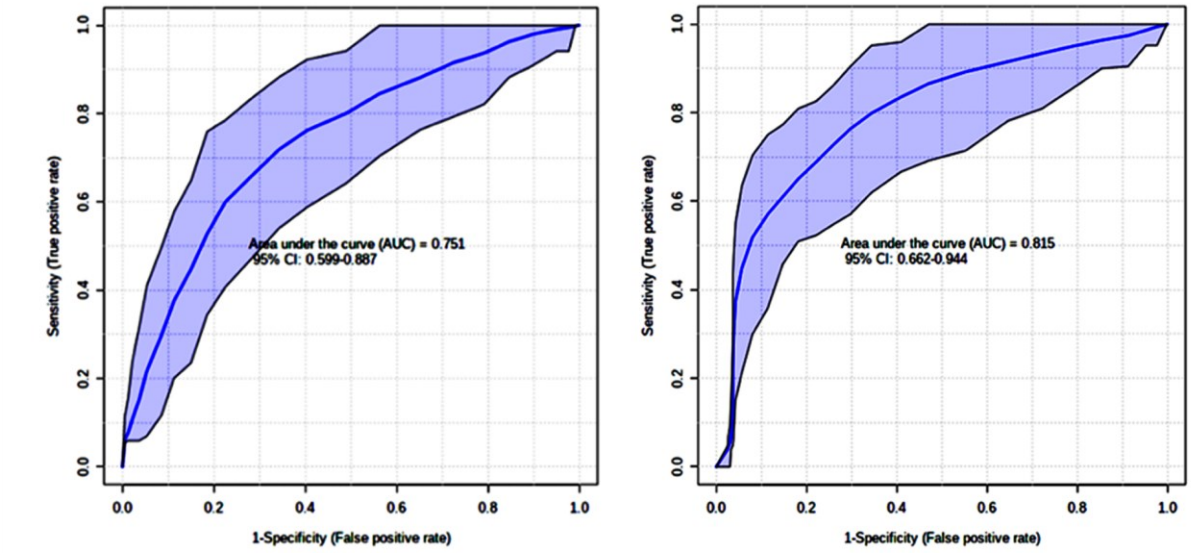

Figure 6.3. *ROC curves for severity (**A**) and outcome (**B**) obtained with the predictive model (RF) on the complete lipidome signature.*

The measurement of a large number of metabolites is challenging for potential fast clinical applications, which on the other hand would be easier with a reduced panel of the highest predictive compounds. Therefore, we aimed to evaluate which lipids could accurately discriminate mild from severe conditions, among the 90 unique lipids that contributed to the model. Hence after a rank aggregation based on the previous models, a final panel of six lipids was built, and their ROC curves are reported in **figure 6.4**. The panel was composed by: LPC O-18:1 (AUC: 0.858, SE: 80%, SP: 81%), LPC O-16:1 (AUC: 0.855, SE: 86%, SP: 75%), LPC O-16:0 (AUC: 0.865, SE: 75%, SP: 90%), PC O-34:3 (AUC: 0.846, SE 80%, SP: 80%), LPC 20:1 (AUC: 0.815, SE: 7815, SP:75%), LPC 18:0 (AUC: 0.800, SE: 65%, SP: 75%), p-value < 0.001.

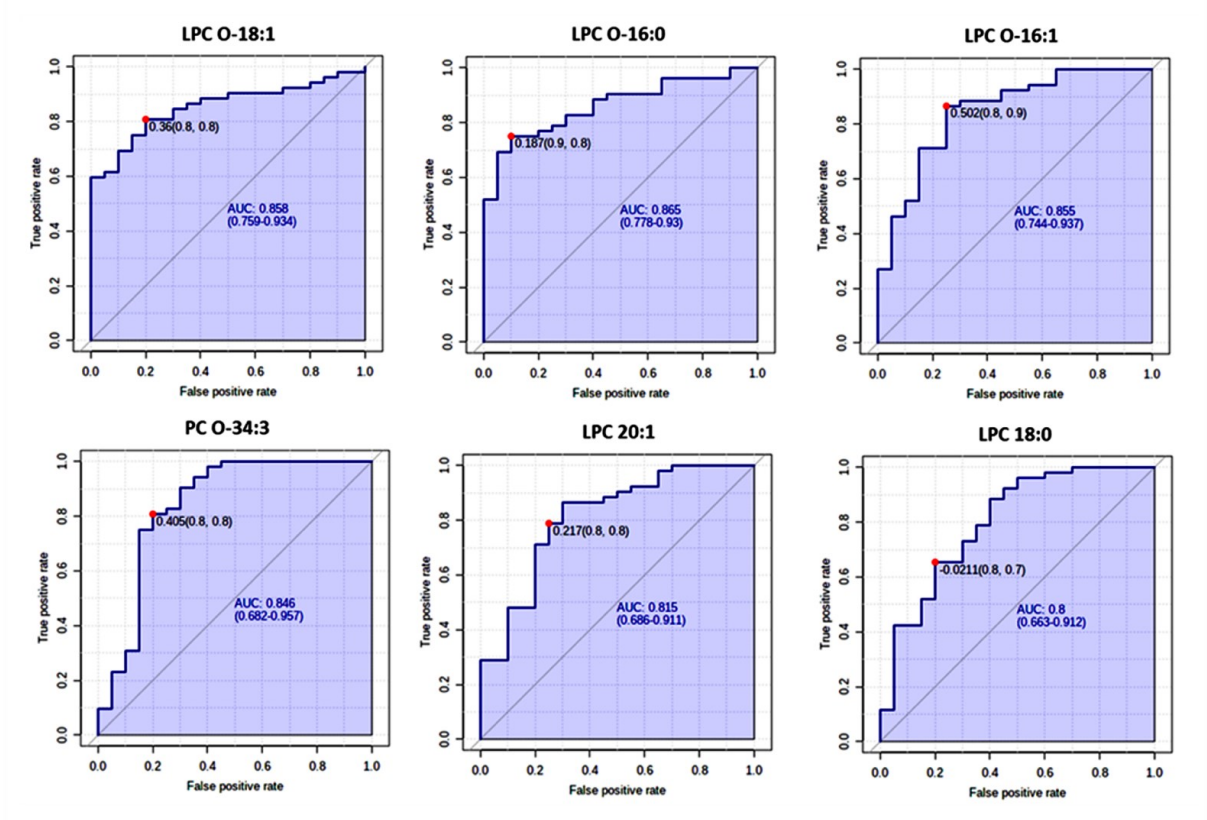

Figure 6.4. *ROC curves with the optimal cutoff calculated for each ROC analysis of the restricted lipid panel composed by LPC O-18:1, LPC O-16:1, LPC O-16:0, PC O-34:3, LPC 20:1, LPC 18:0.*

By using this restricted panel of lipids, the RF results highlighted a comparable predictive potential, with similar AUC values to the model built on the complete lipid profile, for severity (AUC= 0.777, 95% CI: 0.639-0.904, **figure 6.5**) and outcome (AUC= 0.789, 95% CI: 0.658-0.910, **figure 6.6**) respectively. These results are in line to other studies in which metabolomics have been used to identify metabolites associated to the severity status [17,18]. The models performances in cross validation for both analyses are comparable. In terms of accuracy and MCC, severity and outcome RF models achieved both 75% and ~0.50. Sensitivity and specificity are 73% and 78% for the mild class while for the survivor class are 69% and 81% respectively. Applying the model to the external test set the severity is predicted with accuracy of 70% and

0.41 MCC. The sensitivity of mild class prediction is 88% and specificity is 50%. While for the outcome model, the test set is predicted with accuracy of 67% and MCC of 0.32; sensitivity and specificity were 71% and 62% respectively for the survivor class. Accordingly, LPCs, LPC-Os and PC-O levels were significantly lower in the mild group with respect to severe (**figure 6.5**). The evaluation of the same lipids' panel in the subdivision of patients into survivors and non-survivors revealed the predictive potential of these molecules, which appeared substantially reduced in the non-survivor group (**figure 6.6**) as compared both to healthy subjects and survivors.

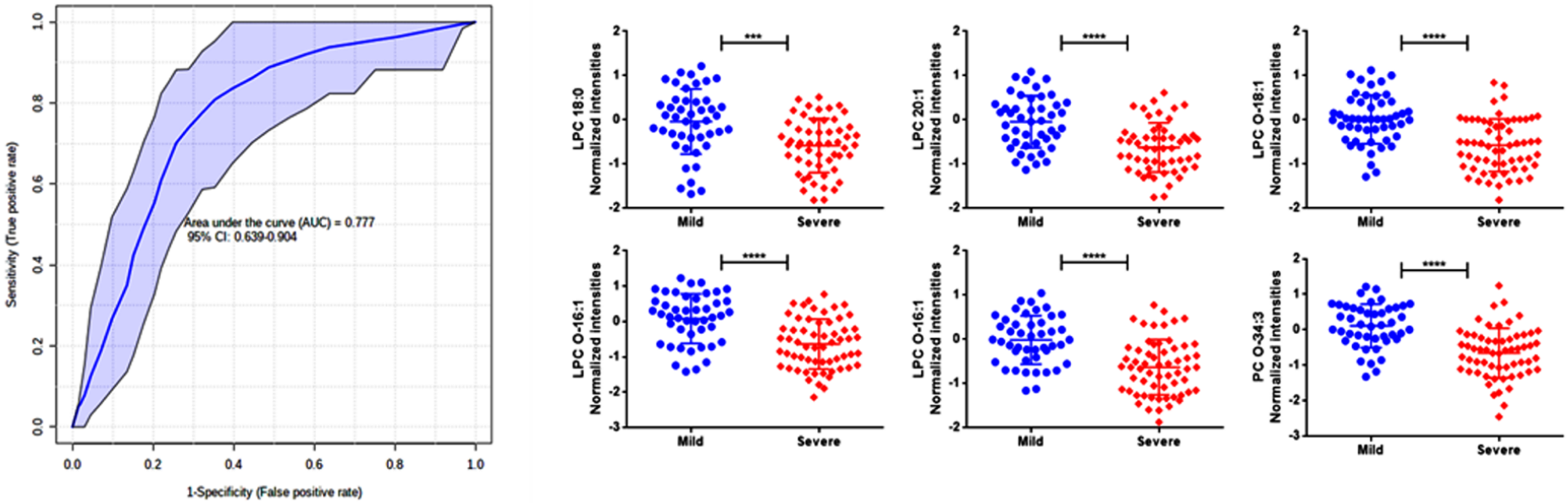

Figure 6.5. *ROC curves for severity obtained with the predictive model (RF) on the reduced lipid panel composed by LPC O-18:1, PC O-34:3, LPC 20:1, LPC O-16:1, LPC 18:0, LPC O-16:0 and comparison of normalized intensity of the selected lipid panel in Mild (blue) and Severe (red) patients. Results are expressed as mean ± SD. Unpaired t-test was performed (***: p= 0.0001; ****: p < 0.0001).*

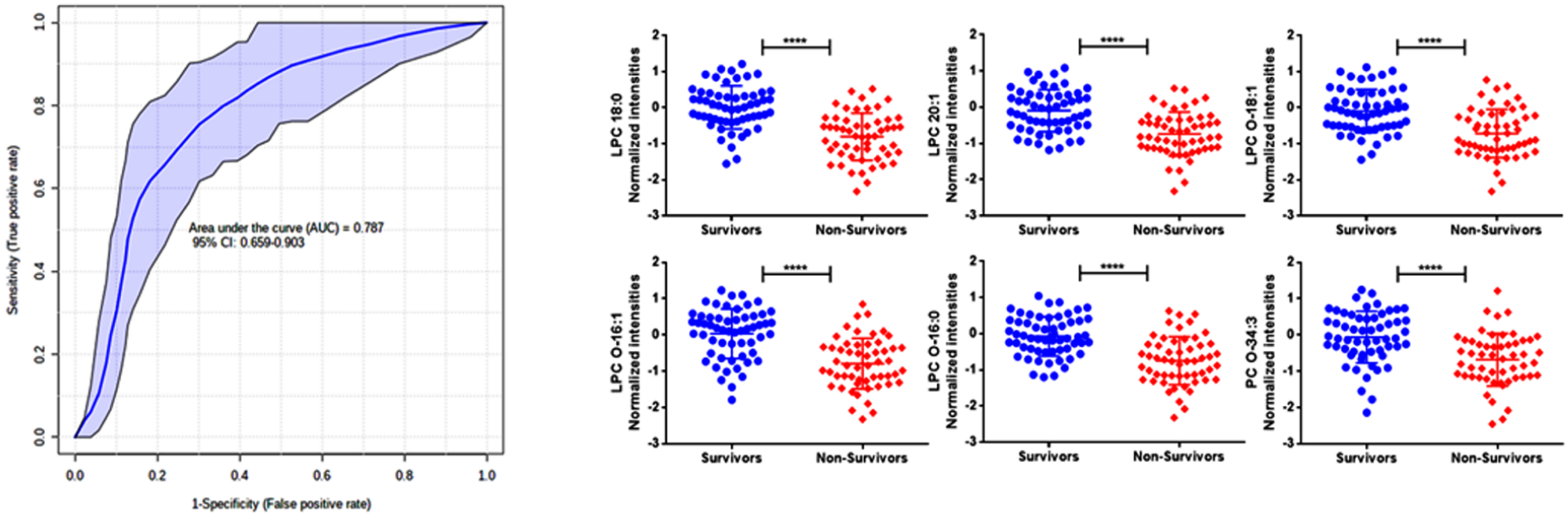

Figure 6.6. *ROC curves for outcome obtained with the predictive model (RF) on the reduced lipid panel composed by LPC O-18:1, PC O-34:3, LPC 20:1, LPC O-16:1, LPC 18:0, LPC O-16:0 and comparison of normalized intensity of the selected lipid panel in survivor (blues) compared to non-survivor patients (red). Results are expressed as mean ± SD. Unpaired t-test was performed (***: p= 0.0001; ****: p < 0.0001).*

Moreover, the LPCs, LPC-Os and PC-O levels in survivor and non-survivor have been evaluated for each phenotype (Mild and Severe). Again, in the severe group, their levels were consistently lower in non-survivor as compared to survivors (**supporting information figure S5.5**). The identified lipid panel could be used not only at t0 but over the course of the disease. In fact, re-building the model with the 25 longitudinal (t1) patients, 21 were correctly classified for their outcome, survivors and non survivors, showing the ability of the lipid panel in highlighting the dynamic changes of disease (**figure 5.7**).

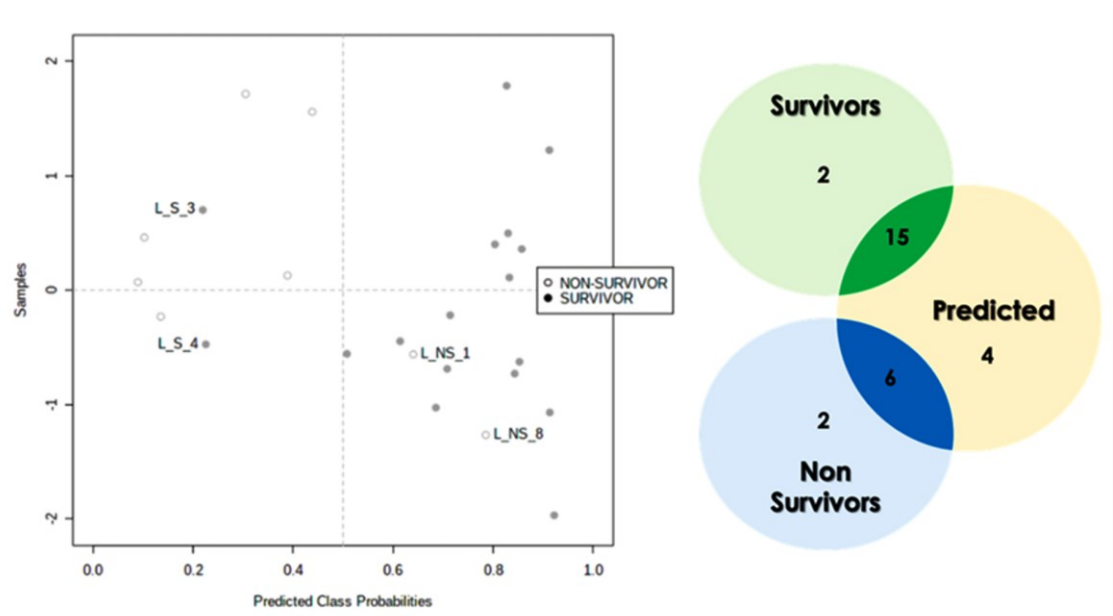

Figure 6.7. *Confusion matrix representing the performance of the model applied to 25 longitudinal (t1) Covid-19 patients. Samples classified into the wrong group were labeled (S: survivors, NS: non-survivors).*

Several conditions and demographic factors, such as age and comorbidities, predispose to a severe Covid-19 phenotype or even fatal outcome [19]. As indicated in **tables 6.1-6.3**, sex and age represent the only demographic factors within our patient cohort that resulted statistically

significant between mild and severe groups. Thus, we performed a new co-variate using linear models. As reported in the supporting information **figure S5.6**, this analysis revealed that, independently by age, the LPCs, LPC-Os and PC-O package reduction remain significantly associated with the outcome in males in the severe non-survivor group. This result is in agreement with the previous observation [20]. Moreover, the top features for the ML model remain unchanged regardless of patient demographic and reflected the severity and outcome trend (**supporting information figure S5.7**).

6.4. Discussion

Covid-19 evolves rapidly and dramatically, so the identification of early markers capable of predicting the patient's trajectory is essential. The target of our study was to identify a potential lipidomic signature that could mirror the severity and predict the short-term mortality of Covid-19 disease at the time of hospitalization, by using untargeted lipidomics, through the employment of a UHPLC-TIMS-MS approach which adds further confidence to lipid annotation [21]. We found that, among the different lipid classes, glycerophospholipids were the most discriminant between mild and severe conditions as well as with respect to non-Covid-19 patients; in particular several LPCs, LPC-Os and PC-O were the lipids with highest statistical significance, with a progressive decrease in relation to the severity status. Then, we sought if the lipidome signature could be used as a prognostic tool to identify potential progression from mild to severe condition and intra-hospital mortality. Using the entire dataset, we built a machine learning model that showed reasonable accuracy to predict the disease state. Interestingly, using a restricted panel of six lipids selected across the entire lipid profile, the model showed the comparable results for severity and outcome. Covid-19 pathogenesis is still not completely understood and lipids play a key role for SARS-CoV-2 replication [22] as observed for other human

coronavirus infections [23], suggesting that SARS-CoV-2 hijacks the host's lipid metabolism [24,25]. Indeed, lipidic profile can mirror a patient's biological status where internal and/or external perturbations activate molecular pathways involved in the immune response and metabolism. Our results show changes in LPCs and PCs in Covid-19 patients, and in particular, lower-level predicts intra-hospital mortality. A similar pattern was observed in patients with Ebola Virus Disease (EVD), where liver dysfunction and decay of choline metabolism affect LPCs and PCs synthesis and are associated with the severity of the disease. Furthermore, the following increase in LPCs and PCs in survivors confirm their potential use as a marker of severity [4]. Similarly, changes in LPCs and PCs in our cohort of Covid-19 patients can reflect the biological status and predict severity and mortality. Recently, several studies carried out in Italian cohorts investigated the possible relationship of lipidic profiles and infection-pathology severity revealing the alterations in serum concentrations of different lipids [6,15]. Our findings showing LPCs and PCs decrease could be an essential aspect to monitor during Covid-19 disease progression and fits with the observations of Fraser et al. [26] where the creatinine/arginine ratio was predictive of Covid-19 related mortality, and that a depressed plasma LPCs profile discern between Covid-19 and healthy patients. Recently, the discovery of a V-shape trend of lipids profile after patient recovery from severe status [18], fully support the important role of changed lipids profile in our study across survivors and non-survivors patients. Our data demonstrate that, within the entire lipidome signature, the progressive decrease of LPCs, LPC-Os and PC-O owns the highest accuracy in discriminating both severity and outcome. Previous targeted-MS based lipidomics studies were conducted to distinguish between asymptomatic Covid-19 and healthy subjects [27], or in diagnostics, to discriminate symptomatic Covid-19 and healthy patients, as a new tool to augment RT-PCR strategy [28]. In other studies, with comparable

numbers of patients, different proteomic and metabolomic profiles were demonstrated to be associated with clinical phenotypes of Covid-19, from mild to severe [29]. Other studies, have further supported and evidenced the potential role of the lipidomic profiles in Covid-19 in categorizing hospitalized Covid-19 patients, connecting the return to baseline levels to disease recovery [18]. Our study, while of relatively small size but comparable to other studies, is the first to propose, to our knowledge, that a restricted subset of six lipids (LPC O-18:1, PC O-34:3, LPC 20:1, LPC O-16:1, LPC 18:0, LPC O-16:0) not highlighted previously, could potentially predict intra-hospital mortality already at the time of the admission, in both mild and severe Covid-19 patients, and identify those patients requiring tight monitoring and/or intensive treatment. Finally, at a translational level, our results, unveiling a panel of LPCs, LPC-Os and PC-O predicting the severity and mortality in hospitalized Covid-19 patients, could suggest the potential employment of this simplified lipid panel as a predictive tool in faster, targeted approaches, using multiple reaction monitoring (MRM) strategy to obtain absolute quantitative data that could be easier employed in a clinical setting.

6.5. Limitation of the study

Firstly, our results were based on a single Italian cohort of Covid-19 patients, thus future studies with larger cohorts including different racial, ethnic, and geographical cohorts will be necessary for extending our current understanding of lipid metabolic dysregulation. In addition, the number of healthy subjects is relatively small. Before the translation to clinical settings, the prognostic value of the identified lipid panel on Covid-19 outcome should be applied to large and separate patients' cohorts, using targeted mass spectrometry methods and absolute quantification. Furthermore, even if our approach can be defined untargeted, and combines different tools for lipids ID assessment, particular lipid classes could be not detected by our method such

as Amadori-like phosphatidylethanolamines [30] or oxidized lipids, such as oxylipins, that require targeted or pseudo targeted approaches. In addition, other important polar metabolites could be included in the analysis, such as amino acids and acylcarnitines, to enrich the model.

6.6. Materials and methods

6.6.1. Study design and participants

A cohort of 99 patients diagnosed with Covid-19 (SARS-CoV-2 infection) admitted at the University Hospital "Giovanni Da Procida", Salerno, Italy, was enrolled between October 2020 and March 2021. The cohort's median age was 68 years old, and the female proportion was 61%. At admission, patients were classified according to the clinical phenotype following World Health Organization (WHO) severity score as Mild patients (hospitalized patients requiring or not supplemental oxygen; n = 45), or Severe patients (hospitalized patients requiring non-invasive ventilation or high-flow oxygen therapy; intubation and mechanical ventilation, or ventilation with additional organ support; n = 54) [World Health Organization. WHO R&D Blueprint. Novel Coronavirus: COVID-19 Therapeutic Trial Synopsis. Draft February 18, 2020 [www.who.int/blueprint/priority-diseases/key-action/COVID-19_Treatment_Trial_Design_Master_Protocol_synopsis_Final_18022020.pdf]. Patients were further followed up until hospital discharge or death and subdivided into survivors (Mild, n = 37; Severe, n = 20) and non-survivors (Mild, n = 8; Severe, n = 34).

Blood samples from all patients were collected at the time of admission (Time 0). In a subgroup of patients (n = 25) we collected a second blood sample (Time 1) in correspondence of clinical and symptoms changes (phenotypical switch).

Healthy and SARS-CoV-2 negative subjects (n = 21) of age 50.21 ± 10.29 and 50% of females were recruited from healthcare workers at the University Hospital "San Giovanni di Dio e Ruggi d'Aragona".

The study protocol was approved by the local Ethics Committee (prot./SCCE no. 71262, May 2020). All methods and experimental procedures were performed under the Declaration of Helsinki.

6.6.2. Blood sample Processing

From each patient, 5-8 mL of whole blood was drawn into EDTA vacutainers and centrifuged at 1.000 g for 20 minutes at 25°C to separate blood cells and plasma. After collection, plasma samples were aliquoted and stored at – 80°C until analysis.

6.6.3. Plasma lipidome extraction

Before extraction, samples were randomized and split in regular sub-groups. Lipids were extracted following the Matyash et al. protocol [31], with slight modifications: briefly, 20 µL of plasma were thawed on ice and added to 225 µL of ice cold MeOH containing a mix of deuterated standards (Splash Lipidomix®, Avanti Polar Lipids, Alabaster, AL, U.S.A) and vortexed for 10 s. Subsequently, 750 µL of cold methyl tert-butyl ether (MTBE) were transferred to the tube and the solution was shaken in a thermomixer (Eppendorf) for 10 min, 300 rpm at 4°C. Then, 188 µL of H_2O were added and samples were vortexed for 20 s and centrifuged at 14680 rpm, for 10 min at 4°C to induce phase separation. The upper layer was collected and evaporated using a SpeedVac (Savant, Thermo Scientific, Milan, Italy). The dried samples were dissolved in 100 µL of BuOH/IPA/H_2O 8/23/69 (v/v) before the UHPLC-TIMS analysis. A quality control (QC) sample was prepared by pooling the same aliquot (3 µL) from each sample. Unless

otherwise described, all solvents and additives were LC-MS grade and purchased by Merck (Darmstadt, Germany).

6.6.4. RP-UHPLC-TIMS-Q-TOF method parameters

UHPLC-TIMS analyses were performed on a Thermo Ultimate RS 3000 UHPLC coupled online to a TimsTOF Pro quadrupole Time of flight (Q-TOF) (Bruker Daltonics, Bremen, Germany) equipped with an Apollo II electrospray ionization (ESI) probe. The separation was performed with an Acquity UPLC CSH C18 column (100 × 2.1 mm; 1.7 µm) protected with a VanGuard CSH precolumn (5.0 × 2.1 mm; 1.7 µm, 130 Å) (Waters, Milford, MA, U.S.A). The column temperature was set at 55°C, a flow rate of 0.4 mL/min was used, mobile phase consisted of (A): ACN/H_2O with 10 mM $HCOONH_4$ and 0.1% HCOOH 60:40 (v/v) and (B): IPA/ACN with 10 mM $HCOONH_4$ and 0.1% HCOOH 90:10 (v/v). The following gradient has been used: 0 min, 40% B; 2 min, 43% B; 2.10 min, 50% B; 12 min, 54% B; 12.10 min, 70% B; 17 min, 99% B; 17.10 min, 99% B; 17.2, 40% B and then 2.8 min for column re-equilibration. The analyses were performed in data-dependent parallel accumulation serial fragmentation (DDA-PASEF) with both positive and negative ionization, in separate runs. The injection volume was set at 3 µL for the positive mode and 5 µL for the negative mode. Source parameters: Nebulizer gas (N_2) pressure: 4.0 Bar, Dry gas (N_2): 10 l/min, Dry temperature: 250°C. Mass spectra were recorded in the range m/z 100–1500, with an accumulation and ramp time to 100 ms each. The ion mobility was scanned from 0.55 to 1.70 Vs/cm^2. Precursors for data-dependent acquisition were isolated within ± 2 m/z and fragmented with an ion mobility-dependent collision energy, 30 eV in positive mode, and 40 eV in negative mode. The total acquisition cycle was of 0.32 s and comprised one full TIMS-MS scan and two PASEF MS/MS scans. Exclusion time was set to 0.1 min, Ion charge control (ICC) was set to 7.5 Mio. The instrument

was calibrated for both mass and mobility using the ESI-L Low Concentration Tuning Mix with the following composition: [m/z, 1/K0: (322.0481, 0.7318 Vs cm^{-2}), (622.0290, 0.9848 Vs cm^{-2}), (922.0098, 1.1895 Vs cm^{-2}), (1221,9906, 1.3820 Vs cm^{-2})] in positive mode and [m/z, 1/K0: (301.99814, 0.6678 Vs cm^{-2}), (601.97897, 0.8781 Vs cm^{-2}), (1033.98811, 1.2525 Vs cm^{-2}), (1333.96894, 1.4015 Vs cm^{-2})] in negative mode.

6.6.5. RP-UHPLC-TIMS-Q-TOF data analysis and processing

4D data alignment, filtering and annotation was performed with Metaboscape 2021 (Bruker) employing a feature finding algorithm (T-Rex 4D) that automatically extracts buckets from raw files. At the beginning of each LC-MS run, a mixture (1:1 v/v) of 10mM sodium formate calibrant solution and ESI-L Low Concentration Tuning Mix was injected to recalibrate, respectively, both the mass and mobility data. Feature detection was set to 500 and 250 counts for positive and negative modes. The minimum number of data points in the 4D TIMS space was set to 100, and recursive feature extraction was used. Lipid annotation was performed first with a rule-based annotation and subsequently using the LipidBlast spectral library of MS DIAL (http://prime.psc.riken.jp/compms/msdial/main.html) with the following parameters: tolerance: narrow 2 ppm, wide 10 ppm; mSigma: narrow 30, wide 250, MS/MS score: narrow 800, wide 150, cross collisional section % (CCS %): narrow 2, wide 5. The spectra were processed in positive mode using $[M+H]^+$, $[M+Na]^+$, $[M+K]^+$, $[M+H\text{-}H_2O]^+$ and $[M+NH_4]^+$ ions in positive mode, while $[M-H]^-$, $[M+Cl]^-$, $[M+HCOO]^-$ and $[M\text{-}H_2O]^-$ in negative mode, the assignment of the molecular formula was performed for the detected features using Smart Formula™ (SF). For the assessment of repeatability and instrument stability over time, a QC strategy was applied [22] using pooled plasma samples inserted during the batch regularly together with a mixture of authentic lipid standards [LightSPLASH®, Avanti Polar Lipids] to monitor

specific retention time and response modification of lipid subclasses. Samples were injected in randomized order and blank samples were injected regularly and used to assess and exclude background signals.

6.6.6. Statistical analysis

Univariate and multivariate statistics was performed with MetaboAnalyst 5.0 (https://www.metaboanalyst.ca). Data preprocessing consisted of the following steps: all lipids missing in more than 50% in QCs and 75% in real samples were excluded, furthermore all lipids with a coefficient of variation (CV %) higher than 35% among QCs samples were discarded. In order to flatten the differences between samples and to avoid bias in the statistical analysis, we first normalized lipid intensities with the corresponding deuterated internal standard and then the dataset was log transformed and auto scaled. A preliminary investigation was carried out using Principal Component Analysis (PCA) on pre-processed data. Then, Partial Least Square Discriminant Analysis (PLS-DA) model was built in order to discriminate between healthy patients and mild and severe covid patients. K-fold cross-validation was performed, splitting the data into 10 subgroups to select the optimal number of Latent Variables (nLVs). The nLVs were selected maximizing the accuracy in cross validation. PLSDA solves classification problems with more than 2 classes and in the scenario where there is a high number of variables and low samples [32]. Statistical analysis between patients' characteristics were analyzed using student t test using SPSS v25.

Variable importance in projection (VIP) scores, based on PLS-DA results, and Significance analysis of Metabolomics (SAM), giving a delta value of 1.5, were used to identify lipids responsible for the maximum separation of the groups. For univariate data analysis, one-way ANOVA corrected by Fisher's LSD post hoc analysis for intergroup comparison (Covid (-),

Mild, Severe) was performed, setting a threshold of significance of false discovery rate (FDR) adjusted p-value of 0.01. Receiver operating characteristic (ROC) analysis was carried out with the Biomarker analysis tool in Metaboanalyst 5.0. A random forest (RF) machine learning (ML) algorithm was performed, after splitting the cohort in a training set and a test set, was tested as a predictive model. Lipid features were ranked according to the specific metrics of each modeling method (p-values, absolute loading values from PCA, the variable importance in projection from PLS-DA, delta value on SAM analysis, and the feature importance from the RF model). A multivariate ROC curve model was compared with the whole lipid profile.

6.7. Conclusions

Covid-19 is a well-documented metabolic disease. Lipidomics can be a useful tool to identify potential new diagnostic and prognostic biomarkers. We developed an UHPLC-TIMS/MS method, that allowed to increase the confidence of the identified molecules being identified on 4 dimensions (RT, MS, MS/MS, CCS).

The combined HRMS and statistics approach let us possible to identify a signature of six lipids with an apparently correlation with the severity of the Covid-19 disease. The analysis on longitudinal patients seem to confirm the predictive power of these molecules, which are therefore candidates as potential prognostic biomarkers of Covid-19.

6.8. References

[1] Livingston E. and Bucher K. Coronavirus Disease 2019 (COVID-19) in Italy. *JAMA*. **2020**. 323 (14): 1335.

[2] Ayres J.S. A metabolic handbook for the COVID-19 pandemic. *Nat Metab*. **2020**. 2: 572-585.

[3] De Bruin S., Bos L.D., Van Roon M.A., Tuip-De Boer A.M., Schuurman A.R., Koel-Simmelinck M.J.A., Bogaard H.J., Tuinman P.R., Van Agtmael M.A., Hamann J., Teunissen C.E., Wiersinga W.J., Koos Zwinderman A.H., Brouwer M.C., Van De Beek D., Vlaar A.P.J., Amsterdam UMC COVDI-19 Biobank Investigators. Clinical features and prognostic factors in Covid-19: A prospective cohort study. *EBioMedicine.* **2021**. 67: 103378.

[4] Kyle J.E., Burnum-Johnson K.E., Wendler J.P., Eisfeld A.J., Halfmann P.J., Watanabe T., Sahr F., Smith R.D., Kawaoka Y., Water, K.M., Metz T.O. Plasma lipidome reveals critical illness and recovery from human Ebola virus disease. *Proc Natl Acad Sci U S A*. **2019**. 116: 3919-3928.

[5] Wu D., Shu T., Yang X., Song J.X., Zhang M., Yao C., Liu W., Huang M., Yu Y., Yang Q., Zhu T., Xu J., Mu J., Wang Y., Wang H., Tang T., Ren Y., Wu Y., Lin S.H., Qiu Y., Zhang D.Y., Shang Y., Zhou X. Plasma metabolomic and lipidomic alterations associated with COVID-19. *Natl Sci Rev*. **2020**. 7: 1157-1168.

[6] Caterino, M., Gelzo M., Sol S., Fedele R., Annunziata A., Calabrese C., Fiorentino G., D'Abbraccio M., Dell'Isola C., Fusco F.M., Parrella R., Fabbrocini G., Gentile I., Andolfo I., Capasso M., Costanzo M., Daniele A., Marchese E., Polito R., Russo R., Missero C., Ruoppolo M., Castaldo G. Dysregulation of lipid metabolism and pathological inflammation in patients with COVID-19. *Sci Rep*. **2021**, 11 (1): 2941.

[7] Eisfeld A.J., Halfmann P.J., Wendler J.P., Kyle J.E., Burnum-Johnson K.E., Peralta Z., Maemura T., Walters K.B., Watanabe T., Fukuyama S., Yamashita M., Jacobs J.M., Kim Y.M., Casey C.P., Stratton K.G., Webb-Robertson B.M., Gritsenko M.A., Monroe M.E., Weitz K.K., Shukla A.K., Tian M., Neumann G., Reed J.L., Van Bakel H., Metz T.O., Smith R.D., Waters K.M., N'jai A., Sahr F., Kawaoka Y. Multi-platform 'Omics Analysis of Human Ebola Virus Disease Pathogenesis. *Cell Host Microbe*. **2017**. 22: 817-829.

[8] Queiroz A., Pinto I.F.D., Lima M., Giovanetti M., De Jesus J.G., Xavier J., Barreto F.K., Canuto G.A.B., Do Amaral H.R., De Filippis A.M.B., Mascarenhas D.L., Falcao M.B., Santos N.P., Azevedo V.A.C., Yoshinaga M.Y., Miyamoto S., Alcantara L.C.J. (2019). Lipidomic Analysis Reveals Serum Alteration of Plasmalogens in Patients Infected With ZIKA Virus. *Front Microbiol*. **2019**. 10: 753.

[9] Rezaei A., Neshat S., Heshmat-Ghahdarijani K. Alterations of Lipid Profile in COVID-19: A Narrative Review. *Curr Probl Cardiol*. **2021**. 47 (3): 100907.

[10] Ebrahimi K.H., Mccullagh J.S.O. A lipidomic view of SARS-CoV-2. *Biosci Rep*. **2021**. 41 (8): BSR20210953.

[11] Li Y., Zhang Y., Lu R., Dai M., Shen M., Zhang J., Cui Y., Liu B., Lin F., Chen L., Han D., Fan Y., Zeng Y., Li W., Li S., Chen X., Li H., Pan P. Lipid metabolism changes in patients with severe COVID-19. *Clin Chim Acta*. **2021**. 517: 66-73.

[12] Schwarz B., Sharma L., Roberts L., Peng X., Bermejo S., Leighton I., Casanovas-Massana A., Minasyan M., Farhadian S., Ko A.I., Yale I.T., Dela Cruz C.S., Bosio C.M. Cutting Edge: Severe SARS-CoV-2 Infection in Humans Is Defined by a Shift in the Serum Lipidome, Resulting in Dysregulation of Eicosanoid Immune Mediators. *J Immunol*. **2021**. 206: 329-334.

[13] Holcapek M., Liebisch G., Ekroos K. Lipidomic Analysis. *Anal Chem*. **2019**. 90: 4249-4257.

[14] Song J.W., Lam S.M., Fan X., Cao W.J., Wang S.Y., Tian H., Chua G.H., Zhang C., Meng F.P., X, Z., Fu J.L., Huang L., Xia P., Yang T., Zhang S., Li B., Jiang,T.J., Wang R., Wang Z., Shi M., Zhang J.Y., Wang F.S., Shui G. Omics-Driven Systems Interrogation of Metabolic Dysregulation in COVID-19 Pathogenesis. *Cell Metab*. **2020**. 32 (2):188-202.

[15] Barberis E., Timo S., Amede E., Vanella V.V., Puricelli C., Cappellano G., Raineri D., Cittone M.G., Rizzi E., Pedrinelli A.R., Vassia V., Casciaro F.G., Priora S., Nerici I., Galbiati A., Hayden E., Falasca M., Vaschetto R., Sainaghi P.P., Dianzani U., Rolla R., Chiocchetti A., Baldanzi G., Marengo E., Manfredi M. Large-Scale Plasma Analysis Revealed New Mechanisms and Molecules Associated with the Host Response to SARS-CoV-2. *Int J Mol Sci*. **2020**. 21 (22): 8623.

[16] Wu D., Shu T., Yang X., Song J.X., Zhang M., Yao C., Liu W., Huang M., Yu Y., Yang Q., Zhu T., Xu J., Mu J., Wang Y., Wang H., Tang T., Ren Y., Wu Y., Lin S.H., Qiu Y., Zhang D.Y., Shang Y., Zhou X. Plasma metabolomic and lipidomic alterations associated with COVID-19. *Natl Sci Rev*. **2020** .7 (7): 1157-1168.

[17] Roberts I., Wright Muelas M., Taylor J.M., Davison A.S., Xu Y., Grixti J.M., Gotts N., Sorokin A., Goodacre R., Kell D.B. Untargeted metabolomics of COVID-19 patient serum reveals potential prognostic markers of both severity and outcome. *Metabolomics*. **2021**. 18 (1): 6.

[18] Sindelar M., Stancliffe E., Schwaiger-Haber M., Anbukumar D.S., Adkins-Travis K., Goss C.W., O'halloran J.A., Mudd P.A., Liu W.C., Albrecht R.A., Garcia-Sastre A., Shriver

L.P., Patti G.J. Longitudinal metabolomics of human plasma reveals prognostic markers of COVID-19 disease severity. *Cell Rep Med*. **2021**. 2 (8): 100369.

[19] Iaccarino G., Grassi G., Borghi C., Ferri C., Salvetti M., Volpe M., Investigators S.-R. Age and Multimorbidity Predict Death Among COVID-19 Patients: Results of the SARS-RAS Study of the Italian Society of Hypertension. *Hypertension*. **2020**. 76: 366-372.

[20] Gebhard C., Regitz-Zagrosek V., Neuhauser H.K., Morgan R., Klein S.L. Impact of sex and gender on COVID-19 outcomes in Europe. *Biol Sex Differ*. **2020**. 11 (1): 29.

[21] Vasilopoulou C.G., Sulek K., Brunner A.D., Meitei N.S., Schweiger-Hufnagel U., Meyer S.W., Barsch A., Mann M., Meier F. Trapped ion mobility spectrometry and PASEF enable in-depth lipidomics from minimal sample amounts. *Nat Commun*. **2020**. 11 (1): 331.

[22] Abu-Farha M., Thanaraj T.A., Qaddoumi M.G., Hashem A., Abubaker J., Al-Mulla F. The Role of Lipid Metabolism in COVID-19 Virus Infection and as a Drug Target. *Int J Mol Sci*. **2020**. 21 (10): 3544.

[23] Yan B., Chu H., Yang D., Sze K.H., Lai P.M., Yuan S., Shuai H., Wang Y., Kao R.Y., Chan J.F., Yuen K.Y. Characterization of the Lipidomic Profile of Human Coronavirus-Infected Cells: Implications for Lipid Metabolism Remodeling upon Coronavirus Replication. *Viruses*. **2019**. 11 (1): 73.

[24] Wei X., Zeng W., Su J., Wan H., Yu X., Cao X., Tan W., Wang H. Hypolipidemia is associated with the severity of COVID-19. *J Clin Lipidol*. **2020**. 14 (3): 297-304.

[25] Nardacci R., Colavita F., Castilletti C., Lapa D., Matusali G., Meschi S., Del Nonno F., Colombo D., Capobianchi M.R., Zumla A., Ippolito G., Piacentini M., Falasca L. Evidences for lipid involvement in SARS-CoV-2 cytopathogenesis. *Cell Death Dis*. **2021**. 12 (3): 263.

[26] Fraser D.D., Slessarev M., Martin C.M., Daley M., Patel M.A., Miller M.R., Patterson E.K., O'gorman D.B., Gill S.E., Wishart D.S., Mandal R., Cepinskas G. Metabolomics Profiling of Critically Ill Coronavirus Disease 2019 Patients: Identification of Diagnostic and Prognostic Biomarkers. *Crit Care Explor*. **2020**. 2 (10): e0272.

[27] Hao Y., Zhang Z., Feng G., Chen M., Wan Q., Lin J., Wu L., Nie W., Chen S. Distinct lipid metabolic dysregulation in asymptomatic COVID-19. *iScience*. **2021**. 24 (9): 102974.

[28] Gray N., Lawler N.G., Zeng A.X., Ryan M., Bong S.H., Boughton B.A., Bizkarguenaga M., Bruzzone C., Embade N., Wist J., Holmes E., Millet O., Nicholson J.K., Whiley L. Diagnostic Potential of the Plasma Lipidome in Infectious Disease: Application to Acute SARS-CoV-2 Infection. *Metabolites*. **2021**. 11 (7): 467.

[29] Shen B., Yi X., Sun Y., Bi X., Du J., Zhang C., Quan S., Zhang F., Sun R., Qian L., Ge W., Liu W., Liang S., Chen H., Zhang Y., Li J., Xu J., He Z., Chen B., Wang J., Yan H., Zheng Y., Wang D., Zhu J., Kong Z., Kang Z., Liang X., Ding X., Ruan G., Xiang N., Cai X., Gao H., Li L., Li S., Xiao Q., Lu T., Zhu Y., Liu H., Chen H., Guo T. Proteomic and Metabolomic Characterization of COVID-19 Patient Sera. *Cell*. **2020** .182 (1): 59-72.

[30] Miyazawa T., Ibusuki D., Yamashita S., Nakagawa K. Analysis of amadori-glycated phosphatidylethanolamine in the plasma of healthy subjects and diabetic patients by liquid chromatography-tandem mass spectrometry. *Ann N Y Acad Sci*. **2008**. 1126: 291-294.

[31] Matyash V., Liebisch G., Kurzchalia T.V., Shevchenko A., Schwudke D. Lipid extraction by methyl-tert-butyl ether for high-throughput lipidomics. *J Lipid Res*. **2008**. 49 (5): 1137-1146.

[32] Guardia M.D.L., GonzáLvez A. Food protected designation of origin: methodologies and applications. Oxford: Elsevier Science & Technology. **2013**.

CHAPTER VII

Supporting information

7.1. Supporting information for Chapter II: "Targeting the ASMase/S1P pathway protects from sortilin-evoked vascular damage in hypertension"

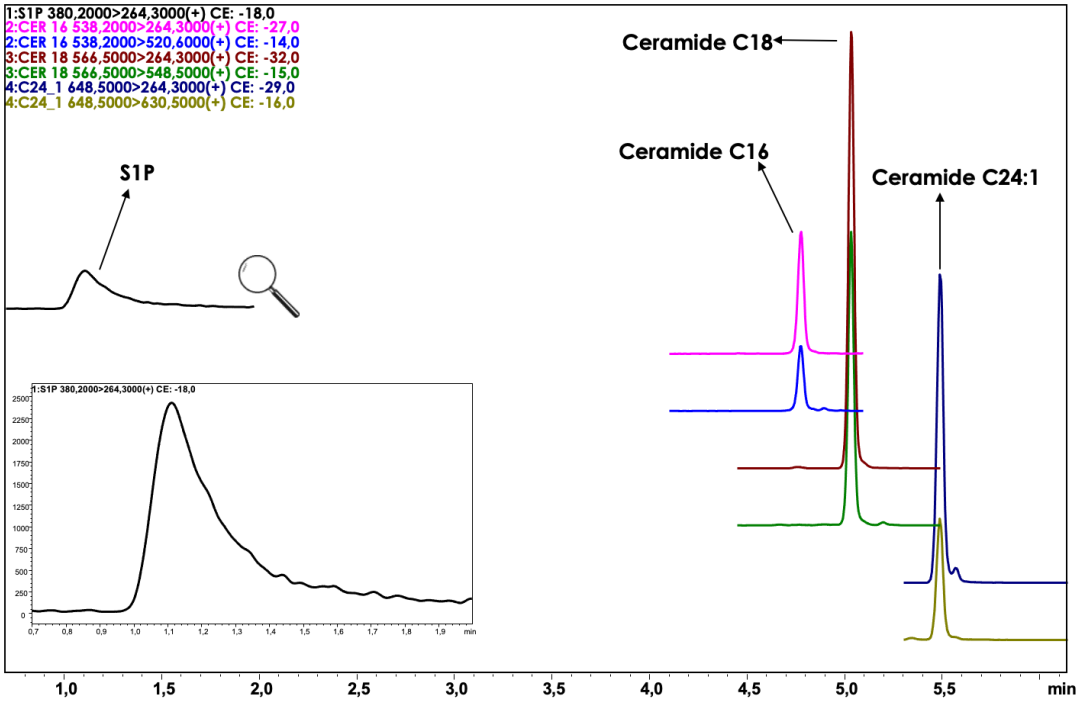

Figure S1.1. *Multiple reaction monitoring (MRM) chromatogram for sphingolipids extract.*

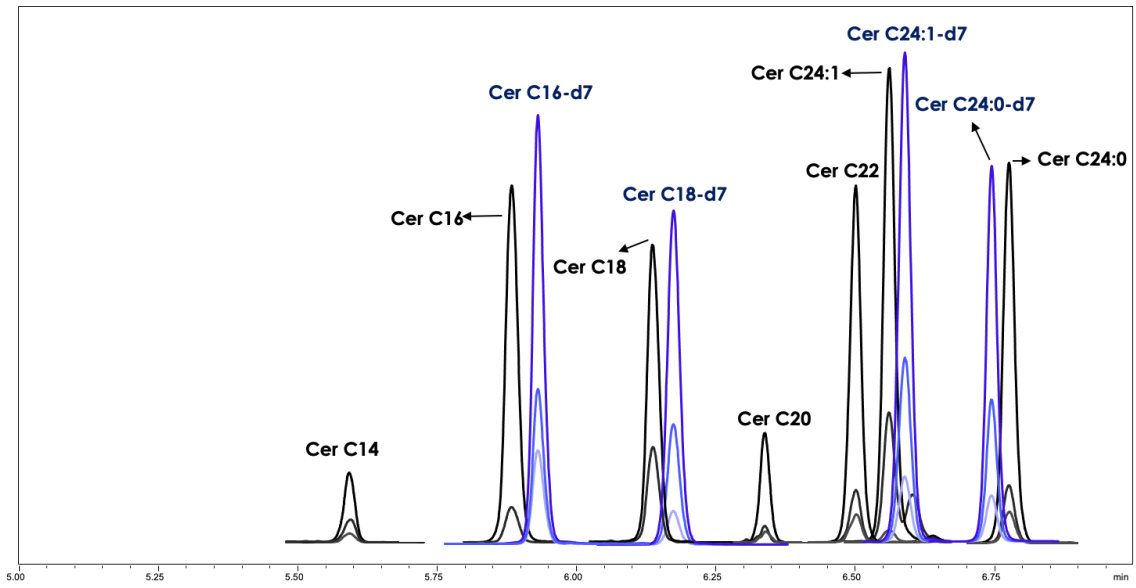

Figure S1.2. *Multiple reaction monitoring chromatogram of the monitored final ceramides panel, including sphingolipids optimized by LipidCreator. An overlay of MRM transitions of each sphingolipid is shown.*

7.1.1. Fast untargeted profiling of sphingolipids alteration by MRMS (Magnetic Resonance Mass Spectrometry)

7.1.1.1. Extraction

Twenty-four patients with hypertension (defined as DBP ≥90 mmHg and/or SBP ≥140 mm Hg or on the basis of use of anti-hypertensive medication) and 9 healthy donor control subjects (non-smokers and non-diabetic) without previous cardiovascular events and not on statin therapy, belonging to the Campania Salute Network Registry, were studied. Plasma samples were thawed and extracted with methanol (MeOH) and methyl-tert-butyl ether (MTBE). Briefly, 225 µL of MeOH was added to 20 µL of plasma and the mixture was vortexed for 10 seconds. Then 750 µL of MTBE was added and the obtained solution was incubated at 300 rpm for six minutes at 4°C. Afterwards, 188 µL of H_2O was added to induce phase separation and the mixture was vortexed for 20 seconds. After centrifuging for five minutes at 14680 rpm, 650 µL of the upper

organic phase was transferred into a new vial and dried. For mass spectrometric analysis, the sample (organic phase) was solubilized in 200 µL of 5 mM ammonium acetate 90% MeOH/DCM (2:1v/v).

7.1.1.2. MS Analysis

Analyses were performed by direct infusion using electrospray ionization with a 250 µL syringe at a flow rate of 2 µL/min. Data were acquired on a solariX XR 7T (Bruker Daltonik GmbH, Bremen, Germany). The instrument was tuned and calibrated with a standard solution of NaTFA (0.1 mg/mL in 50% acetonitrile). Mass spectra were acquired in broadband mode in the range 100-1200 *m/z* with an ion accumulation time of 10 ms. 32 single scans were added for the final mass spectrum using 2 million data points (2M). Nebulizing gas pressure was set to 1 bar. Drying gas pressure was set to 4 L/min at a temperature of 200°C. Both positive and negative ionization modes were employed. Five measurement replicates of each sample were performed.

7.1.1.3. Data processing

Peak alignment and putative annotation of compounds based on accurate MS measurements was performed in MetaboScape 4.0 (Bruker Daltonik GmbH, Bremen,Germany). LipidMAPS was used as the analyte list for compound identification.

7.1.1.4. Results and Discussion

In order to have a look at possible further altered sphingolipids in the context of hypertension, but not monitorable with the targeted developed approach, we decided to investigate the analytical potential of the FT-ICR system. Indeed, the untargeted lipidome profiling is usually carried out by liquid chromatography coupled to tandem mass spectrometry (LC-MS/MS). As an alternative to LC-MS/MS, which can suffer of long analysis time and lack of reproducibility due to retention time drift, direct infusion Fourier transform ion cyclotron resonance mass

spectrometry (FT-ICR/MS) provides very fine isotopic distribution as well as high mass accuracy for metabolite identification, allowing analysis without front-end separation step and derivatization. This MRMS workflow maximizes high throughput in metabolic profiles and 37 sphingolipids (SPs), belonging to different subclasses and shown in the fold-change graph (**figure S1.3**), were putatively annotated with very good mass accuracy (average error <0.1 ppm). Interestingly, the results revealed an increase in the average intensities of several deoxyceramides and three sphinganines (**figure S1.4**). These results should be further confirmed by a prospective large cohort and the identification corroborated by a deep MS/MS investigation.

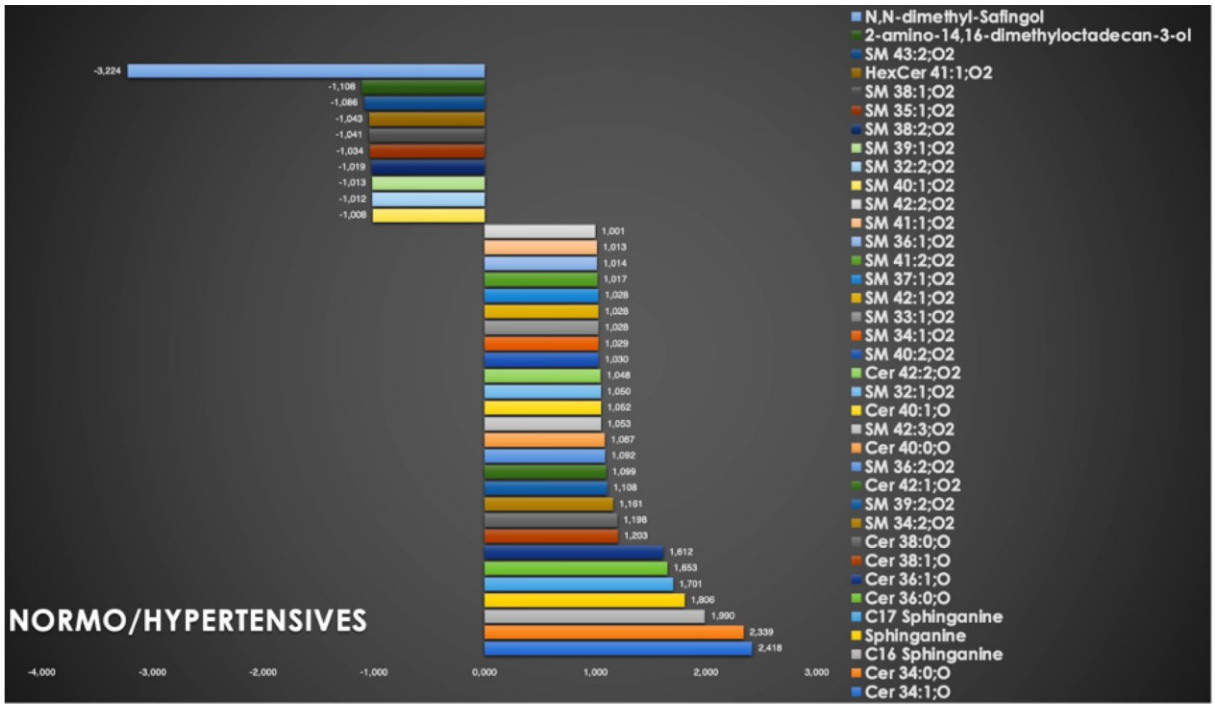

Figure S1.3. *Fold change bar graph of the putative sphingolipids identified in human plasma samples in the direction normotensives/hypertensives (SM: sphingomyelin; Cer: ceramide, HexCer: hexosylceramide).*

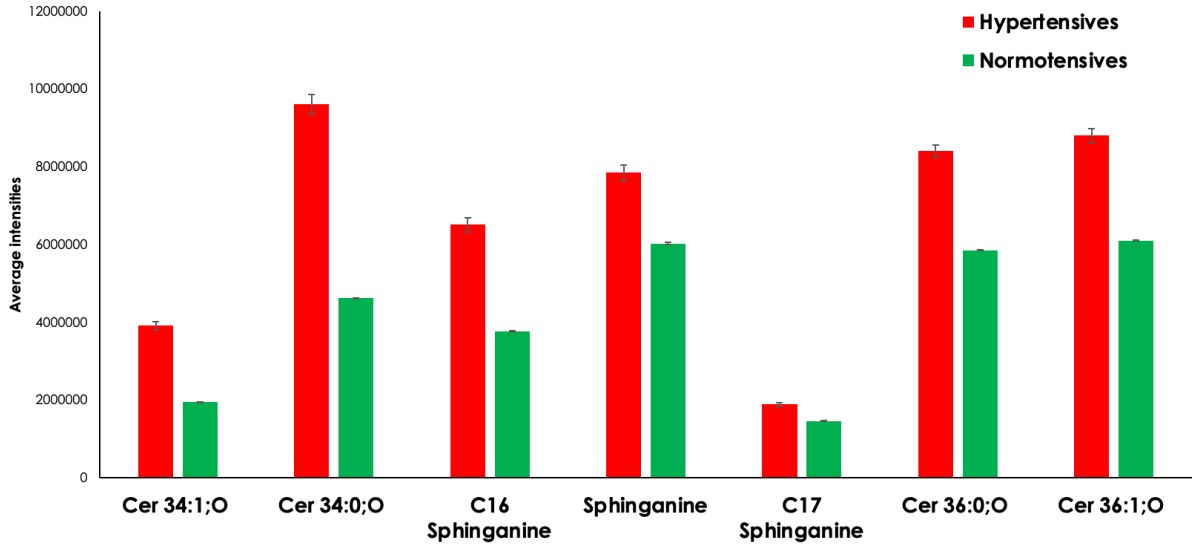

Figure S1.4. *Bar graph of the most dysregulated SPs. Results are expressed as mean ± s.e.m.*

7.2. Supporting information for Chapter III: "Analysis of the metabolic switch induced by the Spirulina peptide SP6 in high fat diet ApoE$^{-/-}$ mice model: a direct infusion FT-ICR-MS based approach"

7.2.1. Detailed SP6 peptide synthesis

The synthesis of peptide (SP6) was performed according to the solid phase approach using standard Fmoc methodology by Biotage Initiator^{+} Alstra automated microwave synthesizer (Biotage, Uppsala, Sweden). Peptides were synthesized on a Fmoc-L-Ile-Wang resin (0.6-0.7 mmol/g, 100 mg), previously deprotected with 25% piperidine/DMF (1 x 3 min, 1 x 10 min) at room temperature. The resin was then washed with DMF (4 x 4.5 mL) and the following protected amino acids were added on to the resin stepwise. Coupling reactions were performed using Nα-Fmoc amino acids (4.0 eq., 0.5 M), HBTU (3eq, 0.6 M), HOAt (3 eq, 0.5 M), and DIEA (6 eq, 2 M) in N-methyl-2-pyrrolidone (NMP) for 10 min at 75°C (2 ×). After each coupling step, the Fmoc protecting group was removed as described above. The resin was washed with DMF (4 × 4.5 mL) after each coupling and deprotection step. The N-terminal Fmoc group was removed, the resin was washed with DCM (7 x) and the peptide was released from the resin with TFA/TIS/H_2O (90:5:5) for 3 h. The resin was removed by filtration, and the crude peptide was recovered by precipitation with cold anhydrous ethyl ether to give a white powder and then lyophilized. The yield of SP6 was 40%. Identity and purity of peptide was assessed by UHPLC-PDA-MS.

7.2.2. Detailed parameters for MSDIAL

Alignement of Profile Q-Exactive files was performed with MS tolerance set at 0.01 for MS and 0.025 for MS/MS with retention time tolerance of 0.1 min. Minimum peak height for detection was set to 10000 amplitude value. Lipid identification was performed with internal Lipidblast library while metabolites with internal libraries ESI POS and ESI NEG

All_Public_MS/MS. All metabolites' annotations were based on mass accuracy, isotopic pattern and spectral matching, rev.dot product, score cut off was 70%. All reported spectral matches were manually revised for correct assignment, adducts with sodium, formate and acetate were allowed for adduct correction. The alignment was performed only on matched MS/MS metabolites blank corrected.

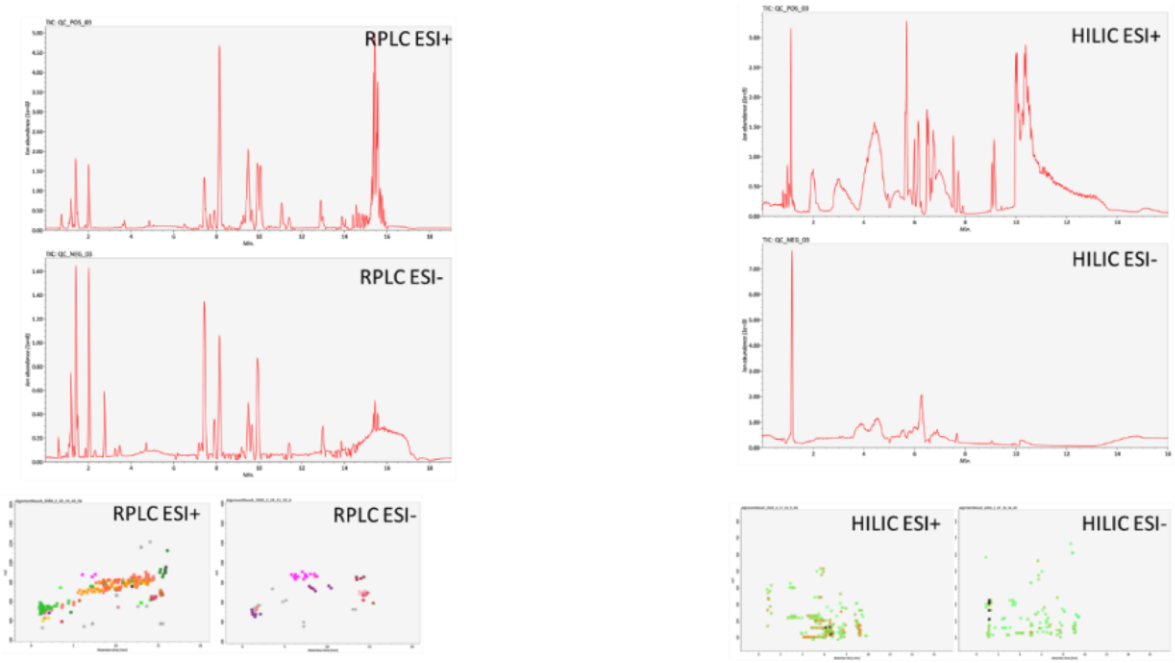

Figure S2.1. *BPC of UHPLC-HRMS/MS in both ESI polarities (RPLC+/- and HILIC+/-).*

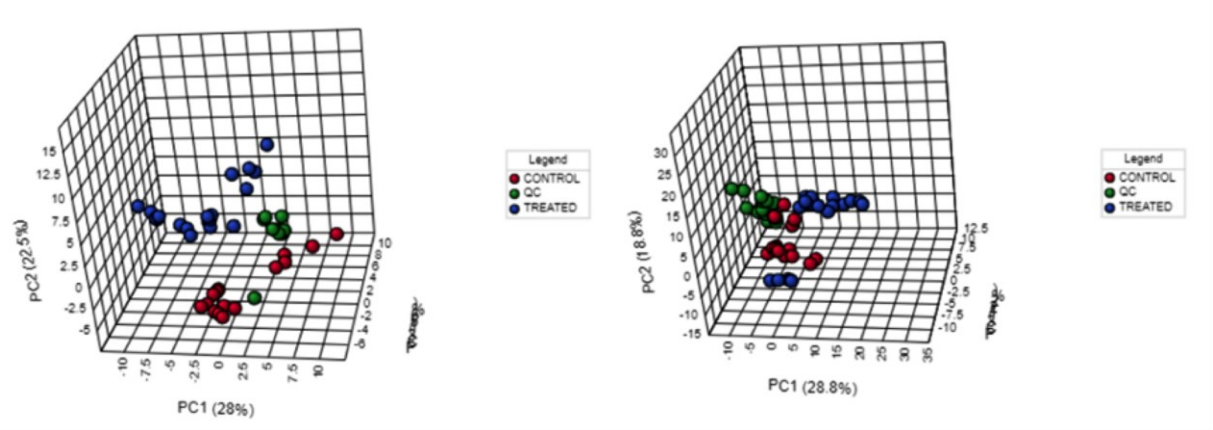

Figure S2.2. *Synchronized PCA 3D plots of polar (left) and lipid (right) showing the satisfactory clustering of QC samples.*

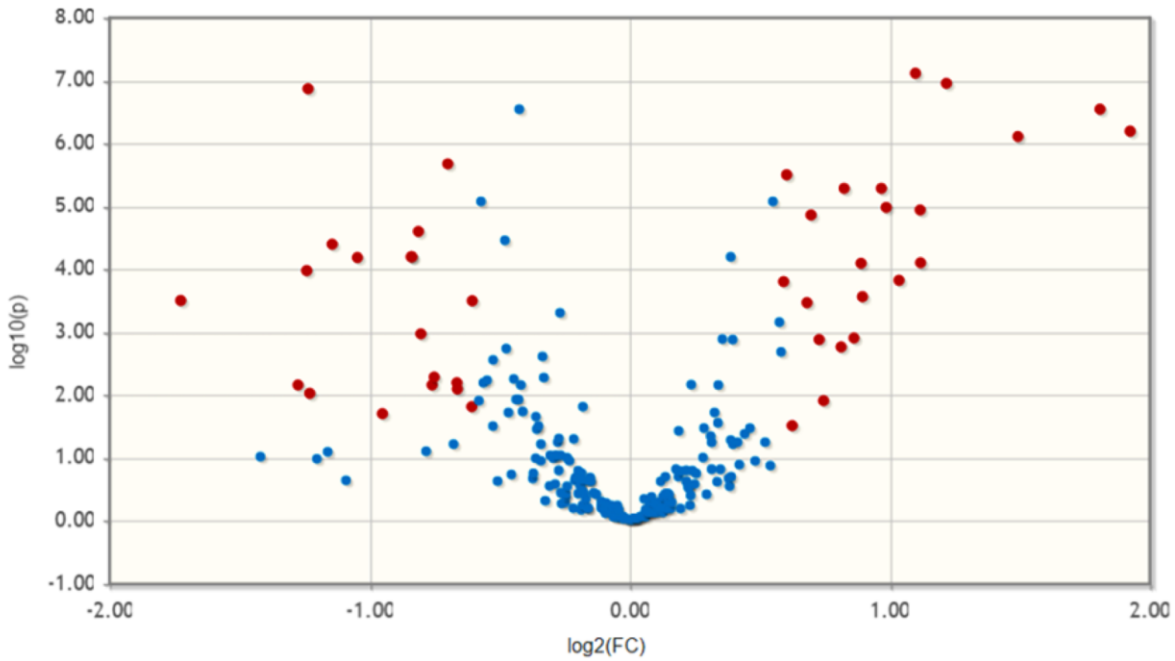

Figure S2.3. *Volcano plot of metabolites with FC (>1; <-1) or p<0.05.*

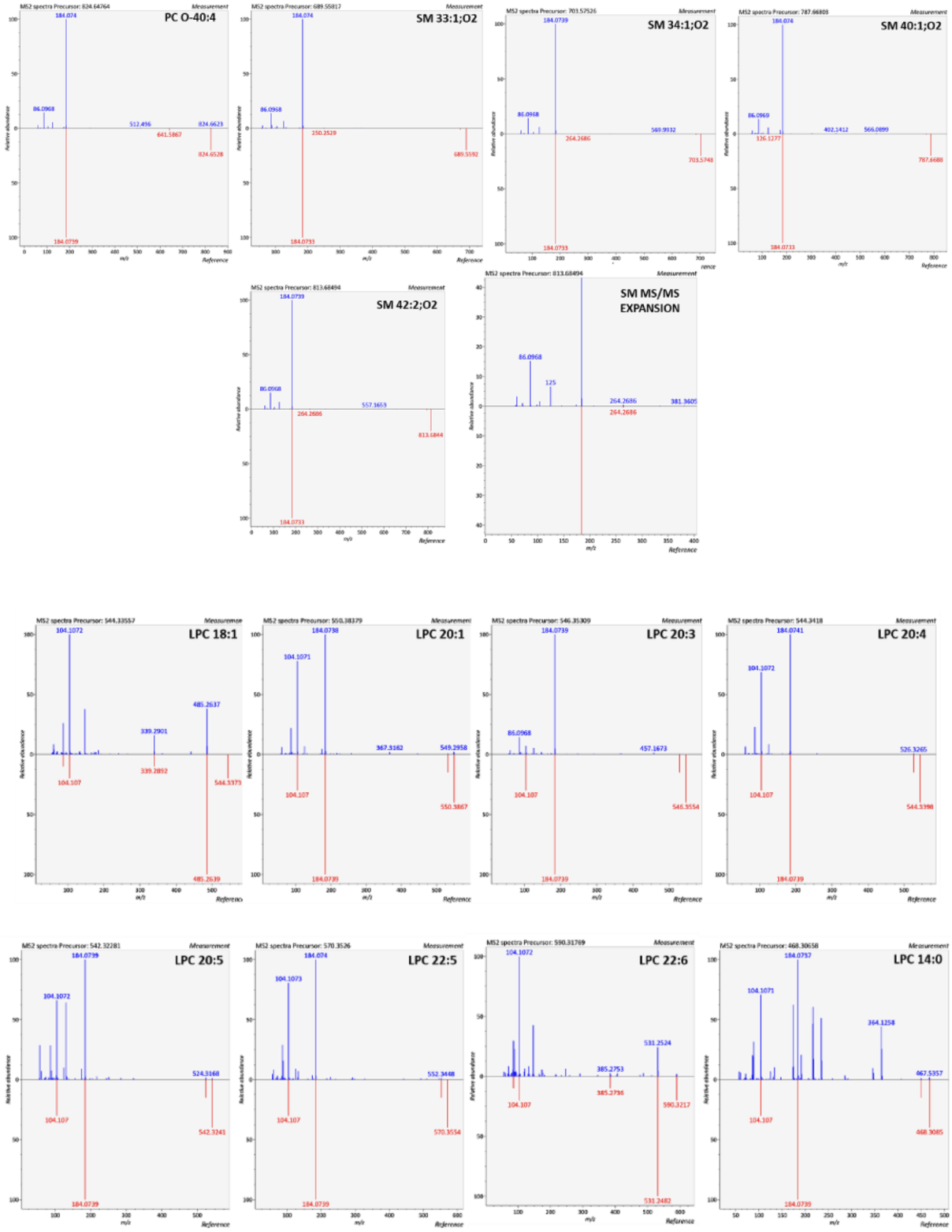
PC O-40:4
SM 33:1;O2
SM 34:1;O2
SM 40:1;O2
SM 42:2;O2
SM MS/MS EXPANSION
LPC 18:1
LPC 20:1
LPC 20:3
LPC 20:4
LPC 20:5
LPC 22:5
LPC 22:6
LPC 14:0

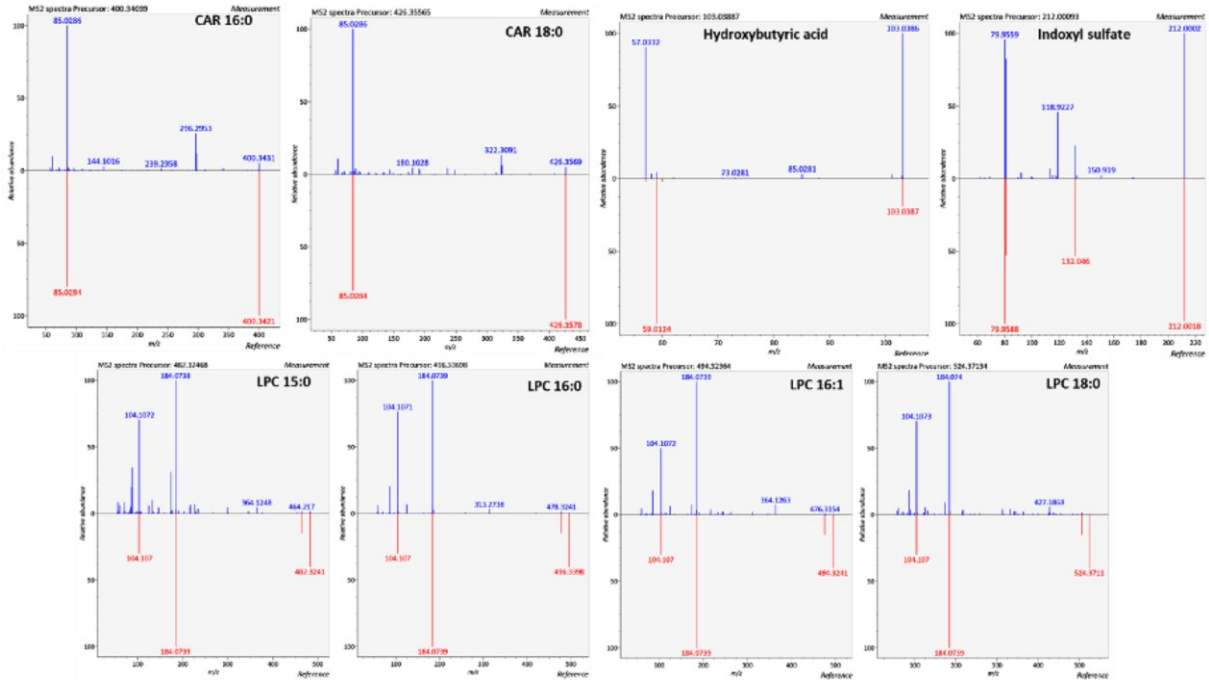

Figure S2.4. *HCD MS/MS spectra comparison with reference of statistically relevant metabolites reported in* ***chapter III table 3.1****.*

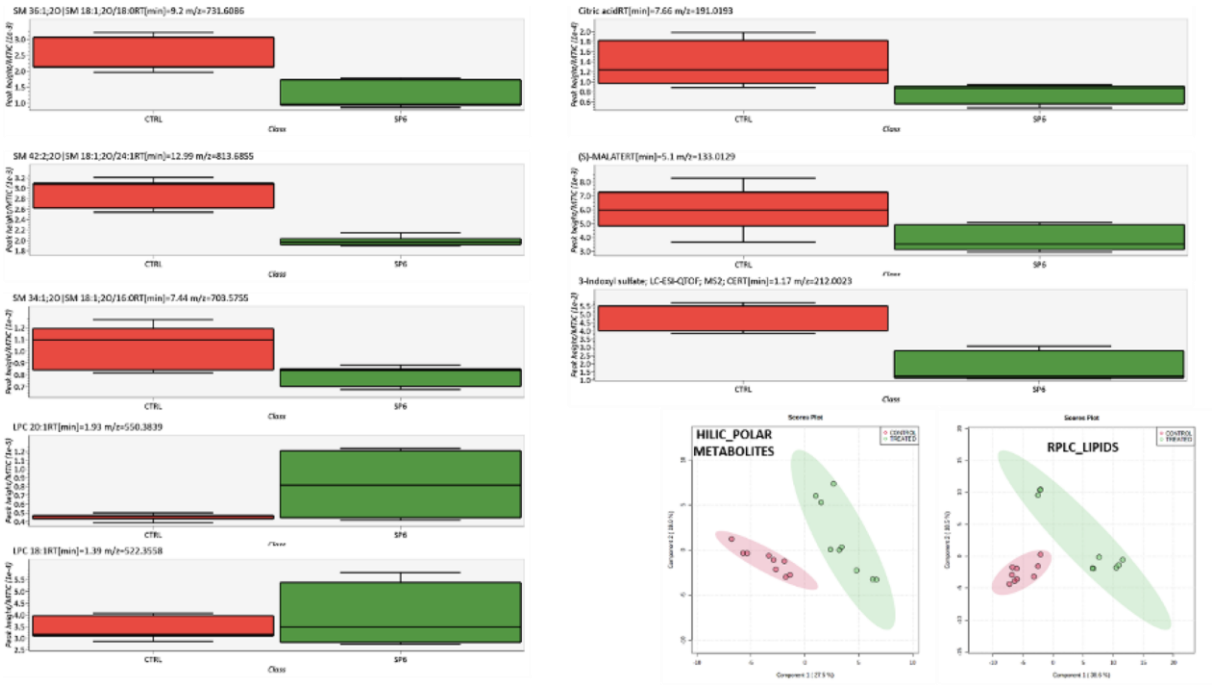

Figure S2.5. *UHPLC-HRMS/MS statistical analysis.*

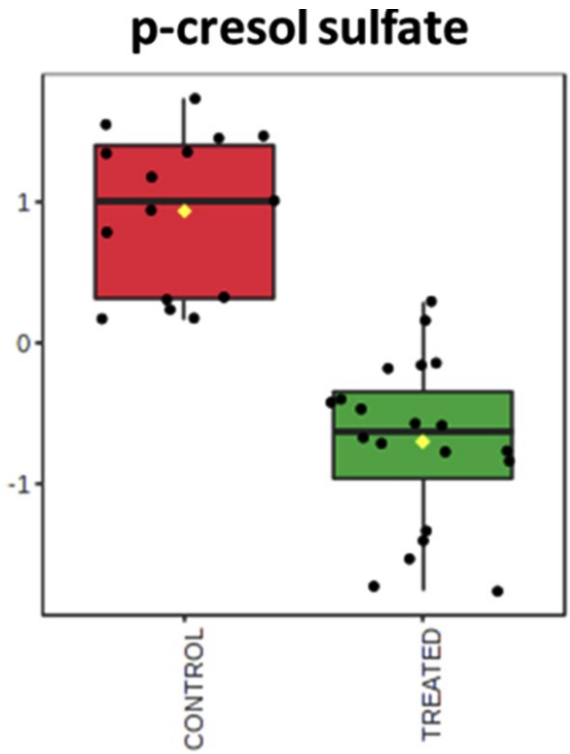

Figure S2.6. *Box plot relative to p-cresol sulfate (DI-FT-ICR).*

Table S2.1: List of all metabolites annotated with MSI level 2 or 3 by DI-FT-ICR (left) and listed in alphabetical order of biochemical class; metabolites in bold are those reported in table 1 and cited through the manuscript. The annotation of these metabolites is further supported by UHPLC-HRMS/MS with HILIC or RP separation mode (right). MS/MS spectra of statistically relevant metabolites are reported in **figure 3.4** or **figure S3.4**. CV % values are relative to signal intensity (for DI-FT-ICR analysis) or to peak area (for UHPLC-HRMS/MS analysis) and have been calculated on the QC samples inserted randomly in the batch. All remaining metabolites detected and annotated with UHPLC-HRMS/MS were not included in the supporting material. These data are available from the authors upon reasonable request.

DI-FT-ICR PLATFORM						UHPLC-HRMS/MS PLATFORM						
m/z meas.	**Compound name (HMDB or LIPIDMAPS)**	**BIOCHEMICAL CLASS/SUBCLASS**	**Mol. Formula**	**error [ppm]**	**QC CV %**	**m/z meas.**	**RT (RP/HILIC)**	**Mol. Formula**	**error [ppm]**	**Fragments**	**FC**	**QC CV %**
103.04007	Hydroxybutyric acid	Alpha hydroxy acids and derivatives	$C_4H_8O_3$	0.03	3.65	103.03883	1.12	$C_4H_8O_3$	1.17	57, 73, 85	1.65	5.13
125.00110	Lactic acid	Alpha hydroxy acids and derivatives	$C_3H_6O_3$	-0.01	0.95							
118.08625	Betaine	Amino acids, peptides, and analogues	$C_5H_{11}NO_2$	-0.12	1.29							
132.07674	Creatine	Amino acids, peptides, and analogues	$C_4H_9N_3O_2$	-0.10	7.55							
146.04588	Glutamic acid	Amino acids, peptides, and analogues	$C_5H_9NO_4$	-0.15	6.90	146.04489	7.44	$C_5H_9NO_4$	0.99	128, 102	1.42	4.85
145.06186	Glutamine	Amino acids, peptides, and analogues	$C_5H_{10}N_2O_3$	-0.07	5.34	145.06056	7.69	$C_5H_{10}N_2O_3$	1.3	127, 109, 101	1.01	1.49
132.10189	Leu/Isoleucine	Amino acids, peptides, and analogues	$C_6H_{13}NO_2$	-0.11	0.11							
147.11279	Lysine	Amino acids, peptides, and analogues	$C_6H_{14}N_2O_2$	-0.11	4.26							
166.08624	Phenylalanine	Amino acids, peptides, and analogues	$C_9H_{11}NO_2$	-0.16	6.66							
138.05253	Proline	Amino acids, peptides, and analogues	$C_5H_9NO_2$	-0.07	1.62							
128.03531	Pyroglutamic acid	Amino acids, peptides, and analogues	$C_5H_7NO_3$	-0.07	6.44							
227.07908	Tryptophan	Amino acids, peptides, and analogues	$C_{11}H_{12}N_2O_2$	-0.08	2.91							

133.01424	Malic acid	Beta hydroxy acids and derivatives	$C_4H_6O_5$	-0.08	6.32	133.01286	5.10	$C_4H_6O_5$	1.15	71, 115, 89	1.57	5.47
199.03787	Deoxy Hexose	Carbohydrates and carbohydrate conjugates	$C_6H_{12}O_5$	0.00	1.38							
135.02989	Erythronic acid	Carbohydrates and carbohydrate conjugates	$C_4H_8O_5$	-0.01	8.75							
179.05611	Hexose	Carbohydrates and carbohydrate conjugates	$C_6H_{12}O_6$	0.00	2.09							
185.02222	Pentose	Carbohydrates and carbohydrate conjugates	$C_5H_{10}O_5$	-0.08	3.54							
160.13319	2-Aminooctanoic acid	Carboxylic acids and derivatives	$C_8H_{17}NO_2$	-0.09	2.46							
175.02480	Ascorbic acid	Dihydrofurans	$C_6H_8O_6$	-0.02	3.29							
204.12302	Acetylcarnitine	Fatty acid esters	$C_9H_{17}NO_4$	-0.09	5.14							
372.31090	CAR 14:0	Fatty acid esters	$C_{21}H_{41}NO_4$	0.26	5.04							
400.34224	CAR 16:0	Fatty acid esters	$C_{23}H_{45}NO_4$	0.40	6.06	400.34045	1.42	$C_{23}H_{46}NO_4$	1.68	296, 85	1.21	0.77
428.37337	CAR 18:0	Fatty acid esters	$C_{25}H_{49}NO_4$	-0.18	6.41							
426.35771	CAR 18:1	Fatty acid esters	$C_{25}H_{47}NO_4$	-0.21	0.64	426.35547	1.50	$C_{25}H_{48}NO_4$	2.32	322, 85	1.34	1.68
232.15431	CAR 4:0	Fatty acid esters	$C_{11}H_{21}NO_4$	-0.21	0.62							
246.17003	CAR 5:0	Fatty acid esters	$C_{12}H_{23}NO_4$	0.18	2.15							
400.34207	Palmitoylcarnitine	Fatty acid esters	$C_{23}H_{45}NO_4$	-0.15	2.53							
171.13905	FA 10:0	Fatty Acyls [FA]	$C_{10}H_{20}O_2$	0.01	8.55							
185.15470	FA 11:0	Fatty Acyls [FA]	$C_{11}H_{22}O_2$	0.03	4.92							
199.17032	FA 12:0	Fatty Acyls [FA]	$C_{12}H_{24}O_2$	-0.18	8.74							
239.16175	FA 12:0;O	Fatty Acyls [FA]	$C_{12}H_{24}O_3$	-0.07	6.91							
253.14100	FA 12:1;O2	Fatty Acyls [FA]	$C_{12}H_{22}O_4$	-0.27	7.79							
251.12542	FA 12:2;O2	Fatty Acyls [FA]	$C_{12}H_{20}O_4$	0.27	2.31							
227.20164	FA 14:0	Fatty Acyls [FA]	$C_{14}H_{28}O_2$	0.01	9.30							
227.20164	FA 14:0	Fatty Acyls [FA]	$C_{14}H_{28}O_2$	-0.04	4.66							
241.18093	FA 14:1;O	Fatty Acyls [FA]	$C_{14}H_{26}O_3$	0.08	6.27							
281.17230	FA 14:1;O2	Fatty Acyls [FA]	$C_{14}H_{26}O_4$	-0.22	4.64							
235.13397	FA 14:4;O	Fatty Acyls [FA]	$C_{14}H_{20}O_3$	0.08	7.29							

241.21730	FA 15:0	Fatty Acyls [FA]	$C_{15}H_{30}O_2$	0.00	5.55
277.19396	FA 15:0	Fatty Acyls [FA]	$C_{15}H_{30}O_2$	-0.01	6.66
241.21624	FA 15:1	Fatty Acyls [FA]	$C_{15}H_{28}O_2$	0.18	6.23
255.19656	FA 15:1;O	Fatty Acyls [FA]	$C_{15}H_{28}O_3$	-0.08	6.13
255.23295	FA 16:0	Fatty Acyls [FA]	$C_{16}H_{32}O_2$	0.00	8.97
291.20962	FA 16:0	Fatty Acyls [FA]	$C_{16}H_{32}O_2$	-0.04	5.16
271.22787	FA 16:0;O	Fatty Acyls [FA]	$C_{16}H_{32}O_3$	-0.04	8.07
287.22280	FA 16:0;O2	Fatty Acyls [FA]	$C_{16}H_{32}O_4$	-0.18	3.92
253.21729	FA 16:1	Fatty Acyls [FA]	$C_{16}H_{30}O_2$	-0.01	7.81
253.21730	FA 16:1	Fatty Acyls [FA]	$C_{16}H_{30}O_2$	-0.03	4.50
269.21222	FA 16:1;O	Fatty Acyls [FA]	$C_{16}H_{30}O_3$	-0.08	9.87
285.20714	FA 16:1;O2	Fatty Acyls [FA]	$C_{16}H_{30}O_4$	0.00	6.36
269.21115	FA 16:2;O	Fatty Acyls [FA]	$C_{16}H_{28}O_3$	-0.07	4.13
265.18092	FA 16:3;O	Fatty Acyls [FA]	$C_{16}H_{26}O_3$	0.08	3.87
269.24860	FA 17:0	Fatty Acyls [FA]	$C_{17}H_{34}O_2$	-0.03	2.98
305.22527	FA 17:0	Fatty Acyls [FA]	$C_{17}H_{34}O_2$	-0.07	9.38
301.23844	FA 17:0;O2	Fatty Acyls [FA]	$C_{17}H_{34}O_4$	-0.33	7.95
267.23296	FA 17:1	Fatty Acyls [FA]	$C_{17}H_{32}O_2$	0.05	6.73
285.24247	FA 17:1;O	Fatty Acyls [FA]	$C_{17}H_{32}O_3$	0.15	7.66
283.26425	FA 18:0	Fatty Acyls [FA]	$C_{18}H_{36}O_2$	0.01	6.96
319.24091	FA 18:0	Fatty Acyls [FA]	$C_{18}H_{36}O_2$	-0.04	6.46
299.25918	FA 18:0;O	Fatty Acyls [FA]	$C_{18}H_{36}O_3$	-0.37	1.51
315.25408	FA 18:0;O2	Fatty Acyls [FA]	$C_{18}H_{36}O_4$	0.08	8.95
281.24860	FA 18:1	Fatty Acyls [FA]	$C_{18}H_{34}O_2$	0.02	6.09
317.22526	FA 18:1	Fatty Acyls [FA]	$C_{18}H_{34}O_2$	-0.07	2.19
297.24352	FA 18:1;O	Fatty Acyls [FA]	$C_{18}H_{34}O_3$	0.10	3.73
313.23844	FA 18:1;O2	Fatty Acyls [FA]	$C_{18}H_{34}O_4$	-0.20	9.55

279.23295	FA 18:2	Fatty Acyls [FA]	$C_{18}H_{32}O_2$	-0.01	5.69
315.20961	FA 18:2	Fatty Acyls [FA]	$C_{18}H_{32}O_2$	-0.34	4.29
297.24249	FA 18:2;O	Fatty Acyls [FA]	$C_{18}H_{32}O_3$	0.03	6.38
319.22433	FA 18:2;O	Fatty Acyls [FA]	$C_{18}H_{32}O_3$	-0.31	4.66
291.19657	FA 18:4;O	Fatty Acyls [FA]	$C_{18}H_{28}O_3$	-0.06	2.43
297.27990	FA 19:0	Fatty Acyls [FA]	$C_{19}H_{38}O_2$	0.11	2.95
295.26426	FA 19:1	Fatty Acyls [FA]	$C_{19}H_{36}O_2$	-0.13	6.70
313.27378	FA 19:1;O	Fatty Acyls [FA]	$C_{19}H_{36}O_3$	0.26	7.92
329.26870	FA 19:1;O2	Fatty Acyls [FA]	$C_{19}H_{36}O_4$	0.25	7.33
311.29555	FA 20:0	Fatty Acyls [FA]	$C_{20}H_{40}O_2$	0.05	10.88
309.27990	FA 20:1	Fatty Acyls [FA]	$C_{20}H_{38}O_2$	0.03	6.93
327.28944	FA 20:1;O	Fatty Acyls [FA]	$C_{20}H_{38}O_3$	0.12	5.82
341.26974	FA 20:1;O2	Fatty Acyls [FA]	$C_{20}H_{38}O_4$	0.24	8.29
307.26425	FA 20:2	Fatty Acyls [FA]	$C_{20}H_{36}O_2$	-0.03	8.70
403.23276	FA 20:3;O6	Fatty Acyls [FA]	$C_{20}H_{34}O_8$	0.28	4.86
303.23293	FA 20:4	Fatty Acyls [FA]	$C_{20}H_{32}O_2$	-0.27	3.27
303.23295	FA 20:4	Fatty Acyls [FA]	$C_{20}H_{32}O_2$	0.07	0.63
319.22787	FA 20:4;O	Fatty Acyls [FA]	$C_{20}H_{32}O_3$	0.06	4.54
343.22434	FA 20:4;O	Fatty Acyls [FA]	$C_{20}H_{32}O_3$	-0.07	3.02
303.23192	FA 20:5	Fatty Acyls [FA]	$C_{20}H_{30}O_2$	0.27	6.38
325.31120	FA 21:0	Fatty Acyls [FA]	$C_{21}H_{42}O_2$	-0.13	7.33
341.30510	FA 21:1;O	Fatty Acyls [FA]	$C_{21}H_{40}O_3$	0.17	4.60
357.30000	FA 21:1;O2	Fatty Acyls [FA]	$C_{21}H_{40}O_4$	0.09	3.63
355.28440	FA 21:2;O2	Fatty Acyls [FA]	$C_{21}H_{38}O_4$	0.34	10.18
339.32685	FA 22:0	Fatty Acyls [FA]	$C_{22}H_{44}O_2$	0.14	6.78
403.30655	FA 22:0;O4	Fatty Acyls [FA]	$C_{22}H_{44}O_6$	0.06	3.17
371.31566	FA 22:1;O2	Fatty Acyls [FA]	$C_{22}H_{42}O_4$	0.16	5.17

331.26425	FA 22:4	Fatty Acyls [FA]	$C_{22}H_{36}O_2$	-0.17	5.32
327.23295	FA 22:6	Fatty Acyls [FA]	$C_{22}H_{32}O_2$	-0.01	5.11
363.20962	FA 22:6	Fatty Acyls [FA]	$C_{22}H_{32}O_2$	0.09	7.93
369.33654	FA 23:1;O	Fatty Acyls [FA]	$C_{23}H_{44}O_3$	0.27	10.10
367.35817	FA 24:0	Fatty Acyls [FA]	$C_{24}H_{48}O_2$	0.06	6.52
383.35207	FA 24:1;O	Fatty Acyls [FA]	$C_{24}H_{46}O_3$	0.12	4.92
397.33235	FA 24:1;O2	Fatty Acyls [FA]	$C_{24}H_{46}O_4$	0.07	1.67
381.37378	FA 25:0	Fatty Acyls [FA]	$C_{25}H_{50}O_2$	-0.60	8.25
419.31567	FA 26:5;O2	Fatty Acyls [FA]	$C_{26}H_{42}O_4$	0.14	1.97
179.05613	FA 6:0;O4	Fatty Acyls [FA]	$C_6H_{12}O_6$	-0.08	9.28
167.06786	FA 7:1;O	Fatty Acyls [FA]	$C_7H_{12}O_3$	-0.12	10.96
165.08858	FA 8:1	Fatty Acyls [FA]	$C_8H_{14}O_2$	-0.09	2.29
157.08700	FA 8:1;O	Fatty Acyls [FA]	$C_8H_{14}O_3$	-0.14	0.67
195.06276	FA 8:2;O2	Fatty Acyls [FA]	$C_8H_{12}O_4$	-0.11	9.09
157.12339	FA 9:0	Fatty Acyls [FA]	$C_9H_{18}O_2$	0.00	3.82
537.48890	FAHFA 34:1;O	Fatty Acyls [FA]	$C_{34}H_{66}O_4$	0.22	0.60
535.47324	FAHFA 34:2;O	Fatty Acyls [FA]	$C_{34}H_{64}O_4$	0.17	8.93
563.50453	FAHFA 36:2;O	Fatty Acyls [FA]	$C_{36}H_{68}O_4$	0.12	7.96
205.15978	FAL 14:3	Fatty Acyls [FA]	$C_{14}H_{22}O$	-0.05	1.43
145.05063	Methylglutaric acid	Fatty Acyls [FA]	$C_6H_{10}O_4$	-0.02	3.06
468.30864	NA 27:6;O3	Fatty Acyls [FA]	$C_{27}H_{43}NO_4$	0.27	6.52
272.25845	unknown FA	Fatty Acyls [FA]	$C_{16}H_{33}NO_2$	0.13	8.04
288.25338	unknown FA	Fatty Acyls [FA]	$C_{16}H_{33}NO_3$	0.25	9.21
300.28976	unknown FA	Fatty Acyls [FA]	$C_{18}H_{37}NO_2$	0.16	5.24
507.51365	WE 34:1	Fatty Acyls [FA]	$C_{34}H_{66}O_2$	0.64	3.81
521.52929	WE 35:1	Fatty Acyls [FA]	$C_{35}H_{68}O_2$	0.30	4.11
535.54495	WE 36:1	Fatty Acyls [FA]	$C_{36}H_{70}O_2$	0.47	2.90

286.27411	NAE 15:0	Fatty amides [FA08]	$C_{17}H_{35}NO_2$	0.16	6.03							
298.27411	NAE 16:1	Fatty amides [FA08]	$C_{18}H_{35}NO_2$	0.34	5.40							
314.30543	NAE 17:0	Fatty amides [FA08]	$C_{19}H_{39}NO_2$	0.32	5.40							
328.32108	NAE 18:0	Fatty amides [FA08]	$C_{20}H_{41}NO_2$	0.15	10.08							
322.27413	NAE 18:3	Fatty amides [FA08]	$C_{20}H_{35}NO_2$	0.27	6.50				n.d			
331.28435	MG 16:0	Glycerolipids [GL]	$C_{19}H_{38}O_4$	0.15	8.46							
359.31566	MG 18:0	Glycerolipids [GL]	$C_{21}H_{42}O_4$	0.15	3.61							
377.26621	MG 18:2	Glycerolipids [GL]	$C_{21}H_{38}O_4$	0.03	8.64							
280.09201	Glycerophospho-choline	Glycerophospholipids [GP]	$C_8H_{20}NO_6P$	-0.11	5.52							
490.29033	LPC 14:0	Glycerophospholipids [GP]	$C_{22}H_{46}NO_7P$	0.12	5.11	468.30658	1.05	$C_{22}H_{46}NO_7P$	1.89	450, 184, 104	1.32	5.47
482.32422	LPC 15:0	Glycerophospholipids [GP]	$C_{23}H_{48}NO_7P$	0.19	5.13	482.32498	1.20	$C_{23}H_{48}NO_7P$	0.85	464, 184, 104	1.51	6.20
518.32162	LPC 16:0	Glycerophospholipids [GP]	$C_{24}H_{50}NO_7P$	-0.14	3.12	518.32007	1.40	$C_{24}H_{50}NO_7P$	1.65	459, 313, 104	1.84	2.13
516.30599	LPC 16:1	Glycerophospholipids [GP]	$C_{24}H_{48}NO_7P$	-0.07	3.40	494.32391	1.11	$C_{24}H_{48}NO_7P$	0.22	476, 184, 104	1.74	0.94
494.32420	LPC 16:1/LPE 19:1	Glycerophospholipids [GP]	$C_{24}H_{48}NO_7P$	0.31	5.89							
546.35293	LPC 18:0	Glycerophospholipids [GP]	$C_{26}H_{54}NO_7P$	-0.14	2.75							
526.29299	LPC 18:0/LPE 21:0	Glycerophospholipids [GP]	$C_{27}H_{44}NO_7P$	0.20	1.56							
544.33724	LPC 18:1	Glycerophospholipids [GP]	$C_{26}H_{52}NO_7P$	-0.59	3.63	544.33551	1.48	$C_{26}H_{52}NO_7P$	0.61	504, 184, 104	1.44	2.87
542.32164	LPC 18:2	Glycerophospholipids [GP]	$C_{26}H_{50}NO_7P$	-0.54	1.03	520.34058	1.18	$C_{26}H_{50}NO_7P$	0.8	502, 184, 104	1.58	1.21
520.33990	LPC 18:2	Glycerophospholipids [GP]	$C_{26}H_{50}NO_7P$	0.44	4.14							
572.36859	LPC 20:1	Glycerophospholipids [GP]	$C_{28}H_{56}NO_7P$	-0.10	0.37	550.38385	2.09	$C_{28}H_{56}NO_7P$	2.99	532, 184, 104	2.12	0.61

568.33711	LPC 20:3	Glycerophospholipids [GP]	$C_{28}H_{52}NO_7P$	-0.25	6.12	546.35284	1.29	$C_{28}H_{52}NO_7P$	2.57	184, 104	1.18	5.01
566.32163	LPC 20:4	Glycerophospholipids [GP]	$C_{28}H_{50}NO_7P$	-0.08	2.67	566.31805	1.15	$C_{28}H_{50}NO_7P$	3.67	507, 361, 104	1.25	4.66
544.34011	LPC 20:4	Glycerophospholipids [GP]	$C_{28}H_{50}NO_7P$	0.74	3.75							
564.30598	LPC 20:5	Glycerophospholipids [GP]	$C_{28}H_{48}NO_7P$	0.17	4.30	542.32343	0.97	$C_{28}H_{48}NO_7P$	0.67	524, 184, 104	1.12	0.66
592.33726	LPC 22:5	Glycerophospholipids [GP]	$C_{30}H_{52}NO_7P$	-0.15	5.34	570.35284	1.185	$C_{30}H_{52}NO_7P$	2.57	552, 184, 104	1.55	1.46
570.35568	LPC 22:5	Glycerophospholipids [GP]	$C_{30}H_{52}NO_7P$	0.79	2.08							
590.32164	LPC 22:6	Glycerophospholipids [GP]	$C_{30}H_{50}NO_7P$	-0.07	3.17	568.33630	1.08	$C_{30}H_{50}NO_7P$	3.48	184, 104	1.02	0.96
568.34000	LPC 22:6	Glycerophospholipids [GP]	$C_{30}H_{50}NO_7P$	0.61	5.05							
630.44690	LPC 24:0	Glycerophospholipids [GP]	$C_{32}H_{66}NO_7P$	-0.01	7.88							
482.36061	LPC O-16:0	Glycerophospholipids [GP]	$C_{24}H_{52}NO_6P$	0.45	5.01							
510.39188	LPC O-18:0	Glycerophospholipids [GP]	$C_{26}H_{56}NO_6P$	0.07	5.50							
508.37626	LPC O-18:1	Glycerophospholipids [GP]	$C_{26}H_{54}NO_6P$	0.39	4.55							
530.35805	LPC O-18:1	Glycerophospholipids [GP]	$C_{26}H_{54}NO_6P$	-0.29	8.94							
538.42322	LPC O-20:0	Glycerophospholipids [GP]	$C_{28}H_{60}NO_6P$	0.37	4.75							
454.29294	LPC13:0	Glycerophospholipids [GP]	$C_{21}H_{44}NO_7P$	0.48	5.30							
478.29294	LPE 18:2	Glycerophospholipids [GP]	$C_{23}H_{44}NO_7P$	0.24	1.09	478.2915	1.235	$C_{23}H_{44}NO_7P$	1.32	337	2.71	3.77
532.33729	LPE 20:0	Glycerophospholipids [GP]	$C_{25}H_{52}NO_7P$	-0.13	6.58							
502.29300	LPE 20:4	Glycerophospholipids [GP]	$C_{25}H_{44}NO_7P$	0.59	4.97							
548.27474	LPE 22:6	Glycerophospholipids [GP]	$C_{27}H_{44}NO_7P$	0.27	3.39							
580.36205	LPS 22:0	Glycerophospholipids [GP]	$C_{28}H_{56}NO_9P$	0.15	9.98							
578.34644	LPS 22:1/PC 20:1;O	Glycerophospholipids [GP]	$C_{28}H_{54}NO_9P$	0.17	6.96							
706.53844	PC 30:0/PE 33:0	Glycerophospholipids [GP]	$C_{38}H_{76}NO_8P$	0.64	4.23							
756.55130	PC 32:0	Glycerophospholipids [GP]	$C_{40}H_{80}NO_8P$	0.07	1.62							
734.56966	PC 32:0/PE 35:0	Glycerophospholipids [GP]	$C_{40}H_{80}NO_8P$	0.54	2.46				n.d			
788.61668	PC 36:1/PE 39:1	Glycerophospholipids [GP]	$C_{44}H_{86}NO_8P$	0.62	2.11							

786.60099	PC 36:2/PE 39:2	Glycerophospholipids [GP]	$C_{44}H_{84}NO_8P$	0.54	1.75							
814.63272	PC 38:2/ PE 41:2	Glycerophospholipids [GP]	$C_{46}H_{88}NO_8P$	0.92	5.91							
812.61693	PC 38:3/PE 41:3	Glycerophospholipids [GP]	$C_{46}H_{86}NO_8P$	0.91	3.82							
810.60095	PC 38:4/PE 41:4	Glycerophospholipids [GP]	$C_{46}H_{84}NO_8P$	0.51	1.86				n.d			
806.56963	PC 38:6/PE 41:6	Glycerophospholipids [GP]	$C_{46}H_{80}NO_8P$	0.47	1.41							
834.60101	PC 40:6/PE 43:6	Glycerophospholipids [GP]	$C_{48}H_{84}NO_8P$	0.60	1.76				n.d			
468.30864	PC O-14:0/LPE 17:0	Glycerophospholipids [GP]	$C_{22}H_{46}NO_7P$	0.19	6.52							
496.33989	PC O-16:0/LPE 19:0	Glycerophospholipids [GP]	$C_{24}H_{50}NO_7P$	0.38	3.66							
510.35552	PC O-17:0/LPE 20:0	Glycerophospholipids [GP]	$C_{25}H_{52}NO_7P$	0.21	5.17							
524.37121	PC O-18:0	Glycerophospholipids [GP]	$C_{26}H_{54}NO_7P$	0.46	2.59							
522.35552	PC O-18:1/LPC 18:1	Glycerophospholipids [GP]	$C_{26}H_{52}NO_7P$	0.36	3.71							
550.38688	PC O-20:1/LPC 20:1	Glycerophospholipids [GP]	$C_{28}H_{56}NO_7P$	0.52	6.57							
720.59034	PC O-32:0/PE O-35:0	Glycerophospholipids [GP]	$C_{40}H_{82}NO_7P$	0.51	6.00							
718.57479	PC O-32:1/PE O-35:1	Glycerophospholipids [GP]	$C_{40}H_{80}NO_7P$	0.81	4.23							
746.60610	PC O-34:1/PE O-37:1	Glycerophospholipids [GP]	$C_{42}H_{84}NO_7P$	0.69	4.61							
744.59037	PC O-34:2/PE O-37:2	Glycerophospholipids [GP]	$C_{42}H_{82}NO_7P$	0.43	2.15							
774.63734	PC O-36:1/PE O-39:1	Glycerophospholipids [GP]	$C_{44}H_{88}NO_7P$	0.68	1.53							
768.59044	PC O-36:4	Glycerophospholipids [GP]	$C_{44}H_{82}NO_7P$	0.61	0.74							
796.62182	PC O-38:4	Glycerophospholipids [GP]	$C_{46}H_{86}NO_7P$	0.62	5.88							
794.60607	PC O-38:5	Glycerophospholipids [GP]	$C_{46}H_{84}NO_7P$	0.58	3.09							
824.65303	PC O-40:4	Glycerophospholipids [GP]	$C_{48}H_{90}NO_7P$	0.57	4.04	824.64703	12.72	$C_{48}H_{90}NO_7P$	5.74	184, 512	1.11	0.45
818.60598	PC O-40:7	Glycerophospholipids [GP]	$C_{48}H_{84}NO_7P$	0.41	0.87							
724.52789	PE O-36:5	Glycerophospholipids [GP]	$C_{41}H_{74}NO_7P$	0.80	3.03				n.d			

885.54976	PI 38:4	Glycerophospholipids [GP]	$C_{47}H_{83}O_{13}P$	0.06	3.16							
816.57602	PS 38:1	Glycerophospholipids [GP]	$C_{44}H_{84}NO_{10}P$	-0.03	11.20							
844.60744	PS 40:1	Glycerophospholipids [GP]	$C_{46}H_{88}NO_{10}P$	0.13	4.72							
215.03406	Paraxanthine	Imidazopyrimidines	$C_7H_8N_4O_2$	-0.30	1.49							
167.02105	Uric acid	Imidazopyrimidines	$C_5H_4N_4O_3$	-0.10	3.50							
145.01424	Oxoglutaric acid	Keto acids and derivatives	$C_5H_6O_5$	-0.01	6.33							
115.04006	Alpha-ketoisovaleric acid	Organic acids and derivatives	$C_5H_8O_3$	-0.08	7.17							
117.01933	Methylmalonic acid	Organic acids and derivatives	$C_4H_6O_4$	-0.04	2.73							
212.00228	Indoxyl sulfate	Organic sulfuric acids and derivatives	$C_8H_7NO_4S$	-0.14	7.37	212.00226	1.17	$C_8H_7NO_4S$	0.04	79, 132	2.38	5.29
187.00704	p-Cresol sulfate	Organic sulfuric acids and derivatives	$C_7H_8O_4S$	-0.04	7.49	n.d						
301.14099	Alpha-CEHC	Organoheterocyclic compounds	$C_{16}H_{22}O_4$	-0.18	3.82							
162.11245	L-Carnitine	Organonitrogen compounds	$C_7H_{15}NO_3$	-0.14	7.77							
218.10339	Pantothenic acid	Organooxygen compounds	$C_9H_{17}NO_5$	-0.05	5.69							
124.00739	Taurine	Organosulfonic acids and derivatives	$C_2H_7NO_3S$	-0.04	1.90							
263.04401	Deoxyuridine	Pyrimidine nucleosides	$C_9H_{12}N_2O_5$	0.17	8.95							
277.05965	Thymidine	Pyrimidine nucleosides	$C_{10}H_{14}N_2O_5$	0.08	2.08							
274.27411	C16 Sphinganine	Sphingolipids [SP]	$C_{16}H_{35}NO_2$	0.16	8.12							
288.28976	C17 Sphinganine	Sphingolipids [SP]	$C_{17}H_{37}NO_2$	0.14	6.22							
512.50365	Cer 32:0;O2	Sphingolipids [SP]	$C_{32}H_{65}NO_3$	-0.23	6.97							
524.54024	Cer 34:0;O	Sphingolipids [SP]	$C_{34}H_{69}NO_2$	0.16	6.63							
540.53490	Cer 34:0;O2	Sphingolipids [SP]	$C_{34}H_{69}NO_3$	-0.30	2.11							
572.52502	Cer 34:0;O4	Sphingolipids [SP]	$C_{34}H_{69}NO_5$	0.10	2.39							
522.52456	Cer 34:1;O	Sphingolipids [SP]	$C_{34}H_{67}NO_2$	0.11	4.36							
552.57154	Cer 36:0;O	Sphingolipids [SP]	$C_{36}H_{73}NO_2$	0.37	7.70							
568.56625	Cer 36:0;O2	Sphingolipids [SP]	$C_{36}H_{73}NO_3$	-0.25	5.85							
550.55591	Cer 36:1;O	Sphingolipids [SP]	$C_{36}H_{71}NO_2$	0.18	6.54							

596.59750	Cer 38:0;O2	Sphingolipids [SP]	$C_{38}H_{77}NO_3$	-0.29	0.13							
689.55927	SM 33:1;O2	Sphingolipids [SP]	$C_{38}H_{77}N_2O_6P$	0.41	2.33							
703.57504	SM 34:1;O2	Sphingolipids [SP]	$C_{39}H_{79}N_2O_6P$	0.51	4.17	703.57550	7.44	$C_{39}H_{79}N_2O_6P$	0.67	264, 184	1.09	2.33
701.55943	SM 34:2;O2	Sphingolipids [SP]	$C_{39}H_{77}N_2O_6P$	0.62	1.91							
731.60637	SM 36:1;O2	Sphingolipids [SP]	$C_{41}H_{83}N_2O_6P$	0.23	5.51	731.60858	9.20	$C_{41}H_{83}N_2O_6P$	2.44	264, 184	1.85	0.29
759.63717	SM 38:1;O2	Sphingolipids [SP]	$C_{43}H_{87}N_2O_6P$	-0.29	4.52							
787.66893	SM 40:1;O2	Sphingolipids [SP]	$C_{45}H_{91}N_2O_6P$	0.43	6.09	787.66803	12.84	$C_{45}H_{91}N_2O_6P$	0.73	184	3.74	3.89
815.70066	SM 42:1;O2	Sphingolipids [SP]	$C_{47}H_{95}N_2O_6P$	0.94	4.91							
813.68478	SM 42:2;O2	Sphingolipids [SP]	$C_{47}H_{93}N_2O_6P$	0.76	4.86	813.68549	12.99	$C_{47}H_{93}N_2O_6P$	1.1	264, 184	1.25	1.28
316.28469	SPB 18:1;O3	Sphingolipids [SP]	$C_{18}H_{37}NO_3$	0.12	7.08							
302.30532	Sphinganine	Sphingolipids [SP]	$C_{18}H_{39}NO_2$	-0.16	2.17							
330.33670	Sphingoid bases un-known/N-N dime-thylsaphingol	Sphingolipids [SP]	$C_{20}H_{43}NO_2$	0.16	5.78							
500.27834	ST 24:1;O5;G	Sphingolipids [SP]	$C_{26}H_{43}NO_6$	0.21	2.42							
391.28438	ST 24:2;O4	Sphingolipids [SP]	$C_{24}H_{38}O_4$	0.17	2.90							
465.30445	ST 27:1;O;S	Sphingolipids [SP]	$C_{27}H_{46}O_4S$	0.12	9.21							
547.39947	ST 27:2;O;Hex	Sphingolipids [SP]	$C_{33}H_{54}O_6$	0.15	1.41							
433.33133	ST 27:2;O4	Sphingolipids [SP]	$C_{27}H_{44}O_4$	0.17	6.60							
447.34706	ST 28:2;O4	Sphingolipids [SP]	$C_{28}H_{46}O_4$	0.24	9.76							
429.37379	ST 29:1;O2	Sphingolipids [SP]	$C_{29}H_{50}O_2$	0.22	9.19							
489.39494	ST 31:1;O4	Sphingolipids [SP]	$C_{31}H_{54}O_4$	-0.01	4.97							
671.57397	CE 18:2	Sterol Lipids [ST]	$C_{45}H_{76}O_2$	0.32	0.66							
695.57392	CE 20:4	Sterol Lipids [ST]	$C_{47}H_{76}O_2$	0.31	8.55							
465.30439	Cholesterol sulfate	Sterol Lipids [ST]	$C_{27}H_{46}O_4S$	-0.53	3.35							
191.01970	Citric acid	Tricarboxylic acids and derivatives	$C_6H_8O_7$	-0.05	3.44	191.01932	7.66	$C_6H_8O_7$	0.41	173, 111, 87	1.86	7.41
339.23296	unknown	unknown	$C_{24}H_{32}O_2$	-0.10	4.07							

637.54135	unknown	unknown	$C_{40}H_{74}O_6$	0.15	8.25

7.3. Supporting information for Chapter IV: "Dysregulated endocannabinoid pathway and its role in AP-4 deficiency syndrome"

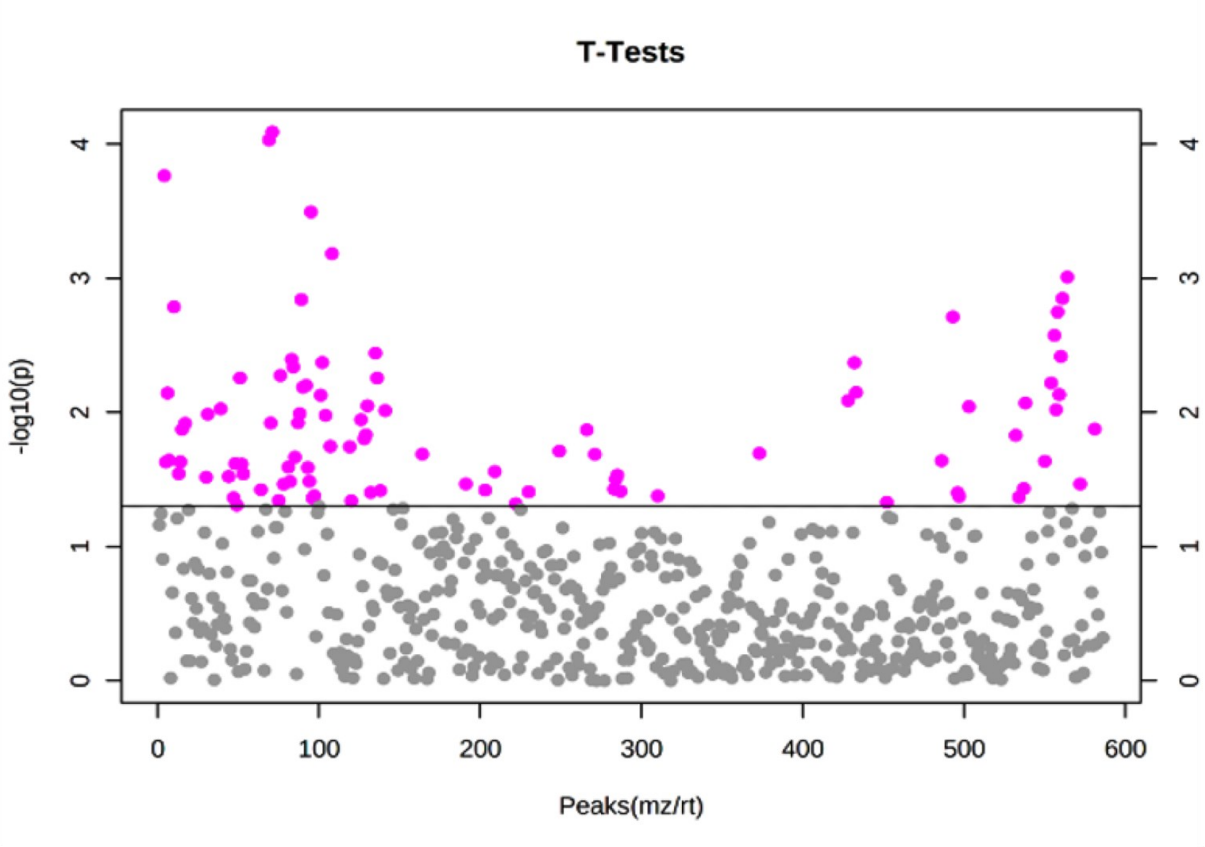

Figure S3.1. *T-test analysis, p-value threshold <0.05 (pink dots: significant lipids; grey dots: unsignificant lipids).*

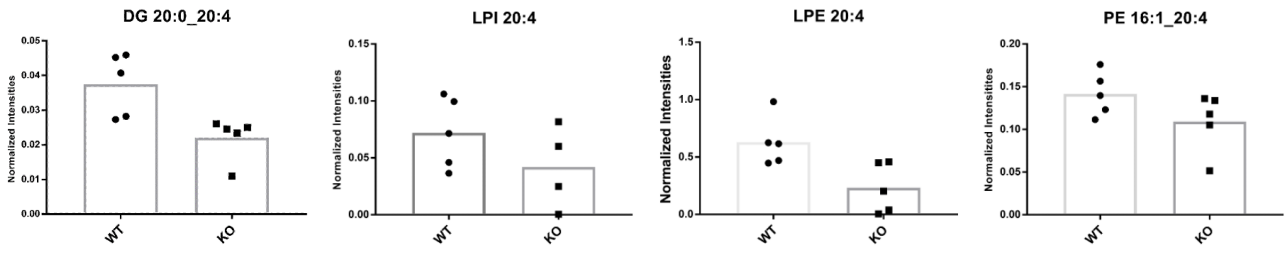

Figure S3.2. *Analysis of lipids containing the acyl chain 20:4.*

Table S3.1. *Putative identified lipids in brain extract.*

RT [min]	CCS (Å²)	m/z meas.	Ions	Compound	Molecular Formula	Mob. 1/K0	MS/MS score	Δm/z [ppm]	ΔCCS [%]
13.58	205.0	379.2843	$[M+H]^+$. $[M+H-H_2O]^+$	2-Arachidonoylglycerol	$C_{23}H_{38}O_4$	0.988	m.c.	m.c.	2.1
16.09	182.5	303.234	$[M-H]^-$	Arachidonic acid	$C_{20}H_{32}O_2$	0.872	m.c.	m.c.	1.3
32.19	283.4	614.587	$[M+NH_4]^+$	CE 14:0	$C_{41}H_{72}O_2$	1.384	976.5	-0.046	3.3
32.65	285.7	642.6185	$[M+NH_4]^+$	CE 16:0	$C_{43}H_{76}O_2$	1.397	974	0.139	2.3
32.13	283.6	640.603	$[M+NH_4]^+$	CE 16:1	$C_{43}H_{74}O_2$	1.386	971.2	0.549	2.6
32.85	287.8	656.6343	$[M+NH_4]^+$	CE 17:0	$C_{44}H_{78}O_2$	1.407	971	0.483	2.3
32.35	285.2	654.6189	$[M+NH_4]^+$	CE 17:1	$C_{44}H_{76}O_2$	1.395	943	0.736	1.8
33.11	289.8	670.6498	$[M+NH_4]^+$	CE 18:0	$C_{45}H_{80}O_2$	1.418	975.8	0.13	1.7
32.17	288.6	666.6187	$[M+NH_4]^+$. $[M+H]^+$. $[M+Na]^+$	CE 18:2	$C_{45}H_{76}O_2$	1.412	977	0.461	2.3
31.82	287.6	664.6045	$[M+NH_4]^+$	CE 18:3	$C_{45}H_{74}O_2$	1.407	979.1	2.583	3
33.02	291.8	696.6664	$[M+NH_4]^+$	CE 20:1	$C_{47}H_{82}O_2$	1.429	975.2	1.836	1.1
32.59	292.9	694.6503	$[M+NH_4]^+$	CE 20:2	$C_{47}H_{80}O_2$	1.434	981.1	1.004	2.3
32.2	292.4	692.6347	$[M+NH_4]^+$	CE 20:3	$C_{47}H_{78}O_2$	1.432	980.5	1.03	2.4
31.89	291.5	690.6189	$[M+NH_4]^+$. $[M+H]^+$. $[M+Na]^+$	CE 20:4	$C_{47}H_{76}O_2$	1.427	978.1	0.739	2
32.23	296.3	718.6502	$[M+NH_4]^+$	CE 22:4	$C_{49}H_{80}O_2$	1.451	982.7	0.766	0.7
28.45	265.3	568.5654	$[M+H]^+$	Cer 18:0;2O/18:0	$C_{36}H_{73}NO_3$	1.293	380.8	-1.154	0.6
29.71	279.2	650.6432	$[M+H]^+$	Cer 18:0;2O/24:1	$C_{42}H_{83}NO_3$	1.365	178.6	-1.896	0.7
28.14	263.6	566.5501	$[M+H]^+$	Cer 18:1;2O/18:0	$C_{36}H_{71}NO_3$	1.285	970.8	-0.97	0.5
29.57	274.8	622.613	$[M+H]^+$. $[M+H]^+$. $[M+H-H_2O]^+$	Cer 18:1;2O/22:0	$C_{40}H_{79}NO_3$	1.343	867.3	-0.46	0.7

29.83	277.3	636.6292	$[M+H]^+$	Cer 18:1;2O/23:0	$C_{41}H_{81}NO_3$	1.355	959.9	0.417	1.3
30.05	280	650.6446	$[M+H]^+$	Cer 18:1;2O/24:0	$C_{42}H_{83}NO_3$	1.369	965.6	0.127	1.2
29.52	277.7	648.6284	$[M+H]^+$. $[M+H-H_2O]^+$	Cer 18:1;2O/24:1	$C_{42}H_{81}NO_3$	1.358	922.3	-0.815	0.9
28.28	264.7	592.566	$[M+H]^+$	Cer 18:2;2O/20:0	$C_{38}H_{73}NO_3$	1.291	909.5	-0.444	0.1
29.07	270	620.5975	$[M+H]^+$	Cer 18:2;2O/22:0	$C_{40}H_{77}NO_3$	1.319	961.9	0.068	0.3
29.38	273	634.6124	$[M+H]^+$. $[M+H-H_2O]^+$	Cer 18:2;2O/23:0	$C_{41}H_{79}NO_3$	1.334	849.9	-1.442	0.1
29.02	273.8	646.6129	$[M+H]^+$. $[M+H-H_2O]^+$	Cer 18:2;2O/24:1	$C_{42}H_{79}NO_3$	1.339	830	-0.571	0.4
30.25	282.5	664.6606	$[M+H]^+$. $[M+H-H_2O]^+$	Cer 20:1;2O/23:0	$C_{43}H_{85}NO_3$	1.382	946.2	1.219	0.5
29.98	283	676.6604	$[M+H]^+$. $[M+H-H_2O]^+$	Cer 20:1;2O/24:1	$C_{44}H_{85}NO_3$	1.385	966.7	0.123	0.1
30.41	329.3	1036.879	$[M+H]^+$	Cer related molecule	$C_{62}H_{117}NO_{10}$	1.622	398.7	3.574	2.4
26.33	262.7	630.5093	$[M+NH_4]^+$,$[M+H]^+$	DG 14:0_22:6	$C_{39}H_{66}O_5$	1.283	348.3	-0.275	0.6
28.45	262	598.5405	$[M+NH_4]^+$. $[M+H-H_2O]^+$. $[M+Na]^+$. $[M+H]^+$	DG 16:0_17:1	$C_{36}H_{68}O_5$	1.279	723.8	0.023	0.9
28.37	260.5	610.5396	$[M+NH_4]^+$	DG 16:0_18:2	$C_{37}H_{68}O_5$	1.272	789.5	-1.079	0.9
27.26	262.8	632.5247	$[M+NH_4]^+$	DG 16:0_20:5	$C_{39}H_{66}O_5$	1.284	878.5	-0.374	1
27.24	257	582.5089	$[M+NH_4]^+$. $[M+Na]^+$	DG 16:1_16:1	$C_{35}H_{64}O_5$	1.254	976.1	-0.539	1.6
28.19	261.6	610.5405	$[M+NH_4]^+$. $[M+H]^+$. $[M+Na]^+$. $[M+H-H_2O]^+$	DG 16:1_18:1	$C_{37}H_{68}O_5$	1.278	860.8	-0.243	1.4
28.54	264.8	624.5566	$[M+NH_4]^+$	DG 17:0_18:2	$C_{38}H_{70}O_5$	1.294	938.9	0.845	1.3
28.42	268.1	648.5563	$[M+NH_4]^+$	DG 17:0_20:4	$C_{40}H_{70}O_5$	1.311	681.6	0.319	1.8
30.41	281.1	696.6506	$[M+NH_4]^+$. $[M+H]^+$. $[M+H-H_2O]^+$	DG 18:0_22:1	$C_{43}H_{82}O_5$	1.377	745.9	0.609	1.8
29.25	276.9	690.6035	$[M+NH_4]^+$	DG 18:0_22:4	$C_{43}H_{76}O_5$	1.356	946.6	0.507	1.8
28.88	266.8	638.5718	$[M+NH_4]^+$. $[M+H-H_2O]^+$. $[M+Na]^+$	DG 18:1_18:1	$C_{39}H_{72}O_5$	1.304	967	-0.071	1.9

28.04	266.6	660.5562	$[M+NH_4]^+$. $[M+H]^+$. $[M+Na]^+$	DG 18:1_20:4	$C_{41}H_{70}O_5$	1.304	800	0.079	1.6
27.72	270.2	684.5567	$[M+NH_4]^+$	DG 18:1_22:6	$C_{43}H_{70}O_5$	1.322	775.6	0.741	2
27.22	262.8	658.5407	$[M+NH_4]^+$	DG 18:2_20:4	$C_{41}H_{68}O_5$	1.285	885.6	0.072	1.8
29.7	272.6	654.6029	$[M+NH_4]^+$. $[M+H]^+$	DG 19:0_18:1	$C_{40}H_{76}O_5$	1.333	865.5	-0.329	1.5
29.14	273.4	676.587	$[M+NH_4]^+$	DG 19:0_20:4	$C_{42}H_{74}O_5$	1.338	709.8	-0.279	1
29.45	276.5	690.6037	$[M+NH_4]^+$	DG 20:0_20:4	$C_{43}H_{76}O_5$	1.354	632.8	1.066	1.5
26.93	266.7	682.5407	$[M+NH_4]^+$	DG 20:4_20:4	$C_{43}H_{68}O_5$	1.305	894.8	0.281	1.6
29.40	278.3	716.6203	$[M+H]^+$	DG 20:4_20:4	$C_{43}H_{68}O_5$	1.363	326.7	2.174	2
30.19	278.3	682.6345	$[M+NH_4]^+$. $[M+H]^+$	DG 21:0_18:1	$C_{42}H_{80}O_5$	1.362	920.6	0.233	2.5
29.97	282.3	718.636	$[M+NH_4]^+$	DG 22:0_20:4	$C_{45}H_{80}O_5$	1.383	789.7	1.875	1.5
29.4	266.6	614.5716	$[M+NH_4]^+$. $[M+Na]^+$. $[M+H-H_2O]^+$. $[M+H]^+$	DG 34:0	$C_{37}H_{72}O_5$	1.302	879.4	-0.19	0.7
28.77	264.1	612.556	$[M+NH_4]^+$	DG 34:1	$C_{37}H_{70}O_5$	1.29	966.8	-0.162	0.7
29.12	266.9	626.5716	$[M+NH_4]^+$. $[M+H-H_2O]^+$. $[M+H]^+$	DG 35:1	$C_{38}H_{72}O_5$	1.304	910.7	-0.355	0.8
29.43	270.0	640.5876	$[M+NH_4]^+$. $[M+H]^+$	DG 36:1	$C_{39}H_{74}O_5$	1.32	854.0	0.247	1.9
28.36	266.4	636.556	$[M+NH_4]^+$. $[M+NH_4]^+$. $[M+H]^+$	DG 36:3	$C_{39}H_{70}O_5$	1.302	959.7	-0.148	1.3
29.92	275.7	668.619	$[M+NH_4]^+$. $[M+H]^+$. $[M+NH_4]^+$	DG 38:1	$C_{41}H_{78}O_5$	1.349	963.8	0.415	1.6
29.41	272.0	666.6031	$[M+NH_4]^+$	DG 38:2	$C_{41}H_{76}O_5$	1.331	973.2	-0.401	1.2
29.27	273.3	664.5871	$[M+NH_4]^+$. $[M+H]^+$. $[M+NH_4]^+$	DG 38:3	$C_{41}H_{74}O_5$	1.337	856.1	-0.67	2.1
29.10	271.8	664.5869	$[M+NH_4]^+$	DG 38:3	$C_{41}H_{74}O_5$	1.329	960.3	-0.33	1.5
28.29	269	660.5556	$[M+NH_4]^+$	DG 38:5	$C_{41}H_{70}O_5$	1.316	781.5	-0.594	1.7
27.66	268.5	658.5404	$[M+NH_4]^+$. $[M+NH_4]^+$. $[M+H]^+$	DG 38:6	$C_{41}H_{68}O_5$	1.313	782.5	0.214	2.1

30.52	280.9	684.6496	$[M+NH_4]^+$	DG 39:0	$C_{42}H_{82}O_5$	1.375	637.4	0.17	1.5
29.92	278	694.6347	$[M+NH_4]^+$	DG 40:2	$C_{43}H_{80}O_5$	1.361	870.4	0.579	1.4
29.65	279.1	692.6189	$[M+NH_4]^+$	DG 40:3	$C_{43}H_{78}O_5$	1.366	959.7	0.149	2.3
28.57	274.2	686.5718	$[M+NH_4]^+$. $[M+H]^+$. $[M+NH_4]^+$	DG 40:6	$C_{43}H_{72}O_5$	1.342	822	0.06	2.0
30.85	286.2	712.6815	$[M+NH_4]^+$	DG 41:0	$C_{44}H_{86}O_5$	1.402	796.6	0.169	0.5
30.57	284.1	710.6661	$[M+NH_4]^+$. $[M+H]^+$. $[M+NH_4]^+$	DG 41:1	$C_{44}H_{84}O_5$	1.391	967.9	0.566	1.4
30.14	280.6	708.6509	$[M+NH_4]^+$. $[M+H]^+$	DG 41:2	$C_{44}H_{82}O_5$	1.374	755.6	1.202	1.3
30.74	287.2	724.6817	$[M+NH_4]^+$. $[M+H]^+$	DG 42:1	$C_{45}H_{86}O_5$	1.407	967.2	0.396	1.6
30.32	283.5	722.6666	$[M+NH_4]^+$	DG 42:2	$C_{45}H_{84}O_5$	1.389	964.6	1.317	1.1
28.42	282.5	718.6352	$[M+NH_4]^+$	DG 42:4	$C_{45}H_{80}O_5$	1.384	708.1	1.095	1.9
29.69	282.5	718.6352	$[M+NH_4]^+$	DG 42:4	$C_{45}H_{80}O_5$	1.384	708.1	1.095	1.9
30.68	289.3	750.6985	$[M+NH_4]^+$	DG 44:2	$C_{47}H_{88}O_5$	1.418	860.6	1.937	0.6
29.88	267.8	616.534	$[M+NH_4]^+$. $[M+NH_4]^+$. $[M+H]^+$	DG O-36:6	$C_{39}H_{66}O_4$	1.308	535.3	6.807	3.9
31.1	283.4	700.6276	$[M+NH_4]^+$. $[M+H]^+$. $[M+NH_4]^+$	DG O-42:6	$C_{45}H_{78}O_4$	1.388	962	5.331	2.6
29.5	303.5	830.7098	$[M+H]^+$	HexCer 18:0;2O/24:0;O	$C_{48}H_{95}NO_9$	1.491	348.8	2.014	0.6
30.09	325.1	982.83	$[M+H]^+$	HexCer 18:0;3O/34:2;(2OH)	$C_{58}H_{111}NO_{10}$	1.601	193.6	3.681	1.8
27.16	284.5	728.6034	$[M+H]^+$. $[M+NH_4]^+$. $[M+H-H_2O]^+$. $[M+H]^+$. $[M+H]^+$	HexCer 18:1;2O/18:0	$C_{42}H_{81}NO_8$	1.394	816.8	-0.612	0.9
26.85	288.3	744.5989	$[M+H]^+$	HexCer 18:1;2O/18:0;O	$C_{42}H_{81}NO_9$	1.413	789.8	0.987	1.6
25.73	281.9	726.5883	$[M+H]^+$	HexCer 18:1;2O/18:1	$C_{42}H_{79}NO_8$	1.382	358.8	0.698	0.5
28.14	289	756.6351	$[M+H]^+$	HexCer 18:1;2O/20:0	$C_{44}H_{85}NO_8$	1.417	775.6	0.827	3.1
28.89	293.8	784.667	$[M+H]^+$	HexCer 18:1;2O/22:0	$C_{46}H_{89}NO_8$	1.442	706.9	1.076	0.7

28.15	292.8	782.6511	$[M+H]^+$	HexCer 18:1;2O/22:1	$C_{46}H_{87}NO_8$	1.437	779.1	0.663	0.4
27.89	296	798.6459	$[M+H]^+$. $[M+H-H_2O]^+$	HexCer 18:1;2O/22:1;O	$C_{46}H_{87}NO_9$	1.453	823.7	0.773	0.1
29.18	296.2	798.6831	$[M+H]^+$	HexCer 18:1;2O/23:0	$C_{47}H_{91}NO_8$	1.454	775.6	1.725	0.4
29.02	299.9	814.6792	$[M+H]^+$. $[M+H-H_2O]^+$	HexCer 18:1;2O/23:0;O	$C_{47}H_{91}NO_9$	1.472	826.6	3.241	0.4
29.45	298.7	812.6993	$[M+H]^+$. $[M+H-H_2O]^+$	HexCer 18:1;2O/24:0	$C_{48}H_{93}NO_8$	1.466	742.3	2.317	0.9
29.3	302.3	828.6947	$[M+H]^+$. $[M+H-H_2O]^+$. $[M+Na]^+$	HexCer 18:1;2O/24:0;O	$C_{48}H_{93}NO_9$	1.485	825.4	2.877	0.7
28.61	301.2	826.6785	$[M+H]^+$. $[M+H-H_2O]^+$	HexCer 18:1;2O/24:1;O	$C_{48}H_{91}NO_9$	1.479	826.1	2.175	0.4
29.56	303.7	842.7102	$[M+H]^+$	HexCer 18:1;2O/25:0;O	$C_{49}H_{95}NO_9$	1.492	799.9	3.086	0.2
29.14	301.9	840.6942	$[M+H]^+$	HexCer 18:1;2O/25:1;O	$C_{49}H_{93}NO_9$	1.483	482.8	2.195	0.3
28.95	303.8	840.694	$[M+H]^+$. $[M+H-H_2O]^+$	HexCer 18:1;2O/25:1;O	$C_{49}H_{93}NO_9$	1.493	807.5	1.689	0.3
29.91	302.8	840.7298	$[M+H]^+$	HexCer 18:1;2O/26:0	$C_{50}H_{97}NO_8$	1.488	572.4	1.388	1.4
29.37	302.9	838.7141	$[M+H]^+$. $[M+H-H_2O]^+$	HexCer 18:1;2O/26:1	$C_{50}H_{95}NO_8$	1.488	510.2	0.989	0.4
29.23	305.8	854.7086	$[M+H]^+$. $[M+H-H_2O]^+$	HexCer 18:1;2O/26:1;O	$C_{50}H_{95}NO_9$	1.503	744.1	1.131	0.2
30.21	325.7	966.8359	$[M+H]^+$	HexCer 18:1;2O/34:1;O	$C_{58}H_{111}NO_9$	1.604	306.4	2.714	1.2
30.38	327.7	1010.863	$[M+H]^+$	HexCer 18:1;2O/36:1;2O	$C_{60}H_{115}NO_{10}$	1.614	181.1	2.961	1.6
30.51	329.7	994.868	$[M+H]^+$	HexCer 18:1;2O/36:1;O	$C_{60}H_{115}NO_9$	1.624	396.9	3.812	0.8
30.52	331.4	1020.885	$[M+H]^+$	HexCer 18:1;2O/38:2;O	$C_{62}H_{117}NO_9$	1.633	346.5	4.243	1
28.11	294.9	798.6462	$[M+H]^+$	HexCer 18:2;2O/22:0;O	$C_{46}H_{87}NO_9$	1.447	755.8	1.2	
27.28	290.9	780.6349	$[M+H]^+$	HexCer 18:2;2O/22:1	$C_{46}H_{85}NO_8$	1.427	756.7	0.021	0.4
28.48	297	812.6623	$[M+H]^+$. $[M+H-H_2O]^+$	HexCer 18:2;2O/23:0;O	$C_{47}H_{89}NO_9$	1.458	791.4	1.57	0.6
28.24	295.7	808.6667	$[M+H]^+$. $[M+NH_4]^+$	HexCer 18:2;2O/24:1	$C_{48}H_{89}NO_8$	1.452	619	0.665	0.4

28.08	298.6	824.6612	$[M+H]^+$. $[M+H-H_2O]^+$	HexCer 18:2;2O/24:1;O	$C_{48}H_{89}NO_9$	1.466	718.2	-0.153	0.2
29.78	306.1	856.7246	$[M+H]^+$. $[M+H-H_2O]^+$	HexCer 20:1;2O/24:0;O	$C_{50}H_{97}NO_9$	1.504	701.2	1.468	0.7
29.69	310	882.7425	$[M+H]^+$	HexCer 20:2;2O/26:0;O	$C_{52}H_{99}NO_9$	1.524	524.9	3.07	0.8
29.37	300.2	830.6715	$[M+HCOO]^-$. $[M-H]^-$	HexCer 40:0;2O	$C_{46}H_{91}NO_8$	1.474	868.5	-1.323	0
29.24	302.5	846.6662	$[M+HCOO]^-$	HexCer 40:0;3O	$C_{46}H_{91}NO_9$	1.486	747.2	-1.614	0.4
29.48	305.1	860.6815	$[M+HCOO]^-$. $[M-H]^-$	HexCer 41:0;3O	$C_{47}H_{93}NO_9$	1.499	802.7	-1.995	0.1
29.31	303.2	858.6671	$[M+HCOO]^-$. $[M-H]^-$	HexCer 41:1;3O	$C_{47}H_{91}NO_9$	1.49	772.5	-0.566	0.4
28.79	299.6	840.6559	$[M+HCOO]^-$. $[M-H]^-$	HexCer 41:2;2O	$C_{47}H_{89}NO_8$	1.472	781.7	-1.325	0.6
29.75	307.8	874.6971	$[M+HCOO]^-$. $[M-H]^-$	HexCer 42:0;3O	$C_{48}H_{95}NO_9$	1.513	766.6	-2.003	0.2
29.12	302.4	854.672	$[M+HCOO]^-$	HexCer 42:2;2O	$C_{48}H_{91}NO_8$	1.486	803.9	-0.857	0.1
28.57	301.2	852.656	$[M+HCOO]^-$. $[M-H]^-$	HexCer 42:3;2O	$C_{48}H_{89}NO_8$	1.48	774	-1.158	0
30.02	310.9	900.7131	$[M+HCOO]^-$. $[M+Cl]^-$	HexCer 44:1;3O	$C_{50}H_{97}NO_9$	1.529	727.2	-1.632	0.4
29.48	309.7	898.6977	$[M+HCOO]^-$. $[M-H]^-$	HexCer 44:2;3O	$C_{50}H_{95}NO_9$	1.523	748.4	-1.358	0.2
28.53	291.4	770.6499	$[M+H]^+$	HexCer 16:1;2O/23:0	$C_{45}H_{87}NO_8$	1.429	687.5	-0.802	0.4
7.51	234.3	526.3152	$[M+HCOO]^-$	LPC 15:0	$C_{23}H_{48}NO_7P$	1.14	953.6	0.258	1.1
9.76	237.8	540.3306	$[M+HCOO]^-$	LPC 16:0	$C_{24}H_{50}NO_7P$	1.158	925.9	0.174	2.2
12.91	241.7	554.3464	$[M+HCOO]^-$	LPC 17:0	$C_{25}H_{52}NO_7P$	1.178	1000	0.143	1.1
14.54	245.2	568.3619	$[M+HCOO]^-$	LPC 18:0	$C_{26}H_{54}NO_7P$	1.195	957.7	-0.201	1
10.12	236.8	522.355	$[M+H]^+$	LPC 18:1	$C_{26}H_{52}NO_7P$	1.152	956.2	-0.476	0.1
15.22	245	538.3866	$[M+H]^+$	LPC 19:0	$C_{27}H_{56}NO_7P$	1.193	962.4	-0.024	1.2
12.74	240.2	536.3707	$[M+H]^+$	LPC 19:1	$C_{27}H_{54}NO_7P$	1.17	997.3	-0.643	1.5

16.3	249.8	552.402	$[M+H]^+$	LPC 20:0	$C_{28}H_{58}NO_7P$	1.217	998.4	-0.577	1.3
14.4	243.9	550.3864	$[M+H]^+$. $[M+Na]^+$	LPC 20:1	$C_{28}H_{56}NO_7P$	1.188	979.8	-0.652	1.5
13.66	245.8	550.3863	$[M+H]^+$	LPC 20:1	$C_{28}H_{56}NO_7P$	1.197	994.2	-0.901	1.6
8.09	243	588.3306	$[M+HCOO]^-$. $[M+Cl]^-$	LPC 20:4	$C_{28}H_{50}NO_7P$	1.186	924	-0.196	1.5
7.6	243.1	588.3307	$[M+HCOO]^-$	LPC 20:4	$C_{28}H_{50}NO_7P$	1.186	856.3	0.112	1.6
16.83	250.3	578.4179	$[M+H]^+$. $[M+Na]^+$	LPC 22:1	$C_{30}H_{60}NO_7P$	1.221	958.5	-0.269	1.4
11.71	249.3	616.3615	$[M+HCOO]^-$	LPC 22:4	$C_{30}H_{54}NO_7P$	1.218	895.8	-0.733	1.4
7.54	246.6	612.3302	$[M+HCOO]^-$	LPC 22:6	$C_{30}H_{50}NO_7P$	1.204	870.1	-0.07	1.5
22.93	260.8	608.4653	$[M+H]^+$	LPC 24:0	$C_{32}H_{66}NO_7P$	1.273	949.8	0.168	0.7
19.57	256.3	606.4491	$[M+H]^+$	LPC 24:1	$C_{32}H_{64}NO_7P$	1.251	979.6	-0.664	0.9
7.27	206.4	438.2635	$[M-H]^-$	LPE 15:0	$C_{20}H_{42}NO_7P$	0.999	984.8	1.875	2.3
9.48	210.4	452.2789	$[M-H]^-$	LPE 16:0	$C_{21}H_{44}NO_7P$	1.019	982.1	1.41	2.9
5.27	207.4	450.2632	$[M-H]^-$	LPE 16:1	$C_{21}H_{42}NO_7P$	1.005	978.5	1.237	3.1
14.77	217.7	480.3102	$[M-H]^-$	LPE 18:0	$C_{23}H_{48}NO_7P$	1.057	976.8	1.463	2.7
12.11	214.1	478.2944	$[M-H]^-$	LPE 18:1	$C_{23}H_{46}NO_7P$	1.039	979.1	0.978	2.8
12.96	219.4	494.3254	$[M-H]^-$	LPE 19:0	$C_{24}H_{50}NO_7P$	1.066	202.2	0.462	0.5
13.1	218.8	492.3102	$[M-H]^-$	LPE 19:1	$C_{24}H_{48}NO_7P$	1.063	970.6	1.376	2.5
17.06	224.6	508.3412	$[M-H]^-$	LPE 20:0	$C_{25}H_{52}NO_7P$	1.092	970.2	0.63	2.8
14.71	222.4	506.3258	$[M-H]^-$	LPE 20:1	$C_{25}H_{50}NO_7P$	1.081	975.4	1.187	3.1
13.94	231.1	508.3393	$[M+H]^+$	LPE 20:1	$C_{25}H_{50}NO_7P$	1.124	983.8	-0.975	1.1
13.76	230.9	508.3392	$[M+H]^+$	LPE 20:1	$C_{25}H_{50}NO_7P$	1.122	982.8	-0.82	1

13.08	221.6	504.31	$[M-H]^-$	LPE 20:2	$C_{25}H_{48}NO_7P$	1.077	963.4	1.095	3.3
12.77	221.2	504.31	$[M-H]^-$	LPE 20:2	$C_{25}H_{48}NO_7P$	1.075	968.3	1.019	3.2
9.91	217.7	502.2943	$[M-H]^-$	LPE 20:3	$C_{25}H_{46}NO_7P$	1.058	961.3	0.594	2.3
7.47	216.9	500.2789	$[M-H]^-$	LPE 20:4	$C_{25}H_{44}NO_7P$	1.054	969.9	1.112	3.3
4.74	215.9	498.2631	$[M-H]^-$	LPE 20:5	$C_{25}H_{42}NO_7P$	1.049	951.4	0.666	2.7
15.98	225.4	520.3411	$[M-H]^-$	LPE 21:1	$C_{26}H_{52}NO_7P$	1.097	950.3	0.582	2.3
17.31	229.1	534.3568	$[M-H]^-$	LPE 22:1	$C_{27}H_{54}NO_7P$	1.115	960.4	0.484	2.8
17.59	229.9	534.3568	$[M-H]^-$	LPE 22:1	$C_{27}H_{54}NO_7P$	1.119	983.3	0.575	3.2
15.62	227.8	532.341	$[M-H]^-$	LPE 22:2	$C_{27}H_{52}NO_7P$	1.109	983.5	0.468	2.6
13.55	224.7	530.325	$[M-H]^-$	LPE 22:3	$C_{27}H_{50}NO_7P$	1.094	950.6	-0.065	2.9
14.05	225.9	530.3254	$[M-H]^-$	LPE 22:3	$C_{27}H_{50}NO_7P$	1.099	981.9	0.363	3.4
13.08	233.1	532.339	$[M+H]^+$	LPE 22:3	$C_{27}H_{50}NO_7P$	1.135	781.4	-1.424	1.8
11.89	223.2	528.3096	$[M-H]^-$	LPE 22:4	$C_{27}H_{48}NO_7P$	1.086	963.5	0.032	2.6
10.17	229.7	530.3238	$[M+H]^+$	LPE 22:4	$C_{27}H_{48}NO_7P$	1.118	986.6	-0.65	1.3
9.04	222.1	526.2937	$[M-H]^-$	LPE 22:5	$C_{27}H_{46}NO_7P$	1.081	966.9	-0.324	3.3
7.38	221.5	524.2791	$[M-H]^-$	LPE 22:6	$C_{27}H_{44}NO_7P$	1.078	834.7	0.872	3.4
13.29	229.5	554.3251	$[M-H]^-$	LPE 24:5	$C_{29}H_{50}NO_7P$	1.118	969.5	-0.141	3.2
12.82	229	554.3235	$[M-H]^-$	LPE 24:5	$C_{29}H_{50}NO_7P$	1.116	988.9	-3.716	2.9
11.34	227.8	552.3089	$[M-H]^-$	LPE 24:6	$C_{29}H_{48}NO_7P$	1.11	506.4	-1.467	2.3
26.91	275.8	726.5429	$[M+H]^+$	LPE 36:4	$C_{41}H_{76}NO_7P$	1.352	964.1	-0.436	0.7
27.77	281.7	754.5738	$[M+H]^+$	LPE 38:4	$C_{43}H_{80}NO_7P$	1.382	924.7	-1.167	0.3

12.43	209.6	436.2841	$[M-H]^-$	LPE O-16:1	$C_{21}H_{44}NO_6P$	1.015	832	1.808	3
15.86	216.5	464.3152	$[M-H]^-$	LPE O-18:1	$C_{23}H_{48}NO_6P$	1.05	838.5	1.641	3.4
15.88	224.0	464.3155	$[M-H]^-$	LPE O-18:1	$C_{23}H_{48}NO_6P$	1.086	383.7	1.657	7
13.28	214.9	462.2997	$[M-H]^-$	LPE O-18:2	$C_{23}H_{46}NO_6P$	1.042	831.9	1.528	3.8
15.59	229.5	492.3443	$[M+H]^+$	LPE O-20:2	$C_{25}H_{50}NO_6P$	1.115	925.9	-1.389	2.3
10.58	221.1	509.2889	$[M-H]^-$	LPG 18:1	$C_{24}H_{47}O_9P$	1.075	909.6	0.807	0.1
6.83	223.9	531.273	$[M-H]^-$	LPG 20:4	$C_{26}H_{45}O_9P$	1.09	967.3	0.365	3.4
4.52	229.6	557.2731	$[M-H]^-$	LPI 15:0	$C_{24}H_{47}O_{12}P$	1.119	950.1	-0.423	3.3
7.00	232.9	571.289	$[M-H]^-$	LPI 16:0	$C_{25}H_{49}O_{12}P$	1.136	831.3	0.315	3.5
12.86	239.9	599.3202	$[M-H]^-$	LPI 18:0	$C_{27}H_{53}O_{12}P$	1.171	835.8	-0.022	2.7
9.51	236.4	597.305	$[M-H]^-$	LPI 18:1	$C_{27}H_{51}O_{12}P$	1.154	838.6	0.699	2.3
4.66	240.6	619.2887	$[M-H]^-$	LPI 20:4	$C_{29}H_{49}O_{12}P$	1.175	956.8	-0.239	3.2
5.41	240.7	619.2886	$[M-H]^-$	LPI 20:4	$C_{29}H_{49}O_{12}P$	1.176	821.5	-0.446	3.3
4.66	244.5	643.2889	$[M-H]^-$	LPI 22:6	$C_{31}H_{49}O_{12}P$	1.195	922.3	0.216	3.1
4.76	216.2	482.2529	$[M-H]^-$	LPS 15:0	$C_{21}H_{42}NO_9P$	1.05	854.1	0.931	3.1
7.94	224.3	522.2813	$[M-H]^-$	LPS 18:1	$C_{24}H_{46}NO_9P$	1.091	825.3	0.125	3.1
4.82	230.4	568.2684	$[M-H]^-$	LPS 22:6	$C_{28}H_{44}NO_9P$	1.123	800.1	0.322	2.9
25.00	282	750.5281	$[M+HCOO]^-$	PC 14:0_16:0	$C_{38}H_{76}NO_8P$	1.383	897.5	-1.410	0.9
23.15	280.3	748.5123	$[M+HCOO]^-$	PC 14:0_16:1	$C_{38}H_{74}NO_8P$	1.374	863.8	-1.520	0.7
25.78	281.0	720.5544	$[M+H]^+$	PC 15:0_16:0	$C_{39}H_{78}NO_8P$	1.377	994.0	0.913	0.2
27.34	291.7	804.5749	$[M+HCOO]^-$	PC 16:0_18:1	$C_{42}H_{82}NO_8P$	1.432	540.2	-1.268	0.1

25.57	289.8	802.5594	$[M+HCOO]^-$	PC 16:0_18:2	$C_{42}H_{80}NO_8P$	1.422	952.1	-1.137	0.1
25.60	283.6	758.5702	$[M+H]^+$	PC 16:0_18:2	$C_{42}H_{80}NO_8P$	1.391	994.2	1.158	0.6
29.19	280.7	772.5849	$[M-H]^-$	PC 16:0_20:1	$C_{43}H_{84}NO_8P$	1.377	923.9	-1.612	0.8
25.13	283.6	758.5707	$[M+H]^+$	PC 16:1_18:1	$C_{42}H_{80}NO_8P$	1.391	616.9	1.461	0.6
28.99	294	790.6317	$[M+H]^+$	PC 18:0_18:0	$C_{44}H_{88}NO_8P$	1.443	931.9	-0.782	0.6
28.92	302.6	860.6372	$[M+HCOO]^-$	PC 18:0_20:1	$C_{46}H_{90}NO_8P$	1.487	860.4	-1.607	0.3
27.69	299.5	856.6061	$[M+HCOO]^-$	PC 18:0_20:3	$C_{46}H_{86}NO_8P$	1.472	522.4	-1.399	0.3
23.32	289.6	830.5716	$[M+H]^+$. $[M+Na]^+$. $[M+H]^+$	PC 18:2_22:6	$C_{48}H_{80}NO_8P$	1.422	996.9	2.614	0.7
30.01	311.0	902.6852	$[M+HCOO]^-$	PC 19:1_22:0	$C_{49}H_{96}NO_8P$	1.53	630.5	-0.903	0.4
23.71	298.5	874.5589	$[M+HCOO]^-$	PC 20:4_20:4	$C_{48}H_{80}NO_8P$	1.467	740	-1.921	1.3
17.44	248.7	592.3968	$[M+H]^+$	PC 22:1	$C_{30}H_{58}NO_8P$	1.214	600.9	-0.734	0.5
30.26	313.2	916.7004	$[M+HCOO]^-$	PC 24:0_18:1	$C_{50}H_{98}NO_8P$	1.541	625.1	-0.843	0.3
22.54	273.2	678.5068	$[M+H]^+$. $[M+Na]^+$	PC 28:0	$C_{36}H_{72}NO_8P$	1.337	998	0.167	0.1
23.69	275.9	692.5233	$[M+H]^+$	PC 29:0	$C_{37}H_{74}NO_8P$	1.351	552.8	0.974	0.1
24.69	278.8	706.5389	$[M+H]^+$	PC 30:0	$C_{38}H_{76}NO_8P$	1.366	996.6	1.237	0.2
23.97	278.1	718.5386	$[M+H]^+$	PC 31:1	$C_{39}H_{76}NO_8P$	1.363	988.1	0.483	0.2
26.53	284.4	734.5713	$[M+H]^+$	PC 32:0	$C_{40}H_{80}NO_8P$	1.394	997.8	2.731	0.4
25.77	282.1	732.5544	$[M+H]^+$	PC 32:1	$C_{40}H_{78}NO_8P$	1.383	994.9	0.789	1.3
25.47	285.8	776.5436	$[M+HCOO]^-$	PC 32:1	$C_{40}H_{78}NO_8P$	1.402	836.3	-1.391	0.5
25.21	285.8	776.5438	$[M+HCOO]^-$. $[M+Cl]^-$	PC 32:1	$C_{40}H_{78}NO_8P$	1.402	886.4	-1.145	0.5
23.32	278.3	730.5388	$[M+H]^+$	PC 32:2	$C_{40}H_{76}NO_8P$	1.364	997.0	0.869	0.2

22.97	277.3	728.5232	$[M+H]^+$	PC 32:3	$C_{40}H_{74}NO_8P$	1.359	992.8	1.019	0.3
27.60	290.3	792.5746	$[M+HCOO]^-$	PC 33:0	$C_{41}H_{82}NO_8P$	1.425	363.3	-1.782	0.2
26.00	283.6	746.5703	$[M+H]^+$	PC 33:1	$C_{41}H_{80}NO_8P$	1.390	993.8	1.207	0.5
24.28	280.9	744.5548	$[M+H]^+$	PC 33:2	$C_{41}H_{78}NO_8P$	1.377	946.2	1.361	0.5
28.09	293	806.5904	$[M+HCOO]^-$	PC 34:0	$C_{42}H_{84}NO_8P$	1.438	826.3	-1.534	0.1
27.83	289.1	762.6025	$[M+H]^+$. $[M+Na]^+$. $[M+H]^+$	PC 34:0	$C_{42}H_{84}NO_8P$	1.418	995	2.26	0.4
26.94	291.7	804.5757	$[M+HCOO]^-$	PC 34:1	$C_{42}H_{82}NO_8P$	1.432	803.8	-0.35	0.1
25.82	285.1	758.5702	$[M+H]^+$	PC 34:2	$C_{42}H_{80}NO_8P$	1.398	996.5	0.96	0.1
23.65	281	756.5545	$[M+H]^+$	PC 34:3	$C_{42}H_{78}NO_8P$	1.378	995.4	1.051	0.8
23.04	280.3	754.539	$[M+H]^+$	PC 34:4	$C_{42}H_{76}NO_8P$	1.375	996.8	1.126	0.8
27.46	289.1	774.603	$[M+H]^+$	PC 35:1	$C_{43}H_{84}NO_8P$	1.418	884.7	2.67	0.6
26.19	286.7	772.5866	$[M+H]^+$	PC 35:2	$C_{43}H_{82}NO_8P$	1.406	925.4	2.687	0.4
24.09	283.3	768.5546	$[M+H]^+$	PC 35:4	$C_{43}H_{78}NO_8P$	1.39	993.1	1.146	0.2
27.93	291.6	788.6186	$[M+H]^+$	PC 36:1	$C_{44}H_{86}NO_8P$	1.431	994.6	2.981	1.3
27.18	289.2	786.6018	$[M+H]^+$	PC 36:2	$C_{44}H_{84}NO_8P$	1.419	996.1	1.131	0.7
26.39	288.5	784.586	$[M+H]^+$	PC 36:3	$C_{44}H_{82}NO_8P$	1.415	995.0	1.3	2.0
25.94	287.5	784.5859	$[M+H]^+$	PC 36:3	$C_{44}H_{82}NO_8P$	1.411	992.0	1.039	0.3
25.36	293.3	826.5601	$[M+HCOO]^-$. $[M+Cl]^-$	PC 36:4	$C_{44}H_{80}NO_8P$	1.44	890.4	-0.256	0.4
25.04	286.6	782.5716	$[M+H]^+$. $[M+K]^+$. $[M+H]^+$. $[M+Na]^+$	PC 36:4	$C_{44}H_{80}NO_8P$	1.406	996.5	2.758	1.4
23.83	283.7	780.5551	$[M+H]^+$	PC 36:5	$C_{44}H_{78}NO_8P$	1.392	995.2	1.73	0.5
23.34	283.7	780.5555	$[M+H]^+$	PC 36:5	$C_{44}H_{78}NO_8P$	1.392	995.8	2.121	0.3

22.51	282.7	778.5394	$[M+H]^+$. $[M+Na]^+$	PC 36:6	$C_{44}H_{76}NO_8P$	1.387	995.7	1.625	0.6
21.99	281.4	778.5383	$[M+H]^+$	PC 36:6	$C_{44}H_{76}NO_8P$	1.381	995.4	0.733	1.8
24.28	286.4	794.5705	$[M+H]^+$	PC 37:5	$C_{45}H_{80}NO_8P$	1.406	995.2	1.529	0.4
23.58	285.7	792.5556	$[M+H]^+$	PC 37:6	$C_{45}H_{78}NO_8P$	1.402	988.5	2.372	0.6
28.95	296.3	816.6493	$[M+H]^+$	PC 38:1	$C_{46}H_{90}NO_8P$	1.455	993.7	2.012	0.9
27.45	292.7	812.6168	$[M+H]^+$	PC 38:3	$C_{46}H_{86}NO_8P$	1.437	994.5	0.481	0.6
26.68	298.5	854.5906	$[M+HCOO]^-$	PC 38:4	$C_{46}H_{84}NO_8P$	1.467	918.5	-1.277	0.4
26.14	290.5	810.6011	$[M+H]^+$	PC 38:4	$C_{46}H_{84}NO_8P$	1.426	997.0	0.608	0.5
26.38	291.2	810.6023	$[M+H]^+$	PC 38:4	$C_{46}H_{84}NO_8P$	1.43	995.1	2.018	0.2
25.21	289.6	808.5866	$[M+H]^+$	PC 38:5	$C_{46}H_{82}NO_8P$	1.422	995.0	1.97	0.7
25.81	290.2	808.5855	$[M+H]^+$	PC 38:5	$C_{46}H_{82}NO_8P$	1.425	994.7	0.304	0.6
24.5	289.4	806.5709	$[M+H]^+$	PC 38:6	$C_{46}H_{80}NO_8P$	1.421	995.7	1.83	0.5
23.79	287.3	806.5713	$[M+H]^+$	PC 38:6	$C_{46}H_{80}NO_8P$	1.411	994.1	2.293	0.7
22.81	286.2	804.5553	$[M+H]^+$	PC 38:7	$C_{46}H_{78}NO_8P$	1.405	994.6	1.494	0.6
23.45	286.9	804.5549	$[M+H]^+$	PC 38:7	$C_{46}H_{78}NO_8P$	1.409	993.9	1.444	0.1
29.31	299	830.6665	$[M+H]^+$	PC 39:1	$C_{47}H_{92}NO_8P$	1.468	800.6	3.035	1.3
27.57	294	824.6205	$[M+H]^+$	PC 39:4	$C_{47}H_{86}NO_8P$	1.444	657.9	5.363	0.4
26.25	291.8	822.6011	$[M+H]^+$	PC 39:5	$C_{47}H_{84}NO_8P$	1.433	995	0.447	0.8
25.7	291.1	820.5867	$[M+H]^+$	PC 39:6	$C_{47}H_{82}NO_8P$	1.43	995	1.643	0.2
23.84	289.4	818.5714	$[M+H]^+$	PC 39:7	$C_{47}H_{80}NO_8P$	1.421	993.7	2.223	0.1
27.98	303.8	882.6218	$[M+HCOO]^-$	PC 40:4	$C_{48}H_{88}NO_8P$	1.494	793.8	-1.386	0.5

27.75	296.6	838.6336	$[M+H]^+$	PC 40:4	$C_{48}H_{88}NO_8P$	1.457	996.7	2.075	0.8
27.51	295.8	838.6317	$[M+H]^+$	PC 40:4	$C_{48}H_{88}NO_8P$	1.453	974.3	0.313	1.1
26.93	294.8	836.6161	$[M+H]^+$	PC 40:5	$C_{48}H_{86}NO_8P$	1.448	983	-0.275	0.7
27.40	295.6	836.6156	$[M+H]^+$	PC 40:5	$C_{48}H_{86}NO_8P$	1.452	991.4	-0.256	0.4
26.76	301.8	878.591	$[M+HCOO]^-$	PC 40:6	$C_{48}H_{84}NO_8P$	1.484	848	-0.681	0.8
26.44	294.1	834.6032	$[M+H]^+$	PC 40:6	$C_{48}H_{84}NO_8P$	1.444	996.1	2.951	0.4
24.76	292.3	832.5875	$[M+H]^+$	PC 40:7	$C_{48}H_{82}NO_8P$	1.436	995.6	2.934	0.5
24.25	291.4	832.5863	$[M+H]^+$	PC 40:7	$C_{48}H_{82}NO_8P$	1.431	991.6	1.361	0.5
24.61	299.5	876.575	$[M+HCOO]^-$	PC 40:7	$C_{48}H_{82}NO_8P$	1.472	692.1	-1.191	0.9
22.03	287.7	828.5557	$[M+H]^+$	PC 40:9	$C_{48}H_{78}NO_8P$	1.413	768.5	2.394	0.7
29.18	301.8	856.6828	$[M+H]^+$	PC 41:2	$C_{49}H_{94}NO_8P$	1.483	979.8	2.735	1.3
25.77	294.4	846.6025	$[M+H]^+$	PC 41:7	$C_{49}H_{84}NO_8P$	1.447	834.6	2.015	0.6
22.85	292	854.5722	$[M+H]^+$. $[M+Na]^+$. $[M+H]^+$. $[M+Na]^+$. $[M+K]^+$	PC 42:10	$C_{50}H_{80}NO_8P$	1.435	995.5	3.199	0.6
21.56	290.2	852.5563	$[M+H]^+$	PC 42:11	$C_{50}H_{78}NO_8P$	1.426	979.1	2.944	0.9
29.61	311.8	914.685	$[M+HCOO]^-$	PC 42:2	$C_{50}H_{96}NO_8P$	1.534	817.1	-0.615	0.5
28.49	300.8	866.6651	$[M+H]^+$	PC 42:4	$C_{50}H_{92}NO_8P$	1.478	995.1	2.023	0.6
27.78	299.1	862.6328	$[M+H]^+$	PC 42:6	$C_{50}H_{88}NO_8P$	1.47	965.5	0.853	0.4
26.04	296.1	860.6184	$[M+H]^+$	PC 42:7	$C_{50}H_{86}NO_8P$	1.455	989.4	2.42	0.8
26.48	297.2	860.6183	$[M+H]^+$	PC 42:7	$C_{50}H_{86}NO_8P$	1.461	994.2	2.23	0.5
25.05	294.6	858.6025	$[M+H]^+$	PC 42:8	$C_{50}H_{84}NO_8P$	1.447	995	2.075	0.7
24.82	295.3	858.6022	$[M+H]^+$	PC 42:8	$C_{50}H_{84}NO_8P$	1.451	988.1	1.737	0.4

23.78	293.2	856.5868	$[M+H]^+$	PC 42:9	$C_{50}H_{82}NO_8P$	1.441	989.1	2	0.6
23.29	293.7	856.585	$[M+H]^+$	PC 42:9	$C_{50}H_{82}NO_8P$	1.443	919.5	0.217	0.4
24.18	294.6	856.5867	$[M+H]^+$	PC 42:9	$C_{50}H_{82}NO_8P$	1.448	995	1.867	0.1
29.98	305.7	884.7132	$[M+H]^+$	PC 43:2	$C_{51}H_{98}NO_8P$	1.503	992.1	3.478	1.7
24.29	297.3	882.6028	$[M+H]^+$	PC 44:10	$C_{52}H_{84}NO_8P$	1.462	995.4	2.379	0.6
23.68	296.9	880.5861	$[M+H]^+$	PC 44:11	$C_{52}H_{82}NO_8P$	1.46	972.7	1.078	0.1
23.05	295	880.5864	$[M+H]^+$	PC 44:11	$C_{52}H_{82}NO_8P$	1.45	992.7	1.475	0.6
22.37	294.4	878.5733	$[M+H]^+$	PC 44:12	$C_{52}H_{80}NO_8P$	1.447	997.9	4.418	0.6
30.21	317	942.7155	$[M+HCOO]^-$	PC 44:2	$C_{52}H_{100}NO_8P$	1.56	642	-1.897	0.4
30.45	309.6	898.7302	$[M+H]^+$	PC 44:2	$C_{52}H_{100}NO_8P$	1.523	995.1	4.699	1.4
29.75	302.3	896.7143	$[M+H]^+$	PC 44:3	$C_{52}H_{98}NO_8P$	1.486	995	4.512	2.9
26.38	299.1	886.6336	$[M+H]^+$	PC 44:8	$C_{52}H_{88}NO_8P$	1.471	997.5	2.07	1.1
26.00	301.9	910.6345	$[M+H]^+$	PC 46:10	$C_{54}H_{88}NO_8P$	1.485	953.4	2.677	1.6
23.67	299.8	906.6022	$[M+H]^+$	PC 46:12	$C_{54}H_{84}NO_8P$	1.475	991.7	1.477	1
27.76	287.1	764.5786	$[M+HCOO]^-$	PC O-16:0_16:0	$C_{40}H_{82}NO_7P$	1.408	943.1	-2.972	0.9
28.78	296.5	818.6276	$[M+HCOO]^-$	PC O-16:0_20:1	$C_{44}H_{88}NO_7P$	1.456	767.3	-0.348	0.2
28.78	292.4	792.6099	$[M+HCOO]^-$	PC O-18:0_16:0	$C_{42}H_{86}NO_7P$	1.435	935.2	-3.649	0.7
26.11	280	692.559	$[M+H]^+$	PC O-30:0	$C_{38}H_{78}NO_7P$	1.371	999.8	0.228	1.1
25.82	277.3	690.5434	$[M+H]^+$	PC O-30:1	$C_{38}H_{76}NO_7P$	1.357	777.1	0.309	0.6
27.57	285.2	720.5897	$[M+H]^+$	PC O-32:0	$C_{40}H_{82}NO_7P$	1.398	998.1	-0.357	0.4
27.39	282.9	718.5748	$[M+H]^+$	PC O-32:1	$C_{40}H_{80}NO_7P$	1.386	996.6	0.474	0.3

26.05	280.2	716.5592	$[M+H]^+$	PC O-32:2	$C_{40}H_{78}NO_7P$	1.373	750.1	0.506	0.4
28.95	290.3	748.6192	$[M+H]^+$	PC O-34:0	$C_{42}H_{86}NO_7P$	1.423	999.4	-3.249	0.2
27.62	288	746.6065	$[M+H]^+$	PC O-34:1	$C_{42}H_{84}NO_7P$	1.412	999.2	1.052	0.5
27.65	290.6	788.5829	$[M+HCOO]^-$	PC O-34:2	$C_{42}H_{82}NO_7P$	1.426	474.6	2.974	0.8
27.44	286.4	744.5905	$[M+H]^+$	PC O-34:2	$C_{42}H_{82}NO_7P$	1.404	995	0.713	1.1
23.21	280.4	738.544	$[M+H]^+$	PC O-34:5	$C_{42}H_{76}NO_7P$	1.375	999.8	1.262	0.5
21.37	278.5	780.5172	$[M+HCOO]^-$	PC O-34:6	$C_{42}H_{74}NO_7P$	1.366	564.7	-1.658	1.8
23.92	283.1	752.5596	$[M+H]^+$	PC O-35:5	$C_{43}H_{78}NO_7P$	1.388	999.8	0.852	0.4
26.30	276.8	748.5289	$[M+H]^+$	PC O-35:7	$C_{43}H_{74}NO_7P$	1.357	667.1	1.649	1.0
29.41	297.5	820.6418	$[M+HCOO]^-$	PC O-36:0	$C_{44}H_{90}NO_7P$	1.461	741.3	-2.05	1.0
28.70	296.4	816.6125	$[M+HCOO]^-$	PC O-36:2	$C_{44}H_{86}NO_7P$	1.455	849.7	-0.265	1.1
28.50	291.6	772.6228	$[M+H]^+$	PC O-36:2	$C_{44}H_{86}NO_7P$	1.431	996.7	1.356	0.9
26.35	287.4	768.5903	$[M+H]^+$	PC O-36:4	$C_{44}H_{82}NO_7P$	1.41	998.9	0.103	0.1
26.09	285.4	766.5739	$[M+H]^+$	PC O-36:5	$C_{44}H_{80}NO_7P$	1.4	405.7	-1.03	0.1
14.53	297.9	824.5805	$[M+HCOO]^-$	PC O-37:5	$C_{45}H_{82}NO_7P$	1.463	200.6	-0.52	2.0
28.49	294.6	798.6396	$[M+H]^+$	PC O-38:3	$C_{46}H_{88}NO_7P$	1.446	996.6	3.194	2.1
26.4	290.5	794.6058	$[M+H]^+$	PC O-38:5	$C_{46}H_{84}NO_7P$	1.426	976.9	-0.717	0.4
26.21	289.3	792.5897	$[M+H]^+$	PC O-38:6	$C_{46}H_{82}NO_7P$	1.42	987.5	-0.525	0.7
25.88	289.8	792.5895	$[M+H]^+$	PC O-38:6	$C_{46}H_{82}NO_7P$	1.423	996.1	-0.821	0.5
27.19	293.8	818.6068	$[M+H]^+$	PC O-40:7	$C_{48}H_{84}NO_7P$	1.443	999.8	1.118	0.2
29.12	273.4	728.559	$[M-H]^-$	PC P-18:1_16:0	$C_{41}H_{80}NO_7P$	1.34	200.5	-1.264	3.1

28.55	276.5	752.5565	$[M-H]^-$	PC-O-15:0_20:4	$C_{43}H_{80}NO_7P$	1.356	785.5	-5.841	2.6
23.57	271	712.4911	$[M+H]^+$	PE 14:0_20:4	$C_{39}H_{70}NO_8P$	1.328	795.1	-0.004	1.6
23.99	264	710.4764	$[M-H]^-$	PE 14:0_20:4	$C_{39}H_{70}NO_8P$	1.293	926	-0.043	2.5
23.04	272.2	736.492	$[M+H]^+$	PE 14:0_22:6	$C_{41}H_{70}NO_8P$	1.334	930.4	1.155	1.0
27.75	267.6	716.5223	$[M-H]^-$	PE 16:0_18:1	$C_{39}H_{76}NO_8P$	1.311	323.5	-1.88	1.4
26.13	276.7	740.526	$[M+H]^+$	PE 16:0_20:4	$C_{41}H_{74}NO_8P$	1.356	939.8	4.24	1.2
23.86	272.6	738.5075	$[M+H]^+$	PE 16:1_20:4	$C_{41}H_{72}NO_8P$	1.336	944.7	0.795	1.3
29.82	289.2	786.6059	$[M+H]^+$	PE 17:1_22:1	$C_{44}H_{84}NO_8P$	1.419	661.8	6.696	0.7
28.58	269.2	718.5384	$[M-H]^-$	PE 18:0_16:0	$C_{39}H_{78}NO_8P$	1.319	896.6	-1.135	1.3
28.08	284.3	770.5703	$[M+H]^+$	PE 18:0_18:0	$C_{43}H_{80}NO_8P$	1.394	919.6	1.371	0.1
28.90	286.7	774.6021	$[M+H]^+$	PE 18:0_20:1	$C_{43}H_{84}NO_8P$	1.407	963.3	1.902	0.1
28.33	277.7	768.5531	$[M-H]^-$	PE 18:0_20:3	$C_{43}H_{80}NO_8P$	1.362	305.2	-2.187	1.1
28.59	279.3	770.5692	$[M-H]^-$	PE 18:1_20:1	$C_{43}H_{82}NO_8P$	1.37	886.0	-1.662	1.0
28.58	289.3	798.6016	$[M+H]^+$	PE 18:1_22:2	$C_{45}H_{84}NO_8P$	1.42	387.4	1.785	1.1
24.16	269.1	714.5076	$[M+H]^+$	PE 18:2_16:1	$C_{39}H_{72}NO_8P$	1.318	979.9	1.368	0.1
24.25	276.3	786.5069	$[M-H]^-$	PE 18:2_22:6	$C_{45}H_{74}NO_8P$	1.356	899.3	-1.274	1.8
28.44	294.2	802.6373	$[M+H]^+$	PE 20:0_20:1	$C_{45}H_{88}NO_8P$	1.444	316.8	6.655	0.8
26.15	288.8	796.5864	$[M+H]^+$	PE 20:0_20:4	$C_{45}H_{82}NO_8P$	1.417	991.1	1.598	0.7
28.53	278.5	768.5537	$[M-H]^-$	PE 20:3_18:0	$C_{43}H_{80}NO_8P$	1.366	944.7	-1.119	1.5
26.58	270	738.507	$[M-H]^-$	PE 20:4_16:0	$C_{41}H_{74}NO_8P$	1.324	921.8	-1.231	1.6
24.28	267.9	736.4915	$[M-H]^-$	PE 20:4_16:1	$C_{41}H_{72}NO_8P$	1.313	873.2	-1.158	1.6

27.89	276.6	766.5388	$[M-H]^-$	PE 20:4_18:0	$C_{43}H_{78}NO_8P$	1.357	912.1	-0.644	1.2
26.59	274.5	764.5225	$[M-H]^-$	PE 20:4_18:1	$C_{43}H_{76}NO_8P$	1.346	910.5	-1.274	1.2
24.09	279.4	788.5252	$[M+H]^+$	PE 20:4_20:4	$C_{45}H_{74}NO_8P$	1.371	737.4	3.532	0.2
23.03	275	784.4915	$[M-H]^-$	PE 20:4_20:5	$C_{45}H_{72}NO_8P$	1.35	899.5	-1.113	0.3
25.00	273.3	762.5073	$[M-H]^-$	PE 20:5_18:1	$C_{43}H_{74}NO_8P$	1.34	696.1	-0.887	0.8
14.97	233.7	536.3345	$[M+H]^+$	PE 21:1	$C_{26}H_{50}NO_8P$	1.138	982.2	-0.499	1.6
28.53	282.7	794.5696	$[M-H]^-$	PE 22:4_18:0	$C_{45}H_{82}NO_8P$	1.388	928.6	-1.003	0.3
23.77	271.9	760.4915	$[M-H]^-$	PE 22:6_16:1	$C_{43}H_{72}NO_8P$	1.333	862.4	-1.05	1.1
25.82	278.9	788.5226	$[M-H]^-$	PE 22:6_18:1	$C_{45}H_{76}NO_8P$	1.369	800.1	-1.254	1.3
25.36	285.8	838.5381	$[M-H]^-$	PE 22:6_22:4	$C_{49}H_{78}NO_8P$	1.404	856.7	-1.379	0.6
17.42	245.9	578.3804	$[M+H]^+$	PE 24:1	$C_{29}H_{56}NO_8P$	1.199	997.5	-2.302	0.6
17.43	252.8	628.3973	$[M+H]^+$	PE 28:4	$C_{33}H_{58}NO_8P$	1.235	383.7	0.248	1.9
27.25	274.9	718.5386	$[M+H]^+$	PE 34:1	$C_{39}H_{76}NO_8P$	1.347	952.5	0.617	0.8
26.12	272.2	716.523	$[M+H]^+$	PE 34:2	$C_{39}H_{74}NO_8P$	1.333	965.4	0.783	0.8
28.63	274.2	744.5548	$[M-H]^-$	PE 36:1	$C_{41}H_{80}NO_8P$	1.344	407.5	-0.161	2.0
28.22	280.8	746.5705	$[M+H]^+$	PE 36:1	$C_{41}H_{80}NO_8P$	1.377	897.0	1.478	1.0
27.33	277.8	744.5542	$[M+H]^+$	PE 36:2	$C_{41}H_{78}NO_8P$	1.362	944	0.582	0.7
27.82	272.2	742.538	$[M-H]^-$	PE 36:2	$C_{41}H_{78}NO_8P$	1.335	793.7	-1.736	0.8
26.32	275.4	742.5395	$[M+H]^+$	PE 36:3	$C_{41}H_{76}NO_8P$	1.35	951.4	1.828	0.7
24.3	273.6	738.508	$[M+H]^+$	PE 36:5	$C_{41}H_{72}NO_8P$	1.341	938.7	1.733	0.1
24.44	273.1	760.4938	$[M-H]^-$	PE 37:0	$C_{43}H_{72}NO_8P$	1.339	392.7	2.154	1.7

24.1	275.4	750.5082	$[M+H]^+$	PE 37:6	$C_{42}H_{72}NO_8P$	1.35	891.1	1.891	0.4
27.38	282.3	768.5548	$[M+H]^+$	PE 38:4	$C_{43}H_{78}NO_8P$	1.385	939.8	1.413	0.1
26.02	278.7	766.539	$[M+H]^+$	PE 38:5	$C_{43}H_{76}NO_8P$	1.367	875.5	1.083	0.4
25.17	278.4	764.5238	$[M+H]^+$	PE 38:6	$C_{43}H_{74}NO_8P$	1.366	925.3	1.832	0.5
23.33	275	762.508	$[M+H]^+$	PE 38:7	$C_{43}H_{72}NO_8P$	1.349	915.4	1.493	0.2
29.20	285	798.601	$[M-H]^-$	PE 40:2	$C_{45}H_{86}NO_8P$	1.399	662.1	-0.994	0.2
28.09	287.3	796.5862	$[M+H]^+$	PE 40:4	$C_{45}H_{82}NO_8P$	1.41	945.9	1.382	0.4
27.89	287.5	796.5859	$[M+H]^+$	PE 40:4	$C_{45}H_{82}NO_8P$	1.411	968.1	1.243	0.3
27.58	280.6	790.5396	$[M-H]^-$	PE 40:6	$C_{45}H_{78}NO_8P$	1.377	938.0	0.458	2.4
23.80	286.5	822.5296	$[M-H]^-$	PE 40:6	$C_{45}H_{78}NO_{10}P$	1.407	792.0	0.395	2.4
23.80	278.9	788.5237	$[M+H]^+$	PE 40:8	$C_{45}H_{74}NO_8P$	1.369	906.2	1.656	0.4
27.1	287.3	818.5705	$[M+H]^+$	PE 42:7	$C_{47}H_{80}NO_8P$	1.411	1000	1.177	1.1
24.01	284.4	836.5224	$[M-H]^-$	PE 44:11	$C_{49}H_{76}NO_8P$	1.397	794.7	-1.607	0.5
23.35	283.6	834.508	$[M-H]^-$	PE 44:12	$C_{49}H_{74}NO_8P$	1.393	956.6	0.147	0.5
22.85	284.7	836.5246	$[M+H]^+$	PE 44:12	$C_{49}H_{74}NO_8P$	1.398	944.1	2.55	0.4
24.14	289.9	864.5564	$[M+H]^+$	PE 46:12	$C_{51}H_{78}NO_8P$	1.425	918.2	3.029	0.1
30.80	324.7	994.8195	$[M-H]^-$	PE 54:2	$C_{59}H_{114}NO_8P$	1.599	584.3	-1.426	0.8
30.51	323.3	992.8041	$[M-H]^-$	PE 54:3	$C_{59}H_{112}NO_8P$	1.592	611.6	-1.149	0.8
30.80	324.2	1020.836	$[M-H]^-$	PE 56:3	$C_{61}H_{116}NO_8P$	1.597	633.0	-1.23	2.3
30.40	323.3	1016.804	$[M-H]^-$	PE 56:5	$C_{61}H_{112}NO_8P$	1.592	390.9	-2.686	1.7
30.05	323.5	1012.771	$[M-H]^-$	PE 56:7	$C_{61}H_{108}NO_8P$	1.594	366.8	-2.872	0.7

29.96	280.8	758.6039	$[M-H]^-$	PE O-18:1_20:0	$C_{43}H_{86}NO_7P$	1.377	969.3	-3.463	2.7
28.4	267	700.5279	$[M-H]^-$	PE O-18:2_16:0	$C_{39}H_{76}NO_7P$	1.308	304.1	-1.257	2.5
28.06	276	704.5575	$[M+H]^+$	PE O-34:1	$C_{39}H_{78}NO_7P$	1.352	963.4	-1.971	1.5
27.94	274.3	702.5434	$[M+H]^+$	PE O-34:2	$C_{39}H_{76}NO_7P$	1.343	869.5	0.44	1.5
26.86	272.2	700.5281	$[M+H]^+$	PE O-34:3	$C_{39}H_{74}NO_7P$	1.333	930.9	0.783	1.2
28.29	277	716.5599	$[M+H]^+$	PE O-35:2	$C_{40}H_{78}NO_7P$	1.357	914.6	0.951	1.2
28.7	269.9	714.543	$[M-H]^-$	PE O-35:2	$C_{40}H_{78}NO_7P$	1.322	806.2	-1.857	2.1
28.64	279.9	730.5756	$[M+H]^+$	PE O-36:2	$C_{41}H_{80}NO_7P$	1.372	926.6	1.203	1.0
28.04	278.1	728.5593	$[M+H]^+$	PE O-36:3	$C_{41}H_{78}NO_7P$	1.363	949	0.462	1.3
28.44	271.7	726.5436	$[M-H]^-$	PE O-36:3	$C_{41}H_{78}NO_7P$	1.331	744.5	-0.758	1.1
27.26	269.7	722.5121	$[M-H]^-$	PE O-36:5	$C_{41}H_{74}NO_7P$	1.322	985.6	-1.214	3
24.02	270.7	720.4984	$[M+H]^+$	PE O-36:7	$C_{41}H_{70}NO_7P$	1.326	860.5	2.635	1.4
28.96	282.3	744.5914	$[M+H]^+$	PE O-37:2	$C_{42}H_{82}NO_7P$	1.384	817.4	1.39	0.9
28.70	274.8	740.5587	$[M-H]^-$	PE O-37:3	$C_{42}H_{80}NO_7P$	1.347	806.4	-1.764	2.9
29.48	279.7	756.5908	$[M-H]^-$	PE O-38:2	$C_{43}H_{84}NO_7P$	1.372	973.8	-0.518	2.8
29.06	278	754.5744	$[M-H]^-$	PE O-38:3	$C_{43}H_{82}NO_7P$	1.363	956.3	-1.558	2.9
28.51	282.2	754.5751	$[M+H]^+$	PE O-38:4	$C_{43}H_{80}NO_7P$	1.384	940.5	1.046	1.1
28.46	276.3	750.5433	$[M-H]^-$	PE O-38:5	$C_{43}H_{78}NO_7P$	1.355	974.3	-1.176	3
27.33	274.2	748.5279	$[M-H]^-$	PE O-38:6	$C_{43}H_{76}NO_7P$	1.344	974	-0.781	2.7
29.74	282.4	770.6059	$[M-H]^-$	PE O-39:2	$C_{44}H_{86}NO_7P$	1.385	811.1	-0.88	2.8
29.53	288	772.6224	$[M+H]^+$	PE O-39:2	$C_{44}H_{86}NO_7P$	1.413	629.4	2.032	0.2

28.96	285.5	770.6066	$[M+H]^+$	PE O-39:3	$C_{44}H_{84}NO_7P$	1.401	822.4	0.824	0.1
28.55	278.9	764.5601	$[M-H]^-$	PE O-39:5	$C_{44}H_{80}NO_7P$	1.368	980.1	-0.251	3.1
28.71	279.1	764.5599	$[M-H]^-$	PE O-39:5	$C_{44}H_{80}NO_7P$	1.369	988.2	-0.269	2.4
29.24	288.6	784.6222	$[M+H]^+$	PE O-40:3	$C_{45}H_{86}NO_7P$	1.416	827.7	1.309	0.4
29.24	283.2	780.5899	$[M-H]^-$	PE O-40:4	$C_{45}H_{84}NO_7P$	1.390	967.9	-1.689	2.6
28.81	281.8	778.5751	$[M-H]^-$	PE O-40:5	$C_{45}H_{82}NO_7P$	1.382	972.9	-0.95	2.5
26.33	280.2	774.5443	$[M+H]^+$	PE O-40:8	$C_{45}H_{76}NO_7P$	1.375	928.1	1.467	0.1
24.79	278.2	772.5279	$[M+H]^+$	PE O-40:9	$C_{45}H_{74}NO_7P$	1.365	679.6	0.469	0.3
30.13	288.7	798.6373	$[M-H]^-$	PE O-41:2	$C_{46}H_{90}NO_7P$	1.417	816.7	-1.021	0.7
29.73	286.5	796.6218	$[M-H]^-$	PE O-41:3	$C_{46}H_{88}NO_7P$	1.406	881.9	-0.926	0.8
30.34	291.8	812.6529	$[M-H]^-$	PE O-42:2	$C_{47}H_{92}NO_7P$	1.433	920.9	-1.256	2.6
29.93	290.1	810.637	$[M-H]^-$	PE O-42:3	$C_{47}H_{90}NO_7P$	1.425	793.5	-1.506	2.8
30.36	289.7	812.6572	$[M+H]^+$	PE O-42:3	$C_{47}H_{90}NO_7P$	1.423	375.5	5.443	1.1
29.13	291.5	808.6222	$[M+H]^+$	PE O-42:5	$C_{47}H_{86}NO_7P$	1.431	927.3	0.952	2.2
28.99	291.5	808.6232	$[M+H]^+$	PE O-42:5	$C_{47}H_{86}NO_7P$	1.431	748.4	2.13	0.1
28.36	289.3	806.6042	$[M+H]^+$	PE O-42:6	$C_{47}H_{84}NO_7P$	1.420	870.5	-2.102	0.3
28.58	285.7	802.5707	$[M-H]^-$	PE O-42:7	$C_{47}H_{82}NO_7P$	1.402	956	-4.644	2.9
28.50	288.5	804.5901	$[M+H]^+$	PE O-42:7	$C_{47}H_{82}NO_7P$	1.416	932.8	0.361	0.3
30.32	295.8	838.6681	$[M-H]^-$	PE O-44:3	$C_{49}H_{94}NO_7P$	1.453	840.8	-2.056	1.8
29.94	285.7	784.6216	$[M-H]^-$	PE O-18:1_22:1	$C_{45}H_{88}NO_7P$	1.402	868.3	-1.172	2.1
28.23	279.6	774.5439	$[M-H]^-$	PE P-18:0_22:6	$C_{45}H_{78}NO_7P$	1.372	943.7	-0.812	2.7

25.99	274.3	747.5166	$[M-H]^-$	PG 16:0_18:1/BMP 16:0_18:1	$C_{40}H_{77}O_{10}P$	1.345	208.3	-2.042	2.0
24.44	276.6	769.5016	$[M-H]^-$	PG 16:0_20:4/BMP 36:4	$C_{42}H_{75}O_{10}P$	1.357	861.7	-1.199	2.3
23.08	289	819.5171	$[M-H]^-$	PG 18:1_22:6	$C_{46}H_{77}O_{10}P$	1.419	444.4	-1.272	3.2
29.37	297.6	831.619	$[M-H]^-$	PG 20:0_20:1	$C_{46}H_{89}O_{10}P$	1.462	260.6	8.339	4.6
28.74	295.7	829.6032	$[M-H]^-$	PG 20:1_20:1/BMP 40:2	$C_{46}H_{87}O_{10}P$	1.452	687.1	7.695	4.4
21.43	290.8	841.502	$[M-H]^-$	PG 20:4_22:6	$C_{48}H_{75}O_{10}P$	1.428	943.9	-0.558	3.2
25.68	285.6	766.559	$[M+NH_4]^+$	PG 34:1/BMP 34:1	$C_{40}H_{77}O_{10}P$	1.401	941.7	-0.575	1.4
24.21	282.1	764.5497	$[M+NH_4]^+$	PG 34:2/BMP 34:2	$C_{40}H_{75}O_{10}P$	1.384	829.6	7.389	1.8
28.73	292.1	803.5876	$[M-H]^-$	PG 38:1	$C_{44}H_{85}O_{10}P$	1.434	494.6	8.298	3.8
24.31	289.3	814.5653	$[M+NH_4]^+$. $[M+H]^+$	PG 38:5/BMP 38:5	$C_{44}H_{77}O_{10}P$	1.421	906.8	6.7	1.2
23.71	289.7	812.5451	$[M+NH_4]^+$. $[M+H]^+$. $[M+NH_4]^+$	PG 38:6/BMP 38:6	$C_{44}H_{75}O_{10}P$	1.422	917.9	2.197	1.4
30.29	308.6	887.6823	$[M-H]^-$	PG 44:1	$C_{50}H_{97}O_{10}P$	1.517	615.6	8.566	2.9
21.04	294.3	865.5027	$[M-H]^-$	PG 44:12	$C_{50}H_{75}O_{10}P$	1.447	923.5	0.183	4.0
28.54	285.9	761.5776	$[M-H]^-$	PG O-20:1_16:0	$C_{42}H_{83}O_9P$	1.402	759.8	9.766	3.9
30.2	303.2	845.669	$[M-H]^-$	PG O-20:1_22:0	$C_{48}H_{95}O_9P$	1.49	733.8	5.918	3.9
29.23	291.6	789.6083	$[M-H]^-$	PG O-38:1	$C_{44}H_{87}O_9P$	1.431	822	8.663	3.5
28.57	289.5	787.5932	$[M-H]^-$	PG O-38:2	$C_{44}H_{85}O_9P$	1.421	265.1	9.165	3.9
29.77	297.4	817.6404	$[M-H]^-$	PG O-40:1	$C_{46}H_{91}O_9P$	1.46	757.6	9.455	4.8
29.22	295.2	815.6245	$[M-H]^-$	PG O-40:2	$C_{46}H_{89}O_9P$	1.449	570.6	9.064	4.7
30.16	306.6	871.6838	$[M-H]^-$	PG O-44:2	$C_{50}H_{97}O_9P$	1.507	439.4	4.554	3.3
23.2	289.1	814.561	$[M+NH_4]^+$	PG 39:5 /BMP 39:5	$C_{44}H_{77}O_{10}P$	1.42	924.3	1.946	0.3

22.79	291.7	838.5617	$[M+NH_4]^+$. $[M+H]^+$	PG 40:7 /BMP 40:7	$C_{46}H_{77}O_{10}P$	1.433	824.5	2.635	0.2
24.02	291.1	857.5181	$[M-H]^-$	PI 16:0_20:4	$C_{45}H_{79}O_{13}P$	1.431	775.5	-0.586	2.5
21.89	300.7	929.5182	$[M-H]^-$	PI 20:4_22:6	$C_{51}H_{79}O_{13}P$	1.48	699	-0.251	2.7
27.23	298.7	882.6083	$[M+NH_4]^+$	PI 36:1	$C_{45}H_{85}O_{13}P$	1.468	931.6	1.845	1.4
23.65	295.4	876.5617	$[M+NH_4]^+$. $[M+Na]^+$	PI 36:4	$C_{45}H_{79}O_{13}P$	1.452	927.8	2.413	1.5
26.50	296.5	885.5491	$[M-H]^-$	PI 38:4	$C_{47}H_{83}O_{13}P$	1.458	197	-1.014	1.9
24.23	295.1	883.5335	$[M-H]^-$	PI 38:5	$C_{47}H_{81}O_{13}P$	1.451	401.1	-0.706	2.7
23.89	297.7	902.5778	$[M+NH_4]^+$. $[M+H]^+$	PI 38:5	$C_{47}H_{81}O_{13}P$	1.464	906.7	2.868	1.4
23.20	297.2	900.5621	$[M+NH_4]^+$	PI 38:6	$C_{47}H_{79}O_{13}P$	1.462	925.1	2.749	1.5
23.77	298.7	907.5336	$[M-H]^-$	PI 40:7	$C_{49}H_{81}O_{13}P$	1.469	209.5	-0.503	1.7
22.91	298.4	926.5782	$[M+NH_4]^+$	PI 40:7	$C_{49}H_{81}O_{13}P$	1.468	881.2	3.131	0.2
23.40	299.8	926.5786	$[M+NH_4]^+$. $[M+H]^+$	PI 40:7	$C_{49}H_{81}O_{13}P$	1.475	914.7	3.762	0.7
22.37	298.2	905.518	$[M-H]^-$	PI 40:8	$C_{49}H_{79}O_{13}P$	1.466	737.9	-0.578	3.1
22.01	298.3	924.5622	$[M+NH_4]^+$	PI 40:8	$C_{49}H_{79}O_{13}P$	1.468	873.6	2.746	0.8
23.84	283.6	806.4968	$[M-H]^-$	PS 16:0_22:6	$C_{44}H_{74}NO_{10}P$	1.392	348.7	-1.128	1.6
24.41	275.8	758.497	$[M-H]^-$	PS 16:1_18:1	$C_{40}H_{74}NO_{10}P$	1.352	559.8	-0.936	1.8
28.74	289.7	816.5748	$[M-H]^-$	PS 18:0_20:1	$C_{44}H_{84}NO_{10}P$	1.422	649.6	-1.53	1.9
22.62	286.7	830.4977	$[M-H]^-$	PS 18:2_22:6	$C_{46}H_{74}NO_{10}P$	1.408	770	-0.059	2.9
26.48	285.5	824.5443	$[M-H]^-$	PS 19:0_20:4	$C_{45}H_{80}NO_{10}P$	1.402	569	-0.879	1.4
24.52	288.1	846.5273	$[M-H]^-$	PS 19:1_22:6	$C_{47}H_{78}NO_{10}P$	1.415	532.6	-1.855	1.7
23.09	290.9	856.5126	$[M-H]^-$	PS 20:3_22:6	$C_{48}H_{76}NO_{10}P$	1.43	455.6	-1.004	3.4

24.52	284.1	808.5125	$[M-H]^-$	PS 20:4_18:1	$C_{44}H_{76}NO_{10}P$	1.395	179	-1.23	1.5
23.99	287.4	832.5124	$[M-H]^-$	PS 22:6_18:1	$C_{46}H_{76}NO_{10}P$	1.412	249.5	-1.172	2.0
29.37	295.3	844.6065	$[M-H]^-$	PS 40:1	$C_{46}H_{88}NO_{10}P$	1.451	234.3	-0.844	2.1
27.85	291.2	838.559	$[M-H]^-$	PS 40:4	$C_{46}H_{82}NO_{10}P$	1.43	285.4	-1.609	2.0
26.34	289.3	834.5289	$[M-H]^-$	PS 40:6	$C_{46}H_{78}NO_{10}P$	1.421	675.7	-0.238	2.5
27.36	288.9	848.5449	$[M-H]^-$	PS 41:6	$C_{47}H_{80}NO_{10}P$	1.42	157.8	-0.212	1.3
23.62	294.9	882.5277	$[M-H]^-$	PS 44:10	$C_{50}H_{78}NO_{10}P$	1.45	684	-1.48	3.7
21.68	292.8	878.4976	$[M-H]^-$	PS 44:12	$C_{50}H_{74}NO_{10}P$	1.44	884.3	-0.12	2.9
28.80	271	662.5723	$[M+NH_4]^+$. $[M+H-H_2O]^+$	Stearoyl-arachidonoyl-glycerol	$C_{41}H_{72}O_5$	1.326	m.c	m.c.	1.9
27.75	301.3	864.6299	$[M+H]^+$	SHexCer 40:1	$C_{46}H_{89}NO_{11}S$	1.481	853.6	6.022	0.5
28.22	302.8	878.6409	$[M+H]^+$	SHexCer 41:1	$C_{47}H_{91}NO_{11}S$	1.488	753.4	2.613	0.3
28.54	305.3	892.6566	$[M+H]^+$. $[M+H-H_2O]^+$	SHexCer 42:1	$C_{48}H_{93}NO_{11}S$	1.501	802.2	2.464	0.2
27.72	303.8	890.6406	$[M+H]^+$	SHexCer 42:2	$C_{48}H_{91}NO_{11}S$	1.494	803.7	2.135	0.3
27.55	307.7	906.636	$[M+H]^+$	SHexCer 42:2;3O	$C_{48}H_{91}NO_{12}S$	1.514	470.7	2.346	0.4
22.49	278	675.5435	$[M+H]^+$. $[M+Na]^+$	SM 32:1	$C_{37}H_{75}N_2O_6P$	1.36	1000	-0.039	0.8
21.96	278	675.5432	$[M+H]^+$	SM 32:1	$C_{37}H_{75}N_2O_6P$	1.36	1000	-0.626	0.2
23.58	280.2	689.5593	$[M+H]^+$	SM 33:1	$C_{38}H_{77}N_2O_6P$	1.372	1000	0.304	1.1
24.49	282.6	703.5754	$[M+H]^+$	SM 34:1	$C_{39}H_{79}N_2O_6P$	1.384	983.9	0.668	2.1
24.69	282.9	703.5753	$[M+H]^+$	SM 34:1	$C_{39}H_{79}N_2O_6P$	1.385	976.4	0.412	2.2
22.46	279.6	701.5579	$[M+H]^+$	SM 34:2	$C_{39}H_{77}N_2O_6P$	1.369	992.4	-1.068	0.5
22.79	279.8	701.5593	$[M+H]^+$	SM 34:2	$C_{39}H_{77}N_2O_6P$	1.37	1000	-0.141	0.8

25.76	285.1	717.5904	$[M+H]^+$	SM 35:1	$C_{40}H_{81}N_2O_6P$	1.397	1000	-0.123	0.3
23.91	282.3	715.5751	$[M+H]^+$	SM 35:2	$C_{40}H_{79}N_2O_6P$	1.383	1000	0.916	0.1
27.19	290.2	733.6197	$[M+H]^+$	SM 36:0	$C_{41}H_{85}N_2O_6P$	1.422	954.3	-2.656	1.3
24.92	285.3	729.5915	$[M+H]^+$. $[M+Na]^+$	SM 36:2	$C_{41}H_{81}N_2O_6P$	1.398	924.7	1.308	2.3
27.31	290	745.622	$[M+H]^+$	SM 37:1	$C_{42}H_{85}N_2O_6P$	1.422	980.4	0.184	3.5
27.83	293.1	759.6381	$[M+H]^+$	SM 38:1	$C_{43}H_{87}N_2O_6P$	1.437	935.7	0.836	2.1
28.05	292.8	759.6371	$[M+H]^+$	SM 38:1	$C_{43}H_{87}N_2O_6P$	1.436	955.6	0.048	0.9
26.95	290.6	757.6221	$[M+H]^+$	SM 38:2	$C_{43}H_{85}N_2O_6P$	1.425	1000	0.871	0.4
28.45	295.2	773.6526	$[M+H]^+$	SM 39:1	$C_{44}H_{89}N_2O_6P$	1.448	441.8	-0.67	0.9
29.05	299.2	789.6845	$[M+H]^+$	SM 40:0	$C_{45}H_{93}N_2O_6P$	1.469	807.2	0.081	0.9
28.76	297.4	787.6701	$[M+H]^+$	SM 40:1	$C_{45}H_{91}N_2O_6P$	1.46	969.4	1.841	1.3
28.83	311.3	787.6705	$[M+H]^+$	SM 40:1	$C_{45}H_{91}N_2O_6P$	1.528	907.9	2.299	4.0
27.83	295.6	785.6533	$[M+H]^+$	SM 40:2	$C_{45}H_{89}N_2O_6P$	1.451	1000	0.386	1.1
29.35	300.1	801.6883	$[M+H]^+$	SM 41:1	$C_{46}H_{93}N_2O_6P$	1.473	1000	4.409	0.6
28.32	297.7	799.6705	$[M+H]^+$	SM 41:2	$C_{46}H_{91}N_2O_6P$	1.461	791.5	1.802	0.3
28.98	302.3	815.7022	$[M+H]^+$	SM 42:1	$C_{47}H_{95}N_2O_6P$	1.484	1000	2.736	0.1
29.53	303	815.7024	$[M+H]^+$	SM 42:1	$C_{47}H_{95}N_2O_6P$	1.488	856	2.943	1.1
28.70	300.4	813.6865	$[M+H]^+$	SM 42:2	$C_{47}H_{93}N_2O_6P$	1.475	958	2.386	2.1
28.05	297.8	811.6702	$[M+H]^+$	SM 42:3	$C_{47}H_{91}N_2O_6P$	1.462	1000	1.456	0.8
23.61	286.5	721.5849	$[M+H]^+$	SM 34:0;3O	$C_{39}H_{81}N_2O_7P$	1.404	812.9	-0.626	0.3
23.87	289.3	719.5703	$[M+H]^+$	SM 34:1;3O	$C_{39}H_{79}N_2O_7P$	1.417	894.2	0.613	1.5

24.24		745.5862	$[M+H]^+$	SM 36:2;3O	$C_{41}H_{81}N_2O_7P$	1.42	894.2	1.368	0.4
28.42	299.6	805.6805	$[M+H]^+$	SM 40:0;3O	$C_{45}H_{93}N_2O_7P$	1.471	894.2	1.382	1.1
29.13	304.7	833.711	$[M+H]^+$	SM 42:0;3O	$C_{47}H_{97}N_2O_7P$	1.497	891.9	0.75	1.0
28.35	302.2	831.6944	$[M+H]^+$	SM 42:1;3O	$C_{47}H_{95}N_2O_7P$	1.484	893.5	-0.664	1.3
30.89	298.1	780.7088	$[M+NH_4]^+$. $[M+Na]^+$	TG 14:0_15:0_16:1	$C_{48}H_{90}O_6$	1.463	837.2	1.555	0.9
31.33	302.6	796.7404	$[M+NH_4]^+$	TG 14:0_16:0_16:0	$C_{49}H_{94}O_6$	1.485	864.3	2.002	0.4
31.06	301.1	794.7249	$[M+NH_4]^+$	TG 14:0_16:0_16:1	$C_{49}H_{92}O_6$	1.478	884.6	2.105	0.7
31.37	306	822.7563	$[M+NH_4]^+$	TG 14:0_16:0_18:1	$C_{51}H_{96}O_6$	1.503	833.4	2.198	0.6
30.85	310.5	868.7417	$[M+NH_4]^+$	TG 14:0_16:0_22:6	$C_{55}H_{94}O_6$	1.526	713.7	3.394	0.5
30.81	299.3	792.7091	$[M+NH_4]^+$. $[M+Na]^+$	TG 14:0_16:1_16:1	$C_{49}H_{90}O_6$	1.469	890.4	1.997	2.1
31.09	304.3	820.7407	$[M+NH_4]^+$. $[M+Na]^+$	TG 14:0_16:1_18:1	$C_{51}H_{94}O_6$	1.495	831.3	2.321	0.6
30.56	308.1	866.7218	$[M+NH_4]^+$	TG 14:0_16:1_22:6	$C_{55}H_{92}O_6$	1.514	774.9	-0.656	0.4
30.37	311.5	940.7428	$[M+NH_4]^+$	TG 14:0_22:6_22:6	$C_{61}H_{94}O_6$	1.533	861.7	4.505	1.3
30.54	297.0	790.6925	$[M+NH_4]^+$	TG 14:1_16:1_16:1	$C_{49}H_{88}O_6$	1.458	915.4	0.734	0.3
30.84	302.8	818.7244	$[M+NH_4]^+$	TG 14:1_16:1_18:1	$C_{51}H_{92}O_6$	1.487	869.8	1.475	2.6
31.21	303.5	808.7406	$[M+NH_4]^+$	TG 15:0_16:0_16:1	$C_{50}H_{94}O_6$	1.490	888.3	2.116	2.1
31.48	308.7	836.7721	$[M+NH_4]^+$	TG 15:0_16:0_18:1	$C_{52}H_{98}O_6$	1.516	760.7	2.323	0.3
30.96	301.7	806.7245	$[M+NH_4]^+$	TG 15:0_16:1_16:1	$C_{50}H_{92}O_6$	1.481	890	1.5	0.9
31.23	307.0	834.7562	$[M+NH_4]^+$	TG 15:0_16:1_18:1	$C_{52}H_{96}O_6$	1.508	785.7	2.007	0.9
30.70	300.1	804.7085	$[M+NH_4]^+$	TG 15:1_16:1_16:1	$C_{50}H_{90}O_6$	1.473	859.5	1.333	0.9
30.99	305.2	832.7402	$[M+NH_4]^+$	TG 15:1_16:1_18:1	$C_{52}H_{94}O_6$	1.499	813.6	1.528	0.3

31.77	309.8	838.7879	$[M+NH_4]^+$	TG 16:0_16:0_17:0	$C_{52}H_{100}O_6$	1.522	903.4	2.514	1.2
31.16	315.1	896.7736	$[M+NH_4]^+$	TG 16:0_16:0_22:6	$C_{57}H_{98}O_6$	1.55	679.5	3.192	0.6
31.09	307.3	846.7562	$[M+NH_4]^+$. $[M+Na]^+$	TG 16:0_16:1_18:2	$C_{53}H_{96}O_6$	1.51	897.6	2.07	1.1
30.86	313.2	894.7582	$[M+NH_4]^+$	TG 16:0_16:1_22:6	$C_{57}H_{96}O_6$	1.54	647.3	4.218	0.2
32.1	313.8	866.8199	$[M+NH_4]^+$	TG 16:0_17:0_18:0	$C_{54}H_{104}O_6$	1.543	601.7	3.141	1.7
31.78	313	864.804	$[M+NH_4]^+$	TG 16:0_17:0_18:1	$C_{54}H_{102}O_6$	1.538	885.8	2.739	0.7
31.94	315.6	878.8196	$[M+NH_4]^+$	TG 16:0_18:0_18:1	$C_{55}H_{104}O_6$	1.552	915.8	2.836	0.6
32.45	315.5	894.8517	$[M+NH_4]^+$	TG 16:0_18:0_19:0	$C_{56}H_{108}O_6$	1.551	722.8	3.633	1.4
32.27	317.8	906.8514	$[M+NH_4]^+$	TG 16:0_18:0_20:1	$C_{57}H_{108}O_6$	1.563	862.4	3.241	1.6
32.82	319.3	922.8835	$[M+NH_4]^+$	TG 16:0_18:0_21:0	$C_{58}H_{112}O_6$	1.571	741.8	4.244	1.7
33.03	321.4	936.8995	$[M+NH_4]^+$	TG 16:0_18:0_22:0	$C_{59}H_{114}O_6$	1.581	814.7	4.324	2.0
31.45	319.4	924.8049	$[M+NH_4]^+$. $[M+Na]^+$	TG 16:0_18:0_22:6	$C_{59}H_{102}O_6$	1.571	722.9	3.635	0.3
31.79	315.7	890.8201	$[M+NH_4]^+$	TG 16:0_18:1_19:1	$C_{56}H_{104}O_6$	1.552	798.1	3.636	1.1
31.15	315.8	922.789	$[M+NH_4]^+$	TG 16:0_18:1_22:6	$C_{59}H_{100}O_6$	1.554	713.8	3.503	0.8
30.92	313.8	920.7734	$[M+NH_4]^+$	TG 16:0_18:2_22:6	$C_{59}H_{98}O_6$	1.544	663	3.715	0.9
33.44	324.1	964.9316	$[M+NH_4]^+$	TG 16:0_20:0_22:0	$C_{61}H_{118}O_6$	1.596	668.9	5.044	2.4
32.84	321.9	948.8996	$[M+NH_4]^+$	TG 16:0_20:1_21:0	$C_{60}H_{114}O_6$	1.584	619	4.41	1.8
30.95	315.2	946.7888	$[M+NH_4]^+$	TG 16:0_20:3_22:6	$C_{61}H_{100}O_6$	1.551	675.9	3.14	1.5
30.81	319.4	944.7742	$[M+NH_4]^+$	TG 16:0_20:4_22:6	$C_{61}H_{98}O_6$	1.572	815.5	4.045	0.1
30.69	322.3	968.7747	$[M+NH_4]^+$	TG 16:0_22:6_22:6	$C_{63}H_{98}O_6$	1.587	871.4	4.303	0.4
31.50	311.9	862.7882	$[M+NH_4]^+$	TG 16:1_17:0_18:1	$C_{54}H_{100}O_6$	1.533	752.3	2.804	0.2

31.25	310.1	860.7715	$[M+NH_4]^+$	TG 16:1_17:1_18:1	$C_{54}H_{98}O_6$	1.524	854.5	1.152	0.1
31.03	308.5	858.7567	$[M+NH_4]^+$	TG 16:1_17:1_18:2	$C_{54}H_{96}O_6$	1.516	774.8	2.957	0.1
31.13	310.1	872.7725	$[M+NH_4]^+$. $[M+Na]^+$	TG 16:1_18:1_18:2	$C_{55}H_{98}O_6$	1.524	931.8	2.738	0.5
32.11	316.3	918.8527	$[M+NH_4]^+$	TG 16:1_18:1_21:0	$C_{58}H_{108}O_6$	1.556	589	4.684	1.8
30.64	315	918.7576	$[M+NH_4]^+$	TG 16:1_18:2_22:6	$C_{59}H_{96}O_6$	1.55	775.5	3.09	1.2
32.46	317.5	920.8676	$[M+NH_4]^+$	TG 17:0_16:1_22:0	$C_{58}H_{110}O_6$	1.562	569.6	3.9	1.8
32.10	315.4	892.8359	$[M+NH_4]^+$	TG 17:0_18:0_18:1	$C_{56}H_{106}O_6$	1.551	678.9	3.595	1.3
31.52	314.1	888.8037	$[M+NH_4]^+$	TG 17:1_18:1_18:1	$C_{56}H_{102}O_6$	1.545	894.6	2.528	0.4
31.88	318.4	928.836	$[M+NH_4]^+$	TG 18:0_18:0_20:4	$C_{59}H_{106}O_6$	1.567	750.8	3.648	1.2
31.76	319.7	952.8381	$[M+NH_4]^+$	TG 18:0_18:0_22:6	$C_{61}H_{106}O_6$	1.574	657.8	4.799	1.3
31.63	314.8	902.8194	$[M+NH_4]^+$. $[M+Na]^+$	TG 18:0_18:1_18:2	$C_{57}H_{104}O_6$	1.548	874.2	2.622	1.1
32.25	318.6	932.8681	$[M+NH_4]^+$	TG 18:0_18:1_20:1	$C_{59}H_{110}O_6$	1.568	760.7	4.225	2.0
32.64	321	960.8997	$[M+NH_4]^+$	TG 18:0_18:1_22:1	$C_{61}H_{114}O_6$	1.58	646.3	4.674	2.6
32.07	320.5	956.8674	$[M+NH_4]^+$	TG 18:0_18:1_22:3	$C_{61}H_{110}O_6$	1.578	780.4	3.395	1.8
31.74	320.4	978.8548	$[M+NH_4]^+$	TG 18:0_20:1_22:6	$C_{63}H_{108}O_6$	1.577	754.7	6.4	2.3
30.98	326.4	996.8063	$[M+NH_4]^+$	TG 18:0_22:6_22:6	$C_{65}H_{102}O_6$	1.608	610.9	4.7	0.1
32.23	320.2	958.8818	$[M+NH_4]^+$	TG 18:1_18:1_22:1	$C_{61}H_{112}O_6$	1.576	835.3	1.808	2.6
31.28	311.4	896.7764	$[M+NH_4]^+$	TG 18:1_18:2_18:3	$C_{57}H_{98}O_6$	1.532	897.7	5.724	1.1
33.22	323.5	976.9314	$[M+NH_4]^+$	TG 18:1_20:0_21:0	$C_{62}H_{118}O_6$	1.593	624.5	5.017	2.8
31.44	320.4	976.8379	$[M+NH_4]^+$	TG 18:1_20:1_22:6	$C_{63}H_{106}O_6$	1.577	699.0	5.606	1.7
30.81	322.6	970.7901	$[M+NH_4]^+$	TG 18:1_20:4_22:6	$C_{63}H_{100}O_6$	1.588	718.1	4.211	0.3

30.63	310.6	894.7535	$[M+NH_4]^+$	TG 18:2_18:2_18:3	$C_{57}H_{96}O_6$	1.527	933.4	-2.155	0.4
31.46	305.1	810.7563	$[M+NH_4]^+$	TG 47:0	$C_{50}H_{96}O_6$	1.498	935.4	2.231	0.3
31.96	312.8	852.8038	$[M+NH_4]^+$. $[M+Na]^+$	TG 50:0	$C_{53}H_{102}O_6$	1.537	928.7	2.783	1.3
31.63	311.2	850.788	$[M+NH_4]^+$	TG 50:1	$C_{53}H_{100}O_6$	1.529	949.6	2.517	0.3
30.81	304.8	844.7403	$[M+NH_4]^+$	TG 50:4	$C_{53}H_{94}O_6$	1.497	956.5	1.936	0.3
32.29	316.6	880.8355	$[M+NH_4]^+$. $[M+NH_4]^+$. $[M+Na]^+$	TG 52:0	$C_{55}H_{106}O_6$	1.556	946.7	3.061	1.6
31.62	313.9	876.8039	$[M+NH_4]^+$	TG 52:2	$C_{55}H_{102}O_6$	1.543	946.2	2.778	1.1
31.39	311.7	874.7878	$[M+NH_4]^+$	TG 52:3	$C_{55}H_{100}O_6$	1.532	906	2.406	0.1
31.25	311.9	872.7726	$[M+NH_4]^+$	TG 52:4	$C_{55}H_{98}O_6$	1.533	889.5	2.965	0.6
31.92	316.3	904.8355	$[M+NH_4]^+$	TG 54:2	$C_{57}H_{106}O_6$	1.556	832.3	2.96	1.3
31.57	315.9	900.8034	$[M+NH_4]^+$	TG 54:4	$C_{57}H_{102}O_6$	1.554	798.1	2.683	0.5
31.39	314.3	900.8037	$[M+NH_4]^+$	TG 54:4	$C_{57}H_{102}O_6$	1.546	934.1	2.908	0.2
31.15	311.5	898.7892	$[M+NH_4]^+$	TG 54:5	$C_{57}H_{100}O_6$	1.532	826.4	3.992	1.4
30.61	311.3	892.7417	$[M+NH_4]^+$	TG 54:8	$C_{57}H_{94}O_6$	1.531	647.2	3.317	1.0
33.21	322.2	950.9154	$[M+NH_4]^+$	TG 57:0	$C_{60}H_{116}O_6$	1.586	688.8	4.473	2.5
33.02	322.9	962.9154	$[M+NH_4]^+$	TG 58:1	$C_{61}H_{116}O_6$	1.589	725	4.604	2.5
31.2	315.6	948.805	$[M+NH_4]^+$	TG 58:8	$C_{61}H_{102}O_6$	1.553	736.7	3.752	1.5
31.11	317.6	972.8053	$[M+NH_4]^+$	TG 60:10	$C_{63}H_{102}O_6$	1.564	768.3	4.152	1.8

m.c.: manual curation

Table S3.2. *VIP SCORE results.*

Compound	Comp. 1	Comp. 2	Comp. 3	Comp. 4	Comp. 5
DG 42:1	2.0916	1.9565	1.9227	1.9129	1.9124
DG 41:1	2.0862	1.9442	1.9106	1.8999	1.8994
BMP 42:10	2.0598	1.9325	1.8991	1.8898	1.8893
HexCer 18:1;2O/26:0	2.0282	1.8947	1.862	1.8517	1.8513
HexCer 20:2;2O/26:0;O	1.9848	1.8552	1.8269	1.8166	1.8161
TG 18:1_18:1_22:1	1.9566	1.8109	1.7801	1.77	1.7695
TG 18:0_20:1_22:6	1.9279	1.784	1.7557	1.7458	1.7453
HexCer 18:1;2O/24:0	1.9263	1.786	1.7559	1.7468	1.7463
CE 18:0	1.9158	1.9287	1.9028	1.8924	1.8918
TG 18:0_18:1_20:1	1.9082	1.7659	1.7353	1.7258	1.7253
SM 38:1_B	1.9007	1.7732	1.7465	1.7366	1.7361
TG 18:0_18:0_22:6	1.871	1.7313	1.7049	1.6962	1.6958
LPC 24:0	1.8399	1.7026	1.678	1.6685	1.6681
TG 18:0_18:1_22:3	1.8339	1.697	1.6685	1.6606	1.6603
HexCer 18:1;2O/20:0	1.8282	1.7071	1.6777	1.6727	1.6723
HexCer 18:2;2O/22:0;O	1.8224	1.6907	1.6616	1.6555	1.6552
PG 39:5 /BMP 39:5	1.8221	1.6892	1.6623	1.6546	1.6541
HexCer 18:1;2O/22:0	1.8136	1.6885	1.6604	1.655	1.6546
DG O-36:6	1.7968	1.663	1.6355	1.6296	1.6292
DG 21:0_18:1	1.7917	1.679	1.6525	1.6471	1.6467
LPC 24:1	1.7916	1.6745	1.6457	1.6386	1.6382
TG 17:1_18:1_18:1	1.781	1.6598	1.6326	1.6302	1.6298
HexCer 18:1;2O/25:0;O	1.7759	1.6739	1.647	1.6405	1.6401
HexCer 18:1;2O/24:0;O	1.7721	1.6651	1.641	1.6347	1.6343
PG 40:7 /BMP 40:7	1.7606	1.6291	1.6132	1.6051	1.6046
CE 16:0	1.7591	1.7753	1.751	1.7411	1.7406
TG 18:0_18:1_22:1	1.7556	1.6361	1.6159	1.6075	1.607
HexCer 18:1;2O/38:2;O	1.7544	1.6346	1.6199	1.6126	1.6122
PG 34:2/BMP 34:2	1.7423	1.6123	1.5982	1.595	1.5945
TG 16:0_18:1_19:1	1.7364	1.6107	1.5833	1.5778	1.5776
LPC 20:4_A	1.7299	1.607	1.5834	1.5812	1.5808
SM 42:0;3O	1.7278	1.7507	1.724	1.7147	1.7143
DG 17:0_20:4	1.7228	1.5948	1.5809	1.5719	1.5716
TG 18:0_18:1_18:2	1.7207	1.6063	1.5972	1.5909	1.5905
LPE 18:1	1.7185	1.5988	1.5716	1.5627	1.5623
HexCer 18:1;2O/23:0;O	1.711	1.6416	1.6155	1.6092	1.6088
Cer related molecule	1.7095	1.5914	1.5819	1.5744	1.5741
HexCer 18:2;2O/23:0;O	1.7067	1.5796	1.5523	1.5483	1.5479
LPC 19:1	1.6957	1.5753	1.549	1.5403	1.5399
HexCer 18:1;2O/23:0	1.6878	1.5625	1.5375	1.5332	1.5329
DG 41:2	1.6871	1.5752	1.5526	1.5468	1.5465
CE 22:4	1.6863	1.6954	1.6665	1.657	1.6565
TG 54_5	1.6715	1.5979	1.6075	1.599	1.5986

CE 20:3	1.6705	1.6639	1.6429	1.6371	1.6367
PC 42:11	1.6693	1.5726	1.5893	1.5803	1.5798
LPC 20:1_B	1.6558	1.6582	1.6325	1.6242	1.624
TG 16:0_18:0_18:1	1.6543	1.5328	1.5185	1.5099	1.5095
LPC 20:1_A	1.6446	1.5222	1.4963	1.4926	1.4922
HexCer 20:1;2O/24:0;O	1.623	1.5901	1.5637	1.5568	1.5565
HexCer d16:1/23:0	1.6219	1.5012	1.4785	1.4755	1.4751
PC 39:5	1.6089	1.4969	1.4714	1.4631	1.4627
PE 46:12	1.602	1.4887	1.4676	1.461	1.4606
LPE 24:5_A	1.5998	1.4835	1.4607	1.4596	1.4593
PC 42:7_B	1.5991	1.4815	1.4602	1.4535	1.4533
HexCer 18:1;2O/22:1	1.5904	1.4749	1.4498	1.4464	1.4461
CE 16:1	1.581	1.5749	1.5563	1.5506	1.5502
SM 35:1	1.5796	1.5511	1.5328	1.5267	1.5265
TG 16:1_18:1_21:0	1.5779	1.461	1.4422	1.4351	1.4351
CE 20:2	1.5758	1.643	1.6289	1.6205	1.6201
CE 14:0	1.5753	1.5637	1.5376	1.5296	1.5294
DG 20:0_20:4	1.5701	1.4536	1.445	1.4395	1.4391
DG 22:0_20:4	1.5685	1.4619	1.4367	1.4366	1.4365
HexCer 18:1;2O/18:0;O	1.559	1.5582	1.5318	1.5245	1.5242
HexCer 18:1;2O/25:1;O_A	1.557	1.4448	1.4199	1.419	1.4188
PC 32:1_C	1.5442	1.4591	1.4474	1.4395	1.4391
CE 20:1	1.5369	1.6161	1.5947	1.587	1.5866
DG 34:0	1.5364	1.4219	1.4263	1.4202	1.4198
PC 44:8	1.5322	1.4499	1.4254	1.4173	1.4169
DG 18:1_22:6	1.5272	1.4133	1.4063	1.3997	1.3994
Cer 20:1;2O/24:1	1.5249	1.4138	1.3913	1.3881	1.3879
PC 44:3	1.5179	1.4063	1.3878	1.38	1.3796
HexCer 18:1;2O/25:1;O_B	1.5105	1.4031	1.3788	1.3838	1.3834
HexCer 18:1;2O/18:1	1.51	1.3993	1.3844	1.3808	1.3806
PC 16:0_18:2_B	1.5013	1.4271	1.4136	1.4064	1.4066
TG 50_1	1.5012	1.3924	1.389	1.3814	1.381

A, B, C indicate potential isomers.

Table S3.3. *Volcano Plot results.*

Compound	Fold Change (FC)	log2(FC)	raw pvalue	-log10(pvalue)
DG 42:1	2.3984	1.2621	$8.1252e^{-05}$	4.0902
DG 41:1	2.1043	1.0733	$9.3214e^{-05}$	4.0305
BMP 42:10	2.7033	1.4347	0.00017214	3.7641
HexCer 18:1;2O/26:0	3.442	1.7833	0.00032057	3.4941
HexCer 20:2;2O/26:0;O	3.3384	1.7391	0.00065606	3.1831
HexCer 18:1;2O/24:0	3.946	1.9804	0.0014421	2.841
CE 18:0	0.36618	-1.4494	0.0016357	2.7863
SM 38:1_B	6.8151	2.7687	0.0019427	2.7116
LPC 24:0	3.0408	1.6045	0.0036173	2.4416
HexCer 18:1;2O/20:0	2.134	1.0935	0.0040284	2.3949
PG 39:5 /BMP 39:5	2.7386	1.4534	0.0042597	2.3706
HexCer 18:1;2O/22:0	2.22	1.1505	0.0045893	2.3382
DG O-36:6	2.4643	1.3012	0.0053023	2.2755
LPC 24:1	2.517	1.3317	0.0055402	2.2565
HexCer 18:1;2O/25:0;O	2.9985	1.5842	0.0062974	2.2008
HexCer 18:1;2O/24:0;O	2.183	1.1263	0.0064878	2.1879
PG 40:7 /BMP 40:7	2.2497	1.1697	0.0071026	2.1486
CE 16:0	0.41106	-1.2826	0.0071825	2.1437
HexCer 18:1;2O/38:2;O	3.3051	1.7247	0.0074481	2.128
PG 34:2/BMP 34:2	2.1053	1.074	0.0081596	2.0883
LPC 20:4_A	0.05756	-4.1188	0.0089335	2.049

A, B, C indicate potential isomers.

Table S3.4. *SAM results.*

Compound	d.value	stdev	rawp	q.value
DG 42:1	7.3331	0.24141	$3.413e^{-02}$	0.0085244
DG 41:1	7.1916	0.24552	$5.1195e^{-05}$	0.0085244
BMP 42:10	6.5846	0.26476	$6.8259e^{-05}$	0.0085244
HexCer 18:1;2O/26:0	6.0079	0.28573	0.00015358	0.014385
HexCer 20:2;2O/26:0;O	5.3871	0.31184	0.00022184	0.016623
TG 18:1_18:1_22:1	5.0577	0.32742	0.0003413	0.021311

TG 18:0_20:1_22:6	4.7665	0.34233	0.00066553	0.031967
HexCer 18:1;2O/24:0	4.7517	0.34312	0.00068259	0.031967
TG 18:0_18:1_20:1	4.5871	0.35208	0.00087031	0.032606
SM 38:1_B	4.5228	0.35568	0.0010239	0.034873
TG 18:0_18:0_22:6	4.2857	0.3695	0.0015358	0.04795
LPC 24:0	4.0632	0.38325	0.0021331	0.054531
TG 18:0_18:1_22:3	4.0228	0.38583	0.0022355	0.054531
HexCer 18:1;2O/20:0	3.9859	0.38821	0.0023549	0.054531
HexCer 18:2;2O/22:0;O	3.9482	0.39066	0.0024573	0.054531
PG 39:5 /BMP 39:5	3.946	0.39081	0.0024744	0.054531
HexCer 18:1;2O/22:0	3.8931	0.39429	0.0026792	0.055764
DG O-36:6	3.7913	0.40113	0.0031229	0.059671
DG 21:0_18:1	3.7614	0.40317	0.0033276	0.059671
LPC 24:1	3.7605	0.40323	0.0033447	0.059671
TG 17:1_18:1_18:1	3.7001	0.40739	0.0037713	0.064224
HexCer 18:1;2O/25:0;O	3.6713	0.4094	0.0040102	0.065323
HexCer 18:1;2O/24:0;O	3.6507	0.41085	0.004198	0.065531
PG 40:7 /BMP 40:7	3.5882	0.41527	0.0046758	0.066445
TG 18:0_18:1_22:1	3.5621	0.41714	0.0048976	0.066445
HexCer 18:1;2O/38:2;O	3.5556	0.41761	0.0049659	0.066445
PG 34:2/BMP 34:2	3.4932	0.42213	0.0053413	0.066856
TG 16:0_18:1_19:1	3.4637	0.4243	0.0055119	0.066856
SM 42:0;3O	3.4212	0.42743	0.0058874	0.066856
DG 17:0_20:4	3.3971	0.42923	0.0060239	0.066856
TG 18:0_18:1_18:2	3.3871	0.42997	0.0061604	0.066856
LPE 18:1	3.3765	0.43077	0.0062457	0.066856
HexCer 18:1;2O/23:0;O	3.341	0.43344	0.0066894	0.067803
Cer related molecule	3.3342	0.43395	0.0067406	0.067803
HexCer 18:2;2O/23:0;O	3.3209	0.43496	0.0068771	0.067803
LPC 19:1	3.271	0.43877	0.0076962	0.073933
HexCer 18:1;2O/23:0	3.2355	0.4415	0.0082935	0.075502
DG 41:2	3.2325	0.44174	0.0083618	0.075502
TG 54_5	3.1648	0.44701	0.0093515	0.079419
PC 42:11	3.1555	0.44774	0.0095392	0.079419
LPC 20:1_B	3.0991	0.45221	0.010427	0.084201
TG 16:0_18:0_18:1	3.0928	0.45272	0.010563	0.084201
LPC 20:1_A	3.0535	0.45585	0.011399	0.088974
HexCer 20:1;2O/24:0;O	2.9685	0.46274	0.013259	0.10012
HexCer d16:1/23:0	2.9643	0.46309	0.013362	0.10012

A, B, C indicate potential isomers.

7.4. Supporting information for Chapter V: "Pre-formed gradients for high-throughput and robust nanoflow lipidomics with trapped ion mobility and PASEF"

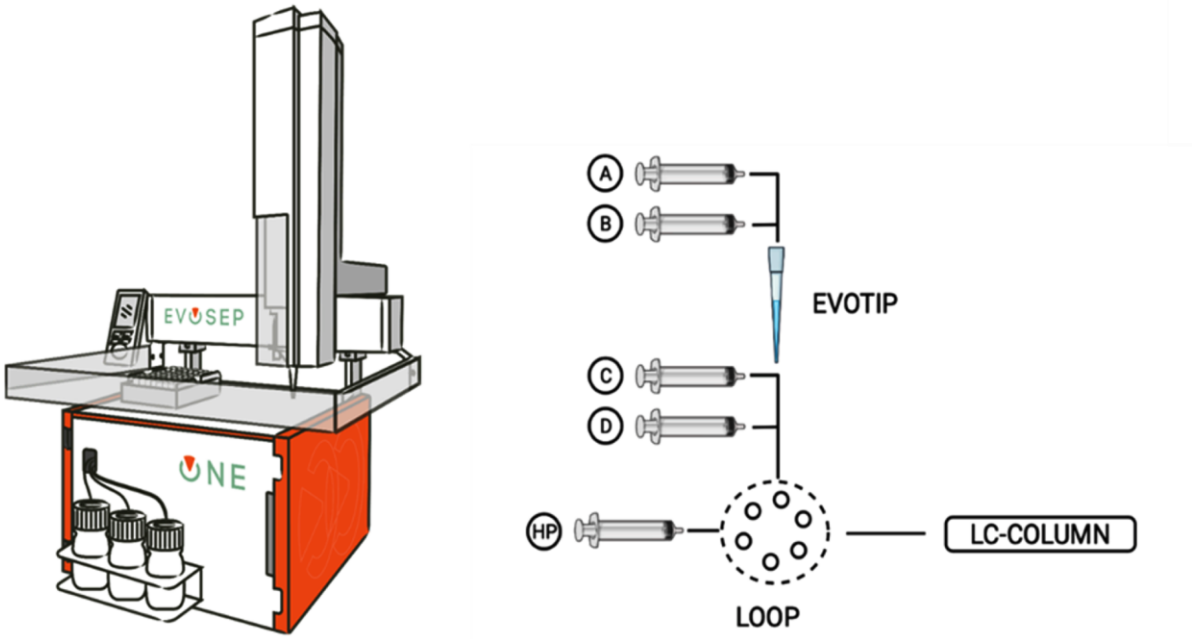

Figure S4.1. *Schematic representation of Evosep One. Lipids are eluted from the C18 disk contained into the Evotip. Pumps C and D form the final gradient which is stored in the loop and then pushed over the column by HP (high pressure) pump.*

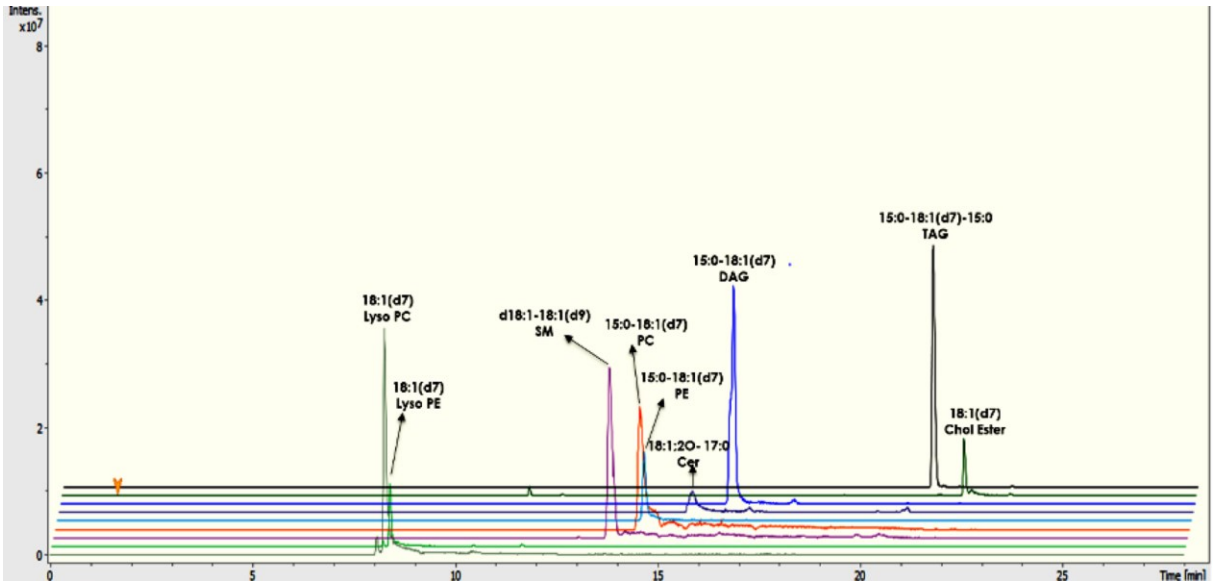

Figure S4.2. *Extracted ion chromatograms (EIC) of lipid standard mix.*

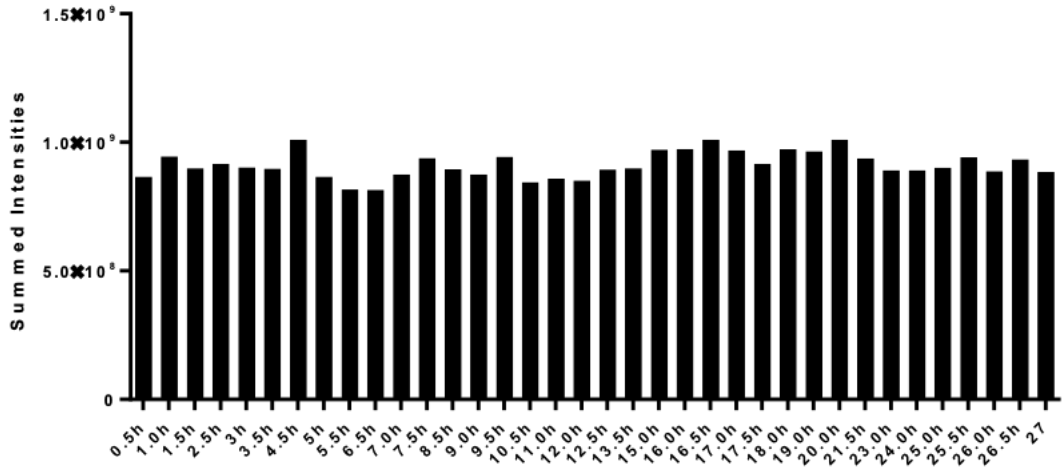

Figure S4.3. *Summed intensities variation of identified lipids over 27 h with Evosep One.*

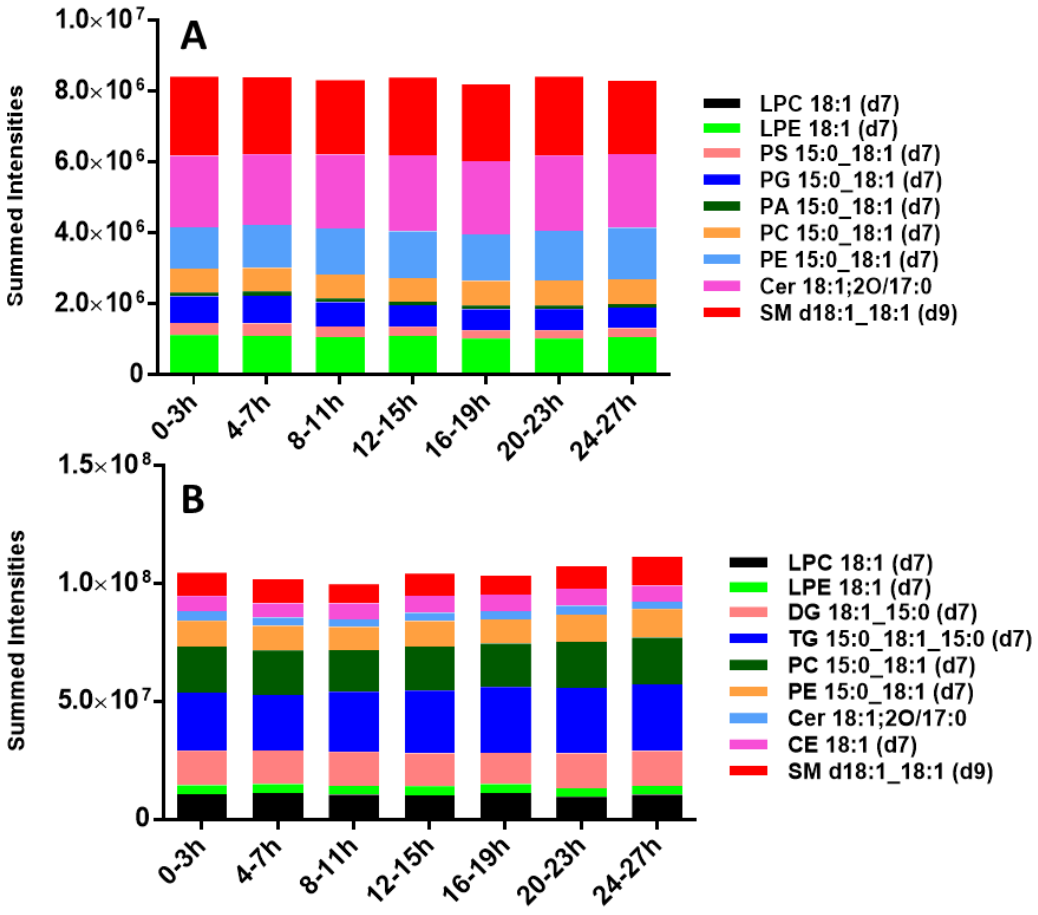

Figure S4.4. *Summed intensities variation over 27 h of internal standard lipids in negative (**A**) and positive mode (**B**).*

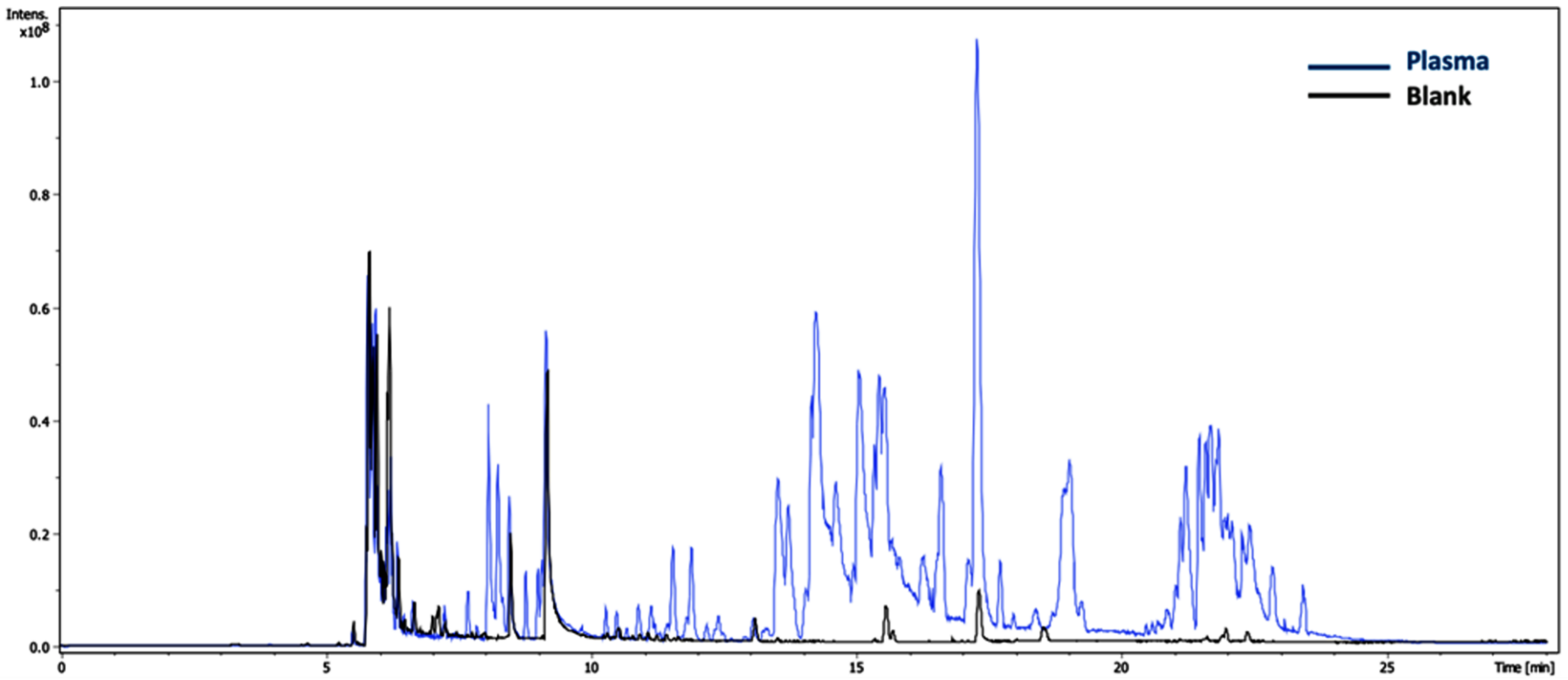

Figure S4.5. *BPC comparison between a plasma run (blue) and the consecutive blank injection (black).*

Table S4.1. *List of lipids identified starting from 1 µL of plasma with Evosep One coupled to TimsTOF Pro.*

RT [min]	CCS (Å²)	m/z meas.	M meas.	Ions	Name	Molecular Formula	MS/MS score	Δm/z [ppm]
21.86	281.2	614.5874	596.5536	$[M+NH_4]^+$	CE 14:0	$C_{41}H_{72}O_2$	732.9	0.556
21.29	277.3	612.572	594.5381	$[M+NH_4]^+$	CE 14:1	$C_{41}H_{70}O_2$	937.0	1.061
22.15	281.9	628.6028	610.5689	$[M+NH_4]^+$	CE 15:0	$C_{42}H_{74}O_2$	624.7	0.082
22.44	282.9	642.6181	624.5843	$[M+NH_4]^+$	CE 16:0	$C_{43}H_{76}O_2$	711.9	-0.271
21.85	281.6	640.6028	622.569	$[M+NH_4]^+$	CE 16:1	$C_{43}H_{74}O_2$	672.6	0.225
21.42	281.2	638.5867	620.5529	$[M+NH_4]^+$	CE 16:2	$C_{43}H_{72}O_2$	690.0	-0.572
22.58	284.9	656.6337	638.5999	$[M+NH_4]^+$	CE 17:0	$C_{44}H_{78}O_2$	881.4	-0.585
22.13	283.3	654.6182	636.5844	$[M+NH_4]^+$	CE 17:1	$C_{44}H_{76}O_2$	689.2	-0.238
21.68	283	652.6028	634.569	$[M+NH_4]^+$	CE 17:2	$C_{44}H_{74}O_2$	741.0	0.139
22.88	287.4	670.6488	652.615	$[M+NH_4]^+$	CE 18:0	$C_{45}H_{80}O_2$	684.2	-1.253
22.37	285.6	668.6339	650.6001	$[M+NH_4]^+$	CE 18:1	$C_{45}H_{78}O_2$	700.8	-0.145
21.94	286.1	666.6198	648.586	$[M+NH_4]^+$	CE 18:2	$C_{45}H_{76}O_2$	671.5	2.204
21.56	288.7	664.6021	646.5684	$[M+NH_4]^+$, $[M+NH_4]^+$, $[M+H]^+$	CE 18:3	$C_{45}H_{74}O_2$	978.7	-0.846
21.13	285.7	662.5867	644.5529	$[M+NH_4]^+$	CE 18:4	$C_{45}H_{72}O_2$	737.9	-0.557
22.1	289	680.6339	662.6	$[M+NH_4]^+$	CE 19:2	$C_{46}H_{78}O_2$	362.3	-0.076
21.45	286.4	676.6027	658.5688	$[M+NH_4]^+$	CE 19:4	$C_{46}H_{74}O_2$	688.9	0.177
22.82	289.7	696.6648	678.631	$[M+NH_4]^+$	CE 20:1	$C_{47}H_{82}O_2$	736.1	-0.674
22.46	290.4	694.6492	676.6154	$[M+NH_4]^+$	CE 20:2	$C_{47}H_{80}O_2$	815.7	-1.266
22.05	289.9	692.6338	674.6	$[M+NH_4]^+$	CE 20:3	$C_{47}H_{78}O_2$	688.4	-0.239
22.19	289.9	692.6337	674.5998	$[M+NH_4]^+$	CE 20:3	$C_{47}H_{78}O_2$	635.3	-1.805
21.73	289.3	690.6194	672.5849	$[M+NH_4]^+$, $[M+H]^+$	CE 20:4	$C_{47}H_{76}O_2$	969.7	1.744
21.33	286.9	688.603	670.5691	$[M+NH_4]^+$, $[M+Na]^+$	CE 20:5	$C_{47}H_{74}O_2$	979.9	0.266
23.40	293.6	712.6952	694.6613	$[M+NH_4]^+$	CE 21:0	$C_{48}H_{86}O_2$	773.6	-1.420

23.23	295.2	724.6964	706.6626	$[M+NH_4]^+$	CE 22:1	$C_{49}H_{86}O_2$	731.9	0.130
22.52	296.2	720.6658	702.632	$[M+NH_4]^+$	CE 22:3	$C_{49}H_{82}O_2$	1000	1.145
22.12	293.7	718.6491	700.6152	$[M+NH_4]^+$	CE 22:4	$C_{49}H_{80}O_2$	908.8	-0.253
10.90	244.9	484.4725	483.4652	$[M+H]^+$	Cer 14:0;2O/16:0	$C_{30}H_{61}NO_3$	178.6	0.118
11.98	252.3	512.5038	511.4965	$[M+H]^+$	Cer 16:0;O2/16:0	$C_{32}H_{65}NO_3$	560.8	0.041
9.34	262.6	590.5151	589.5078	$[M+H]^+$	Cer 16:0;O2/21:4;O	$C_{37}H_{67}NO_4$	772.5	1.501
17.86	280.8	670.6347	669.6274	$[M+H]^+$	Cer 17:0;O3/24:0;O	$C_{41}H_{83}NO_5$	883.2	0.479
15.13	261.8	556.5295	555.5223	$[M+H]^+$	Cer 18:0;O2/16:0;O	$C_{34}H_{69}NO_4$	1000	-0.719
18.58	274.3	624.6289	623.6217	$[M+H]^+$	Cer 18:0;O2/22:0	$C_{40}H_{81}NO_3$	754.2	0.086
19.35	279.7	652.6599	651.6526	$[M+H]^+$	Cer 18:0;O2/24:0	$C_{42}H_{85}NO_3$	800.8	-0.520
19.71	282.4	666.6757	665.6685	$[M+H]^+$	Cer 18:0;O2/25:0	$C_{43}H_{87}NO_3$	649.2	-0.322
17.40	278.2	656.6182	655.6109	$[M+H]^+$	Cer 18:0;O3/22:0;O	$C_{40}H_{81}NO_5$	1000	-0.856
18.29	283.5	684.6484	683.6412	$[M+H]^+$	Cer 18:0;O3/24:0;O	$C_{42}H_{85}NO_5$	821.8	-2.170
13.52	252.8	508.4733	507.4661	$[M+H]^+$	Cer 18:1;O2/14:1	$C_{32}H_{61}NO_3$	383.6	1.804
15.25	256.9	538.5193	537.512	$[M+H]^+$	Cer 18:1;O2/16:0	$C_{34}H_{67}NO_3$	796.1	-0.065
14.68	259.2	536.5039	535.4966	$[M+H]^+$	Cer 18:1;O2/16:1	$C_{34}H_{65}NO_3$	1000	0.340
16.35	262.6	566.55	565.5427	$[M+H]^+$	Cer 18:1;O2/18:0	$C_{36}H_{71}NO_3$	778.6	-1.227
18.28	273.1	622.613	621.6057	$[M+H]^+$	Cer 18:1;O2/22:0	$C_{40}H_{79}NO_3$	756.9	-0.513
18.69	276.1	636.6289	635.6217	$[M+H]^+$	Cer 18:1;O2/23:0	$C_{41}H_{81}NO_3$	657.5	-0.536
19.08	278.5	650.6441	649.6369	$[M+H]^+$	Cer 18:1;O2/24:0	$C_{42}H_{83}NO_3$	905.0	-0.731
19.22	278.3	650.6445	649.6372	$[M+H]^+$	Cer 18:1;O2/24:0	$C_{42}H_{83}NO_3$	856.3	0.198
19.45	280.5	664.6598	663.6528	$[M+H]^+$, $[M+H-H_2O]^+$	Cer 18:1;O2/25:0	$C_{43}H_{85}NO_3$	276.2	-0.471
19.80	283.7	678.6754	677.6677	$[M+H]^+$, $[M+Na]^+$	Cer 18:1;O2/26:0	$C_{44}H_{87}NO_3$	656.0	-0.615
17.31	276.9	634.6125	633.6052	$[M+H]^+$	Cer 18:2;O2/23:0	$C_{41}H_{79}NO_3$	363.2	-1.273
16.84	277.6	650.6078	649.6005	$[M+H]^+$	Cer 18:2;O2/23:0;O	$C_{41}H_{79}NO_4$	307.1	-0.282
17.29	280.2	664.6234	663.6161	$[M+H]^+$	Cer 18:2;O2/24:0;O	$C_{42}H_{81}NO_4$	420.4	-0.367

18.18	281.9	662.6447	661.6374	$[M+H]^+$	Cer 18:2;O2/25:0	$C_{43}H_{83}NO_3$	344.0	0.06
17.75	283.0	678.6392	677.6319	$[M+H]^+$	Cer 18:2;O2/25:0;O	$C_{43}H_{83}NO_4$	416.4	-0.513
18.59	284.8	676.6596	675.6523	$[M+H]^+$	Cer 18:2;O2/26:0	$C_{44}H_{85}NO_3$	488.7	-0.636
18.17	285.4	692.6548	691.6475	$[M+H]^+$	Cer 18:2;O2/26:0;O	$C_{44}H_{85}NO_4$	410.6	-0.557
20.37	287.4	694.7063	693.6991	$[M+H]^+$	Cer 19:0;2O/26:0	$C_{45}H_{91}NO_3$	181.6	-1.434
16.81	274.4	620.5982	619.5909	$[M+H]^+$	Cer 19:0;O2/21:2	$C_{40}H_{77}NO_3$	1000	1.005
19.75	287	696.6862	695.6789	$[M+H]^+$	Cer 19:0;O2/25:0;O	$C_{44}H_{89}NO_4$	1000	-0.59
18.50	275.5	636.6294	635.6221	$[M+H]^+$	Cer 19:1;O2/22:0	$C_{41}H_{81}NO_3$	388.1	0.937
19.46	290.3	726.695	725.6877	$[M+H]^+$	Cer 20:0;3O/25:0;(2OH)	$C_{45}H_{91}NO_5$	706.5	-1.933
19.80	292.6	740.7123	739.705	$[M+H]^+$	Cer 20:0;3O/26:0;(2OH)	$C_{46}H_{93}NO_5$	766.5	-0.55
17.71	269.3	596.5975	595.5903	$[M+H]^+$	Cer 20:0;O2/18:0	$C_{38}H_{77}NO_3$	772.8	-0.154
20.05	284.9	680.6911	679.6836	$[M+H]^+$, $[M+Na]^+$	Cer 20:0;O2/24:0	$C_{44}H_{89}NO_3$	639.1	-0.824
19.08	288.6	712.6806	711.6733	$[M+H]^+$	Cer 20:0;O3/24:0;O	$C_{44}H_{89}NO_5$	633.1	-0.972
20.13	286.1	692.6905	691.6837	$[M+H]^+$, $[M+H-H_2O]^+$	Cer 20:1;2O/25:0	$C_{45}H_{89}NO_3$	774.8	-2.022
20.44	288.9	706.7067	705.6992	$[M+H]^+$, $[M+H-H_2O]^+$	Cer 20:1;2O/26:0	$C_{46}H_{91}NO_3$	864.5	-0.905
20.73	291.2	720.7229	719.715	$[M+H]^+$, $[M+H-H_2O]^+$	Cer 20:1;2O/27:0	$C_{47}H_{93}NO_3$	594.2	0.152
21.00	293.3	734.7384	733.7309	$[M+H]^+$, $[M+H-H_2O]^+$	Cer 20:1;2O/28:0	$C_{48}H_{95}NO_3$	790.3	0.409
22.21	335.7	1040.995	1039.987	$[M+H]^+$	Cer 20:1;2O/48:3;2O	$C_{68}H_{129}NO_5$	768.4	1.366
20.00	294.6	732.722	731.7147	$[M+H]^+$	Cer 20:2;2O/28:0	$C_{48}H_{93}NO_3$	174.5	-1.237
16.21	265.5	582.5466	581.5393	$[M+H]^+$	Cer 21:0;O2/15:1;O	$C_{36}H_{71}NO_4$	790.7	1.715
20.67	289.7	708.722	707.7153	$[M+H]^+$, $[M+Na]^+$	Cer 22:0;2O/24:0	$C_{46}H_{93}NO_3$	206.6	-1.214
20.43	296.9	768.7434	767.7362	$[M+H]^+$	Cer 22:0;3O/26:0;(2OH)	$C_{48}H_{97}NO_5$	860	-0.585
17.56	275.5	640.6214	639.6141	$[M+H]^+$	Cer 22:0;O2/18:0;O	$C_{40}H_{81}NO_4$	211.7	-4.919
21.49	297.5	762.7682	761.761	$[M+H]^+$	Cer 22:1;2O/28:0	$C_{50}H_{99}NO_3$	817.6	-2.704
22.54	339.6	1069.026	1068.019	$[M+H]^+$	Cer 22:1;2O/48:3;2O	$C_{70}H_{133}NO_5$	819.1	0.435
20.37	285	724.6792	723.672	$[M+H]^+$	Cer 24:0;3O/21:1;(2OH)	$C_{45}H_{89}NO_5$	578.2	-4.369

21.69	298	764.784	763.7767	$[M+H]^+$	Cer 26:0;2O/24:0	$C_{50}H_{101}NO_3$	251.3	-1.672
15.93	254.8	558.5092	540.4754	$[M+NH_4]^+$	DG 14:0_16:0	$C_{33}H_{64}O_5$	768.6	0.04
15.57	252.3	544.4937	526.4587	$[M+NH_4]^+$, $[M+H]^+$	DG 15:0_14:0	$C_{32}H_{62}O_5$	890	0.16
16.66	257.4	572.5247	554.4908	$[M+NH_4]^+$	DG 15:0_16:0	$C_{34}H_{66}O_5$	879.3	-0.467
17.18	260.2	586.5404	568.5069	$[M+NH_4]^+$, $[M+Na]^+$, $[M+NH_4]^+$, $[M+NH_4]^+$, $[M+H]^+$, $[M+K]^+$	DG 16:0_16:0	$C_{35}H_{68}O_5$	882.6	-0.171
17.33	259.7	586.5413	568.5074	$[M+NH_4]^+$	DG 16:0_16:0	$C_{35}H_{68}O_5$	770.5	0.403
16.97	259.7	586.5404	568.5065	$[M+NH_4]^+$	DG 16:0_16:0	$C_{35}H_{68}O_5$	601.1	-0.223
16.13	254.9	558.5089	540.4756	$[M+NH_4]^+$, $[M+Na]^+$, $[M+H]^+$	DG 16:0_14:0	$C_{33}H_{64}O_5$	810.5	-0.479
16.41	258.4	584.5245	566.4907	$[M+NH_4]^+$	DG 16:0_16:1	$C_{35}H_{66}O_5$	751.1	-0.574
16.06	258.4	596.5245	578.4907	$[M+NH_4]^+$	DG 17:1_16:1	$C_{36}H_{66}O_5$	624.1	-0.796
18.96	270.7	642.603	624.5694	$[M+NH_4]^+$, $[M+H]^+$, $[M+H-H_2O]^+$, $[M+NH_4]^+$	DG 18:0_18:0	$C_{39}H_{76}O_5$	862.4	-0.088
19.09	270.6	642.6042	624.5703	$[M+NH_4]^+$	DG 18:0_18:0	$C_{39}H_{76}O_5$	723.6	1.893
18.13	265.6	614.5717	596.5382	$[M+NH_4]^+$, $[M+NH_4]^+$, $[M+H]^+$	DG 18:0_16:0	$C_{37}H_{72}O_5$	856.2	-0.257
18.27	265.1	614.5729	596.5391	$[M+NH_4]^+$	DG 18:0_16:0	$C_{37}H_{72}O_5$	891.1	2.285
17.35	265.8	638.5714	620.5377	$[M+NH_4]^+$, $[M+H]^+$, $[M+Na]^+$, $[M+NH_4]^+$	DG 18:1_18:1	$C_{39}H_{72}O_5$	962.9	-0.624
17.25	263.7	612.5558	594.5221	$[M+NH_4]^+$, $[M+H]^+$	DG 18:1_16:0	$C_{37}H_{70}O_5$	928.5	-0.533
16.66	262.2	636.556	618.5222	$[M+NH_4]^+$	DG 18:1_18:2	$C_{39}H_{70}O_5$	935.8	0.041
16.01	258.3	634.5404	616.5066	$[M+NH_4]^+$	DG 18:2_18:2	$C_{39}H_{68}O_5$	734.0	-0.142
16.55	260.8	610.54	592.5062	$[M+NH_4]^+$	DG 18:2_16:0	$C_{37}H_{68}O_5$	630.7	-0.809
16.07	260.1	608.5256	590.4918	$[M+NH_4]^+$	DG 18:2_16:1	$C_{37}H_{66}O_5$	754.0	1.271
18.19	268.7	640.587	622.5531	$[M+NH_4]^+$, $[M+H]^+$	DG 20:1_16:0	$C_{39}H_{74}O_5$	287.1	-0.764
19.68	276.5	670.634	652.6002	$[M+NH_4]^+$	DG 22:0_16:0	$C_{41}H_{80}O_5$	441.2	-0.995
20.57	287.7	714.6029	696.5691	$[M+NH_4]^+$	DG 22:6_20:0	$C_{45}H_{76}O_5$	575.0	-0.305
20.63	284.6	712.68	694.6462	$[M+NH_4]^+$	DG 25:0_16:0	$C_{44}H_{86}O_5$	409.1	-1.377
13.48	236.5	504.4048	486.371	$[M+NH_4]^+$	DG O-28:6	$C_{31}H_{50}O_4$	433.6	-0.095
12.66	253.7	528.4987	510.4648	$[M+NH_4]^+$	DG O-29:1	$C_{32}H_{62}O_4$	926.9	0.34

15.22	242.9	520.4363	502.4025	$[M+NH_4]^+$	DG O-29:5	$C_{32}H_{54}O_4$	592.9	0.576
16.35	257.4	556.5306	538.4968	$[M+NH_4]^+$	DG O-31:1	$C_{34}H_{66}O_4$	1000	1.181
17.20	254	556.5293	538.496	$[M+NH_4]^+$, $[M+H]^+$	DG O-31:1	$C_{34}H_{66}O_4$	442.3	-1.115
11.30	258.2	554.5154	536.4816	$[M+NH_4]^+$	DG O-31:2	$C_{34}H_{64}O_4$	389.1	1.889
16.81	261.3	570.5473	552.5135	$[M+NH_4]^+$	DG O-32:1	$C_{35}H_{68}O_4$	277.0	3.032
15.93	249.2	560.4681	542.4343	$[M+NH_4]^+$	DG O-32:6	$C_{35}H_{58}O_4$	309.6	1.846
12.32	263.7	582.5455	564.5116	$[M+NH_4]^+$	DG O-33:2	$C_{36}H_{68}O_4$	537.1	-0.283
12.65	266.1	596.5611	578.5273	$[M+NH_4]^+$	DG O-34:2	$C_{37}H_{70}O_4$	476.0	-0.078
12.87	266.1	596.5611	578.5273	$[M+NH_4]^+$	DG O-34:2	$C_{37}H_{70}O_4$	467.2	0.348
19.74	268.5	614.6065	596.5727	$[M+NH_4]^+$	DG O-35:0	$C_{38}H_{76}O_4$	360.0	-2.414
20.13	265.9	612.5921	594.5582	$[M+NH_4]^+$	DG O-35:1	$C_{38}H_{74}O_4$	977.2	0.039
13.42	269	610.5769	592.543	$[M+NH_4]^+$	DG O-35:2	$C_{38}H_{72}O_4$	886.0	-0.049
13.55	268.5	610.5768	592.543	$[M+NH_4]^+$	DG O-35:2	$C_{38}H_{72}O_4$	901.4	-0.316
12.52	266.1	608.5615	590.5277	$[M+NH_4]^+$	DG O-35:3	$C_{38}H_{70}O_4$	409.6	0.357
13.76	271.2	624.5925	606.5587	$[M+NH_4]^+$	DG O-36:2	$C_{39}H_{74}O_4$	420.5	-0.258
13.98	271.1	624.5924	606.5586	$[M+NH_4]^+$	DG O-36:2	$C_{39}H_{74}O_4$	423.4	-0.255
14.52	273.7	638.609	620.5752	$[M+NH_4]^+$	DG O-37:2	$C_{40}H_{76}O_4$	512.7	1.27
14.36	273.8	638.6061	620.5723	$[M+NH_4]^+$	DG O-37:2	$C_{40}H_{76}O_4$	400.6	-4.533
14.68	273.7	638.608	620.5742	$[M+NH_4]^+$	DG O-37:2	$C_{40}H_{76}O_4$	539.6	0.168
13.59	271.5	636.593	618.5591	$[M+NH_4]^+$	DG O-37:3	$C_{40}H_{74}O_4$	480.6	0.46
13.81	271.9	636.5923	618.5585	$[M+NH_4]^+$	DG O-37:3	$C_{40}H_{74}O_4$	455.3	-0.627
20.67	274.5	654.6393	636.6055	$[M+NH_4]^+$	DG O-38:1	$C_{41}H_{80}O_4$	383.9	-0.287
14.83	275.8	652.6241	634.5903	$[M+NH_4]^+$	DG O-38:2	$C_{41}H_{78}O_4$	507.9	0.254
15.07	276	652.6243	634.5905	$[M+NH_4]^+$	DG O-38:2	$C_{41}H_{78}O_4$	481.1	0.519
15.6	278.5	666.6401	648.6063	$[M+NH_4]^+$	DG O-39:2	$C_{42}H_{80}O_4$	892.5	0.926
14.68	276.2	664.6243	646.5905	$[M+NH_4]^+$	DG O-39:3	$C_{42}H_{78}O_4$	476.1	0.559

14.89	276.5	664.6243	646.5905	$[M+NH_4]^+$	DG O-39:3	$C_{42}H_{78}O_4$	507.1	0.691
13.77	274.2	662.6086	644.5747	$[M+NH_4]^+$	DG O-39:4	$C_{42}H_{76}O_4$	954.8	1.058
13.97	274.3	662.6083	644.5745	$[M+NH_4]^+$	DG O-39:4	$C_{42}H_{76}O_4$	518.5	0.874
21.61	281.8	696.6856	678.6517	$[M+NH_4]^+$	DG O-41:1	$C_{44}H_{86}O_4$	274.2	-1.319
21.79	284	710.6995	692.6656	$[M+NH_4]^+$	DG O-42:1	$C_{45}H_{88}O_4$	269.1	-3.666
20.91	281.8	700.6271	682.5937	$[M+NH_4]^+$, $[M+H]^+$, $[M+H]^+$, $[M+NH_4]^+$	DG O-42:6	$C_{45}H_{78}O_4$	705.2	4.57
19.07	288.5	698.6077	680.5739	$[M+NH_4]^+$	DG O-42:7	$C_{45}H_{76}O_4$	469	-0.641
19.26	288.1	698.608	680.5742	$[M+NH_4]^+$	DG O-42:7	$C_{45}H_{76}O_4$	524.2	-0.979
18.15	287.8	698.6083	680.5754	$[M+NH_4]^+$, $[M+H-H_2O]^+$, $[M+Na]^+$, $[M+H]^+$	DG O-42:7	$C_{45}H_{76}O_4$	638.3	0.183
18.01	290.5	698.6078	680.574	$[M+NH_4]^+$	DG O-42:7	$C_{45}H_{76}O_4$	671.2	-0.558
17.32	286.7	698.6081	680.5742	$[M+NH_4]^+$	DG O-42:7	$C_{45}H_{76}O_4$	882.6	-0.275
18.21	291.1	696.5921	678.5585	$[M+NH_4]^+$, $[M+H]^+$	DG O-42:8	$C_{45}H_{74}O_4$	621.8	-0.737
18.70	289.1	696.5929	678.5591	$[M+NH_4]^+$	DG O-42:8	$C_{45}H_{74}O_4$	659.8	1.02
22.09	286.9	724.7163	706.6825	$[M+NH_4]^+$	DG O-43:1	$C_{46}H_{90}O_4$	448.8	-1.839
22.19	289	738.7326	720.6988	$[M+NH_4]^+$	DG O-44:1	$C_{47}H_{92}O_4$	462	-1.026
13.66	297.1	862.6255	861.6172	$[M+H]^+$, $[M+Na]^+$	Hex2Cer 18:1;2O/16:0	$C_{46}H_{87}NO_{13}$	505.5	0.324
14.12	278.4	700.5719	699.5646	$[M+H]^+$	HexCer 18:1;O2/16:0	$C_{40}H_{77}NO_8$	663.4	-1.189
8.06	256.7	676.4423	675.435	$[M+H]^+$	HexCer 18:3;O2/14:4;O	$C_{38}H_{61}NO_9$	317.1	0.574
7.50	232.2	482.3242	481.3169	$[M+H]^+$	LPC 15:0	$C_{23}H_{48}NO_7P$	373.9	-0.028
8.22	235	496.3397	495.3327	$[M+H]^+$, $[M+Na]^+$, $[M+H-H_2O]^+$	LPC 16:0	$C_{24}H_{50}NO_7P$	677.5	-0.162
7.65	231.3	494.3251	493.3178	$[M+H]^+$	LPC 16:1	$C_{24}H_{48}NO_7P$	365.2	1.953
7.28	231.5	494.3245	493.3172	$[M+H]^+$	LPC 16:1	$C_{24}H_{48}NO_7P$	937.6	0.587
8.73	238.3	510.3552	509.348	$[M+H]^+$	LPC 17:0	$C_{25}H_{52}NO_7P$	749.1	-0.309
8.58	238.1	510.3554	509.3481	$[M+H]^+$	LPC 17:0	$C_{25}H_{52}NO_7P$	1000	-0.05
7.94	233.8	508.3399	507.3326	$[M+H]^+$	LPC 17:1	$C_{25}H_{50}NO_7P$	1000	0.179
9.27	241.2	524.3714	523.3641	$[M+H]^+$, $[M+H-H_2O]^+$	LPC 18:0	$C_{26}H_{54}NO_7P$	652.2	0.736

8.42	236.9	522.3558	521.3486	$[M+H]^+$	LPC 18:1	$C_{26}H_{52}NO_7P$	638.5	0.818
8.61	237.7	522.3552	521.348	$[M+H]^+$	LPC 18:1	$C_{26}H_{52}NO_7P$	435	-0.337
7.81	232.2	520.3398	519.3325	$[M+H]^+$	LPC 18:2	$C_{26}H_{50}NO_7P$	584.8	0.226
7.62	233.8	520.3396	519.3324	$[M+H]^+$	LPC 18:2	$C_{26}H_{50}NO_7P$	929.9	-0.118
9.39	243.4	550.3868	549.3795	$[M+H]^+$	LPC 20:1	$C_{28}H_{56}NO_7P$	650.2	0.105
8.71	238.6	548.3709	547.3636	$[M+H]^+$	LPC 20:2	$C_{28}H_{54}NO_7P$	709.3	-0.367
7.98	237.1	546.3542	545.3469	$[M+H]^+$	LPC 20:3	$C_{28}H_{52}NO_7P$	881.4	-1.569
7.80	234.8	544.34	543.3327	$[M+H]^+$	LPC 20:4	$C_{28}H_{50}NO_7P$	537.5	0.099
7.62	236.1	544.3399	543.3327	$[M+H]^+$	LPC 20:4	$C_{28}H_{50}NO_7P$	947.1	0.069
7.14	233.0	542.3252	541.3179	$[M+H]^+$	LPC 20:5	$C_{28}H_{48}NO_7P$	865.1	2.313
8.37	242.3	572.3701	571.3628	$[M+H]^+$	LPC 22:4	$C_{30}H_{54}NO_7P$	890.3	-0.292
8.03	237.7	570.3554	569.3481	$[M+H]^+$	LPC 22:5	$C_{30}H_{52}NO_7P$	759.7	-0.107
7.76	236.8	568.3399	567.3326	$[M+H]^+$	LPC 22:6	$C_{30}H_{50}NO_7P$	997.3	0.211
7.59	238.7	568.3393	567.3321	$[M+H]^+$	LPC 22:6	$C_{30}H_{50}NO_7P$	988.9	-0.734
8.28	221	454.2933	453.2861	$[M+H]^+$	LPE 16:0	$C_{21}H_{44}NO_7P$	1000	1.076
9.32	227.8	482.3246	481.3173	$[M+H]^+$	LPE 18:0	$C_{23}H_{48}NO_7P$	538.3	0.903
8.5	222.2	480.3092	479.302	$[M+H]^+$	LPE 18:1	$C_{23}H_{46}NO_7P$	327	1.729
7.88	218	478.2936	477.2864	$[M+H]^+$	LPE 18:2	$C_{23}H_{44}NO_7P$	1000	0.626
7.71	219.2	478.2932	477.2859	$[M+H]^+$	LPE 18:2	$C_{23}H_{44}NO_7P$	808.6	0.977
7.87	220.9	502.2931	501.2858	$[M+H]^+$	LPE 20:4	$C_{25}H_{44}NO_7P$	496.6	0.447
7.72	222.2	502.2929	501.2856	$[M+H]^+$	LPE 20:4	$C_{25}H_{44}NO_7P$	852.2	0.171
7.84	224	526.2938	525.2865	$[M+H]^+$	LPE 22:6	$C_{27}H_{44}NO_7P$	858.2	1.409
15.87	288.2	786.6015	785.5942	$[M+H]^+$	PC 18:0_18:2	$C_{44}H_{84}NO_8P$	922.1	0.988
15.68	290.9	810.6015	809.5942	$[M+H]^+$	PC 18:0_20:4	$C_{46}H_{84}NO_8P$	944.4	1.036
16.64	290	788.616	787.6087	$[M+H]^+$	PC 18:1_18:0	$C_{44}H_{86}NO_8P$	947.1	-0.39
13.59	279.6	756.5539	755.5467	$[M+H]^+$	PC 18:2_16:1	$C_{42}H_{78}NO_8P$	886.1	0.338

13.56	290.3	854.5684	853.5611	$[M+H]^+$	PC 20:4_22:6	$C_{50}H_{80}NO_8P$	886	-1.31
15.05	289.3	808.5846	807.5773	$[M+H]^+$	PC 20:5_18:0	$C_{46}H_{82}NO_8P$	837.8	-0.519
14.05	276.9	706.5379	705.5307	$[M+H]^+$	PC 30:0	$C_{38}H_{76}NO_8P$	973.2	-0.589
14.43	279.3	720.5531	719.5458	$[M+H]^+$	PC 31:0	$C_{39}H_{78}NO_8P$	529.3	-1.78
15.30	282.4	734.5695	733.5623	$[M+H]^+$	PC 32:0	$C_{40}H_{80}NO_8P$	954.1	0.486
15.49	281.8	734.5693	733.562	$[M+H]^+$	PC 32:0	$C_{40}H_{80}NO_8P$	934.6	-0.534
14.29	279.2	732.5541	731.5468	$[M+H]^+$	PC 32:1	$C_{40}H_{78}NO_8P$	973.9	0.471
13.39	276.3	730.5379	729.5307	$[M+H]^+$	PC 32:2	$C_{40}H_{76}NO_8P$	959.3	-0.024
14.83	282.4	746.5698	745.5626	$[M+H]^+$	PC 33:1	$C_{41}H_{80}NO_8P$	905.2	0.604
14.49	279.0	744.5557	743.5485	$[M+H]^+$	PC 33:2	$C_{41}H_{78}NO_8P$	809.7	2.778
13.99	278.6	744.5538	743.5465	$[M+H]^+$	PC 33:2	$C_{41}H_{78}NO_8P$	1000	-0.077
16.55	287.8	762.6014	761.5941	$[M+H]^+$	PC 34:0	$C_{42}H_{84}NO_8P$	920.2	0.476
14.86	281.7	758.5706	757.5633	$[M+H]^+$	PC 34:2	$C_{42}H_{80}NO_8P$	962.9	1.694
13.33	278.9	754.5387	753.5314	$[M+H]^+$	PC 34:4	$C_{42}H_{76}NO_8P$	940.6	0.612
16.05	287.7	774.6001	773.5929	$[M+H]^+$	PC 35:1	$C_{43}H_{84}NO_8P$	967.3	-0.722
15.7	287.4	774.5996	773.5924	$[M+H]^+$	PC 35:1	$C_{43}H_{84}NO_8P$	744.9	-1.817
15.63	285.1	772.5866	771.5793	$[M+H]^+$	PC 35:2	$C_{43}H_{82}NO_8P$	493.9	2.081
14.99	284.7	772.5836	771.5763	$[M+H]^+$	PC 35:2	$C_{43}H_{82}NO_8P$	895.0	-0.314
14.13	282.2	770.5686	769.5613	$[M+H]^+$	PC 35:3	$C_{43}H_{80}NO_8P$	1000	-1.317
13.93	282.1	768.5538	767.5465	$[M+H]^+$	PC 35:4	$C_{43}H_{78}NO_8P$	1000	-0.051
14.98	286.6	784.5861	783.5788	$[M+H]^+$	PC 36:3	$C_{44}H_{82}NO_8P$	916.0	1.069
15.28	286.3	784.5849	783.5776	$[M+H]^+$	PC 36:3	$C_{44}H_{82}NO_8P$	854.8	-0.252
14.09	282.8	782.5685	781.5612	$[M+H]^+$	PC 36:4	$C_{44}H_{80}NO_8P$	895.6	-1.106
13.53	282.2	780.5532	779.5459	$[M+H]^+$	PC 36:5	$C_{44}H_{78}NO_8P$	970.9	-0.489
13.80	283.0	780.5534	779.5461	$[M+H]^+$	PC 36:5	$C_{44}H_{78}NO_8P$	963.0	-0.834
12.86	280.0	778.5376	777.5303	$[M+H]^+$	PC 36:6	$C_{44}H_{76}NO_8P$	946.1	-0.669

13.19	281.0	778.5385	777.5312	$[M+H]^+$	PC 36:6	$C_{44}H_{76}NO_8P$	1000	0.491
17.25	292.2	802.6319	801.6247	$[M+H]^+$	PC 37:1	$C_{45}H_{88}NO_8P$	858.6	0.107
16.43	290.1	800.6167	799.6094	$[M+H]^+$	PC 37:2	$C_{45}H_{86}NO_8P$	1000	-0.122
15.11	288.0	796.5844	795.5772	$[M+H]^+$	PC 37:4	$C_{45}H_{82}NO_8P$	880.7	-0.889
14.90	288.3	796.5842	795.5769	$[M+H]^+$	PC 37:4	$C_{45}H_{82}NO_8P$	1000	-1.04
14.43	285.4	794.5707	793.5634	$[M+H]^+$	PC 37:5	$C_{45}H_{80}NO_8P$	825.3	1.891
13.79	284.5	792.5548	791.5475	$[M+H]^+$	PC 37:6	$C_{45}H_{78}NO_8P$	1000	1.498
16.91	292.1	814.6296	813.6223	$[M+H]^+$	PC 38:2	$C_{46}H_{88}NO_8P$	968.2	-3.366
16.19	291.5	812.6166	811.6093	$[M+H]^+$	PC 38:3	$C_{46}H_{86}NO_8P$	953.1	0.344
16.46	291.3	812.6141	811.6068	$[M+H]^+$	PC 38:3	$C_{46}H_{86}NO_8P$	976.7	-2.109
15.9	291.2	810.6007	809.5934	$[M+H]^+$	PC 38:4	$C_{46}H_{84}NO_8P$	961.0	-0.137
15.35	290.5	810.5998	809.5925	$[M+H]^+$	PC 38:4	$C_{46}H_{84}NO_8P$	983.0	-1.213
14.67	289.1	808.585	807.5777	$[M+H]^+$	PC 38:5	$C_{46}H_{82}NO_8P$	791.7	-0.052
14.39	286.8	806.5703	805.5628	$[M+H]^+$, $[M+Na]^+$	PC 38:6	$C_{46}H_{80}NO_8P$	905.1	1.41
14.73	290.6	820.584	819.5767	$[M+H]^+$	PC 39:6	$C_{47}H_{82}NO_8P$	1000	-1.836
14.97	290.5	820.5861	819.5788	$[M+H]^+$	PC 39:6	$C_{47}H_{82}NO_8P$	546.8	1.293
17.35	295.9	840.6455	839.6382	$[M+H]^+$	PC 40:3	$C_{48}H_{90}NO_8P$	847.9	-2.811
16.89	294.8	838.63	837.6227	$[M+H]^+$	PC 40:4	$C_{48}H_{88}NO_8P$	960.9	-2.194
16.55	294.7	838.6313	837.6241	$[M+H]^+$	PC 40:4	$C_{48}H_{88}NO_8P$	985.4	-0.957
16.23	294.4	836.6155	835.6082	$[M+H]^+$	PC 40:5	$C_{48}H_{86}NO_8P$	1000	-0.63
15.89	293.5	836.6158	835.6086	$[M+H]^+$	PC 40:5	$C_{48}H_{86}NO_8P$	854.5	-0.66
15.56	292.6	834.6006	833.5934	$[M+H]^+$	PC 40:6	$C_{48}H_{84}NO_8P$	976.8	-0.056
14.47	290.6	832.5845	831.5772	$[M+H]^+$	PC 40:7	$C_{48}H_{82}NO_8P$	1000	-0.251
14.69	291.3	832.5848	831.5775	$[M+H]^+$	PC 40:7	$C_{48}H_{82}NO_8P$	1000	-0.187
15.04	291.4	832.5843	831.577	$[M+H]^+$	PC 40:7	$C_{48}H_{82}NO_8P$	1000	-0.923
13.70	288.0	830.5684	829.5611	$[M+H]^+$	PC 40:8	$C_{48}H_{80}NO_8P$	609.5	-0.958

7.86	239.5	570.3542	569.347	$[M+H]^+$	PC O-22:5	$C_{30}H_{52}NO_7P$	996.7	-2.558
16.18	283.6	720.5884	719.5811	$[M+H]^+$	PC O-32:0	$C_{40}H_{82}NO_7P$	875.0	-2.431
16.00	281.2	718.5747	717.5674	$[M+H]^+$	PC O-32:1	$C_{40}H_{80}NO_7P$	1000	0.123
15.10	280.7	718.5755	717.5682	$[M+H]^+$	PC O-32:1	$C_{40}H_{80}NO_7P$	601.1	1.952
14.95	278.5	716.5608	715.5535	$[M+H]^+$	PC O-32:2	$C_{40}H_{78}NO_7P$	956.3	2.906
18.89	292.6	746.6103	745.603	$[M+H]^+$	PC O-34:1	$C_{42}H_{84}NO_7P$	980.2	4.319
16.09	284.1	744.5893	743.582	$[M+H]^+$	PC O-34:2	$C_{42}H_{82}NO_7P$	797.7	-1.047
15.26	280.7	742.5745	741.5672	$[M+H]^+$	PC O-34:3	$C_{42}H_{80}NO_7P$	1000	-0.098
16.65	288.8	772.6205	771.6132	$[M+H]^+$	PC O-36:2	$C_{44}H_{86}NO_7P$	929.4	-1.712
16.46	287.1	770.6044	769.5971	$[M+H]^+$	PC O-36:3	$C_{44}H_{84}NO_7P$	1000	-1.952
15.3	286.4	768.5895	767.5822	$[M+H]^+$	PC O-36:4	$C_{44}H_{82}NO_7P$	940	-0.845
14.61	286.5	766.5755	765.5682	$[M+H]^+$	PC O-36:5	$C_{44}H_{80}NO_7P$	1000	1.37
14.93	283.8	766.5736	765.5663	$[M+H]^+$	PC O-36:5	$C_{44}H_{80}NO_7P$	1000	-1.101
15.11	283.7	766.5743	765.5671	$[M+H]^+$	PC O-36:5	$C_{44}H_{80}NO_7P$	437.0	-0.281
14.42	281.4	764.5587	763.5514	$[M+H]^+$	PC O-36:6	$C_{44}H_{78}NO_7P$	739.9	-0.781
15.46	288.4	780.5905	779.5833	$[M+H]^+$	PC O-37:5	$C_{45}H_{82}NO_7P$	464.0	0.464
15.26	278.5	774.5428	773.5355	$[M+H]^+$	PC O-37:8	$C_{45}H_{76}NO_7P$	570.3	-0.043
17.03	292	798.6364	797.6291	$[M+H]^+$	PC O-38:3	$C_{46}H_{88}NO_7P$	842.3	-0.792
16.32	289.6	794.6053	793.598	$[M+H]^+$	PC O-38:5	$C_{46}H_{84}NO_7P$	990.0	-0.549
15.59	290.1	794.605	793.5978	$[M+H]^+$	PC O-38:5	$C_{46}H_{84}NO_7P$	978.3	-1.032
15.96	290.1	794.6056	793.5983	$[M+H]^+$	PC O-38:5	$C_{46}H_{84}NO_7P$	579.9	-0.494
15.20	288.0	792.5892	791.5819	$[M+H]^+$	PC O-38:6	$C_{46}H_{82}NO_7P$	1000	-1.109
14.92	287.5	790.5741	789.5668	$[M+H]^+$	PC O-38:7	$C_{46}H_{80}NO_7P$	560.7	-0.735
17.69	296.2	824.6529	823.6457	$[M+H]^+$	PC O-40:4	$C_{48}H_{90}NO_7P$	892.1	0.185
17.36	295.6	824.6509	823.6436	$[M+H]^+$	PC O-40:4	$C_{48}H_{90}NO_7P$	844.6	-2.204
16.48	294.3	822.636	821.6287	$[M+H]^+$	PC O-40:5	$C_{48}H_{88}NO_7P$	971.5	-1.227

15.62	292.5	820.6193	819.612	$[M+H]^+$	PC O-40:6	$C_{48}H_{86}NO_7P$	1000	-2.635
17.6	299.4	850.6683	849.661	$[M+H]^+$	PC O-42:5	$C_{50}H_{92}NO_7P$	196.7	-0.008
16.72	296.9	848.6516	847.6443	$[M+H]^+$	PC O-42:6	$C_{50}H_{90}NO_7P$	1000	-1.499
19.97	305.5	880.7187	879.7114	$[M+H]^+$	PC O-44:4	$C_{52}H_{98}NO_7P$	151.0	4.185
18.72	303.4	878.6996	877.6924	$[M+H]^+$	PC O-44:5	$C_{52}H_{96}NO_7P$	231.2	-0.085
17.82	301.6	876.6837	875.6764	$[M+H]^+$	PC O-44:6	$C_{52}H_{94}NO_7P$	796.2	0.074
18.46	301.9	876.6839	875.6766	$[M+H]^+$	PC O-44:6	$C_{52}H_{94}NO_7P$	525.2	-0.171
15.33	273.9	718.5337	717.5264	$[M+H]^+$	PE 21:0_13:1	$C_{39}H_{76}NO_8P$	836.4	-5.716
14.59	271.6	716.5232	715.5159	$[M+H]^+$	PE 34:2	$C_{39}H_{74}NO_8P$	930.4	0.686
16.41	279.4	746.5699	745.5626	$[M+H]^+$	PE 36:1	$C_{41}H_{80}NO_8P$	775.0	0.598
15.46	276.5	744.5547	743.5475	$[M+H]^+$	PE 36:2	$C_{41}H_{78}NO_8P$	1000	1.142
15.67	278.1	744.5539	743.5466	$[M+H]^+$	PE 36:2	$C_{41}H_{78}NO_8P$	529.4	0.139
14.90	274.8	742.5388	741.5315	$[M+H]^+$	PE 36:3	$C_{41}H_{76}NO_8P$	814.3	1.065
14.71	274.5	742.5384	741.5312	$[M+H]^+$	PE 36:3	$C_{41}H_{76}NO_8P$	446.8	0.544
14.53	275.1	740.5229	739.5157	$[M+H]^+$	PE 36:4	$C_{41}H_{74}NO_8P$	850.2	0.65
13.95	271.5	740.5219	739.5146	$[M+H]^+$	PE 36:4	$C_{41}H_{74}NO_8P$	951.1	-0.738
15.64	280.4	768.5541	767.5468	$[M+H]^+$	PE 38:4	$C_{43}H_{78}NO_8P$	679.8	0.281
14.67	276.9	766.5383	765.5311	$[M+H]^+$	PE 38:5	$C_{43}H_{76}NO_8P$	872.5	0.251
15.03	278.1	766.5386	765.5313	$[M+H]^+$	PE 38:5	$C_{43}H_{76}NO_8P$	869.3	0.243
14.40	276.7	764.522	763.5147	$[M+H]^+$	PE 38:6	$C_{43}H_{74}NO_8P$	1000	-0.848
13.88	274.5	764.5232	763.5159	$[M+H]^+$	PE 38:6	$C_{43}H_{74}NO_8P$	388.9	0.459
15.50	281.8	792.554	791.5467	$[M+H]^+$	PE 40:6	$C_{45}H_{78}NO_8P$	647.9	0.278
8.31	224.5	480.3117	479.3044	$[M+H]^+$	PE O-15:1_3:0	$C_{23}H_{46}NO_7P$	797.3	7.216
14.94	275.2	748.5278	747.5205	$[M+H]^+$	PE O-16:1_22:6	$C_{43}H_{74}NO_7P$	942.1	0.29
15.15	269.5	700.5282	699.5209	$[M+H]^+$	PE O-34:3	$C_{39}H_{74}NO_7P$	785.7	0.614
16.97	278.4	730.5774	729.5701	$[M+H]^+$	PE O-36:2	$C_{41}H_{80}NO_7P$	409.0	4.184

16.04	276.6	728.5594	727.5521	$[M+H]^+$	PE O-36:3	$C_{41}H_{78}NO_7P$	876.8	0.733
15.28	273.5	726.5429	725.5357	$[M+H]^+$	PE O-36:4	$C_{41}H_{76}NO_7P$	971.1	-0.584
15.50	273.6	726.5447	725.5375	$[M+H]^+$	PE O-36:4	$C_{41}H_{76}NO_7P$	400.0	1.677
15.11	272.5	724.5276	723.5204	$[M+H]^+$	PE O-36:5	$C_{41}H_{74}NO_7P$	633.2	0.153
14.45	270.9	722.5132	721.5059	$[M+H]^+$	PE O-36:6	$C_{41}H_{72}NO_7P$	1000	1.733
19.68	280.1	746.6071	745.5998	$[M+H]^+$	PE O-37:1	$C_{42}H_{84}NO_7P$	262.1	1.672
15.64	275	738.5436	737.5363	$[M+H]^+$	PE O-37:5	$C_{42}H_{76}NO_7P$	1000	0.88
16.19	278.4	752.5584	751.5511	$[M+H]^+$	PE O-38:5	$C_{43}H_{78}NO_7P$	617.2	-0.237
15.57	276.6	750.5445	749.5372	$[M+H]^+$	PE O-38:6	$C_{43}H_{76}NO_7P$	812.5	1.274
15.24	275.7	750.5432	749.5359	$[M+H]^+$	PE O-38:6	$C_{43}H_{76}NO_7P$	731.3	-0.036
16.31	282.4	778.5743	777.5671	$[M+H]^+$	PE O-40:6	$C_{45}H_{80}NO_7P$	670.5	0.558
16.61	282.8	778.5729	777.5656	$[M+H]^+$	PE O-40:6	$C_{45}H_{80}NO_7P$	177.1	-1.803
12.65	276.6	675.5438	674.5365	$[M+H]^+$	SM 16:1;O2/16:0	$C_{37}H_{75}N_2O_6P$	968.7	0.28
13.87	281.7	703.5762	702.5674	$[M+H]^+$, $[M+H]^+$, $[M+Na]^+$, $[M+H]^+$	SM 18:1;O2/16:0	$C_{39}H_{79}N_2O_6P$	954.9	1.957
14.09	281.2	703.5747	702.5674	$[M+H]^+$	SM 18:1;O2/16:0	$C_{39}H_{79}N_2O_6P$	951.5	-0.034
16.46	291.6	759.6371	758.6298	$[M+H]^+$	SM 18:1;O2/20:0	$C_{43}H_{87}N_2O_6P$	921.1	-0.466
17.66	295.6	787.6691	786.6617	$[M+H]^+$, $[M+Na]^+$	SM 18:1;O2/22:0	$C_{45}H_{91}N_2O_6P$	949.9	0.534
17.55	297.9	813.6848	812.6775	$[M+H]^+$	SM 18:1;O2/24:1	$C_{47}H_{93}N_2O_6P$	870.9	0.584
12.91	278.6	701.5599	700.5526	$[M+H]^+$	SM 18:2;O2/16:0	$C_{39}H_{77}N_2O_6P$	958.5	1.064
11.46	272	647.5117	646.5044	$[M+H]^+$	SM 30:1;O2	$C_{35}H_{71}N_2O_6P$	978.3	-0.823
10.57	265.1	671.4727	670.4655	$[M+H]^+$	SM 31:4;O3	$C_{36}H_{67}N_2O_7P$	166.3	-4.624
13.12	279.5	677.5579	676.5507	$[M+H]^+$	SM 32:0;O2	$C_{37}H_{77}N_2O_6P$	1000	-1.585
15.49	290	745.6256	744.6183	$[M+H]^+$	SM 33:1;2O/4:0	$C_{42}H_{85}N_2O_6P$	999.9	4.168
13.04	279.4	689.559	688.5517	$[M+H]^+$	SM 33:1;O2	$C_{38}H_{77}N_2O_6P$	644.8	0.016
13.26	278.9	689.5594	688.5521	$[M+H]^+$	SM 33:1;O2	$C_{38}H_{77}N_2O_6P$	994.4	0.175
14.4	283.7	705.5893	704.584	$[M+H]^+$, $[M+Na]^+$	SM 34:0;O2	$C_{39}H_{81}N_2O_6P$	947.7	-1.812

14.42	281	703.5745	702.5672	$[M+H]^+$	SM 34:1;O2	$C_{39}H_{79}N_2O_6P$	971.2	-0.126
13.39	287.2	719.5702	718.563	$[M+H]^+$	SM 34:1;O3	$C_{39}H_{79}N_2O_7P$	1000	0.897
13.55	278.5	701.5596	700.5523	$[M+H]^+$	SM 34:2;O2	$C_{39}H_{77}N_2O_6P$	1000	0.243
14.54	286.1	717.5903	716.583	$[M+H]^+$	SM 35:1;O2	$C_{40}H_{81}N_2O_6P$	1000	-0.442
15.64	289.3	733.6202	732.6129	$[M+H]^+$	SM 36:0;O2	$C_{41}H_{85}N_2O_6P$	783.2	-1.959
15.17	287	731.6056	730.5983	$[M+H]^+$	SM 36:1;O2	$C_{41}H_{83}N_2O_6P$	842.7	-0.793
14.38	283.7	729.5902	728.5829	$[M+H]^+$	SM 36:2;O2	$C_{41}H_{81}N_2O_6P$	1000	-0.644
14.13	283.6	729.5897	728.5807	$[M+H]^+$, $[M+Na]^+$	SM 36:2;O2	$C_{41}H_{81}N_2O_6P$	958.8	-0.665
13.34	281.8	727.5748	726.5676	$[M+H]^+$	SM 36:3;O2	$C_{41}H_{79}N_2O_6P$	989.2	0.071
15.89	290.3	745.6219	744.6146	$[M+H]^+$	SM 37:1;O2	$C_{42}H_{85}N_2O_6P$	845.1	-0.097
16.70	291.7	759.6363	758.6291	$[M+H]^+$	SM 38:1;O2	$C_{43}H_{87}N_2O_6P$	985.2	-1.591
15.68	288.9	757.6202	756.6129	$[M+H]^+$	SM 38:2;O2	$C_{43}H_{85}N_2O_6P$	976.1	-2.498
15.12	288.2	753.5875	752.5802	$[M+H]^+$	SM 38:4;O2	$C_{43}H_{81}N_2O_6P$	987.1	-3.4
17.10	293.6	773.6529	772.6456	$[M+H]^+$	SM 39:1;O2	$C_{44}H_{89}N_2O_6P$	955.5	-0.317
16.74	293.6	773.6548	772.6475	$[M+H]^+$	SM 39:1;O2	$C_{44}H_{89}N_2O_6P$	1000	1.659
16.06	292.1	771.6378	770.6305	$[M+H]^+$	SM 39:2;O2	$C_{44}H_{87}N_2O_6P$	1000	0.128
16.38	293.9	785.6522	784.6449	$[M+H]^+$	SM 40:2;O2	$C_{45}H_{89}N_2O_6P$	970.3	-1.067
16.66	294	785.6527	784.6455	$[M+H]^+$	SM 40:2;O2	$C_{45}H_{89}N_2O_6P$	887.9	-0.815
15.48	292.2	783.6371	782.6298	$[M+H]^+$	SM 40:3;O2	$C_{45}H_{87}N_2O_6P$	99.03	-1.007
18.29	297.9	801.6841	800.6788	$[M+H]^+$, $[M+Na]^+$	SM 41:1;O2	$C_{46}H_{93}N_2O_6P$	972.5	-0.495
17.29	295.8	799.6686	798.6613	$[M+H]^+$	SM 41:2;O2	$C_{46}H_{91}N_2O_6P$	965.0	-0.367
16.96	295.8	799.668	798.6608	$[M+H]^+$	SM 41:2;O2	$C_{46}H_{91}N_2O_6P$	914.8	-0.9
16.06	294.2	797.6535	796.6462	$[M+H]^+$	SM 41:3;O2	$C_{46}H_{89}N_2O_6P$	989.1	0.36
19.28	300	815.6983	814.691	$[M+H]^+$	SM 42:1;O2	$C_{47}H_{95}N_2O_6P$	957.6	-2.281
18.88	300.3	815.7001	814.6924	$[M+H]^+$, $[M+Na]^+$	SM 42:1;O2	$C_{47}H_{95}N_2O_6P$	932.8	-0.199
16.91	300.5	831.6911	830.6838	$[M+H]^+$	SM 42:1;O3	$C_{47}H_{95}N_2O_7P$	1000	-4.531

16.58	296.3	811.6687	810.6606	$[M+H]^+$, $[M+Na]^+$	SM 42:3;O2	$C_{47}H_{91}N_2O_6P$	945.3	0.036
15.95	295	809.6522	808.645	$[M+H]^+$	SM 42:4;O2	$C_{47}H_{89}N_2O_6P$	1000	-1.101
15.67	294.9	809.6526	808.6454	$[M+H]^+$	SM 42:4;O2	$C_{47}H_{89}N_2O_6P$	981.0	-0.364
19.53	302.3	829.7133	828.706	$[M+H]^+$	SM 43:1;O2	$C_{48}H_{97}N_2O_6P$	734.7	-2.794
17.17	298.4	825.6848	824.6776	$[M+H]^+$	SM 43:3;O2	$C_{48}H_{93}N_2O_6P$	599.4	0.518
20.40	294.5	778.6908	760.6559	$[M+NH_4]^+$, $[M+Na]^+$	TG 13:0_16:1_16:1	$C_{48}H_{88}O_6$	793.7	-1.45
20.76	293	754.6917	736.6577	$[M+NH_4]^+$, $[M+Na]^+$	TG 14:0_14:0_15:0	$C_{46}H_{88}O_6$	840.8	-0.292
21.03	295.2	768.708	750.674	$[M+NH_4]^+$, $[M+NH_4]^+$, $[M+Na]^+$	TG 14:0_14:0_16:0	$C_{47}H_{90}O_6$	925.8	0.533
20.55	293.7	766.6917	748.6578	$[M+NH_4]^+$, $[M+Na]^+$, $[M+NH_4]^+$	TG 14:0_14:0_16:1	$C_{47}H_{88}O_6$	796.1	-0.266
20.09	292.1	764.6751	746.6421	$[M+NH_4]^+$, $[M+Na]^+$	TG 14:0_14:1_16:1	$C_{47}H_{86}O_6$	843.5	-1.498
21.55	299.7	796.7389	778.705	$[M+NH_4]^+$	TG 14:0_16:0_16:0	$C_{49}H_{94}O_6$	680.1	0.024
23.01	318.8	908.8631	890.8292	$[M+NH_4]^+$	TG 14:0_16:0_24:0	$C_{57}H_{110}O_6$	529.2	-0.796
21.56	304	822.7541	804.7203	$[M+NH_4]^+$	TG 14:0_18:1_16:0	$C_{51}H_{96}O_6$	892.1	-0.347
20.67	299.7	818.7231	800.6893	$[M+NH_4]^+$	TG 14:0_18:2_16:1	$C_{51}H_{92}O_6$	491.9	-0.156
22.92	316.8	894.848	876.8142	$[M+NH_4]^+$	TG 14:0_24:0_15:0	$C_{56}H_{108}O_6$	379.9	-0.447
19.90	292.5	776.6778	758.6441	$[M+NH_4]^+$, $[M+Na]^+$	TG 14:1_15:1_16:1	$C_{48}H_{86}O_6$	887.1	2.01
20.64	296.7	792.7075	774.6737	$[M+NH_4]^+$	TG 14:1_16:1_16:0	$C_{49}H_{90}O_6$	538.6	0.114
21.78	302.7	810.7547	792.7209	$[M+NH_4]^+$	TG 15:0_16:0_16:0	$C_{50}H_{96}O_6$	778.4	0.417
21.38	301.2	808.7385	790.7047	$[M+NH_4]^+$	TG 15:0_16:0_16:1	$C_{50}H_{94}O_6$	663.7	-0.406
21.41	306.9	860.7698	842.7363	$[M+NH_4]^+$, $[M+Na]^+$	TG 15:0_18:1_18:2	$C_{54}H_{98}O_6$	604.3	-0.471
20.97	302.7	832.7388	814.7038	$[M+NH_4]^+$, $[M+Na]^+$	TG 15:1_18:1_16:1	$C_{52}H_{94}O_6$	461.3	0.134
21.41	299.8	796.7386	778.7048	$[M+NH_4]^+$	TG 16:0_15:0_15:0	$C_{49}H_{94}O_6$	673.0	0.082
23.21	321.2	922.8796	904.8458	$[M+NH_4]^+$	TG 16:0_15:0_24:0	$C_{58}H_{112}O_6$	531.3	-0.087
21.67	302	810.7543	792.7205	$[M+NH_4]^+$	TG 16:0_16:0_15:0	$C_{50}H_{96}O_6$	705.8	-0.232
21.77	307.2	848.7686	830.7348	$[M+NH_4]^+$	TG 16:0_16:0_18:2	$C_{53}H_{98}O_6$	664.2	-1.29
22.20	310.6	864.8012	846.7674	$[M+NH_4]^+$	TG 16:0_17:0_18:1	$C_{54}H_{102}O_6$	69.06	-0.289

23.74	327.6	964.927	946.8931	$[M+NH_4]^+$	TG 16:0_17:0_25:0	$C_{61}H_{118}O_6$	458.3	0.264
22.40	312.7	878.8166	860.7827	$[M+NH_4]^+$	TG 16:0_18:1_18:0	$C_{55}H_{104}O_6$	852.7	-0.603
23.52	328.3	976.927	958.8932	$[M+NH_4]^+$	TG 16:0_18:1_25:0	$C_{62}H_{118}O_6$	392.2	0.646
21.25	307.8	872.771	854.7372	$[M+NH_4]^+$	TG 16:0_18:2_18:2	$C_{55}H_{98}O_6$	774.3	1.031
23.22	323.9	948.8955	930.8617	$[M+NH_4]^+$	TG 16:0_25:0_16:1	$C_{60}H_{114}O_6$	407.1	0.258
21.06	298.4	794.7237	776.6899	$[M+NH_4]^+$	TG 16:1_14:0_16:0	$C_{49}H_{92}O_6$	562.6	0.618
20.50	297.9	804.7069	786.6731	$[M+NH_4]^+$	TG 16:1_14:1_17:1	$C_{50}H_{90}O_6$	531.9	-0.933
20.96	299.6	806.7229	788.6891	$[M+NH_4]^+$	TG 16:1_15:1_16:0	$C_{50}H_{92}O_6$	434.9	-0.347
20.2	294.9	790.6909	772.6574	$[M+NH_4]^+$, $[M+Na]^+$	TG 16:1_16:1_14:1	$C_{49}H_{88}O_6$	527.0	-1.543
20.75	302.6	844.7387	826.7048	$[M+NH_4]^+$, $[M+Na]^+$	TG 16:1_16:1_18:2	$C_{53}H_{94}O_6$	670.2	0.294
21.40	304.3	834.754	816.7201	$[M+NH_4]^+$, $[M+Na]^+$	TG 16:1_18:1_15:0	$C_{52}H_{96}O_6$	524.6	-0.506
20.62	305.3	868.7387	850.7048	$[M+NH_4]^+$	TG 16:1_18:3_18:2	$C_{55}H_{94}O_6$	649.2	-0.192
23.11	322.2	934.8798	916.846	$[M+NH_4]^+$	TG 16:1_24:0_16:0	$C_{59}H_{112}O_6$	429.1	0.324
20.99	304.1	844.7394	826.7056	$[M+NH_4]^+$	TG 16:2_18:2_16:0	$C_{53}H_{94}O_6$	388.7	-0.2
22.59	320.7	944.863	926.8292	$[M+NH_4]^+$	TG 16:2_23:0_18:1	$C_{60}H_{110}O_6$	312.2	-1.174
21.82	304.4	824.7696	806.7358	$[M+NH_4]^+$	TG 17:0_15:0_16:0	$C_{51}H_{98}O_6$	852.0	-0.516
23.5	325.2	950.9111	932.8772	$[M+NH_4]^+$	TG 17:0_16:0_24:0	$C_{60}H_{116}O_6$	480.9	-0.007
23.8	329.4	978.9426	960.9087	$[M+NH_4]^+$	TG 17:0_16:0_26:0	$C_{62}H_{120}O_6$	437.5	0.124
22.6	312.2	866.8167	848.7829	$[M+NH_4]^+$	TG 17:0_18:0_16:0	$C_{54}H_{104}O_6$	524.5	-0.454
22.18	313.5	890.8169	872.783	$[M+NH_4]^+$	TG 17:0_18:1_18:1	$C_{56}H_{104}O_6$	690.9	-0.245
21.01	305.1	858.7547	840.7208	$[M+NH_4]^+$	TG 17:1_18:2_16:1	$C_{54}H_{96}O_6$	678.2	0.175
22.02	304.8	824.7703	806.7364	$[M+NH_4]^+$	TG 18:0_16:0_14:0	$C_{51}H_{98}O_6$	824.6	0.122
22.21	307.3	838.7856	820.7517	$[M+NH_4]^+$	TG 18:0_16:0_15:0	$C_{52}H_{100}O_6$	680.8	-0.338
22.43	309.7	852.8009	834.7671	$[M+NH_4]^+$	TG 18:0_16:0_16:0	$C_{53}H_{102}O_6$	696.6	-0.541
23.13	319.5	908.8641	890.8303	$[M+NH_4]^+$	TG 18:0_16:0_20:0	$C_{57}H_{110}O_6$	552.7	0.164
22.79	314.6	880.8329	862.8001	$[M+NH_4]^+$, $[M+Na]^+$	TG 18:0_18:0_16:0	$C_{55}H_{106}O_6$	775.4	0.175

22.91	314.1	880.8296	862.7958	$[M+NH_4]^+$	TG 18:0_18:0_16:0	$C_{55}H_{106}O_6$	750.1	-3.936
22.76	318.3	906.8488	888.815	$[M+NH_4]^+$	TG 18:0_18:0_18:1	$C_{57}H_{108}O_6$	562.7	0.41
22.06	314.5	902.8172	884.7834	$[M+NH_4]^+$	TG 18:0_18:2_18:1	$C_{57}H_{104}O_6$	834.6	0.156
21.78	306	836.7701	818.7362	$[M+NH_4]^+$	TG 18:1_15:0_16:0	$C_{52}H_{98}O_6$	597.3	-0.104
21.67	305.3	836.7687	818.7348	$[M+NH_4]^+$	TG 18:1_16:0_15:0	$C_{52}H_{98}O_6$	602.0	-2.242
22.01	308.2	850.7859	832.7521	$[M+NH_4]^+$	TG 18:1_16:0_16:0	$C_{53}H_{100}O_6$	927.5	0.192
21.78	308.7	862.7855	844.7517	$[M+NH_4]^+$	TG 18:1_16:0_17:1	$C_{54}H_{100}O_6$	753.6	-0.361
21.63	310.4	874.7854	856.7516	$[M+NH_4]^+$	TG 18:1_16:0_18:2	$C_{55}H_{100}O_6$	902.6	-0.818
21.10	301.4	820.7395	802.7056	$[M+NH_4]^+$	TG 18:1_16:1_14:0	$C_{51}H_{94}O_6$	753.9	0.769
21.56	307.2	848.7707	830.7369	$[M+NH_4]^+$	TG 18:1_16:1_16:0	$C_{53}H_{98}O_6$	845.3	0.369
22.79	323.1	958.8797	940.8459	$[M+NH_4]^+$	TG 18:1_16:1_24:1	$C_{61}H_{112}O_6$	387.3	-0.1
22.73	320.9	932.864	914.8301	$[M+NH_4]^+$	TG 18:1_18:0_20:1	$C_{59}H_{110}O_6$	468.7	-0.096
22.00	311.4	876.8022	858.7684	$[M+NH_4]^+$	TG 18:1_18:1_16:0	$C_{55}H_{102}O_6$	913.1	0.848
21.82	311.7	888.8013	870.7675	$[M+NH_4]^+$	TG 18:1_18:1_17:1	$C_{56}H_{102}O_6$	745.5	-0.246
21.39	318.5	948.8034	930.7695	$[M+NH_4]^+$	TG 18:1_18:1_22:6	$C_{61}H_{102}O_6$	353.3	1.927
22.37	315.5	904.8324	886.7985	$[M+NH_4]^+$	TG 18:1_20:1_16:0	$C_{57}H_{106}O_6$	725.4	-0.443
23.71	330.4	990.9437	972.9098	$[M+NH_4]^+$	TG 18:1_26:0_16:0	$C_{63}H_{120}O_6$	398.8	1.406
21.17	304.9	846.7551	828.7213	$[M+NH_4]^+$	TG 18:2_14:0_18:1	$C_{53}H_{96}O_6$	591.3	0.724
20.60	301.3	830.7228	812.6889	$[M+NH_4]^+$	TG 18:2_15:1_16:1	$C_{52}H_{92}O_6$	612.9	-0.759
20.22	297.0	816.7049	798.6711	$[M+NH_4]^+$	TG 18:2_16:1_14:1	$C_{51}H_{90}O_6$	263.7	-3.851
21.31	304.8	846.754	828.7201	$[M+NH_4]^+$	TG 18:2_16:1_16:0	$C_{53}H_{96}O_6$	495.9	-0.262
21.41	310.3	886.7852	868.7514	$[M+NH_4]^+$	TG 18:2_17:1_18:1	$C_{56}H_{100}O_6$	483.9	-0.934
21.63	313.8	900.8012	882.7673	$[M+NH_4]^+$	TG 18:2_18:1_18:1	$C_{57}H_{102}O_6$	854.1	-0.33
22.12	317.6	928.8322	910.7983	$[M+NH_4]^+$	TG 18:2_18:1_20:1	$C_{59}H_{106}O_6$	633.9	-0.572
20.9	306.3	870.7542	852.7204	$[M+NH_4]^+$	TG 18:2_18:2_16:1	$C_{55}H_{96}O_6$	690.5	-0.05
21.26	311.6	898.7858	880.7519	$[M+NH_4]^+$	TG 18:2_18:2_18:1	$C_{57}H_{100}O_6$	792.6	0.01

20.51	307.2	894.7535	876.7207	$[M+NH_4]^+$, $[M+Na]^+$	TG 18:2_18:2_18:3	$C_{57}H_{96}O_6$	810.5	-1.093
20.77	311.8	920.7713	902.7375	$[M+NH_4]^+$	TG 18:2_18:2_20:4	$C_{59}H_{98}O_6$	599.8	0.921
20.43	310.4	918.7541	900.7203	$[M+NH_4]^+$	TG 18:2_18:3_20:4	$C_{59}H_{96}O_6$	300.9	-0.428
20.64	314.2	944.7695	926.7357	$[M+NH_4]^+$	TG 18:2_20:4_20:4	$C_{61}H_{98}O_6$	466.4	-0.704
22.74	325.8	984.8945	966.8607	$[M+NH_4]^+$	TG 18:2_22:1_20:1	$C_{63}H_{114}O_6$	576.7	-1.369
21.00	313.5	920.7702	902.7364	$[M+NH_4]^+$	TG 18:2_22:6_16:0	$C_{59}H_{98}O_6$	627.6	0.015
20.37	301	842.7234	824.6896	$[M+NH_4]^+$	TG 18:3_14:0_18:2	$C_{53}H_{92}O_6$	491.9	-0.506
20.91	300.9	818.7215	800.6877	$[M+NH_4]^+$	TG 18:3_16:0_14:0	$C_{51}H_{92}O_6$	355.0	-2.122
20.88	309.4	896.7702	878.7356	$[M+NH_4]^+$, $[M+Na]^+$	TG 18:3_18:1_18:2	$C_{57}H_{98}O_6$	812.9	-0.021
21.14	311.1	896.7694	878.7356	$[M+NH_4]^+$	TG 18:3_18:2_18:1	$C_{57}H_{98}O_6$	589.7	-0.535
22.21	316.6	916.8328	898.799	$[M+NH_4]^+$	TG 19:1_18:1_18:1	$C_{58}H_{106}O_6$	633.9	-0.09
22.47	318.9	930.8483	912.8145	$[M+NH_4]^+$	TG 20:2_18:0_18:1	$C_{59}H_{108}O_6$	387.7	0.588
21.16	313.8	922.7847	904.7508	$[M+NH_4]^+$	TG 20:4_18:2_18:1	$C_{59}H_{100}O_6$	556.7	-0.809
23.08	324.6	960.8957	942.8618	$[M+NH_4]^+$	TG 22:0_18:1_18:1	$C_{61}H_{114}O_6$	389.4	0.296
21.82	317.1	926.8166	908.7828	$[M+NH_4]^+$	TG 22:4_18:1_16:0	$C_{59}H_{104}O_6$	489.1	-0.802
21.02	316.6	946.7863	928.7525	$[M+NH_4]^+$	TG 22:6_18:1_18:2	$C_{61}H_{100}O_6$	482.5	0.551
22.96	322.3	946.8789	928.8451	$[M+NH_4]^+$	TG 23:0_18:1_16:1	$C_{60}H_{112}O_6$	317.8	-0.541
23.43	323.5	936.8955	918.8617	$[M+NH_4]^+$	TG 24:0_16:0_16:0	$C_{59}H_{114}O_6$	515.9	0.17
22.95	319.7	920.8638	902.83	$[M+NH_4]^+$	TG 24:0_16:1_15:0	$C_{58}H_{110}O_6$	401.8	-0.184
22.58	318.4	918.8487	900.8148	$[M+NH_4]^+$	TG 24:0_16:1_15:1	$C_{58}H_{108}O_6$	399.4	0.339
23.42	326.2	962.9114	944.8776	$[M+NH_4]^+$	TG 24:0_18:1_16:0	$C_{61}H_{116}O_6$	385.6	0.422
23.10	327.1	986.9122	968.8784	$[M+NH_4]^+$	TG 24:0_18:2_18:1	$C_{63}H_{116}O_6$	525.4	1.197

7.5. Supporting information for Chapter VI: "Untargeted Lipidomics Analysis Reveals Specific Lipid Profiles in Hospitalized Covid-19 patients predictive for Severity and Mortality Outcome"

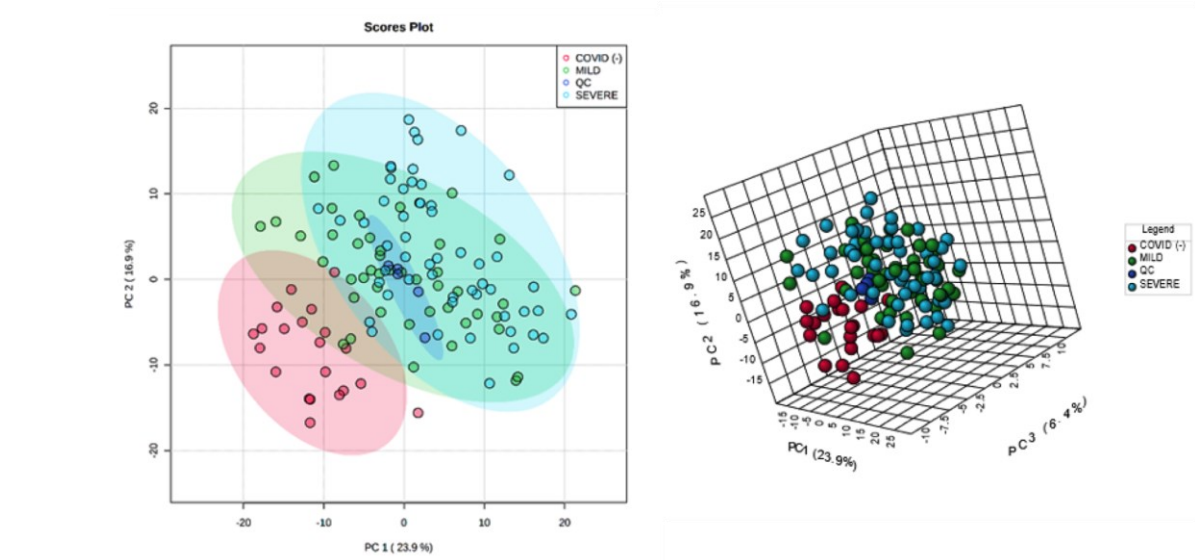

Figure S5.1. *2D left) and 3D right) PCA score plot showing the discrimination of different classes and the clustering of QC samples: Covid (-), red; Mild, green; QC, blue; Severe, light-blue. The repeatability of the system was evaluated using QC samples. The average coefficient of variation (CV %) of the investigated lipids in the pooled QC samples was 12.0 %, this can be also visualized by the satisfactory QC clustering in the score plot of principal component analysis (PCA).*

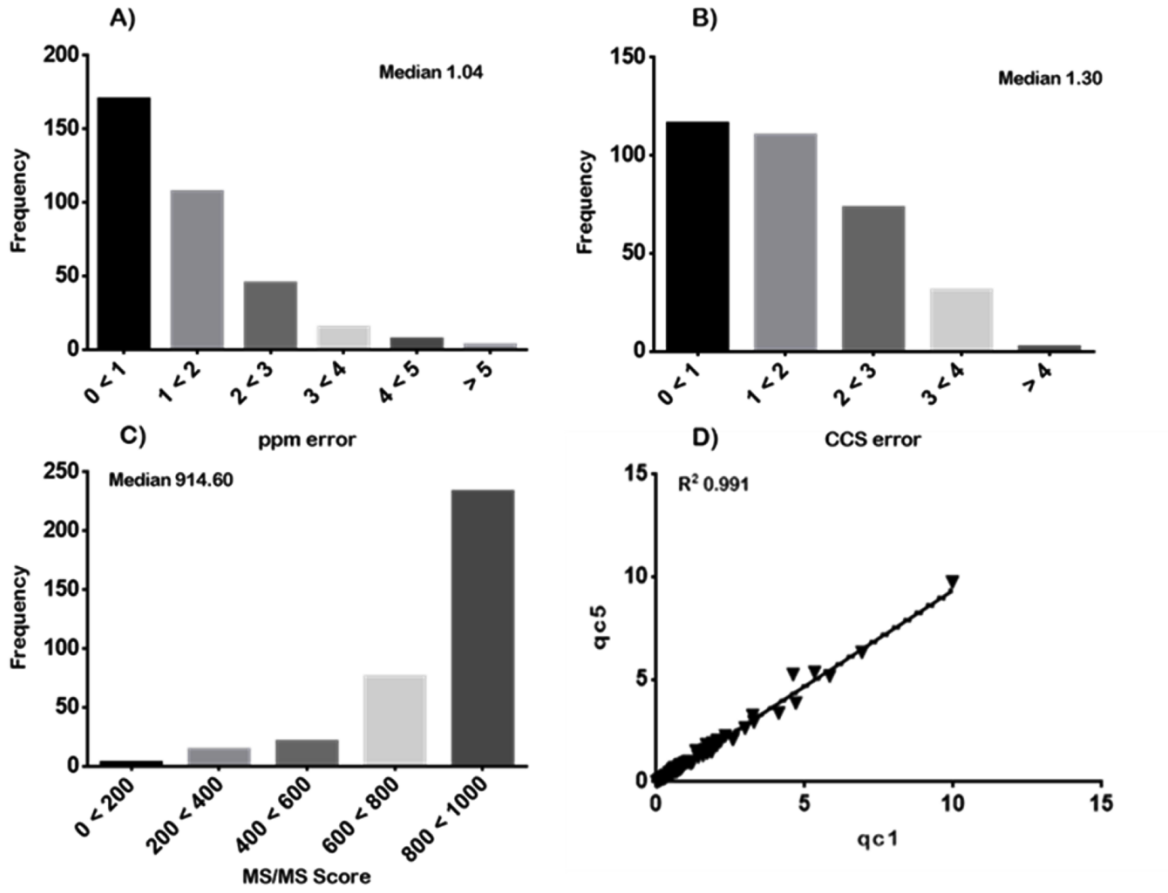

Figure S5.2. *UHPLC-TIMS-MS data were acquired working in parallel accumulation serial fragmentation (PASEF) mode and analyses were acquired in positive and negative ionization mode. Frequency distribution of mass accuracy (**A**), ΔCCS (**B**) MS/MS score (**C**). Pearson correlation of QC replicate injections (**D**). Retention time reproducibility resulted in a median CV value of 0.42 %, prior to the RT alignment. Average MS/MS score, mass accuracy (ppm) and cross collision section error values were, respectively: 914.60 MS/MS score, 0.60 Δppm, 1.30 % ΔCCS.*

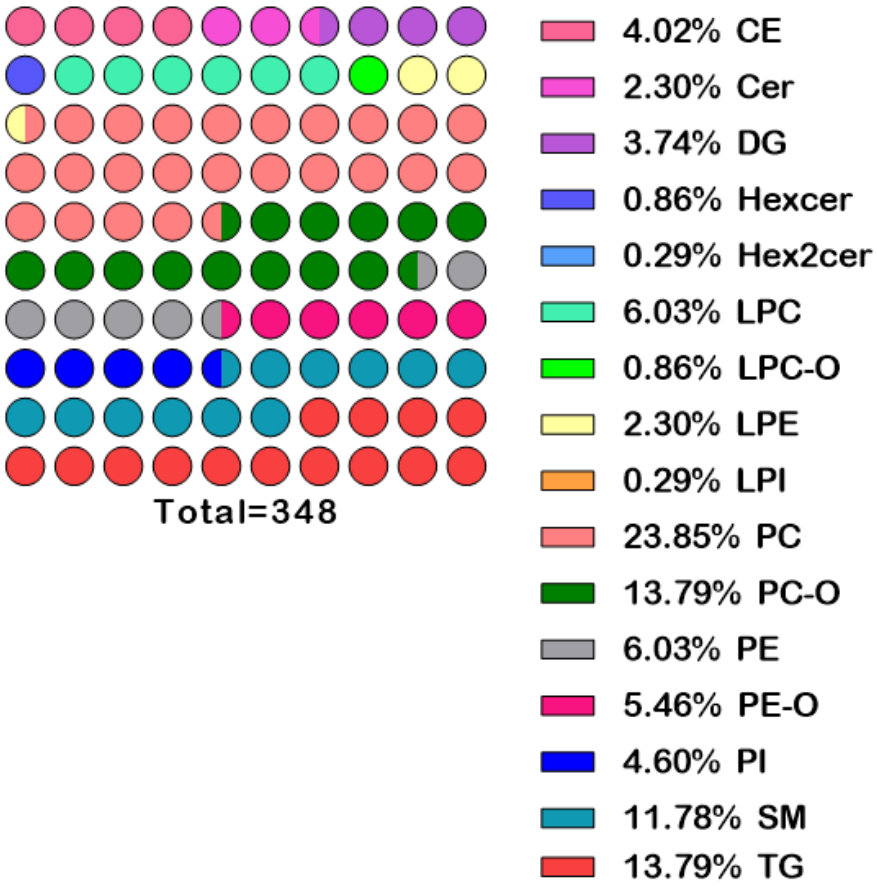

Figure S5.3. *Sub-classification of the 348 putative unique monitored lipids with relative percentages: cholesteryl esters (CEs), diacylglycerols (DGs), triacylglycerols (TGs), phosphatidylinositols (PIs), lysophosphatidylinositol (LPI) lysophosphatidylcholines (LPCs), ether-linked lysophosphatidylcholines (LPC-Os) lysophosphatidylethanolamines (LPEs), phosphatidylcholines (PCs), ether-linked phosphatidylcholines (PC-Os) phosphatidylethanolamines (PEs), ether-linked phosphatidylethanolamines (PE-Os), sphingomyelins (SMs), ceramides (Cers), hexosylceramides (Hexcers), dihexosylceramide (Hex2cer). PCs was the most present lipid subclass in the final dataset, covering the 23.85 % of the annotations, followed by TGs (13.79 %), PC-Os (13.79 %) and SMs (11.78 %). A lower number of PEs (6.03 %), LPCs (6.0 3%), PE-Os (5.46 %), PIs (4.60 %), CEs (4.02 %) and DGs (3.74 %) were annotated. The less present subclasses were: Cers (2.30 %), LPEs (2.30 %), LPC-Os (0.86 %), HexCer (0.86 %) and Hex2Cer (0.29 %).*

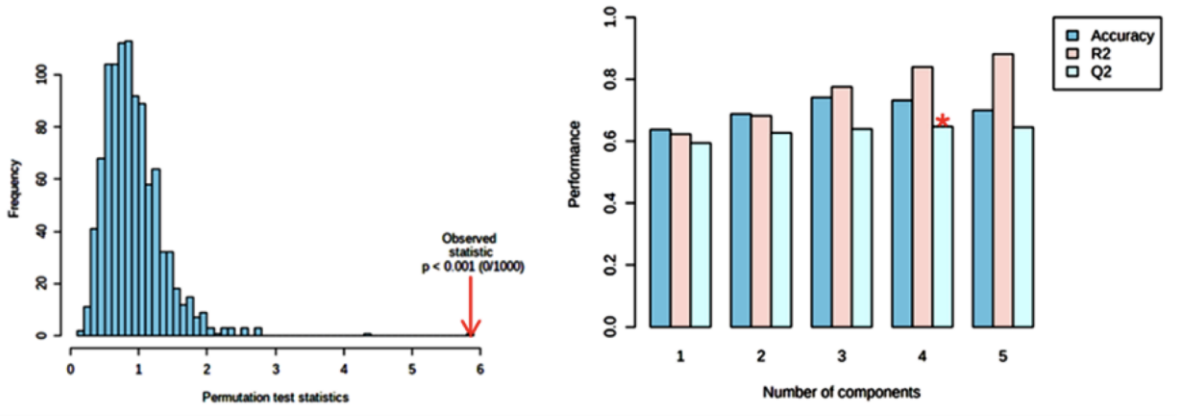

PLS-DA cross validation details:

Measure	1 comps	2 comps	3 comps	4 comps	5 comps
Accuracy	0.63733	0.68333	0.77133	0.74667	0.71533
R2	0.62231	0.68227	0.77572	0.83916	0.88093
Q2	0.59726	0.63227	0.64444	0.65417	0.65772

Figure S5.4. *PLS-DA cross-validation parameters, R^2 and Q^2 results estimated via cross validation and permutation test results based on 1000 iterations.*

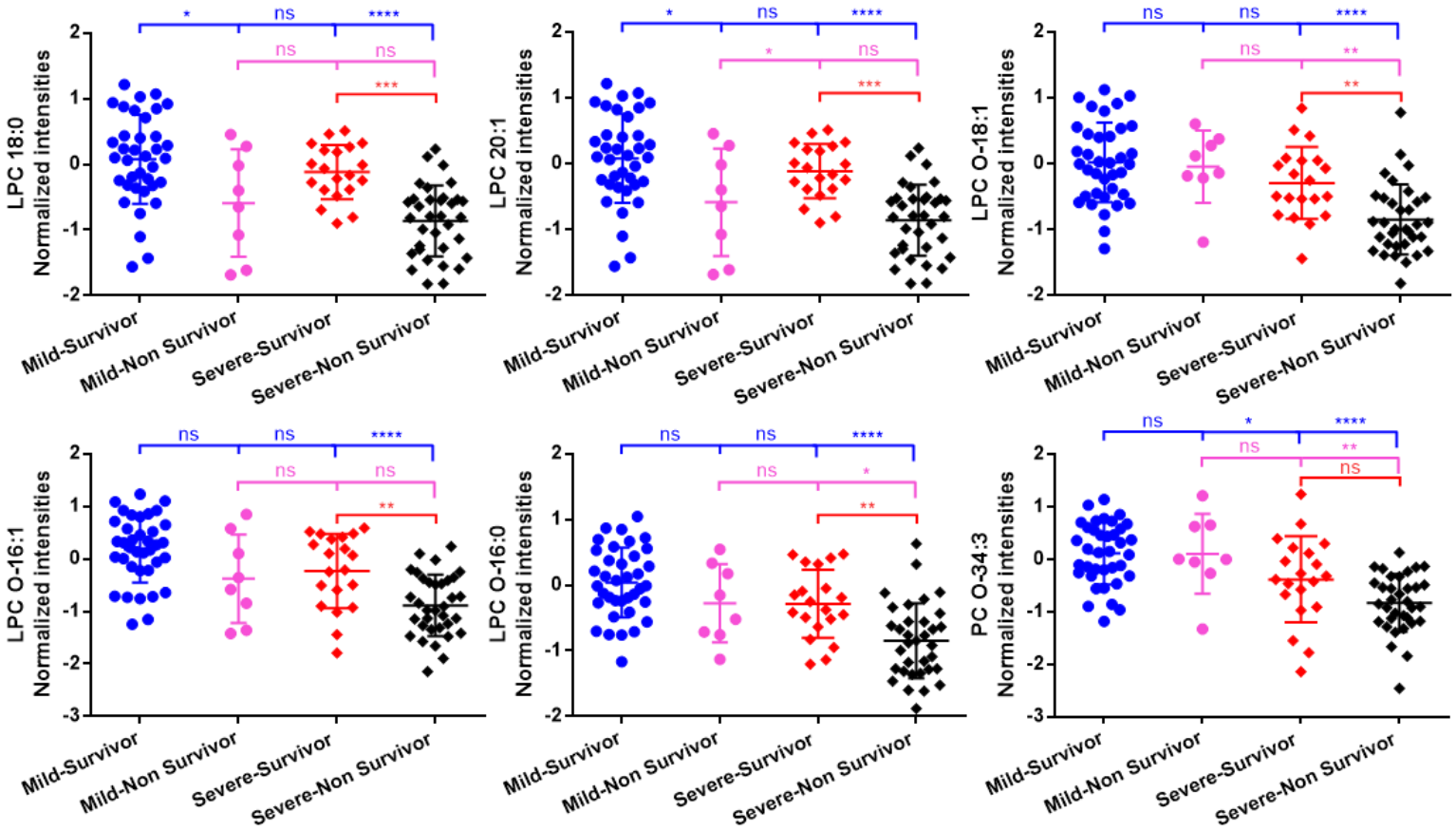

Figure S5.5. *Tukey's multiple comparison test of normalized intensity of the selected lipid panel in Mild-Survivor (blue), Mild-Non Survivor (pink), Severe-Survivor (red) and Severe-Non Survivor (black) patients (ns: not significant, *: $p < 0.05$, **: $p < 0.01$, ***: $p < 0.001$, ****: $p < 0.0001$).*

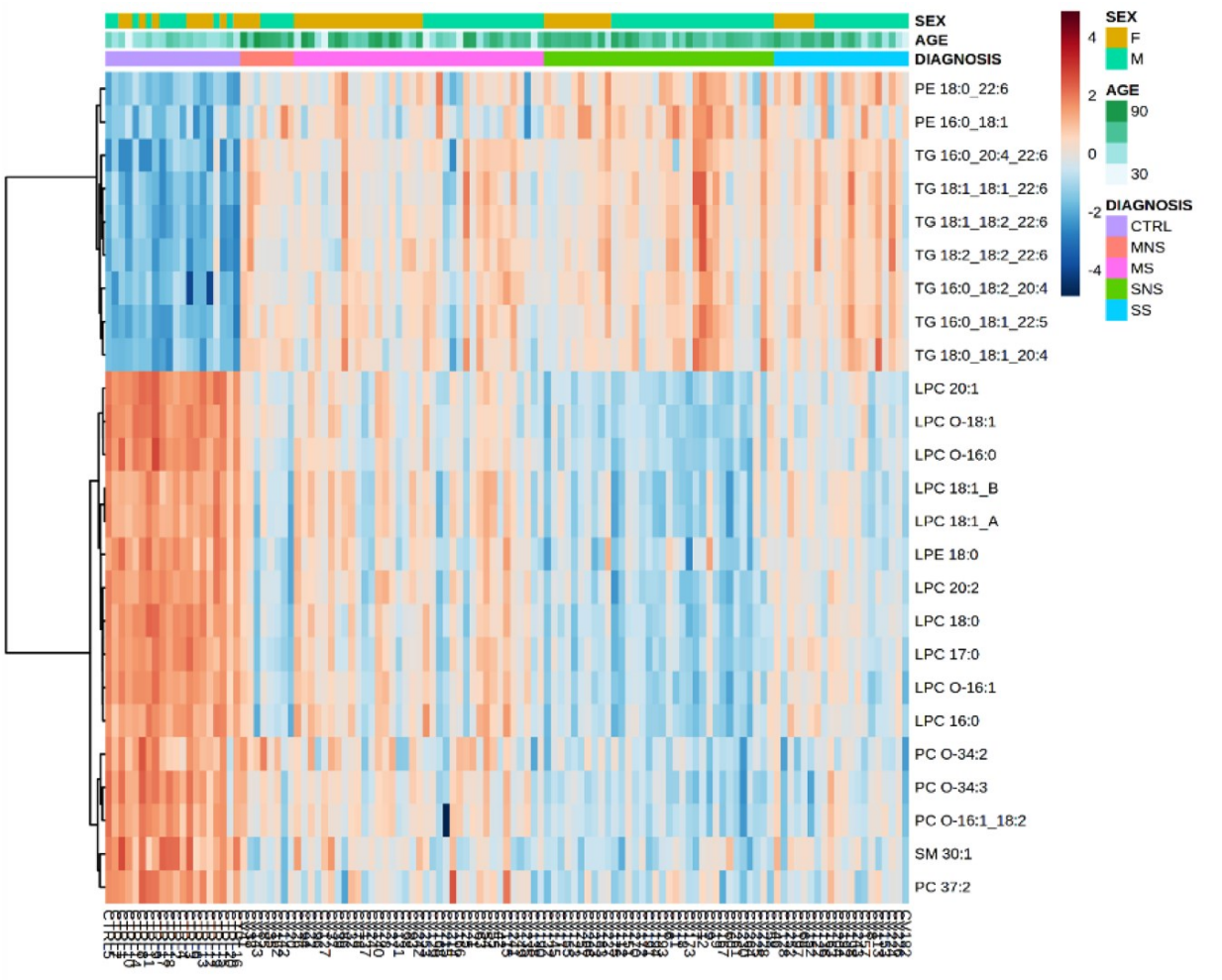

Figure S5.6. *Heatmap of top 25 lipids adjusted for age and sex covariates. (A and B indicate potential isomers).*

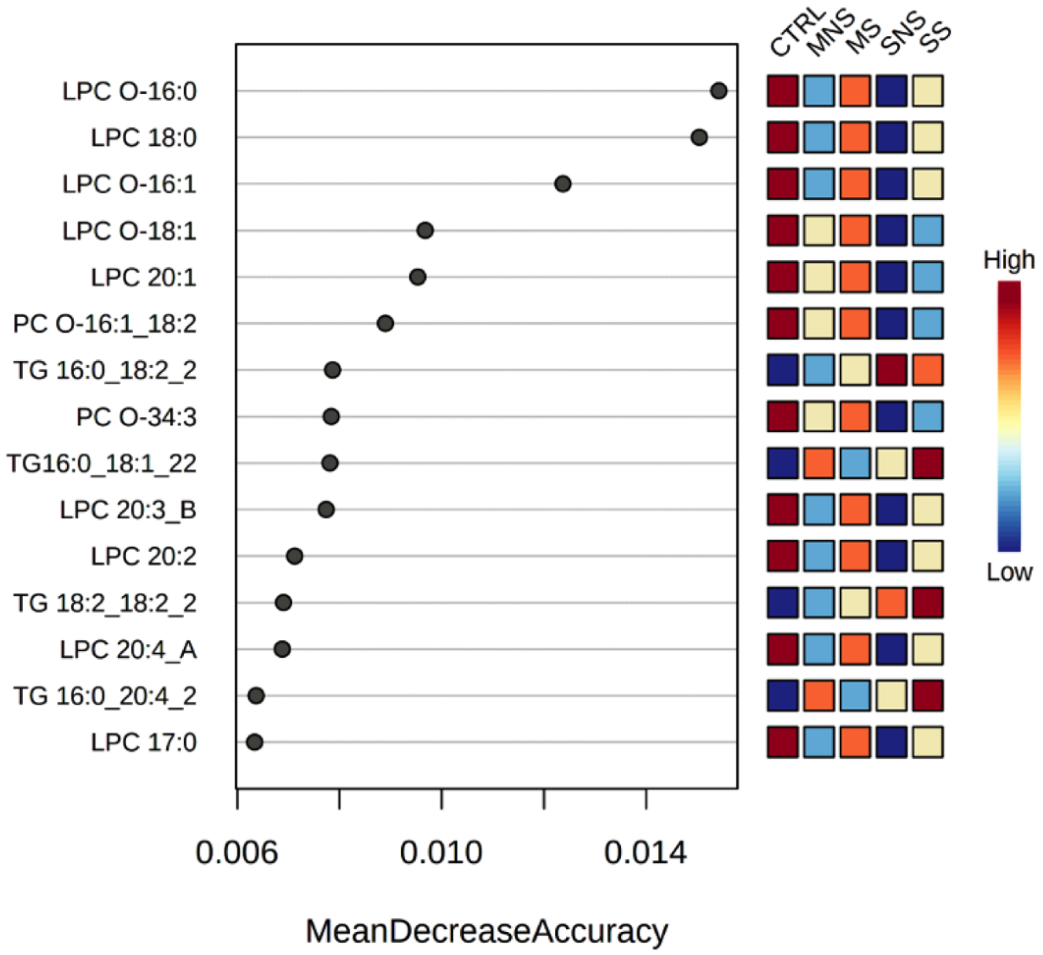

Figure S5.7. *RF features ranked by their contributions to classification accuracy adjusted for covariates sex and age.*

.

Table S5.1. *RP-UHPLC-TIMS-Q-TOF based annotation of lipids in Covid-19 plasma samples, lipids are sorted by class: Lipid annotation was carried out with a combined rule based and spectral library approach following the lipidomic standard initiative guidelines (https://lipidomics-standards-initiative.org/).*

RT [min]	m/z meas	M meas.	Ions	Name	Molecular Formula	MS/MS score	Δm/z [ppm]	ΔCCS [%]	Mob. 1/K0	CCS (Å²)	% QC / SAMPLES
16.63	614.58701	596.55318	$[M+NH_4]^+$	CE 14:0	$C_{41}H_{72}O_2$	937.7	-0.221	2.6	1.375	281.5	80 / 84.8
16.77	628.60242	610.56859	$[M+NH_4]^+$	CE 15:0	$C_{42}H_{74}O_2$	964.7	-0.251	2.3	1.383	283.1	60 / 88.3
16.93	642.61827	624.58457	$[M+NH_4]^+$,$[M+H]^+$	CE 16:0	$C_{43}H_{76}O_2$	969	-0.105	1.9	1.391	284.5	100 / 100
16.62	640.6029	622.56908	$[M+NH_4]^+$	CE 16:1	$C_{43}H_{74}O_2$	972.2	0.363	2.7	1.387	283.8	100 / 100
17.02	656.63389	638.59984	$[M+NH_4]^+$,$[M+Na]^+$	CE 17:0	$C_{44}H_{78}O_2$	949.1	-0.249	2.3	1.407	287.8	80 / 97.2
16.77	654.61831	636.58448	$[M+NH_4]^+$	CE 17:1	$C_{44}H_{76}O_2$	974.1	-0.296	2.3	1.401	286.5	100 / 99.3
17.19	670.64809	652.61562	$[M+NH_4]^+$,$[M+Na]^+$,$[M+K]^+$	CE 18:0	$C_{45}H_80O_2$	963.2	-2.395	1.8	1.42	290.3	100 / 100
16.91	668.63471	650.60088	$[M+NH_4]^+$	CE 18:1	$C_{45}H_{78}O_2$	970.6	1.098	2.2	1.417	289.6	100 / 100
16.65	666.61927	648.58544	$[M+NH_4]^+$	CE 18:2	$C_{45}H_{76}O_2$	965.8	1.380	2.8	1.419	290.1	100 / 100
16.14	662.58708	644.55325	$[M+NH_4]^+$	CE 18:4	$C_{45}H_{72}O_2$	957.2	0.078	4.7	1.418	289.8	100 / 86.9
16.68	692.63403	674.6002	$[M+NH_4]^+$	CE 20:3	$C_{47}H_{78}O_2$	952.4	0.016	3.3	1.444	295	100 / 100
16.48	690.61902	672.58481	$[M+NH_4]^+$,$[M+K]^+$,$[M+H]^+$,$[M+Na]^+$	CE 20:4	$C_{47}H_{76}O_2$	965.6	0.987	2.6	1.436	293.3	100 / 100
16.23	688.60287	670.56886	$[M+NH_4]^+$,$[M+Na]^+$,$[M+H]^+$,$[M+K]^+$	CE 20:5	$C_{47}H_{74}O_2$	960.9	0.259	3.8	1.426	291.3	100 / 100
16.33	714.6185	696.58452	$[M+NH_4]^+$,$[M+H]^+$	CE 22:6	$C_{49}H_{76}O_2$	944.0	0.221	2.4	1.447	295.4	100 / 100
9.93	538.52071	537.51172	$[M+H]^+$,$[M+H-H_2O]^+$,$[M+Na]^+$	Cer 18:1;O2/16:0	$C_{34}H_{67}NO_3$	972.0	2.419	0.1	1.254	257.5	100 / 98.6
14.83	622.61332	621.60604	$[M+H]^+$	Cer 18:1;O2/22:0	$C_40H_{79}NO_3$	884.3	0.071	1.6	1.355	277.4	100 / 100
15.06	636.62892	635.62165	$[M+H]^+$	Cer 18:1;O2/23:0	$C_{41}H_{81}NO_3$	828.3	-0.254	2.9	1.378	281.9	100 / 100
15.27	650.64439	649.63711	$[M+H]^+$	Cer 18:1;O2/24:0	$C_{42}H_{83}NO_3$	747.1	-0.198	2.4	1.385	283.3	100 / 100

14.81	648.6283	647.62102	$[M+H]^+$	Cer 18:1;O2/24:1	$C_{42}H_{81}NO_3$	772.0	-0.870	2.2	1.375	281.2	100 / 100
14.65	634.61329	633.60601	$[M+H]^+$	Cer 18:2;O2/23:0	$C_{41}H_{79}NO_3$	635.7	-0.126	1.0	1.349	275.9	100 / 79.3
14.89	648.62846	647.62089	$[M+H]^+$,$[M+Na]^+$	Cer 18:2;O2/24:0	$C_{42}H_{81}NO_3$	631.5	-0.677	1.8	1.369	280	100 / 79.3
14.57	568.56614	567.55887	$[M+H]^+$	Cer 36:0;O2	$C_{36}H_{73}NO_3$	214.0	-0.220	1.1	1.306	267.9	60 / 89
14.17	612.55589	594.5221	$[M+NH_4]^+$,$[M+Na]^+$	DG 16:0_18:1	$C_{37}H_70O_5$	858.3	-0.416	1.3	1.298	265.9	100 / 100
13.32	610.53999	592.50704	$[M+NH_4]^+$,$[M+K]^+$	DG 16:0_18:2	$C_{37}H_{68}O_5$	890.7	-0.718	1.7	1.283	262.7	100 / 100
12.95	610.53976	592.50593	$[M+NH_4]^+$	DG 16:1_18:1	$C_{37}H_{68}O_5$	914.2	-1.357	0.8	1.271	260.3	100 / 100
10.5	608.52521	590.49132	$[M+NH_4]^+$,$[M+K]^+$,$[M+Na]^+$	DG 16:1_18:2	$C_{37}H_{66}O_5$	814.5	0.317	0.6	1.249	255.8	100 / 93.8
15.16	642.60293	624.56916	$[M+NH_4]^+$,$[M+Na]^+$, $[M+H-H_2O]^+$,$[M+H]^+$,$[M+K]^+$	DG 18:0_18:0	$C_{39}H_{76}O_5$	663.5	-0.302	1.7	1.337	273.5	100 / 100
14.74	640.58666	622.55319	$[M+NH_4]^+$,$[M+K]^+$,$[M+Na]^+$,$[M+H]^+$	DG 18:0_18:1	$C_{39}H_{74}O_5$	888.2	-1.317	2.6	1.329	271.9	100 / 99.3
14.23	638.5717	620.53839	$[M+NH_4]^+$,$[M+K]^+$,$[M+Na]^+[M+H]^+$, $[M+H-H_2O]^+$	DG 18:1_18:1	$C_{39}H_{72}O_5$	935.6	-0.164	2.5	1.312	268.4	100 / 100
13.56	636.55614	618.52238	$[M+NH_4]^+$,$[M+Na]^+$,$[M+K]^+$, $[M+H-H_2O]^+$	DG 18:1_18:2	$C_{39}H_70O_5$	955.0	-0.011	1.8	1.292	264.4	100 / 100
14.04	662.57243	644.53901	$[M+NH_4]^+$,$[M+K]^+$,$[M+Na]^+$	DG 18:1_20:3	$C_{41}H_{72}O_5$	593.1	-0.079	2.9	1.326	271.2	100 / 97.2
12.88	660.55544	642.52212	$[M+NH_4]^+$,$[M+Na]^+$,$[M+K]^+$	DG 18:1_20:4	$C_{41}H_70O_5$	760.6	-1.293	2.3	1.313	268.5	100 / 98.6
11.09	634.54003	616.5065	$[M+NH_4]^+$,$[M+K]^+$	DG 18:2_18:2	$C_{39}H_{68}O_5$	955.2	-0.656	1.6	1.268	259.4	100 / 100
9.69	682.5386	664.50591	$[M+NH_4]^+$,$[M+Na]^+$,$[M+K]^+$	DG 18:2_22:6	$C_{43}H_{68}O_5$	767.3	-2.258	2.2	1.311	267.9	100 / 92.4
15.85	714.60266	696.56934	$[M+NH_4]^+$,$[M+K]^+$,$[M+Na]^+$	DG 22:6_20:0	$C_{45}H_{76}O_5$	656.4	-0.449	0.7	1.432	292.3	80 / 100
7.23	862.62554	861.61706	$[M+H]^+$,$[M+Na]^+$	Hex2Cer 18:1;O2/16:0	$C_{46}H_{87}NO_{13}$	457.2	0.616	2.1	1.505	306.2	100 / 100
14.34	784.66504	783.65594	$[M+H]^+$,$[M+K]^+$	Hex-Cer 18:1;O2/22:0	$C_{46}H_{89}NO_8$	277.4	-1.532	1.4	1.472	300	100 / 100

14.84	812.69664	811.6898	$[M+H]^+$,$[M+Na]^+$,$[M+K]^+$	Hex-Cer 18:1;O2/24:0	$C_{48}H_{93}NO_8$	210.0	-0.958	1.2	1.498	305.1	100 / 99.3
14.32	810.67961	809.67233	$[M+H]^+$	Hex-Cer 18:1;O2/24:1	$C_{48}H_{91}NO_8$	169.7	-2.665	1.5	1.491	303.6	100 / 100
1.11	468.30852	467.30124	$[M+H]^+$	LPC 14:0	$C_{22}H_{46}NO_7P$	990.7	0.184	0.3	1.092	225.1	100 / 100
1.26	482.32419	481.31692	$[M+H]^+$	LPC 15:0	$C_{23}H_{48}NO_7P$	977.8	0.223	0.3	1.107	228	100 / 100
1.47	496.33916	495.3326	$[M+H]^+$,$[M+H-H_2O]^+$,$[M+Na]^+$,$[M+K]^+$	LPC 16:0	$C_{24}H_{50}NO_7P$	987.9	-1.228	1.9	1.13	232.6	100 / 100
1.18	538.31679	493.31859	$[M+HCOO]^-$	LPC 16:1	$C_{24}H_{48}NO_7P$	959.9	3.334	1.4	1.145	235.2	100 / 97.9
1.73	510.35543	509.34815	$[M+H]^+$	LPC 17:0	$C_{25}H_{52}NO_7P$	959.2	-0.023	0.7	1.15	236.5	100 / 100
1.33	508.33968	507.3324	$[M+H]^+$	LPC 17:1	$C_{25}H_{50}NO_7P$	993.7	-0.211	1.8	1.126	231.5	100 / 100
2.06	524.37082	523.36369	$[M+H]^+$,$[M+K]^+$,$[M+Na]^+$	LPC 18:0	$C_{26}H_{54}NO_7P$	973.2	-0.465	0.7	1.169	240.3	100 / 100
1.55	566.34851	521.3503	$[M+HCOO]^-$	LPC 18:1	$C_{26}H_{52}NO_7P$	979.4	3.821	0.7	1.18	242	100 / 100
1.54	522.35552	521.3483	$[M+H]^+$,$[M+Na]^+$,$[M+K]^+$	LPC 18:1	$C_{26}H_{52}NO_7P$	988.8	0.163	0	1.143	234.9	100 / 100
1.26	564.33284	519.33464	$[M+HCOO]^-$	LPC 18:2	$C_{26}H_{50}NO_7P$	975.5	3.902	2.3	1.166	239.3	100 / 100
1.25	520.33948	519.33208	$[M+H]^+$,$[M+K]^+$	LPC 18:2	$C_{26}H_{50}NO_7P$	987	-0.548	1.1	1.117	229.7	100 / 100
2.14	550.38601	549.37873	$[M+H]^+$	LPC 20:1	$C_{28}H_{56}NO_7P$	969.8	-1.382	1.0	1.182	242.6	100 / 100
1.65	548.36906	547.36178	$[M+H]^+$	LPC 20:2	$C_{28}H_{54}NO_7P$	992.3	-4.674	0.4	1.155	237.2	100 / 100
1.37	590.34844	545.35023	$[M+HCOO]^-$	LPC 20:3	$C_{28}H_{52}NO_7P$	973.1	3.605	1.3	1.191	244.1	100 / 98.6
1.36	546.35542	545.34824	$[M+H]^+$,$[M+Na]^+$	LPC 20:3	$C_{28}H_{52}NO_7P$	977.4	0.018	0.1	1.138	233.7	100 / 100
1.21	588.33289	589.34016	$[M-H]^-$	LPC 20:4	$C_{28}H_{50}NO_7P$	975.3	0.657	0.6	1.187	243.3	100 / 100
1.2	544.33975	543.33244	$[M+H]^+$,$[M+Na]^+$	LPC 20:4	$C_{28}H_{50}NO_7P$	989.2	-0.034	0.4	1.132	232.5	100 / 100
1.03	542.32424	541.31696	$[M+H]^+$	LPC 20:5	$C_{28}H_{48}NO_7P$	992.7	0.196	0.4	1.114	228.8	100 / 100
1.49	572.37009	571.36281	$[M+H]^+$	LPC 22:4	$C_{30}H_{54}NO_7P$	679.3	-1.946	0.3	1.165	239	100 / 98.6

1.25	570.35514	569.34786	$[M+H]^+$	LPC 22:5	$C_{30}H_{52}NO_7P$	343.6	-0.402	0.7	1.151	236.1	100 / 100
1.15	568.33974	567.33246	$[M+H]^+$	LPC 22:6	$C_{30}H_{50}NO_7P$	987.4	-0.063	0.2	1.146	235.1	100 / 100
1.72	482.3604	481.35312	$[M+H]^+$	LPC O-16:0	$C_{24}H_{52}NO_6P$	827.2	-0.232	0.9	1.135	233.9	100 / 100
1.64	480.34491	479.33764	$[M+H]^+$	LPC O-16:1	$C_{24}H_{50}NO_6P$	226	0.108	0.7	1.11	228.6	100 / 100
1.81	508.37594	507.36866	$[M+H]^+$	LPC O-18:1	$C_{26}H_{54}NO_6P$	472.9	-0.392	0.8	1.148	236.2	100 / 100
1.55	452.27947	453.28674	$[M-H]^-$	LPE 16:0	$C_{21}H_{44}NO_7P$	983.5	2.659	2.9	1.02	210.4	100 / 97.2
2.18	482.32409	481.31682	$[M+H]^+$	LPE 18:0	$C_{23}H_{48}NO_7P$	968.8	-0.068	1.2	1.088	224.2	100 / 99.3
1.63	478.29539	479.30267	$[M-H]^-$	LPE 18:1	$C_{23}H_{46}NO_7P$	984.6	2.791	3.2	1.043	214.9	100 / 97.2
1.3	478.29276	477.28549	$[M+H]^+$	LPE 18:2	$C_{23}H_{44}NO_7P$	963.6	-0.112	0.4	1.031	212.5	100 / 100
1.31	476.27961	477.28689	$[M-H]^-$	LPE 18:2	$C_{23}H_{44}NO_7P$	953.1	2.749	3.4	1.03	212.2	100 / 97.9
1.26	500.27995	501.28722	$[M-H]^-$	LPE 20:4	$C_{25}H_{44}NO_7P$	956.9	3.335	3.3	1.054	216.9	100 / 99.3
1.19	526.29279	525.28551	$[M+H]^+$	LPE 22:6	$C_{27}H_{44}NO_7P$	943.2	-0.048	0.2	1.069	219.7	100 / 100
1.19	524.28009	525.28736	$[M-H]^-$	LPE 22:6	$C_{27}H_{44}NO_7P$	501.0	3.485	3.2	1.076	221.1	100 / 98.6
1.01	619.29136	620.29863	$[M-H]^-$	LPI 20:4	$C_{29}H_{49}O_{12}P$	743.8	4.056	2.9	1.171	239.8	100 / 93.1
7.36	750.5305	705.53229	$[M+HCOO]^-$	PC 14:0_16:0	$C_{38}H_{76}NO_8P$	802.8	1.943	1.1	1.386	282.7	100 / 95.2
7.33	706.53799	705.53128	$[M+H]^+$,$[M+Na]^+$	PC 30:0	$C_{38}H_{76}NO_8P$	995.4	-0.181	1.3	1.381	281.9	100 / 100
6.24	774.53069	729.53249	$[M+HCOO]^-$	PC 14:0_18:2	$C_{40}H_{76}NO_8P$	822.6	1.921	0.9	1.399	285.2	100 / 100
6.23	730.53825	729.53097	$[M+H]^+$	PC 14:0_18:2	$C_{40}H_{76}NO_8P$	993.6	0.174	0.9	1.378	281.2	100 / 100
5.99	754.53807	753.5308	$[M+H]^+$	PC 14:0_20:4	$C_{42}H_{76}NO_8P$	993.4	-0.051	1.7	1.392	283.9	100 / 97.9
6.00	798.53013	753.53193	$[M+HCOO]^-$	PC 14:0_20:4	$C_{42}H_{76}NO_8P$	809.2	1.297	1.1	1.415	288.3	100 / 99.3
5.81	804.55338	803.54611	$[M+H]^+$	PC 14:1_24:6	$C_{46}H_{78}NO_8P$	981.3	-0.442	0.8	1.424	290	100 / 98.6

8.42	764.54666	719.54846	$[M+HCOO]^-$	PC 15:0_16:0	$C_{39}H_{78}NO_8P$	830.1	2.463	0.8	1.4	285.4	100 / 100
8.68	790.5628	745.56459	$[M+HCOO]^-$	PC 15:0_18:1	$C_{41}H_80NO_8P$	816.1	3.085	0.4	1.42	289.3	100 / 100
7.04	744.5543	743.54702	$[M+H]^+$	PC 15:0_18:2	$C_{41}H_{78}NO_8P$	993.9	0.839	0.5	1.39	283.4	100 / 100
9.61	734.57014	733.56286	$[M+H]^+$	PC 16:0_16:0	$C_40H_80NO_8P$	997.1	0.969	1.8	1.413	288.3	100 / 100
7.64	732.55439	731.54712	$[M+H]^+$	PC 16:0_16:1	$C_40H_{78}NO_8P$	993.3	0.864	1.0	1.395	284.6	100 / 100
7.64	776.54619	731.54799	$[M+HCOO]^-$	PC 16:0_16:1	$C_40H_{78}NO_8P$	815.4	1.971	0.9	1.408	286.9	100 / 100
12.58	762.60047	761.59319	$[M+H]^+$	PC 16:0_18:0	$C_{42}H_{84}NO_8P$	994.0	-0.221	1.1	1.442	294.1	100 / 100
9.88	760.58634	759.57907	$[M+H]^+$	PC 16:0_18:1	$C_{42}H_{82}NO_8P$	994.3	1.658	0.7	1.426	290.9	100 / 100
9.88	804.57834	759.58014	$[M+HCOO]^-$	PC 16:0_18:1	$C_{42}H_{82}NO_8P$	796.7	2.915	0.6	1.44	293.3	100 / 100
8.05	802.56297	757.56477	$[M+HCOO]^-$	PC 16:0_18:2	$C_{42}H_80NO_8P$	785.3	3.278	0.8	1.432	291.7	100 / 100
8.05	758.57043	757.56315	$[M+H]^+$	PC 16:0_18:2	$C_{42}H_80NO_8P$	994.6	1.361	0.8	1.41	287.6	100 / 75.2
6.77	800.54625	755.54805	$[M+HCOO]^-$	PC 16:0_18:3	$C_{42}H_{78}NO_8P$	867.6	1.944	0.8	1.421	289.5	100 / 100
11.34	774.60126	773.59399	$[M+H]^+$	PC 16:0_19:1	$C_{43}H_{84}NO_8P$	992.7	0.596	1.0	1.441	293.7	100 / 100
8.64	784.58611	783.57841	$[M+H]^+$,$[M+H-H_2O]^+$,$[M+K]^+$	PC 16:0_20:3	$C_{44}H_{82}NO_8P$	992.9	1.229	1.0	1.433	292	100 / 100
7.75	782.57031	781.56304	$[M+H]^+$	PC 16:0_20:4	$C_{44}H_80NO_8P$	994.2	1.128	0.7	1.424	290.3	100 / 100
7.75	826.56254	781.56434	$[M+HCOO]^-$	PC 16:0_20:4	$C_{44}H_80NO_8P$	754.5	2.674	0.9	1.446	294.5	100 / 100
6.54	780.5547	779.54713	$[M+H]^+$,$[M+Na]^+$	PC 16:0_20:5	$C_{44}H_{78}NO_8P$	992.5	1.206	1.1	1.413	288	100 / 100
6.55	824.54598	779.54777	$[M+HCOO]^-$	PC 16:0_20:5	$C_{44}H_{78}NO_8P$	724.3	1.59	1.2	1.438	292.9	100 / 100
9.41	810.60106	809.59157	$[M+H]^+$,$[M+Na]^+$	PC 16:0_22:4	$C_{46}H_{84}NO_8P$	989.4	0.423	0.8	1.455	296.4	100 / 100
9.41	854.59239	809.59419	$[M+HCOO]^-$	PC 16:0_22:4	$C_{46}H_{84}NO_8P$	737.1	1.073	0.7	1.471	299.4	100 / 100
7.23	806.57093	805.56365	$[M+H]^+$	PC 16:0_22:6	$C_{46}H_80NO_8P$	992.8	1.852	0.7	1.438	292.9	100 / 100

7.25	850.56167	805.56347	$[M+HCOO]^-$	PC 16:0_22:6	$C_{46}H_80NO_8P$	656.8	1.566	1.1	1.463	297.7	60 / 75.2
6.46	800.54611	755.5479	$[M+HCOO]^-$	PC 16:1_18:2	$C_{42}H_{78}NO_8P$	869.6	1.759	0.3	1.419	289	60 / 77.9
1.45	524.33472	523.32744	$[M+H]^+$	PC 17:0	$C_{25}H_50NO_8P$	971.8	0.096	1.3	1.157	237.8	100 / 98.6
10.91	774.59975	773.59247	$[M+H]^+$	PC 17:0_18:1	$C_{43}H_{84}NO_8P$	991.1	-1.173	1.3	1.445	294.5	100 / 100
11.35	818.59344	773.59523	$[M+HCOO]^-$	PC 17:0_18:1	$C_{43}H_{84}NO_8P$	736.4	2.207	0.7	1.45	295.4	100 / 100
9.25	772.58559	771.57831	$[M+H]^+$	PC 17:0_18:2	$C_{43}H_{82}NO_8P$	989.9	0.568	0.7	1.425	290.5	100 / 100
8.89	772.58508	771.5778	$[M+H]^+$	PC 17:0_18:2	$C_{43}H_{82}NO_8P$	993.7	-0.101	0.8	1.426	290.7	100 / 100
8.87	796.58524	795.57796	$[M+H]^+$	PC 17:0_20:4	$C_{45}H_{82}NO_8P$	994.1	0.210	1.2	1.445	294.3	100 / 100
8.52	840.57776	795.57956	$[M+HCOO]^-$	PC 17:0_20:4	$C_{45}H_{82}NO_8P$	697.1	2.002	1.0	1.461	297.3	100 / 100
8.88	840.57677	795.57857	$[M+HCOO]^-$	PC 17:0_20:4	$C_{45}H_{82}NO_8P$	690.8	0.866	0.9	1.46	297.2	100 / 100
12.91	788.61762	787.61024	$[M+H]^+$,$[M+K]^+$,$[M+Na]^+$	PC 18:0_18:1	$C_{44}H_{86}NO_8P$	991.6	1.569	0.9	1.457	296.8	100 / 100
10.54	830.59336	785.59516	$[M+HCOO]^-$	PC 18:0_18:2	$C_{44}H_{84}NO_8P$	775.4	2.067	0.9	1.458	296.9	100 / 100
10.54	786.60205	785.59431	$[M+H]^+$,$[M+Na]^+$,$[M+K]^+$	PC 18:0_18:2	$C_{44}H_{84}NO_8P$	993.0	1.680	0.9	1.441	293.6	100 / 100
11.35	812.61756	811.60984	$[M+H]^+$,$[M+H-H_2O]^+$,$[M+Na]^+$	PC 18:0_20:3	$C_{46}H_{86}NO_8P$	993.6	1.524	0.9	1.464	298.2	100 / 83.4
12.32	856.60898	811.61078	$[M+HCOO]^-$	PC 18:0_20:3	$C_{46}H_{86}NO_8P$	849.3	1.399	0.8	1.479	301.1	100 / 100
10.12	810.60204	809.59477	$[M+H]^+$	PC 18:0_20:4	$C_{46}H_{84}NO_8P$	992.3	1.616	1.1	1.458	297	100 / 100
10.13	854.59286	809.59466	$[M+HCOO]^-$	PC 18:0_20:4	$C_{46}H_{84}NO_8P$	732.2	1.458	1.0	1.474	300	100 / 100
8.57	852.57706	807.57886	$[M+HCOO]^-$	PC 18:0_20:5	$C_{46}H_{82}NO_8P$	683.6	1.169	1.2	1.469	299	100 / 100
12.29	838.63246	837.62518	$[M+H]^+$	PC 18:0_22:4	$C_{48}H_{88}NO_8P$	989.9	0.483	1.0	1.486	302.5	100 / 100
12.31	882.62262	837.62442	$[M+HCOO]^-$	PC 18:0_22:4	$C_{48}H_{88}NO_8P$	648.9	-0.413	0.9	1.499	305	100 / 100
10.24	836.61665	835.60893	$[M+H]^+$,$[M+Na]^+$	PC 18:0_22:5	$C_{48}H_{86}NO_8P$	989.9	0.304	0.8	1.476	300.5	100 / 100

11.31	880.608	835.6098	$[M+HCOO]^-$	PC 18:0_22:5	$C_{48}H_{86}NO_8P$	772.4	0.796	1.1	1.496	304.4	100 / 100
9.46	878.59257	833.59437	$[M+HCOO]^-$	PC 18:0_22:6	$C_{48}H_{84}NO_8P$	594.8	1.078	1.2	1.49	303.1	100 / 100
10.17	786.60125	785.59398	$[M+H]^+$	PC 18:1_18:1	$C_{44}H_{84}NO_8P$	995.7	0.766	0.8	1.44	293.5	100 / 100
10.19	830.59275	785.59455	$[M+HCOO]^-$	PC 18:1_18:1	$C_{44}H_{84}NO_8P$	839.0	1.322	0.7	1.455	296.3	100 / 100
8.28	784.58606	783.57878	$[M+H]^+$	PC 18:1_18:2	$C_{44}H_{82}NO_8P$	994.2	1.252	0.9	1.431	291.6	100 / 100
7.93	852.57697	807.57877	$[M+HCOO]^-$	PC 18:1_20:4	$C_{46}H_{82}NO_8P$	676.6	1.225	1.1	1.466	298.4	100 / 100
7.45	876.57584	831.57764	$[M+HCOO]^-$	PC 18:1_22:6	$C_{48}H_{82}NO_8P$	627.6	-0.183	1.3	1.48	301.1	100 / 100
9.45	834.60188	833.59205	$[M+H]^+$,$[M+Na]^+$,$[M+K]^+$	PC 20:1_20:5	$C_{48}H_{84}NO_8P$	991.6	1.389	1.5	1.471	299.6	100 / 99.3
9.55	860.61459	859.60732	$[M+H]^+$	PC 20:2_22:5	$C_{50}H_{86}NO_8P$	973.1	-1.957	1.4	1.489	303	100 / 100
5.9	704.52193	703.51466	$[M+H]^+$	PC 30:1	$C_{38}H_{74}NO_8P$	958.2	-0.647	0.8	1.364	278.5	100 / 99.3
8.39	720.5544	719.54713	$[M+H]^+$	PC 31:0	$C_{39}H_{78}NO_8P$	1000	0.695	0.9	1.394	284.5	100 / 100
6.71	718.5348	717.52753	$[M+H]^+$	PC 31:1	$C_{39}H_{76}NO_8P$	966.7	-3.721	0.6	1.379	281.4	100 / 99.3
10.49	748.58506	747.57778	$[M+H]^+$	PC 33:0	$C_{41}H_{82}NO_8P$	1000	-0.032	0.4	1.42	289.7	100 / 100
8.65	746.56964	745.56236	$[M+H]^+$	PC 33:1	$C_{41}H_{80}NO_8P$	963.0	0.264	0.3	1.407	286.9	100 / 100
6.76	756.5539	755.54662	$[M+H]^+$	PC 34:3	$C_{42}H_{78}NO_8P$	951.9	0.217	0.5	1.395	284.4	100 / 75.2
7.27	770.56904	769.56176	$[M+H]^+$	PC 35:3	$C_{43}H_{80}NO_8P$	927.1	-0.612	0.3	1.412	287.8	100 / 96.5
6.81	768.55404	767.54677	$[M+H]^+$	PC 35:4	$C_{43}H_{78}NO_8P$	893.2	0.344	0.7	1.408	287	100 / 100
14.14	790.63206	789.62478	$[M+H]^+$	PC 36:0	$C_{44}H_{88}NO_8P$	623.3	0.170	1.1	1.468	299.1	80 / 96.5
7.23	782.56926	781.56198	$[M+H]^+$	PC 36:4	$C_{44}H_{80}NO_8P$	971.1	-0.175	0.1	1.418	289	100 / 93.1
6.19	780.55374	779.54646	$[M+H]^+$	PC 36:5	$C_{44}H_{78}NO_8P$	975.8	-0.059	0.1	1.41	287.4	100 / 100
5.62	778.53866	777.53138	$[M+H]^+$	PC 36:6	$C_{44}H_{76}NO_8P$	1000	0.658	0.6	1.404	286.1	100 / 100

13.88	802.63125	801.62397	$[M+H]^+$	PC 37:1	$C_{45}H_{88}NO_8P$	1000	-0.896	0.5	1.469	299.2	100 / 99.3
12.11	800.61762	799.61035	$[M+H]^+$	PC 37:2	$C_{45}H_{86}NO_8P$	919.7	1.399	0.4	1.455	296.5	100 / 100
9.52	798.60225	797.59498	$[M+H]^+$	PC 37:3	$C_{45}H_{84}NO_8P$	947.0	1.898	0.6	1.448	294.9	100 / 100
8.53	796.58432	795.57705	$[M+H]^+$	PC 37:4	$C_{45}H_{82}NO_8P$	923.0	-0.972	1.2	1.445	294.5	100 / 100
7.00	794.57007	793.56279	$[M+H]^+$	PC 37:5	$C_{45}H_80NO_8P$	1000	0.864	0.7	1.433	291.9	100 / 90.3
6.38	792.55476	791.54748	$[M+H]^+$	PC 37:6	$C_{45}H_{78}NO_8P$	761.4	1.157	1.4	1.422	289.7	100 / 100
7.93	808.58567	807.57839	$[M+H]^+$	PC 38:5	$C_{46}H_{82}NO_8P$	949.9	0.807	0.7	1.447	294.6	100 / 100
6.25	804.55416	803.54688	$[M+H]^+$	PC 38:7	$C_{46}H_{78}NO_8P$	783.5	0.750	0.9	1.428	290.9	100 / 100
8.26	820.58516	819.57788	$[M+H]^+$	PC 39:6	$C_{47}H_{82}NO_8P$	230.6	0.338	0.9	1.456	296.5	100 / 100
7.69	832.58454	831.57726	$[M+H]^+$	PC 40:7	$C_{48}H_{82}NO_8P$	754.2	-0.639	0.9	1.461	297.4	100 / 75.9
7.44	832.58513	831.57785	$[M+H]^+$	PC 40:7	$C_{48}H_{82}NO_8P$	828.7	0.056	0.9	1.46	297.2	100 / 100
6.18	830.56751	829.56024	$[M+H]^+$	PC 40:8	$C_{48}H_80NO_8P$	586.9	-2.399	0.8	1.443	293.9	100 / 100
7.48	858.59587	857.58859	$[M+H]^+$	PC 42:8	$C_50H_{84}NO_8P$	215.4	-4.990	0.4	1.476	300.4	100 / 98.6
11.38	764.5826	719.58439	$[M+HCOO]^-$	PC O-16:0_16:0	$C_40H_{82}NO_7P$	767.5	1.966	1.2	1.412	288	100 / 100
9.51	788.58258	743.58438	$[M+HCOO]^-$	PC O-16:0_18:2	$C_{42}H_{82}NO_7P$	813.2	1.961	0.6	1.423	289.9	100 / 99.3
9.12	812.5822	767.58399	$[M+HCOO]^-$	PC O-16:0_20:4	$C_{44}H_{82}NO_7P$	704.0	1.364	1.0	1.441	293.4	100 / 100
8.46	836.58218	791.58397	$[M+HCOO]^-$	PC O-16:0_22:6	$C_{46}H_{82}NO_7P$	688.9	1.397	1.1	1.458	296.8	100 / 99.3
10.91	762.56706	717.56886	$[M+HCOO]^-$	PC O-16:1_16:0	$C_40H_80NO_7P$	837.6	2.113	2.1	1.414	288.3	100 / 100
11.22	788.58246	743.58426	$[M+HCOO]^-$	PC O-16:1_18:1	$C_{42}H_{82}NO_7P$	646.6	1.800	1.2	1.433	291.9	100 / 99.3
9.11	786.56691	741.56871	$[M+HCOO]^-$	PC O-16:1_18:2	$C_{42}H_80NO_7P$	789.6	1.657	1.2	1.424	290.2	100 / 99.3
12.00	840.6134	795.6152	$[M+HCOO]^-$	PC O-18:0_20:4	$C_{46}H_{86}NO_7P$	698.3	1.202	1.3	1.468	298.9	100 / 100

11.68	790.59805	745.59985	$[M+HCOO]^-$	PC O-18:1_16:0	$C_{42}H_{84}NO_7P$	678.0	1.755	0.9	1.432	291.8	100 / 99.3
9.29	838.59765	793.59945	$[M+HCOO]^-$	PC O-18:1_20:4	$C_{46}H_{84}NO_7P$	684.7	1.006	1.0	1.46	297.2	100 / 100
8.60	862.59725	817.59905	$[M+HCOO]^-$	PC O-18:1_22:6	$C_{48}H_{84}NO_7P$	533.1	0.623	1.4	1.478	300.7	100 / 99.3
14.04	868.64442	823.64622	$[M+HCOO]^-$	PC O-20:0_20:4	$C_{48}H_90NO_7P$	459.5	0.765	1.4	1.495	304.2	100 / 100
14.02	894.65891	849.6607	$[M+HCOO]^-$	PC O-22:1_20:4	$C_50H_{92}NO_7P$	449.1	-0.481	0.7	1.515	308.2	100 / 100
14.59	922.69079	877.69259	$[M+HCOO]^-$	PC O-24:1_20:4	$C_{52}H_{96}NO_7P$	622.7	0.144	1.0	1.543	313.6	100 / 100
10.88	718.57393	717.56665	$[M+H]^+$	PC O-32:1	$C_40H_80NO_7P$	994.6	-0.804	1.8	1.407	287.2	100 / 100
8.59	716.55803	715.55075	$[M+H]^+$	PC O-32:2	$C_40H_{78}NO_7P$	913.3	-0.935	1.3	1.386	282.8	100 / 98.6
13.92	748.62222	747.61495	$[M+H]^+$	PC O-34:0	$C_{42}H_{86}NO_7P$	947.2	0.989	1.9	1.448	295.4	100 / 100
11.63	746.60576	745.59848	$[M+H]^+$	PC O-34:1	$C_{42}H_{84}NO_7P$	993.8	-0.076	1.6	1.434	292.5	100 / 100
11.2	744.59017	743.5829	$[M+H]^+$	PC O-34:2	$C_{42}H_{82}NO_7P$	993.2	-0.034	1.3	1.422	290	100 / 100
9.09	742.57483	741.56755	$[M+H]^+$	PC O-34:3	$C_{42}H_80NO_7P$	996.4	0.390	0.6	1.403	286.2	100 / 100
13.85	772.62094	771.61367	$[M+H]^+$	PC O-36:2	$C_{44}H_{86}NO_7P$	999.5	-0.495	1.6	1.453	296.3	100 / 99.3
10.15	770.60545	769.59818	$[M+H]^+$	PC O-36:3	$C_{44}H_{84}NO_7P$	999.8	-0.562	0.9	1.433	292.2	100 / 100
9.69	770.60415	769.59688	$[M+H]^+$	PC O-36:3	$C_{44}H_{84}NO_7P$	995.3	-2.144	1.5	1.442	293.9	100 / 100
9.10	768.59072	767.58318	$[M+H]^+$,$[M+Na]^+$	PC O-36:4	$C_{44}H_{82}NO_7P$	995.4	0.720	1.6	1.434	292.3	100 / 100
7.65	766.57436	765.56709	$[M+H]^+$	PC O-36:5	$C_{44}H_80NO_7P$	991.5	-0.048	1.4	1.422	289.9	100 / 98.6
7.24	764.55933	763.55206	$[M+H]^+$	PC O-36:6	$C_{44}H_{78}NO_7P$	998.2	0.452	0.5	1.406	286.6	100 / 95.2
9.88	780.59213	779.58485	$[M+H]^+$	PC O-37:5	$C_{45}H_{82}NO_7P$	366.8	2.681	1.7	1.444	294.4	100 / 100
9.49	780.58942	779.58214	$[M+H]^+$	PC O-37:5	$C_{45}H_{82}NO_7P$	995.7	-0.962	0.9	1.433	292	100 / 100
11.07	796.62038	795.61311	$[M+H]^+$	PC O-38:4	$C_{46}H_{86}NO_7P$	994.5	-1.408	1.7	1.462	297.8	100 / 100

10.43	796.62012	795.61284	$[M+H]^+$	PC O-38:4	$C_{46}H_{86}NO_7P$	997.8	-1.581	1.6	1.46	297.5	100 / 100
10.51	794.60605	793.59877	$[M+H]^+$	PC O-38:5	$C_{46}H_{84}NO_7P$	997.2	0.381	1.6	1.455	296.5	100 / 100
7.74	792.58938	791.58211	$[M+H]^+$	PC O-38:6	$C_{46}H_{82}NO_7P$	999.8	-0.983	1.1	1.445	294.4	100 / 99.3
8.02	790.5746	789.56733	$[M+H]^+$	PC O-38:7	$C_{46}H_80NO_7P$	962.0	0.100	1.3	1.438	293.1	100 / 100
14.05	824.65311	823.64595	$[M+H]^+$,$[M+Na]^+$	PC O-40:4	$C_{48}H_90NO_7P$	998.6	0.390	1.9	1.489	303.3	100 / 100
13.81	824.65188	823.6446	$[M+H]^+$	PC O-40:4	$C_{48}H_90NO_7P$	995.4	-1.093	1.9	1.49	303.4	100 / 100
12.02	822.63701	821.62973	$[M+H]^+$	PC O-40:5	$C_{48}H_{88}NO_7P$	996.8	-0.026	1.5	1.48	301.3	100 / 100
11.27	822.63518	821.62791	$[M+H]^+$	PC O-40:5	$C_{48}H_{88}NO_7P$	999.8	-2.344	1.8	1.483	302	100 / 100
11.10	820.62123	819.61395	$[M+H]^+$	PC O-40:6	$C_{48}H_{86}NO_7P$	995.7	-0.294	1.7	1.478	300.9	100 / 98.6
8.60	818.60589	817.59781	$[M+H]^+$,$[M+Na]^+$	PC O-40:7	$C_{48}H_{84}NO_7P$	976.6	0.042	1.7	1.464	298.1	100 / 100
14.66	854.69864	853.69137	$[M+H]^+$	PC O-42:3	$C_50H_{96}NO_7P$	999.8	-1.039	1.3	1.523	310	100 / 100
14.61	852.68591	851.67864	$[M+H]^+$	PC O-42:4	$C_50H_{94}NO_7P$	974.1	1.866	1.4	1.521	309.5	80 / 100
14.01	850.66899	849.66171	$[M+H]^+$	PC O-42:5	$C_50H_{92}NO_7P$	991.0	0.771	0.7	1.506	306.5	100 / 100
13.88	848.65411	847.64683	$[M+H]^+$	PC O-42:6	$C_50H_90NO_7P$	965.6	1.339	1.0	1.502	305.6	100 / 100
14.58	878.70047	877.69287	$[M+H]^+$,$[M+Na]^+$	PC O-44:5	$C_{52}H_{96}NO_7P$	999.5	0.639	0.8	1.536	312.5	100 / 100
14.1	876.68442	875.67715	$[M+H]^+$	PC O-44:6	$C_{52}H_{94}NO_7P$	992.6	0.279	0.9	1.528	310.8	100 / 100
14.48	876.68203	875.67475	$[M+H]^+$	PC O-44:6	$C_{52}H_{94}NO_7P$	999.8	-2.004	1.0	1.53	311.3	100 / 100
13.79	874.67231	873.66503	$[M+H]^+$	PC O-44:7	$C_{52}H_{92}NO_7P$	984.4	4.123	1.5	1.522	309.6	100 / 98.6
14.42	902.7019	901.69462	$[M+H]^+$	PC O-46:7	$C_{54}H_{96}NO_7P$	984.9	2.353	1.2	1.55	315.1	100 / 100
10.61	716.52558	717.53286	$[M-H]^-$	PE 16:0_18:1	$C_{39}H_{76}NO_8P$	872.1	2.744	2.7	1.315	268.4	100 / 100
8.28	738.50966	739.51694	$[M-H]^-$	PE 16:0_20:4	$C_{41}H_{74}NO_8P$	786.3	2.364	n.r.	1.327	270.8	100 / 100

7.72	762.50961	763.51689	$[M-H]^-$	PE 16:0_22:6	$C_{43}H_{74}NO_8P$	669.8	2.309	n.r.	1.348	274.9	100 / 100
7.72	764.52289	763.51563	$[M+H]^+$,$[M+Na]^+$	PE 16:1_22:5	$C_{43}H_{74}NO_8P$	816.0	0.466	1.3	1.377	280.8	100 / 100
13.63	744.55711	745.56439	$[M-H]^-$	PE 18:0_18:1	$C_{41}H_80NO_8P$	237.9	2.827	2.0	1.349	275.1	100 / 100
11.29	744.55507	743.54779	$[M+H]^+$	PE 18:0_18:2	$C_{41}H_{78}NO_8P$	902.4	1.515	1.9	1.382	281.9	100 / 100
11.29	742.541	743.54828	$[M-H]^-$	PE 18:0_18:2	$C_{41}H_{78}NO_8P$	906.4	2.388	2.9	1.34	273.4	100 / 100
10.83	768.55344	767.54673	$[M+H]^+$,$[M+Na]^+$	PE 18:0_20:4	$C_{43}H_{78}NO_8P$	794.4	-0.343	1.7	1.401	285.7	100 / 100
10.84	766.54091	767.54818	$[M-H]^-$	PE 18:0_20:4	$C_{43}H_{78}NO_8P$	735.4	2.233	1.1	1.36	277.2	100 / 100
10.1	790.54066	791.54794	$[M-H]^-$	PE 18:0_22:6	$C_{45}H_{78}NO_8P$	931.8	1.849	2.7	1.38	281.3	100 / 100
13.62	746.56877	745.5615	$[M+H]^+$	PE 18:1_18:0	$C_{41}H_80NO_8P$	919.6	-0.932	1.1	1.397	285	100 / 99.3
10.91	742.54123	743.5485	$[M-H]^-$	PE 18:1_18:1	$C_{41}H_{78}NO_8P$	978.9	2.720	3.0	1.339	273.1	100 / 99.3
8.87	740.52543	741.5327	$[M-H]^-$	PE 18:1_18:2	$C_{41}H_{76}NO_8P$	866.3	2.737	1.7	1.33	271.3	100 / 98.6
8.5	764.52529	765.53257	$[M-H]^-$	PE 18:1_20:4	$C_{43}H_{76}NO_8P$	949.7	2.406	2.4	1.348	274.9	100 / 99.3
8.63	714.50986	715.51714	$[M-H]^-$	PE 18:2_16:0	$C_{39}H_{74}NO_8P$	844.7	2.782	0.8	1.307	266.8	100 / 100
10.59	718.53897	717.53199	$[M+H]^+$,$[M+Na]^+$	PE 34:1	$C_{39}H_{76}NO_8P$	972.7	0.871	1.2	1.36	277.6	100 / 100
8.62	716.52246	715.51655	$[M+H]^+$,$[M+Na]^+$	PE 34:2	$C_{39}H_{74}NO_8P$	988.1	-0.039	1.8	1.347	274.9	100 / 100
8.27	740.52263	739.51543	$[M+H]^+$,$[M+Na]^+$	PE 36:4	$C_{41}H_{74}NO_8P$	856.7	0.176	2.0	1.366	278.7	100 / 100
6.96	738.50702	737.49974	$[M+H]^+$	PE 36:5	$C_{41}H_{72}NO_8P$	844.3	0.275	1.8	1.352	275.9	100 / 100
10.09	792.55472	791.5474	$[M+H]^+$,$[M+Na]^+$	PE 40:6	$C_{45}H_{78}NO_8P$	937.1	1.174	0.9	1.409	287	100 / 100
7.96	790.54021	789.53293	$[M+H]^+$	PE 40:7	$C_{45}H_{76}NO_8P$	932.7	2.127	0.0	1.39	283.2	100 / 93.1
9.82	700.53217	699.52489	$[M+H]^+$	PE O-16:1_18:2	$C_{39}H_{74}NO_7P$	939.3	4.790	1.7	1.334	272.4	80 / 92.4
9.8	698.51478	699.52206	$[M-H]^-$	PE O-16:1_18:2	$C_{39}H_{74}NO_7P$	983.8	2.617	2.8	1.304	266.3	100 / 96.6

9.35	724.5276	723.52032	$[M+H]^+$	PE O-16:1_20:4	$C_{41}H_{74}NO_7P$	929.7	0.037	2.6	1.354	276.4	100 / 100
9.35	722.51491	723.52218	$[M-H]^-$	PE O-16:1_20:4	$C_{41}H_{74}NO_7P$	955.8	2.634	3.4	1.326	270.6	100 / 100
8.66	748.52778	747.52051	$[M+H]^+$	PE O-16:1_22:6	$C_{43}H_{74}NO_7P$	896.1	0.306	2.3	1.367	278.9	100 / 100
8.69	746.51474	747.52201	$[M-H]^-$	PE O-16:1_22:6	$C_{43}H_{74}NO_7P$	990.8	2.517	3.5	1.345	274.3	100 / 100
14.05	730.57228	729.56501	$[M+H]^+$	PE O-18:1_18:1	$C_{41}H_80NO_7P$	946.5	-3.097	2.3	1.389	283.4	100 / 95.9
14.06	728.56116	729.56844	$[M-H]^-$	PE O-18:1_18:1	$C_{41}H_80NO_7P$	990.8	1.643	3.1	1.344	274.3	100 / 98.6
12.82	728.55824	727.55096	$[M+H]^+$	PE O-18:1_18:2	$C_{41}H_{78}NO_7P$	943.2	-0.798	2.0	1.37	279.6	100 / 98.6
12.24	752.55966	751.55238	$[M+H]^+$	PE O-18:1_20:4	$C_{43}H_{78}NO_7P$	933.2	1.046	1.9	1.389	283.4	100 / 100
12.25	750.54607	751.55334	$[M-H]^-$	PE O-18:1_20:4	$C_{43}H_{78}NO_7P$	948.2	2.339	3.1	1.356	276.6	100 / 100
10.25	750.54386	749.53658	$[M+H]^+$	PE O-18:1_20:5	$C_{43}H_{76}NO_7P$	909.8	0.741	1.5	1.379	281.2	60 / 75.2
13.88	780.58812	779.58084	$[M+H]^+$	PE O-18:1_22:4	$C_{45}H_{82}NO_7P$	928.7	-3.111	1.3	1.423	290	100 / 87.6
13.88	778.57618	779.58346	$[M-H]^-$	PE O-18:1_22:4	$C_{45}H_{82}NO_7P$	931.0	1.075	2.7	1.384	282.2	100 / 98.6
11.37	774.54567	775.55295	$[M-H]^-$	PE O-18:1_22:6	$C_{45}H_{78}NO_7P$	912.9	1.793	3.0	1.375	280.3	100 / 100
9.59	748.53049	749.53777	$[M-H]^-$	PE O-18:2_20:4	$C_{43}H_{76}NO_7P$	870.7	2.485	2.9	1.348	274.9	100 / 100
8.91	774.54335	773.53608	$[M+H]^+$	PE O-18:2_22:6	$C_{45}H_{76}NO_7P$	862.7	0.175	0.9	1.386	282.5	100 / 99.3
8.93	772.5305	773.53778	$[M-H]^-$	PE O-18:2_22:6	$C_{45}H_{76}NO_7P$	932.7	2.343	2.8	1.367	278.6	100 / 98.6
14.09	778.57658	779.58386	$[M-H]^-$	PE O-20:1_20:4	$C_{45}H_{82}NO_7P$	902.4	1.448	2.1	1.386	282.5	100 / 97.9
5.87	807.50424	808.51152	$[M-H]^-$	PI 16:0_16:1	$C_{41}H_{77}O_{13}P$	735.5	2.040	2.9	1.395	284.1	100 / 95.2
6.2	833.5196	834.52688	$[M-H]^-$	PI 16:0_18:2	$C_{43}H_{79}O_{13}P$	299.0	1.255	2.6	1.416	288.4	100 / 100
6	857.51949	858.52677	$[M-H]^-$	PI 16:0_20:4	$C_{45}H_{79}O_{13}P$	645.6	1.098	2.9	1.435	292.1	100 / 100
7.53	835.53538	836.54266	$[M-H]^-$	PI 18:0_16:1	$C_{43}H_{81}O_{13}P$	523.4	1.398	2.7	1.424	289.8	100 / 100

8	861.55086	862.55814	$[M-H]^-$	PI 18:0_18:2	$C_{45}H_{83}O_{13}P$	683.8	1.217	3.8	1.456	296.3	100 / 100
7.74	885.5506	886.55788	$[M-H]^-$	PI 18:0_20:4	$C_{47}H_{83}O_{13}P$	680.9	0.887	3.6	1.471	299.3	100 / 100
7.5	854.57164	836.53782	$[M+NH_4]^+$	PI 34:1	$C_{43}H_{81}O_{13}P$	832.9	-4.266	3.4	1.475	300.1	100 / 100
6.2	852.55963	834.5258	$[M+NH_4]^+$	PI 34:2	$C_{43}H_{79}O_{13}P$	750.2	-0.106	2.7	1.457	296.6	100 / 100
9.76	882.60453	864.57071	$[M+NH_4]^+$	PI 36:1	$C_{45}H_{85}O_{13}P$	933.7	-2.31	1.1.	1.502	305.5	100 / 96.6
8.01	880.59125	862.55727	$[M+NH_4]^+$,$[M+H]^+$	PI 36:2	$C_{45}H_{83}O_{13}P$	794.3	0.304	3.0	1.486	302.2	100 / 100
7.73	880.58707	862.55325	$[M+NH_4]^+$	PI 36:2	$C_{45}H_{83}O_{13}P$	724.6	-2.024	3.1	1.488	302.6	100 / 90
6.64	859.53376	860.54103	$[M-H]^-$	PI 36:3	$C_{45}H_{81}O_{13}P$	222.9	-0.681	0.6	1.439	292.7	100 / 98.6
6	876.56329	858.52947	$[M+NH_4]^+$	PI 36:4	$C_{45}H_{79}O_{13}P$	850.1	3.571	3.2	1.476	300.3	100 / 97.9
8.59	906.60844	888.57262	$[M+NH_4]^+$,$[M+H]^+$	PI 38:3	$C_{47}H_{85}O_{13}P$	892.2	2.063	1.5	1.509	306.8	100 / 91.7
7.74	904.59174	886.55774	$[M+NH_4]^+$,$[M+H]^+$,$[M+Na]^+$	PI 38:4	$C_{47}H_{83}O_{13}P$	717.5	0.906	3.5	1.503	305.7	100 / 100
7.25	928.58829	910.55447	$[M+NH_4]^+$	PI 40:6	$C_{49}H_{83}O_{13}P$	736.1	-2.915	3.2	1.518	308.6	100 / 95.2
6.96	703.57469	702.56741	$[M+H]^+$	SM 18:1;O2/16:0	$C_{39}H_{79}N_2O_6P$	997.8	-0.207	0.8	1.408	287.5	100 / 100
7.18	703.57585	702.56858	$[M+H]^+$	SM 18:1;O2/16:0	$C_{39}H_{79}N_2O_6P$	998.5	1.433	0.7	1.407	287.2	100 / 100
12.44	759.63776	758.63049	$[M+H]^+$	SM 18:1;O2/20:0	$C_{43}H_{87}N_2O_6P$	994.4	0.407	1.1	1.464	298.5	100 / 100
7.07	805.62055	804.61328	$[M+H]^+$	SM 20:2;O2/22:4	$C_{47}H_{85}N_2O_6P$	981.5	-1.053	0.4	1.461	297.5	100 / 95.9
4.29	647.51184	646.50456	$[M+H]^+$	SM 30:1;O2	$C_{35}H_{71}N_2O_6P$	1000	-0.600	2.8	1.348	275.6	80 / 100
5.53	675.54374	674.53646	$[M+H]^+$	SM 32:1;O2	$C_{37}H_{75}N_2O_6P$	950.3	0.269	1.7	1.38	282	100 / 100
4.47	673.52797	672.5207	$[M+H]^+$	SM 32:2;O2	$C_{37}H_{73}N_2O_6P$	982.0	0.086	1.1	1.359	277.8	100 / 100
6.30	689.55922	688.55195	$[M+H]^+$	SM 33:1;O2	$C_{38}H_{77}N_2O_6P$	959.8	0.031	1.2	1.394	284.7	100 / 100
7.97	705.58994	704.58286	$[M+H]^+[M+Na]^+$	SM 34:0;O2	$C_{39}H_{81}N_2O_6P$	993.0	-0.803	1.7	1.429	291.8	100 / 100

6.62	719.56909	718.56181	$[M+H]^+$	SM 34:1;3O	$C_{39}H_{79}N_2O_7P$	928.1	-0.858	3.3	1.442	294.3	100 / 100
5.75	701.5599	700.55187	$[M+H]^+[M+Na]^+$	SM 34:2;O2	$C_{39}H_{77}N_2O_6P$	965.9	1.005	0.8	1.392	284.3	100 / 100
8.21	717.59047	716.58319	$[M+H]^+$	SM 35:1;O2	$C_40H_{81}N_2O_6P$	1000	-0.029	0.7	1.426	291.1	100 / 100
10.47	733.62102	732.61509	$[M+H]^+[M+Na]^+$	SM 36:0;O2	$C_{41}H_{85}N_2O_6P$	952.0	-0.94	1.7	1.456	297.1	100 / 100
9.45	731.60667	730.59974	$[M+H]^+[M+Na]^+$	SM 36:1;O2	$C_{41}H_{83}N_2O_6P$	960.2	0.763	0.6	1.435	292.8	100 / 100
7.50	729.59087	728.5836	$[M+H]^+$	SM 36:2;O2	$C_{41}H_{81}N_2O_6P$	952.8	0.620	0.1	1.419	289.5	100 / 100
7.17	725.55693	724.54965	$[M+H]^+$	SM 36:4;O2	$C_{41}H_{77}N_2O_6P$	920.4	-3.097	2.0	1.416	289	100 / 100
8.6	743.60527	742.59799	$[M+H]^+$	SM 37:2;O2	$C_{42}H_{83}N_2O_6P$	297.1	-1.22	0.9	1.438	293.3	60 / 98.6
13.6	761.65013	760.64285	$[M+H]^+$	SM 38:0;O2	$C_{43}H_{89}N_2O_6P$	901.1	-4.139	0.6	1.476	301	100 / 100
9.85	757.62158	756.6143	$[M+H]^+$	SM 38:2;O2	$C_{43}H_{85}N_2O_6P$	496.0	-0.299	0.7	1.454	296.4	100 / 100
7.49	751.57219	750.56492	$[M+H]^+$	SM 38:5;O2	$C_{43}H_{79}N_2O_6P$	756.7	-3.593	2.8	1.416	288.9	100 / 98.6
13.77	773.65306	772.64515	$[M+H]^+$,$[M+Na]^+$	SM 39:1;O2	$C_{44}H_{89}N_2O_6P$	944.5	-0.113	0.2	1.478	301.2	100 / 100
11.34	771.63738	770.6301	$[M+H]^+$	SM 39:2;O2	$C_{44}H_{87}N_2O_6P$	608.8	-0.496	0.0	1.465	298.7	100 / 100
14.38	789.68198	788.67471	$[M+H]^+$	SM 40:0;O2	$C_{45}H_{93}N_2O_6P$	917.0	-3.014	0.8	1.5	305.6	100 / 99.3
14.13	787.66937	786.6621	$[M+H]^+$	SM 40:1;O2	$C_{45}H_{91}N_2O_6P$	948.9	0.784	0.0	1.487	303.1	100 / 100
12.91	785.65329	784.64587	$[M+H]^+$,$[M+Na]^+$	SM 40:2;O2	$C_{45}H_{89}N_2O_6P$	852.1	0.241	0.2	1.48	301.6	100 / 100
12.39	785.65344	784.64617	$[M+H]^+$	SM 40:2;O2	$C_{45}H_{89}N_2O_6P$	939.4	0.493	0.2	1.479	301.5	100 / 100
7.98	781.62137	780.61409	$[M+H]^+$	SM 40:4;O2	$C_{45}H_{85}N_2O_6P$	163.5	-0.427	0.7	1.452	295.9	100 / 91
9.85	779.60271	778.59543	$[M+H]^+$	SM 40:5;O2	$C_{45}H_{83}N_2O_6P$	184.6	-4.439	0.7	1.452	296	100 / 97.9
14.46	801.68485	800.67797	$[M+H]^+$,$[M+K]^+$,$[M+Na]^+$	SM 41:1;O2	$C_{46}H_{93}N_2O_6P$	914.6	0.52	0.6	1.504	306.3	100 / 100
13.73	799.66899	798.66188	$[M+H]^+$,$[M+Na]^+$	SM 41:2;O2	$C_{46}H_{91}N_2O_6P$	952.0	0.404	0.6	1.493	304.1	100 / 99.3

13.91	799.6691	798.66192	$[M+H]^+$,$[M+K]^+$,$[M+Na]^+$	SM 41:2;O2	$C_{46}H_{91}N_2O_6P$	947.5	0.551	0.4	1.49	303.5	100 / 100
14.72	815.70051	814.69377	$[M+H]^+$,$[M+Na]^+$,$[M+K]^+$	SM 42:1;O2	$C_{47}H_{95}N_2O_6P$	939.5	0.596	0.6	1.518	309.1	100 / 100
14.24	813.68491	812.67712	$[M+H]^+$,$[M+Na]^+$	SM 42:2;O2	$C_{47}H_{93}N_2O_6P$	929.6	0.720	0.8	1.505	306.5	100 / 89.7
14.11	813.68556	812.67786	$[M+H]^+$,$[M+Na]^+$,$[M+K]^+$	SM 42:2;O2	$C_{47}H_{93}N_2O_6P$	949.0	1.445	0.8	1.506	306.7	100 / 100
12.83	811.66973	810.66245	$[M+H]^+$	SM 42:3;O2	$C_{47}H_{91}N_2O_6P$	947.7	1.261	1.00	1.495	304.6	100 / 100
10.27	809.65237	808.6451	$[M+H]^+$	SM 42:4;O2	$C_{47}H_{89}N_2O_6P$	437.7	-0.841	0.3	1.482	301.9	100 / 99.3
5.55	801.59732	800.59004	$[M+H]^+$	SM 42:8;O2	$C_{47}H_{81}N_2O_6P$	201.2	4.989	0.0	1.431	291.5	60 / 97.2
14.93	829.71567	828.70839	$[M+H]^+$	SM 43:1;O2	$C_{48}H_{97}N_2O_6P$	1000	0.138	0.9	1.53	311.5	100 / 100
14.33	827.69971	826.69329	$[M+H]^+$,$[M+Na]^+$	SM 43:2;O2	$C_{48}H_{95}N_2O_6P$	942.1	-0.416	0.3	1.518	309	100 / 100
13.85	825.68408	824.6768	$[M+H]^+$	SM 43:3;O2	$C_{48}H_{93}N_2O_6P$	349.1	-0.330	0.2	1.506	306.7	100 / 97.9
14.69	841.71612	840.70885	$[M+H]^+$	SM 44:2;O2	$C_{49}H_{97}N_2O_6P$	585.3	0.577	0.8	1.533	312.1	100 / 100
15.29	710.63017	692.59828	$[M+NH_4]^+$,$[M+K]^+$,$[M+Na]^+$	TG 10:0_12:0_18:1	$C_{43}H_80O_6$	917.3	1.172	1.9	1.401	286	80 / 91
16.25	820.73988	802.70598	$[M+NH_4]^+$,$[M+Na]^+$	TG 12:0_18:1_18:1	$C_{51}H_{94}O_6$	848.2	1.36	2.7	1.523	310.2	100 / 100
16.01	818.72406	800.68978	$[M+NH_4]^+$,$[M+Na]^+$,$[M+K]^+$	TG 12:0_18:1_18:2	$C_{51}H_{92}O_6$	835.3	1.000	2.9	1.512	308	100 / 100
15.79	816.70765	798.67382	$[M+NH_4]^+$	TG 12:0_18:2_18:2	$C_{51}H_90O_6$	785.6	0.438	3.0	1.502	305.9	100 / 97.9
16.03	844.73946	826.70553	$[M+NH_4]^+$,$[M+K]^+$,$[M+Na]^+$	TG 14:0_18:2_18:2	$C_{53}H_{94}O_6$	825.9	0.951	2.6	1.53	311.5	100 / 100
16.60	836.77105	818.73792	$[M+NH_4]^+$,$[M+K]^+$	TG 15:0_16:0_18:1	$C_{52}H_{98}O_6$	816.6	1.051	2.6	1.552	315.9	100 / 100
16.61	862.78696	844.75313	$[M+NH_4]^+$	TG 15:0_18:1_18:1	$C_{54}H_100O_6$	770.0	1.357	2.4	1.569	319.3	100 / 100
16.17	858.75594	840.72313	$[M+NH_4]^+$,$[M+K]^+$,$[M+Na]^+$	TG 15:0_18:2_18:2	$C_{54}H_{96}O_6$	816.1	1.458	2.5	1.546	314.6	100 / 100
16.73	850.78705	832.75323	$[M+NH_4]^+$	TG 16:0_16:0_18:1	$C_{53}H_100O_6$	867.9	1.454	2.0	1.564	318.3	100 / 100
16.49	848.77178	830.73753	$[M+NH_4]^+$,$[M+K]^+$	TG 16:0_16:1_18:1	$C_{53}H_{98}O_6$	827.3	1.913	2.3	1.554	316.2	100 / 100

16.83	864.80237	846.76855	$[M+NH_4]^+$	TG 16:0_17:0_18:1	$C_{54}H_{102}O_6$	853.6	0.985	2.2	1.582	321.9	100 / 100
16.95	878.81863	860.7848	$[M+NH_4]^+$	TG 16:0_18:0_18:1	$C_{55}H_{104}O_6$	840.3	1.718	2.2	1.595	324.5	100 / 100
16.73	876.80328	858.76946	$[M+NH_4]^+$	TG 16:0_18:1_18:1	$C_{55}H_{102}O_6$	865.2	2.07	2.8	1.586	322.6	100 / 100
16.53	874.78788	856.7535	$[M+NH_4]^+$,$[M+Na]^+$	TG 16:0_18:1_18:2	$C_{55}H_{100}O_6$	785.4	2.358	2.6	1.574	320.2	100 / 100
16.43	924.80278	906.76882	$[M+NH_4]^+$,$[M+Na]^+$	TG 16:0_18:1_22:5	$C_{59}H_{102}O_6$	667.7	1.398	2.6	1.615	328.3	100 / 100
16.33	922.78709	904.75302	$[M+NH_4]^+$,$[M+Na]^+$	TG 16:0_18:1_22:6	$C_{59}H_{100}O_6$	648.8	1.375	2.9	1.612	327.6	100 / 99.3
16.22	896.77173	878.7379	$[M+NH_4]^+$	TG 16:0_18:2_20:4	$C_{57}H_{98}O_6$	640.0	1.785	2.6	1.582	321.7	80 / 98.6
16.22	922.78699	904.7528	$[M+NH_4]^+$,$[M+Na]^+$	TG 16:0_18:2_22:5	$C_{59}H_{100}O_6$	614.2	1.310	2.5	1.603	325.9	100 / 98.6
15.72	866.72322	848.68918	$[M+NH_4]^+$,$[M+Na]^+$,$[M+K]^+$	TG 16:0_18:3_18:4	$C_{55}H_{92}O_6$	638.1	-0.56	1.9	1.531	311.6	100 / 97.9
16.02	944.7718	926.7368	$[M+NH_4]^+$,$[M+K]^+$,$[M+Na]^+$	TG 16:0_20:4_22:6	$C_{61}H_{98}O_6$	580.2	1.909	2.9	1.616	328.3	60 / 93.1
16.09	870.75426	852.72043	$[M+NH_4]^+$	TG 16:1_18:2_18:2	$C_{55}H_{96}O_6$	749.1	-0.145	2.8	1.555	316.3	100 / 97.9
16.83	890.81839	872.78437	$[M+NH_4]^+$,$[M+K]^+$,$[M+Na]^+$	TG 17:0_18:1_18:1	$C_{56}H_{104}O_6$	852.1	1.380	2.1	1.603	326	80 / 100
16.62	888.80255	870.76872	$[M+NH_4]^+$	TG 17:0_18:1_18:2	$C_{56}H_{102}O_6$	740.3	1.292	2.7	1.588	322.9	100 / 100
16.41	886.78689	868.75307	$[M+NH_4]^+$,$[M+K]^+$,$[M+Na]^+$	TG 17:1_18:1_18:2	$C_{56}H_{100}O_6$	777.8	1.224	2.7	1.576	320.6	100 / 100
16.22	934.7907	916.75688	$[M+NH_4]^+$	TG 17:1_18:1_22:6	$C_{60}H_{100}O_6$	578.3	4.995	3.0	1.619	329.1	80 / 95.2
16.67	926.81857	908.78326	$[M+NH_4]^+$,$[M+Na]^+$	TG 18:0_18:1_20:4	$C_{59}H_{104}O_6$	569.9	1.619	2.9	1.621	329.5	100 / 100
16.66	900.80199	882.76816	$[M+NH_4]^+$	TG 18:0_18:2_18:2	$C_{57}H_{102}O_6$	889.6	0.871	3.3	1.601	325.6	80 / 89.6
15.86	894.75388	876.72005	$[M+NH_4]^+$	TG 18:0_18:2_18:5	$C_{57}H_{96}O_6$	404.6	-1.378	1.9	1.562	317.6	100 / 79.3
17.15	906.84946	888.81513	$[M+NH_4]^+$,$[M+K]^+$,$[M+Na]^+$	TG 18:0_20:1_16:0	$C_{57}H_{108}O_6$	705.1	1.127	2.8	1.628	331	100 / 100
16.5	822.75551	804.72158	$[M+NH_4]^+$,$[M+Na]^+$	TG 18:1_16:0_14:0	$C_{51}H_{96}O_6$	899.0	1.205	1.6	1.536	312.8	100 / 100
16.73	902.81869	884.78487	$[M+NH_4]^+$	TG 18:1_18:1_18:1	$C_{57}H_{104}O_6$	808.6	1.746	2.7	1.607	326.8	100 / 100

16.95	904.83445	886.80062	$[M+NH_4]^+$	TG 18:1_18:1_18:0	$C_{57}H_{106}O_6$	676.9	1.863	2.9	1.617	328.8	100 / 100
16.52	900.8026	882.76878	$[M+NH_4]^+$	TG 18:1_18:1_18:2	$C_{57}H_{102}O_6$	845.2	1.262	3.0	1.596	324.5	100 / 100
16.94	930.84942	912.81559	$[M+NH_4]^+$	TG 18:1_18:1_20:1	$C_{59}H_{108}O_6$	818.3	1.300	3.0	1.636	332.5	100 / 100
16.63	952.83442	934.8006	$[M+NH_4]^+$	TG 18:1_18:1_22:4	$C_{61}H_{106}O_6$	744.7	1.858	3.2	1.643	333.8	100 / 100
16.33	948.80333	930.76951	$[M+NH_4]^+$	TG 18:1_18:1_22:6	$C_{61}H_{102}O_6$	576.2	1.961	3.3	1.63	331.3	100 / 99.3
16.31	898.78681	880.75282	$[M+NH_4]^+$,$[M+Na]^+$	TG 18:1_18:2_18:2	$C_{57}H_{100}O_6$	812.8	1.109	2.4	1.584	322.1	100 / 100
17.05	944.86537	926.83154	$[M+NH_4]^+$	TG 18:1_18:2_21:0	$C_{60}H_{110}O_6$	654.5	1.281	4.2	1.664	338.1	100 / 92.4
17.14	958.88106	940.84691	$[M+NH_4]^+$,$[M+Na]^+$	TG 18:1_18:2_22:0	$C_{61}H_{112}O_6$	691.5	0.960	2.9	1.662	337.6	100 / 100
16.12	946.78741	928.75318	$[M+NH_4]^+$,$[M+Na]^+$	TG 18:1_18:2_22:6	$C_{61}H_{100}O_6$	625.9	1.581	3.0	1.619	329.1	100 / 100
17.34	986.91181	968.87799	$[M+NH_4]^+$	TG 18:1_18:2_24:0	$C_{63}H_{116}O_6$	770.0	0.701	3.2	1.687	342.5	100 / 75.2
16.26	846.75602	828.72154	$[M+NH_4]^+$,$[M+K]^+$,$[M+Na]^+$	TG 18:2_18:1_14:0	$C_{53}H_{96}O_6$	689.6	1.787	1.8	1.543	314	100 / 100
16.39	860.77117	842.73837	$[M+NH_4]^+$,$[M+Na]^+$,$[M+K]^+$	TG 18:2_18:1_15:0	$C_{54}H_{98}O_6$	631.0	1.179	1.7	1.558	317.1	100 / 100
16.30	872.77207	854.73728	$[M+NH_4]^+$,$[M+K]^+$,$[M+Na]^+$	TG 18:2_18:1_16:1	$C_{55}H_{98}O_6$	643.0	2.182	2.0	1.563	318	100 / 100
16.00	920.77107	902.73666	$[M+NH_4]^+$,$[M+Na]^+$,$[M+K]^+$	TG 18:2_18:2_20:4	$C_{59}H_{98}O_6$	432.7	1.095	2.0	1.592	323.5	100 / 88.3
15.83	918.75356	900.72099	$[M+NH_4]^+$,$[M+K]^+$,$[M+Na]^+$	TG 18:2_18:2_20:5	$C_{59}H_{96}O_6$	560.8	-0.935	2.6	1.587	322.5	80 / 100
15.89	944.77046	926.7357	$[M+NH_4]^+$,$[M+K]^+$,$[M+Na]^+$	TG 18:2_18:2_22:6	$C_{61}H_{98}O_6$	461.3	0.566	1.9	1.597	324.5	100 / 100
16.82	954.84911	936.81492	$[M+NH_4]^+$,$[M+Na]^+$	TG 18:2_18:3_22:0	$C_{61}H_{108}O_6$	713.3	0.747	3.3	1.653	335.8	100 / 97.9

Rt: retention time; **% QC / SAMPLES**: Percentage of QC and patient samples in which the lipid was detected.

Table S5.2. *ANOVA analysis results.*

Compound	f.value	p.value	-log10 (p)	FDR	Fisher's LSD
LPC 20:1	135.49	$3.50E^{-31}$	30.456	$1.22E^{-28}$	COVID (-) - MILD; COVID (-) - SEVERE; MILD - SEVERE
LPC O-16:0	125.2	$8.48E^{-30}$	29.072	$1.48E^{-27}$	COVID (-) - MILD; COVID (-) - SEVERE; MILD - SEVERE
LPC O-18:1	117.23	$1.13E^{-28}$	27.945	$1.32E^{-26}$	COVID (-) - MILD; COVID (-) - SEVERE; MILD - SEVERE
LPC 18:0	89.504	$2.62E^{-24}$	23.582	$2.28E^{-22}$	COVID (-) - MILD; COVID (-) - SEVERE; MILD - SEVERE
TG 18:1_18:2_22:6	84.754	$1.76E^{-23}$	22.754	$1.23E^{-21}$	MILD - COVID (-); SEVERE - COVID (-)
TG 16:0_20:4_22:6	83.312	$3.19E^{-23}$	22.497	$1.85E^{-21}$	MILD - COVID (-); SEVERE - COVID (-)
TG 16:0_18:1_22:5	82.563	$4.34E^{-23}$	22.362	$2.16E^{-21}$	MILD - COVID (-); SEVERE - COVID (-)
PC O-34:3	80.814	$9.01E^{-23}$	22.045	$3.92E^{-21}$	COVID (-) - MILD; COVID (-) - SEVERE; MILD - SEVERE
LPC O-16:1	79.484	$1.58E^{-22}$	21.801	$5.71E^{-21}$	COVID (-) - MILD; COVID (-) - SEVERE; MILD - SEVERE
TG 16:0_18:2_20:4	79.396	$1.64E^{-22}$	21.785	$5.71E^{-21}$	MILD - COVID (-); SEVERE - COVID (-)
TG 18:2_18:2_22:6	68.901	$1.68E^{-20}$	19.774	$5.32E^{-19}$	MILD - COVID (-); SEVERE - COVID (-)
LPC 17:0	67.915	$2.65E^{-20}$	19.577	$7.69E^{-19}$	COVID (-) - MILD; COVID (-) - SEVERE; MILD - SEVERE
TG 18:1_18:1_22:6	67.1	$3.87E^{-20}$	19.412	$1.04E^{-18}$	MILD - COVID (-); SEVERE - COVID (-)
TG 18:0_18:1_20:4	66.236	$5.80E^{-20}$	19.237	$1.44E^{-18}$	MILD - COVID (-); SEVERE - COVID (-)
LPC 20:2	65.586	$7.87E^{-20}$	19.104	$1.83E^{-18}$	COVID (-) - MILD; COVID (-) - SEVERE; MILD - SEVERE
PE 18:0_22:6	55.399	$1.18E^{-17}$	16.928	$2.57E^{-16}$	MILD - COVID (-); SEVERE - COVID (-); SEVERE - MILD
PE 16:0_22:6	54.537	$1.84E^{-17}$	16.735	$3.77E^{-16}$	MILD - COVID (-); SEVERE - COVID (-); SEVERE - MILD
SM 30:1;O2	54.186	$2.21E^{-17}$	16.656	$4.27E^{-16}$	COVID (-) - MILD; COVID (-) - SEVERE
LPC 16:0	51.213	$1.06E^{-16}$	15.976	$1.93E^{-15}$	COVID (-) - MILD; COVID (-) - SEVERE; MILD - SEVERE
PC 37:2	50.904	$1.25E^{-16}$	15.905	$2.17E^{-15}$	COVID (-) - MILD; COVID (-) - SEVERE
Hex-Cer 18:1;O2/22:0	49.345	$2.88E^{-16}$	15.54	$4.78E^{-15}$	COVID (-) - MILD; COVID (-) - SEVERE
PC O-16:1_18:2	48.384	$4.87E^{-16}$	15.313	$7.70E^{-15}$	COVID (-) - MILD; COVID (-) - SEVERE; MILD - SEVERE
LPE 18:0	48.026	$5.92E^{-16}$	15.227	$8.96E^{-15}$	COVID (-) - MILD; COVID (-) - SEVERE; MILD - SEVERE
LPC 18:1*	47.696	$7.10E^{-16}$	15.149	$1.01E^{-14}$	COVID (-) - MILD; COVID (-) - SEVERE; MILD - SEVERE
TG 16:0_18:1_22:6	47.655	$7.26E^{-16}$	15.139	$1.01E^{-14}$	MILD - COVID (-); SEVERE - COVID (-)
LPC 18:1	46.751	$1.20E^{-15}$	14.922	$1.60E^{-14}$	COVID (-) - MILD; COVID (-) - SEVERE; MILD - SEVERE
PE 16:0_18:1	46.453	$1.41E^{-15}$	14.85	$1.82E^{-14}$	MILD - COVID (-); SEVERE - COVID (-); SEVERE - MILD
TG 18:1_18:1_22:4	44.785	$3.61E^{-15}$	14.443	$4.49E^{-14}$	MILD - COVID (-); SEVERE - COVID (-)
PE 16:0_20:4	43.733	$6.57E^{-15}$	14.183	$7.88E^{-14}$	MILD - COVID (-); SEVERE - COVID (-)
Cer 18:1;O2/24:1	42.886	$1.07E^{-14}$	13.971	$1.24E^{-13}$	MILD - COVID (-); SEVERE - COVID (-)
LPC 17:1	42.115	$1.67E^{-14}$	13.777	$1.88E^{-13}$	COVID (-) - MILD; COVID (-) - SEVERE; MILD - SEVERE

Hex-Cer 18:1;O2/24:0	41.747	$2.07E^{-14}$	13.684	$2.25E^{-13}$	COVID (-) - MILD; COVID (-) - SEVERE
PE 16:1_22:5	41.271	$2.73E^{-14}$	13.563	$2.88E^{-13}$	MILD - COVID (-); SEVERE - COVID (-)
LPC 14:0	40.869	$3.46E^{-14}$	13.461	$3.54E^{-13}$	COVID (-) - MILD; COVID (-) - SEVERE; MILD - SEVERE
LPC 18:2	40.742	$3.73E^{-14}$	13.428	$3.71E^{-13}$	COVID (-) - MILD; COVID (-) - SEVERE; MILD - SEVERE
TG 18:2_18:2_20:5	40.437	$4.47E^{-14}$	13.35	$4.32E^{-13}$	MILD - COVID (-); SEVERE - COVID (-)
LPC 15:0	40.33	$4.76E^{-14}$	13.322	$4.48E^{-13}$	COVID (-) - MILD; COVID (-) - SEVERE; MILD - SEVERE
DG 18:1_20:4	40.251	$4.99E^{-14}$	13.302	$4.57E^{-13}$	MILD - COVID (-); SEVERE - COVID (-)
PC O-16:0_18:2	40.01	$5.75E^{-14}$	13.24	$5.13E^{-13}$	COVID (-) - MILD; COVID (-) - SEVERE; MILD - SEVERE
LPC 18:2*	39.533	$7.64E^{-14}$	13.117	$6.65E^{-13}$	COVID (-) - MILD; COVID (-) - SEVERE; MILD - SEVERE
PE 18:2_16:0	38.615	$1.33E^{-13}$	12.878	$1.13E^{-12}$	MILD - COVID (-); SEVERE - COVID (-); SEVERE - MILD
PC O-34:2	37.966	$1.96E^{-13}$	12.707	$1.59E^{-12}$	COVID (-) - MILD; COVID (-) - SEVERE; MILD - SEVERE
TG 16:0_18:2_22:5	37.965	$1.96E^{-13}$	12.707	$1.59E^{-12}$	MILD - COVID (-); SEVERE - COVID (-)
PE 40:6	35.775	$7.52E^{-13}$	12.124	$5.95E^{-12}$	MILD - COVID (-); SEVERE - COVID (-)
LPC 20:3*	35.027	$1.20E^{-12}$	11.921	$9.27E^{-12}$	COVID (-) - MILD; COVID (-) - SEVERE; MILD - SEVERE
SM 39:1;O2	34.651	$1.52E^{-12}$	11.819	$1.15E^{-11}$	COVID (-) - MILD; COVID (-) - SEVERE
SM 42:1;O2	32.04	$8.01E^{-12}$	11.096	$5.93E^{-11}$	COVID (-) - MILD; COVID (-) - SEVERE
TG 16:0_18:1_18:2	31.476	$1.15E^{-11}$	10.938	$8.37E^{-11}$	MILD - COVID (-); SEVERE - COVID (-)
CE 18:0	31.272	$1.32E^{-11}$	10.88	$9.36E^{-11}$	COVID (-) - MILD; COVID (-) - SEVERE
PC 18:1_18:2	30.952	$1.62E^{-11}$	10.79	$1.13E^{-10}$	COVID (-) - MILD; COVID (-) - SEVERE
SM 40:2;O2	30.812	$1.78E^{-11}$	10.75	$1.21E^{-10}$	COVID (-) - MILD; COVID (-) - SEVERE
DG 18:2_22:6	30.689	$1.93E^{-11}$	10.714	$1.29E^{-10}$	MILD - COVID (-); SEVERE - COVID (-)
LPC 20:3	30.555	$2.11E^{-11}$	10.676	$1.38E^{-10}$	COVID (-) - MILD; COVID (-) - SEVERE; MILD - SEVERE
PE O-18:1_18:2	29.497	$4.24E^{-11}$	10.373	$2.73E^{-10}$	COVID (-) - MILD; COVID (-) - SEVERE
SM 41:1;O2	27.898	$1.24E^{-10}$	9.9067	$7.84E^{-10}$	COVID (-) - MILD; COVID (-) - SEVERE
TG 18:2_18:1_16:1	27.146	$2.07E^{-10}$	9.6849	$1.28E^{-09}$	MILD - COVID (-); SEVERE - COVID (-); SEVERE - MILD
PE 36:4	26.938	$2.38E^{-10}$	9.6228	$1.46E^{-09}$	MILD - COVID (-); SEVERE - COVID (-)
SM 32:2;O2	26.351	$3.57E^{-10}$	9.4479	$2.14E^{-09}$	COVID (-) - MILD; COVID (-) - SEVERE; MILD - SEVERE
LPC 20:4	26.022	$4.48E^{-10}$	9.349	$2.64E^{-09}$	COVID (-) - MILD; COVID (-) - SEVERE; MILD - SEVERE
PE 34:2	25.833	$5.10E^{-10}$	9.2922	$2.96E^{-09}$	MILD - COVID (-); SEVERE - COVID (-); SEVERE - MILD
TG 18:1_18:1_18:2	25.68	$5.67E^{-10}$	9.2462	$3.24E^{-09}$	MILD - COVID (-); SEVERE - COVID (-); SEVERE - MILD
PC 18:0_18:2*	25.594	$6.02E^{-10}$	9.2201	$3.36E^{-09}$	COVID (-) - MILD; COVID (-) - SEVERE
TG 16:0_18:1_18:1	25.581	$6.08E^{-10}$	9.2163	$3.36E^{-09}$	MILD - COVID (-); SEVERE - COVID (-)
PE O-16:1_18:2*	25.444	$6.69E^{-10}$	9.1748	$3.64E^{-09}$	COVID (-) - MILD; COVID (-) - SEVERE
TG 17:0_18:1_18:2	25.09	$8.56E^{-10}$	9.0673	$4.59E^{-09}$	MILD - COVID (-); SEVERE - COVID (-); SEVERE - MILD

PC O-36:3*	24.28	$1.51E^{-09}$	8.8202	$7.87E^{-09}$	COVID (-) - MILD; COVID (-) - SEVERE
LPC 22:4	24.278	$1.52E^{-09}$	8.8195	$7.87E^{-09}$	COVID (-) - MILD; COVID (-) - SEVERE; MILD - SEVERE
TG 17:1_18:1_22:6	24.019	$1.82E^{-09}$	8.7397	$9.32E^{-09}$	MILD - COVID (-); SEVERE - COVID (-)
PC O-16:1_18:1	23.916	$1.96E^{-09}$	8.7081	$9.88E^{-09}$	COVID (-) - MILD; COVID (-) - SEVERE; MILD - SEVERE
PC O-36:3	23.589	$2.47E^{-09}$	8.607	$1.23E^{-08}$	COVID (-) - MILD; COVID (-) - SEVERE; MILD - SEVERE
TG 18:1_18:1_18:0	23.294	$3.05E^{-09}$	8.5155	$1.50E^{-08}$	MILD - COVID (-); SEVERE - COVID (-); SEVERE - MILD
LPC 20:4*	22.724	$4.59E^{-09}$	8.338	$2.22E^{-08}$	COVID (-) - SEVERE; MILD - SEVERE
SM 43:1;O2	22.396	$5.82E^{-09}$	8.2351	$2.77E^{-08}$	COVID (-) - MILD; COVID (-) - SEVERE
DG 18:1_18:2	21.163	$1.43E^{-08}$	7.8448	$6.72E^{-08}$	MILD - COVID (-); SEVERE - COVID (-); SEVERE - MILD
CE 14:0	21.021	$1.59E^{-08}$	7.7995	$7.36E^{-08}$	COVID (-) - MILD; COVID (-) - SEVERE; MILD - SEVERE
PC 36:0	21.004	$1.61E^{-08}$	7.7942	$7.36E^{-08}$	COVID (-) - MILD; COVID (-) - SEVERE
SM 32:1;O2	20.562	$2.23E^{-08}$	7.6526	$1.01E^{-07}$	COVID (-) - MILD; COVID (-) - SEVERE
TG 18:2_18:3_22:0	20.102	$3.13E^{-08}$	7.5041	$1.40E^{-07}$	MILD - COVID (-); SEVERE - COVID (-)
DG 18:2_18:2	20.036	$3.29E^{-08}$	7.4831	$1.45E^{-07}$	MILD - COVID (-); SEVERE - COVID (-); SEVERE - MILD
CE 17:0	19.94	$3.53E^{-08}$	7.4518	$1.54E^{-07}$	COVID (-) - MILD; COVID (-) - SEVERE
SM 39:2;O2	19.208	$6.11E^{-08}$	7.2138	$2.63E^{-07}$	COVID (-) - MILD; COVID (-) - SEVERE
PE O-18:1_20:4	19.117	$6.55E^{-08}$	7.1839	$2.78E^{-07}$	COVID (-) - MILD; COVID (-) - SEVERE
LPC 22:5	19.005	$7.13E^{-08}$	7.1471	$2.99E^{-07}$	COVID (-) - MILD; COVID (-) - SEVERE; MILD - SEVERE
TG 18:1_18:2_18:2	18.925	$7.57E^{-08}$	7.1209	$3.14E^{-07}$	MILD - COVID (-); SEVERE - COVID (-); SEVERE - MILD
TG 16:0_16:0_18:1	18.703	$8.95E^{-08}$	7.0481	$3.67E^{-07}$	MILD - COVID (-); SEVERE - COVID (-)
TG 18:1_18:1_20:1	18.424	$1.11E^{-07}$	6.9561	$4.48E^{-07}$	MILD - COVID (-); SEVERE - COVID (-); SEVERE - MILD
PE 34:1	18.367	$1.16E^{-07}$	6.9371	$4.62E^{-07}$	SEVERE - COVID (-); SEVERE - MILD
LPC 16:1	18.339	$1.18E^{-07}$	6.9281	$4.67E^{-07}$	COVID (-) - MILD; COVID (-) - SEVERE; MILD - SEVERE
PE 18:0_20:4*	18.208	$1.30E^{-07}$	6.8845	$5.10E^{-07}$	MILD - COVID (-); SEVERE - COVID (-)
PE 18:0_20:4	17.975	$1.56E^{-07}$	6.8074	$5.97E^{-07}$	MILD - COVID (-); SEVERE - COVID (-)
CE 18:2	17.974	$1.56E^{-07}$	6.8069	$5.97E^{-07}$	COVID (-) - MILD; COVID (-) - SEVERE
PE O-18:2_20:4	17.887	$1.67E^{-07}$	6.7781	$6.30E^{-07}$	COVID (-) - MILD; COVID (-) - SEVERE; MILD - SEVERE
TG 16:0_18:0_18:1	17.363	$2.49E^{-07}$	6.603	$9.30E^{-07}$	MILD - COVID (-); SEVERE - COVID (-)
PE O-18:1_20:4*	17.353	$2.51E^{-07}$	6.5999	$9.30E^{-07}$	COVID (-) - MILD; COVID (-) - SEVERE
PC 40:8	16.637	$4.38E^{-07}$	6.3589	$1.60E^{-06}$	COVID (-) - SEVERE; MILD - SEVERE
PE O-16:1_20:4*	16.482	$4.94E^{-07}$	6.3064	$1.79E^{-06}$	COVID (-) - MILD; COVID (-) - SEVERE
CE 16:0	16.129	$6.51E^{-07}$	6.1866	$2.33E^{-06}$	COVID (-) - MILD; COVID (-) - SEVERE; MILD - SEVERE
PE 40:7	16.086	$6.73E^{-07}$	6.1719	$2.39E^{-06}$	MILD - COVID (-); SEVERE - COVID (-)
TG 18:2_18:2_20:4	16.074	$6.79E^{-07}$	6.1679	$2.39E^{-06}$	MILD - COVID (-); SEVERE - COVID (-)
TG 18:1_18:1_18:1	15.896	$7.82E^{-07}$	6.107	$2.72E^{-06}$	MILD - COVID (-); SEVERE - COVID (-)

PC 37:3	15.846	$8.13E^{-07}$	6.09	$2.80E^{-06}$	COVID (-) - MILD; COVID (-) - SEVERE
LPE 16:0	15.739	$8.84E^{-07}$	6.0533	$3.02E^{-06}$	COVID (-) - MILD; COVID (-) - SEVERE
DG 18:1_18:1	15.689	$9.20E^{-07}$	6.0363	$3.11E^{-06}$	MILD - COVID (-); SEVERE - COVID (-)
TG 17:1_18:1_18:2	15.547	$1.03E^{-06}$	5.9874	$3.44E^{-06}$	MILD - COVID (-); SEVERE - COVID (-); SEVERE - MILD
SM 18:1;O2/20:0	15.412	$1.15E^{-06}$	5.9412	$3.80E^{-06}$	COVID (-) - MILD; COVID (-) - SEVERE
SM 41:2;O2	15.367	$1.19E^{-06}$	5.9257	$3.90E^{-06}$	COVID (-) - MILD; COVID (-) - SEVERE
TG 17:0_18:1_18:1	15.219	$1.33E^{-06}$	5.8748	$4.34E^{-06}$	MILD - COVID (-); SEVERE - COVID (-); SEVERE - MILD
LPE 18:1	15.197	$1.36E^{-06}$	5.8672	$4.37E^{-06}$	COVID (-) - MILD; COVID (-) - SEVERE
Cer 18:1;O2/16:0	15.186	$1.37E^{-06}$	5.8633	$4.37E^{-06}$	MILD - COVID (-); SEVERE - COVID (-)
PC 18:0_18:2	15.122	$1.44E^{-06}$	5.8414	$4.56E^{-06}$	COVID (-) - MILD; COVID (-) - SEVERE
PC O-38:4*	15.09	$1.48E^{-06}$	5.8303	$4.63E^{-06}$	COVID (-) - MILD; COVID (-) - SEVERE
PE O-16:1_20:4	14.868	$1.76E^{-06}$	5.7536	$5.48E^{-06}$	COVID (-) - MILD; COVID (-) - SEVERE
DG 16:0_18:2	14.77	$1.91E^{-06}$	5.7197	$5.87E^{-06}$	MILD - COVID (-); SEVERE - COVID (-); SEVERE - MILD
PC 16:0_18:0	14.355	$2.66E^{-06}$	5.5754	$8.07E^{-06}$	COVID (-) - MILD; COVID (-) - SEVERE
TG 16:0_17:0_18:1	14.351	$2.67E^{-06}$	5.5738	$8.07E^{-06}$	MILD - COVID (-); SEVERE - COVID (-)
SM 40:1;O2	14.31	$2.76E^{-06}$	5.5596	$8.27E^{-06}$	COVID (-) - MILD; COVID (-) - SEVERE
PC 14:0_18:2	14.003	$3.53E^{-06}$	5.4521	$1.05E^{-05}$	COVID (-) - MILD; COVID (-) - SEVERE
TG 16:1_18:2_18:2	13.966	$3.64E^{-06}$	5.4394	$1.07E^{-05}$	MILD - COVID (-); SEVERE - COVID (-)
PC 37:1	13.887	$3.88E^{-06}$	5.4115	$1.13E^{-05}$	COVID (-) - MILD; COVID (-) - SEVERE
CE 20:3	13.653	$4.68E^{-06}$	5.3293	$1.36E^{-05}$	COVID (-) - MILD; COVID (-) - SEVERE
PC 14:0_20:4*	13.475	$5.42E^{-06}$	5.2664	$1.56E^{-05}$	COVID (-) - MILD; COVID (-) - SEVERE; MILD - SEVERE
PC 14:0_18:2*	13.458	$5.49E^{-06}$	5.2604	$1.57E^{-05}$	COVID (-) - MILD; COVID (-) - SEVERE
TG 15:0_18:2_18:2	12.912	$8.57E^{-06}$	5.0671	$2.42E^{-05}$	MILD - COVID (-); SEVERE - COVID (-)
SM 42:8;O2	12.656	$1.06E^{-05}$	4.9757	$2.97E^{-05}$	MILD - COVID (-); SEVERE - COVID (-)
PC O-38:5	12.557	$1.15E^{-05}$	4.9403	$3.19E^{-05}$	COVID (-) - SEVERE; MILD - SEVERE
PC 18:1_18:1	12.544	$1.16E^{-05}$	4.9356	$3.20E^{-05}$	COVID (-) - MILD; COVID (-) - SEVERE
LPC 20:5	12.526	$1.18E^{-05}$	4.9292	$3.23E^{-05}$	COVID (-) - MILD; COVID (-) - SEVERE
TG 16:0_18:3_18:4	12.48	$1.22E^{-05}$	4.913	$3.32E^{-05}$	MILD - COVID (-); SEVERE - COVID (-)
PI 36:3	12.465	$1.24E^{-05}$	4.9074	$3.34E^{-05}$	COVID (-) - MILD; COVID (-) - SEVERE
PC 18:1_18:1*	12.357	$1.35E^{-05}$	4.8689	$3.60E^{-05}$	COVID (-) - MILD; COVID (-) - SEVERE
PC 38:7	12.353	$1.36E^{-05}$	4.8675	$3.60E^{-05}$	MILD - COVID (-); SEVERE - COVID (-)
PE O-18:1_18:1*	12.308	$1.41E^{-05}$	4.8511	$3.71E^{-05}$	COVID (-) - MILD; COVID (-) - SEVERE
TG 18:2_18:1_15:0	12.011	$1.80E^{-05}$	4.7443	$4.71E^{-05}$	MILD - COVID (-); SEVERE - COVID (-)
DG 16:0_18:1	11.907	$1.96E^{-05}$	4.7069	$5.10E^{-05}$	MILD - COVID (-); SEVERE - COVID (-)
CE 18:1	11.87	$2.03E^{-05}$	4.6935	$5.22E^{-05}$	COVID (-) - MILD; COVID (-) - SEVERE

TG 18:0_18:2_18:5	11.762	$2.21E^{-05}$	4.6547	$5.67E^{-05}$	SEVERE - COVID (-); SEVERE - MILD
PE 18:1_18:0	11.627	$2.48E^{-05}$	4.6056	$6.30E^{-05}$	SEVERE - COVID (-); SEVERE - MILD
PC O-38:4	11.398	$3.00E^{-05}$	4.5224	$7.57E^{-05}$	MILD - COVID (-); MILD - SEVERE
PC O-37:5*	11.38	$3.05E^{-05}$	4.5159	$7.63E^{-05}$	COVID (-) - SEVERE; MILD - SEVERE
PE 18:0_18:1	11.269	$3.35E^{-05}$	4.4755	$8.32E^{-05}$	SEVERE - COVID (-); SEVERE - MILD
PI 36:2*	11.221	$3.48E^{-05}$	4.4583	$8.59E^{-05}$	COVID (-) - MILD; COVID (-) - SEVERE
PC 16:0_20:4	11.17	$3.63E^{-05}$	4.4397	$8.90E^{-05}$	MILD - COVID (-); SEVERE - COVID (-)
PE 18:1_20:4	11.08	$3.92E^{-05}$	4.4067	$9.54E^{-05}$	MILD - COVID (-); SEVERE - COVID (-)
LPE 18:2	10.956	$4.35E^{-05}$	4.3613	0.000105	COVID (-) - MILD; COVID (-) - SEVERE
TG 15:0_18:1_18:1	10.758	$5.14E^{-05}$	4.2889	0.000123	MILD - COVID (-); SEVERE - COVID (-)
PE 18:0_18:2*	10.669	$5.54E^{-05}$	4.2563	0.000132	SEVERE - COVID (-); SEVERE - MILD
PC O-36:2	10.55	$6.13E^{-05}$	4.2123	0.000145	COVID (-) - MILD; COVID (-) - SEVERE
PC 33:0	10.543	$6.17E^{-05}$	4.2099	0.000145	COVID (-) - MILD; COVID (-) - SEVERE
PC 18:0_20:3	10.521	$6.28E^{-05}$	4.2019	0.000147	COVID (-) - MILD; COVID (-) - SEVERE
PC 14:0_20:4	10.499	$6.40E^{-05}$	4.1937	0.000149	COVID (-) - MILD; COVID (-) - SEVERE
CE 17:1	10.149	$8.62E^{-05}$	4.0645	0.000199	COVID (-) - SEVERE
PC 30:0	9.8606	0.0001103	3.9575	0.000252	COVID (-) - MILD; COVID (-) - SEVERE
PE 18:0_18:2	9.7695	0.0001192	3.9236	0.000271	SEVERE - COVID (-); SEVERE - MILD
PC O-32:2	9.4356	0.0001588	3.7991	0.000359	COVID (-) - SEVERE; MILD - SEVERE
PC O-32:1	9.3805	0.0001665	3.7785	0.000374	COVID (-) - SEVERE
PC 17:0_18:2	9.2634	0.0001842	3.7346	0.000411	COVID (-) - MILD
LPC 22:6	9.2412	0.0001878	3.7263	0.000416	COVID (-) - MILD; COVID (-) - SEVERE
TG 16:0_16:1_18:1	9.0808	0.0002158	3.666	0.000475	MILD - COVID (-); SEVERE - COVID (-)
LPE 18:2*	9.0305	0.0002254	3.6471	0.000493	COVID (-) - MILD; COVID (-) - SEVERE
PC O-40:5*	8.8682	0.0002594	3.586	0.000564	MILD - COVID (-); MILD - SEVERE
PC O-16:1_16:0	8.8308	0.000268	3.5719	0.000579	COVID (-) - MILD; COVID (-) - SEVERE
TG 18:1_18:2_22:0	8.603	0.0003268	3.4858	0.000702	SEVERE - COVID (-)
PC 16:0_20:4*	8.4693	0.0003672	3.4351	0.000784	MILD - COVID (-); SEVERE - COVID (-)
PC 16:0_18:1	8.4518	0.0003729	3.4285	0.000787	SEVERE - COVID (-); SEVERE - MILD
PE O-20:1_20:4	8.4506	0.0003733	3.428	0.000787	COVID (-) - MILD; COVID (-) - SEVERE
PC 17:0_18:2*	8.4341	0.0003787	3.4218	0.000794	COVID (-) - MILD; COVID (-) - SEVERE
DG 18:0_18:1	8.0989	0.0005079	3.2942	0.001058	SEVERE - COVID (-); SEVERE - MILD
PC O-42:3	8.0726	0.0005198	3.2842	0.001077	COVID (-) - MILD; COVID (-) - SEVERE
PC O-36:4	7.9579	0.000575	3.2403	0.001184	COVID (-) - SEVERE; MILD - SEVERE
Cer 36:0	7.893	0.0006088	3.2156	0.001246	COVID (-) - MILD; COVID (-) - SEVERE

PI 36:1	7.701	0.0007212	3.142	0.001468	COVID (-) - MILD; COVID (-) - SEVERE
PC 30:1	7.6099	0.0007817	3.107	0.001582	COVID (-) - SEVERE
TG 18:0_20:1_16:0	7.5021	0.00086	3.0655	0.00173	SEVERE - COVID (-)
PE O-16:1_18:2	7.4217	0.0009236	3.0345	0.001847	COVID (-) - MILD; COVID (-) - SEVERE
PC 18:0_18:1	7.3224	0.0010087	2.9963	0.001997	COVID (-) - MILD; COVID (-) - SEVERE
PI 38:3	7.3211	0.0010098	2.9958	0.001997	COVID (-) - MILD; COVID (-) - SEVERE
TG 18:2_18:1_14:0	7.0676	0.0012656	2.8977	0.002488	MILD - COVID (-); SEVERE - COVID (-)
DG 22:6_20:0	7.0334	0.0013048	2.8845	0.002551	MILD - COVID (-)
PE 36:5	6.9934	0.0013522	2.869	0.002629	SEVERE - COVID (-)
PC 16:0_22:6*	6.8385	0.0015531	2.8088	0.003003	SEVERE - COVID (-)
PC 16:0_22:6	6.7731	0.001647	2.7833	0.003167	SEVERE - COVID (-)
TG 15:0_16:0_18:1	6.7056	0.0017497	2.757	0.003346	MILD - COVID (-); SEVERE - COVID (-)
PC 35:3	6.6568	0.001828	2.738	0.003473	COVID (-) - MILD; COVID (-) - SEVERE
PC 16:0_18:1*	6.6518	0.0018362	2.7361	0.003473	SEVERE - COVID (-)
PC O-16:0_20:4	6.5965	0.0019298	2.7145	0.00363	MILD - SEVERE
CE 20:4	6.5847	0.0019503	2.7099	0.003649	MILD - SEVERE
PC 16:0_22:4	6.1362	0.0029227	2.5342	0.005439	MILD - COVID (-); MILD - SEVERE
PC 16:0_16:1	6.0951	0.0030334	2.5181	0.005615	MILD - COVID (-); SEVERE - COVID (-)
PC 15:0_18:2	5.9028	0.0036114	2.4423	0.00665	COVID (-) - MILD
PC O-18:1_20:4	5.8766	0.0036985	2.432	0.006774	MILD - SEVERE
PI 18:0_16:1	5.826	0.0038727	2.412	0.007056	COVID (-) - MILD; COVID (-) - SEVERE
DG 16:1_18:2	5.7813	0.0040334	2.3943	0.007311	MILD - COVID (-); SEVERE - COVID (-)
SM 33:1;O2	5.7631	0.0041008	2.3871	0.007394	COVID (-) - SEVERE
PC O-44:6	5.6877	0.0043921	2.3573	0.007879	MILD - SEVERE
DG 18:0_18:0	5.6701	0.0044631	2.3504	0.007965	SEVERE - COVID (-)
PE O-18:1_22:4*	5.663	0.0044924	2.3475	0.007976	COVID (-) - MILD
PC 36:6	5.6476	0.0045557	2.3414	0.008048	COVID (-) - MILD; COVID (-) - SEVERE

FDR= false discovery rate; *= isomers (our data don't. explain structural isomers or stereoisomers).

Table S5.3. *SAM analysis results.*

Compound	d.value	stdev	rawp	q.value
LPC 20:1	31.41	0.30672	0	0
LPC O-16:0	30.257	0.3239	0	0
LPC O-18:1	29.296	0.33858	0	0
LPC 18:0	25.369	0.40202	0	0
TG 18:1_18:2_22:6	24.588	0.41534	0	0
TG 16:0_20:4_22:6	24.344	0.41957	0	0
TG 16:0_18:1_22:5	24.215	0.4218	0	0
PC O-34:3	23.912	0.42709	0	0
LPC O-16:1	23.678	0.43121	0	0
TG 16:0_18:2_20:4	23.662	0.43148	0	0
TG 18:2_18:2_22:6	21.693	0.46703	0	0
LPC 17:0	21.497	0.47067	0	0
TG 18:1_18:1_22:6	21.333	0.47373	0	0
TG 18:0_18:1_20:4	21.157	0.47701	0	0
LPC 20:2	21.024	0.47951	0	0
PE 18:0_22:6	18.808	0.52239	0	0
PE 16:0_22:6	18.608	0.52637	0	0
SM 30:1;O2	18.526	0.52801	0	0
LPC 16:0	17.819	0.54232	0	0
PC 37:2	17.744	0.54386	0	0
Hex-Cer 18:1;O2/22:0	17.362	0.55172	0	0
PC O-16:1_18:2	17.123	0.55668	0	0
LPE 18:0	17.033	0.55855	0	0
LPC 18:1*	16.95	0.56029	0	0
TG 16:0_18:1_22:6	16.939	0.5605	0	0
LPC 18:1	16.71	0.56532	0	0
PE 16:0_18:1	16.634	0.56692	0	0
TG 18:1_18:1_22:4	16.202	0.57607	0	0
PE 16:0_20:4	15.925	0.582	0	0
Cer 18:1;O2/24:1	15.699	0.58687	0	0
LPC 17:1	15.491	0.59136	0	0

Hex-Cer 18:1;O2/24:0	15.392	0.59353	0	0
PE 16:1_22:5	15.262	0.59636	0	0
LPC 14:0	15.152	0.59878	0	0
LPC 18:2	15.117	0.59955	0	0
TG 18:2_18:2_20:5	15.033	0.60139	0	0
LPC 15:0	15.003	0.60204	0	0
DG 18:1_20:4	14.981	0.60253	0	0
PC O-16:0_18:2	14.914	0.604	0	0
LPC 18:2*	14.781	0.60694	0	0
PE 18:2_16:0	14.523	0.61268	0	0
PC O-34:2	14.339	0.6168	0	0
TG 16:0_18:2_22:5	14.339	0.61681	0	0
PE 40:6	13.705	0.63113	0	0
LPC 20:3*	13.485	0.63618	0	0
SM 39:1;O2	13.373	0.63874	0	0
SM 42:1;O2	12.582	0.65717	0	0
TG 16:0_18:1_18:2	12.407	0.66129	0	0
CE 18:0	12.344	0.66279	0	0
PC 18:1_18:2	12.244	0.66516	0	0
SM 40:2;O2	12.2	0.6662	0	0
DG 18:2_22:6	12.161	0.66713	0	0
LPC 20:3	12.119	0.66812	0	0
PE O-18:1_18:2	11.784	0.67616	0	0
SM 41:1;O2	11.268	0.68868	0	0
TG 18:2_18:1_16:1	11.022	0.69472	0	0
PE 36:4	10.953	0.69642	0	0
SM 32:2;O2	10.758	0.70123	0	0
LPC 20:4	10.648	0.70396	0	0
PE 34:2	10.585	0.70554	0	0
TG 18:1_18:1_18:2	10.534	0.70682	0	0
PC 18:0_18:2*	10.505	0.70754	0	0
TG 16:0_18:1_18:1	10.5	0.70765	0	0
PE O-16:1_18:2*	10.454	0.7088	0	0
TG 17:0_18:1_18:2	10.334	0.71181	0	0
PC O-36:3*	10.058	0.71877	0	0

LPC 22:4	10.057	0.71879	0	0
TG 17:1_18:1_22:6	9.9683	0.72105	0	0
PC O-16:1_18:1	9.9329	0.72195	0	0
PC O-36:3	9.8198	0.72483	0	0
TG 18:1_18:1_18:0	9.7173	0.72744	0	0
LPC 20:4*	9.5184	0.73254	0	0
SM 43:1;O2	9.4029	0.73551	0	0
DG 18:1_18:2	8.9645	0.7469	0	0
CE 14:0	8.9135	0.74823	0	0
PC 36:0	8.9075	0.74839	0	0
SM 32:1;O2	8.7482	0.75257	0	0
TG 18:2_18:3_22:0	8.5809	0.75698	0	0
DG 18:2_18:2	8.5571	0.75761	0	0
CE 17:0	8.5219	0.75854	0	0
SM 39:2;O2	8.2534	0.76568	0	0
PE O-18:1_20:4	8.2197	0.76658	0	0
LPC 22:5	8.1781	0.76769	0	0
TG 18:1_18:2_18:2	8.1485	0.76849	0	0
TG 16:0_16:0_18:1	8.0662	0.77069	0	0
TG 18:1_18:1_20:1	7.9622	0.77349	0	0
PE 34:1	7.9407	0.77407	0	0
LPC 16:1	7.9306	0.77434	0	0
PE 18:0_20:4*	7.8813	0.77567	0	0
PE 18:0_20:4	7.7941	0.77803	0	0
CE 18:2	7.7935	0.77804	0	0
PE O-18:2_20:4	7.761	0.77892	0	0
TG 16:0_18:0_18:1	7.5627	0.78431	0	0
PE O-18:1_20:4*	7.5592	0.78441	0	0
PC 40:8	7.286	0.79188	0	0
PE O-16:1_20:4*	7.2265	0.79352	0	0
CE 16:0	7.0905	0.79727	0	0
PE 40:7	7.0739	0.79774	0	0
TG 18:2_18:2_20:4	7.0693	0.79786	0	0
TG 18:1_18:1_18:1	7.0002	0.79977	0	0
PC 37:3	6.9809	0.80031	0	0

LPE 16:0	6.9393	0.80147	0	0
DG 18:1_18:1	6.92	0.802	0	0
TG 17:1_18:1_18:2	6.8644	0.80355	0	0
SM 18:1;O2/20:0	6.8119	0.80501	0	0
SM 41:2;O2	6.7943	0.8055	0	0
TG 17:0_18:1_18:1	6.7365	0.80712	0	0
LPE 18:1	6.7279	0.80736	0	0
Cer 18:1;O2/16:0	6.7234	0.80748	0	0
PC 18:0_18:2	6.6984	0.80818	0	0
PC O-38:4*	6.6859	0.80853	0	0
PE O-16:1_20:4	6.5987	0.81098	0	0
DG 16:0_18:2	6.5601	0.81206	0	0
PC 16:0_18:0	6.396	0.81669	0	0
TG 16:0_17:0_18:1	6.3942	0.81674	0	0
SM 40:1;O2	6.378	0.81719	0	0
PC 14:0_18:2	6.2556	0.82066	0	0
TG 16:1_18:2_18:2	6.2411	0.82107	0	0
PC 37:1	6.2093	0.82197	0	0
CE 20:3	6.1157	0.82463	0	0
PC 14:0_20:4*	6.044	0.82668	0	0
PC 14:0_18:2*	6.0372	0.82687	0	0
TG 15:0_18:2_18:2	5.8169	0.83319	0	0
SM 42:8;O2	5.7126	0.83619	0	0
PC O-38:5	5.6722	0.83736	0	0
PC 18:1_18:1	5.6669	0.83751	0	0
LPC 20:5	5.6595	0.83773	0	0
TG 16:0_18:3_18:4	5.641	0.83826	0	0
PI 36:3	5.6347	0.83844	0	0
PC 18:1_18:1*	5.5907	0.83972	0	0
PC 38:7	5.5891	0.83976	0	0
PE O-18:1_18:1*	5.5704	0.8403	0	0
TG 18:2_18:1_15:0	5.4485	0.84384	0	0
DG 16:0_18:1	5.4058	0.84509	0	0
CE 18:1	5.3905	0.84553	0	0
TG 18:0_18:2_18:5	5.3462	0.84683	0	0

PE 18:1_18:0	5.29	0.84846	0	0
PC O-38:4	5.195	0.85125	0	0
PC O-37:5*	5.1875	0.85147	$2.87E^{-05}$	$4.68E^{-06}$
PE 18:0_18:1	5.1415	0.85282	$2.87E^{-05}$	$4.68E^{-06}$
PI 36:2*	5.1217	0.8534	$2.87E^{-05}$	$4.68E^{-06}$
PC 16:0_20:4	5.1005	0.85402	$2.87E^{-05}$	$4.68E^{-06}$
PE 18:1_20:4	5.0628	0.85513	$2.87E^{-05}$	$4.68E^{-06}$
LPE 18:2	5.0109	0.85666	$5.75E^{-05}$	$9.05E^{-06}$
TG 15:0_18:1_18:1	4.9281	0.8591	$5.75E^{-05}$	$9.05E^{-06}$
PE 18:0_18:2*	4.8908	0.86021	$5.75E^{-05}$	$9.05E^{-06}$
PC O-36:2	4.8405	0.8617	$5.75E^{-05}$	$9.05E^{-06}$
PC 33:0	4.8378	0.86178	$5.75E^{-05}$	$9.05E^{-06}$
PC 18:0_20:3	4.8286	0.86205	$8.62E^{-05}$	$1.34E^{-05}$
PC 14:0_20:4	4.8192	0.86233	$8.62E^{-05}$	$1.34E^{-05}$
CE 17:1	4.6714	0.86673	0.000115	$1.76E^{-05}$
PC 30:0	4.5489	0.87039	0.000115	$1.76E^{-05}$
PE 18:0_18:2	4.5101	0.87155	0.000144	$2.19E^{-05}$
PC O-32:2	4.3675	0.87583	0.000172	$2.61E^{-05}$
PC O-32:1	4.3439	0.87654	0.000201	$2.95E^{-05}$
PC 17:0_18:2	4.2936	0.87805	0.000201	$2.95E^{-05}$
LPC 22:6	4.2841	0.87834	0.000201	$2.95E^{-05}$
TG 16:0_16:1_18:1	4.2151	0.88043	0.000201	$2.95E^{-05}$
LPE 18:2*	4.1934	0.88108	0.000201	$2.95E^{-05}$
PC O-40:5*	4.1233	0.88321	0.00023	$3.33E^{-05}$
PC O-16:1_16:0	4.1072	0.8837	0.00023	$3.33E^{-05}$
TG 18:1_18:2_22:0	4.0085	0.8867	0.000287	$4.13E^{-05}$
PC 16:0_20:4*	3.9504	0.88847	0.000345	$4.84E^{-05}$
PC 16:0_18:1	3.9428	0.8887	0.000345	$4.84E^{-05}$
PE O-20:1_20:4	3.9422	0.88872	0.000345	$4.84E^{-05}$
PC 17:0_18:2*	3.9351	0.88893	0.000345	$4.84E^{-05}$
DG 18:0_18:1	3.7888	0.89341	0.000402	$5.55E^{-05}$
PC O-42:3	3.7773	0.89376	0.000402	$5.55E^{-05}$
PC O-36:4	3.727	0.8953	0.000402	$5.55E^{-05}$
Cer 36:0	3.6986	0.89618	0.000517	$7.09E^{-05}$
PI 36:1	3.6142	0.89878	0.000546	$7.44E^{-05}$

PC 30:1	3.574	0.90002	0.000603	$8.18E^{-05}$
TG 18:0_20:1_16:0	3.5264	0.90149	0.000661	$8.90E^{-05}$
PE O-16:1_18:2	3.4909	0.90259	0.00069	$9.24E^{-05}$
PC 18:0_18:1	3.4469	0.90395	0.000805	0.0001065
PI 38:3	3.4464	0.90396	0.000805	0.0001065
TG 18:2_18:1_14:0	3.3338	0.90746	0.000891	0.0001166
DG 22:6_20:0	3.3186	0.90793	0.000891	0.0001166
PE 36:5	3.3008	0.90849	0.00092	0.0001197
PC 16:0_22:6*	3.2317	0.91064	0.001063	0.0001376
PC 16:0_22:6	3.2025	0.91156	0.001207	0.0001554
TG 15:0_16:0_18:1	3.1723	0.9125	0.001264	0.0001619
PC 35:3	3.1505	0.91318	0.001293	0.0001638
PC 16:0_18:1*	3.1482	0.91325	0.001293	0.0001638
PC O-16:0_20:4	3.1234	0.91403	0.001322	0.0001656
CE 20:4	3.1182	0.91419	0.001322	0.0001656
PC 16:0_22:4	2.9164	0.92054	0.002213	0.0002757
PC 16:0_16:1	2.8978	0.92112	0.002299	0.0002849
PC 15:0_18:2	2.8108	0.92387	0.002759	0.0003401
PC O-18:1_20:4	2.7989	0.92425	0.00296	0.000363
PI 18:0_16:1	2.7759	0.92498	0.003132	0.0003821
DG 16:1_18:2	2.7556	0.92562	0.003276	0.0003976
SM 33:1;O2	2.7473	0.92588	0.003305	0.000399
PC O-44:6	2.7131	0.92697	0.003649	0.0004383
DG 18:0_18:0	2.7051	0.92722	0.003707	0.0004407
PE O-18:1_22:4*	2.7018	0.92733	0.003707	0.0004407
PC 36:6	2.6948	0.92755	0.003764	0.0004453
Cer 18:2;O2/24:0	2.5409	0.93245	0.005144	0.0006053
SM 42:4;O2	2.5302	0.93279	0.005259	0.0006158
PC O-18:0_20:4	2.4916	0.93403	0.005948	0.0006929
SM 37:2;O2	2.4871	0.93417	0.005977	0.0006929
CE 15:0	2.4358	0.93581	0.006437	0.0007425
PC 18:0_22:4	2.4274	0.93608	0.006523	0.0007488
PC 42:8	2.3933	0.93718	0.006954	0.0007943
PC O-36:5	2.332	0.93914	0.008075	0.0009178
PE O-18:1_22:4	2.2811	0.94078	0.008764	0.0009914

stdev= standard deviation; ***=** isomers (our data don't explain structural isomers or stereoisomers)

CHAPTER VIII

Conclusions

The PhD project aimed to evaluate different analytical techniques for the study of omics sciences, and specially of lipidomics, with the purpose to pinpoint metabolic alterations related to a pathological state or a dietary regime. The research has been focused to develop, apply and validate highly advanced MS-based platforms that can pursue personalized medicine objectives. Indeed, the PhD project had the main goal to identify and highlight potential new biomarkers leading to a better understanding of the pathophysiology of investigated diseases and allowing a timely intervention for a better final care of the patient.

Identifying new biomarkers, as new prognostic or diagnostic tools, represents a constant urgency both for rare diseases with a low incidence and for more widespread pathologies, such as cardiovascular diseases. In this regard, in the first two year of the PhD, the research activity was focused on the application of MS-based strategies in the field of hypertension and atherosclerosis, two of the main risks of CVDs, which are among the main causes of mortality.

Firstly, we attempted to identify a possible correlation among sphingolipids, hypertension and sortilin. To assess this aim, a method was developed and validated for the quantification of S1P and ceramides. The experimental conditions were applied to HUVECs line and to two patients' cohorts, Campania Salute Network study and Moli-Sani population. Remarkable, the results from human plasma samples confirmed the indications obtained from *in vitro* experiments. Indeed, incubation of HUVECs with sortilin induced an increase in the medium culture levels of S1P. These findings have been widely supported by *in vivo* studies where not only elevated sphingosine-1-phosphate plasma levels were associated with hypertension, but

moreover the observed plasma concentration of S1P went hand in hand with blood pressure levels. Furthermore, in confirmation of the correlation between sortilin and S1P (r=0.761, r=0.4648) plasma levels, the activity of ASMase, co-responsible of sphingolipids metabolism, revealed a linear increase with the severity of the hypertension. In conclusion, here we suggest the potential of S1P and sortilin as new biomarkers for hypertension (**chapter II**). Hypertension is often found in combination with atherosclerosis and in addition to the discovery of new biomarkers, nowadays, it is increasingly attractive to look for new biomolecules of natural origin that may counteract the onset of cardiovascular risks or represent a safer adjuvant to drug therapies. To test an antiatherosclerosis potential activity of a novel spirulina peptide with reported antihypertensive properties, namely SP6, we elaborated a direct infusion Fourier transform ion cyclotron resonance mass spectrometry (DI-FT-ICR-MS) untargeted approach. The method allowed to uncover the metabolites and the lipids significantly modulated by SP6 supplemental dietary regime, such as sphingomyelins, glycerophospholipids and TCA intermediates. The results open the way to a large-scale study of SP6 preventive treatment for atherosclerosis and highlight the usefulness of DI-FT-ICR in lipidomic and metabolomic profiling (**chapter III**) before to move to LC-MS/MS approaches. In this regard, ion mobility mass spectrometry (IMS) represents a powerful tool to boost lipidomics profiling, providing additional information, such as cross collision section values, regarding the analysed metabolites. During the PhD project, TIMS technology, coupled to different separation techniques, was employed to investigate lipidomic perturbations of a rare disease like AP-4 deficiency syndrome and of the current infection disease caused by SARS-CoV-2. A nano-LC-TIMS approach led to the identification of 585 lipids in AP-4 deficient brain mice covering 24 lipid subclasses with high MS/MS scores and low ΔCCS errors (%), median values of 889 and 1%, respectively. The developed nLC-TIMS method corroborated the role for AP-4 in the transport of DAGLB and opened to

suggestive new insights of the pathophysiology of this severe childhood hereditary spastic paraplegia. Indeed, the employed strategy, in addition to have provided information about a marked suppression of hexosyl-ceramides in *Ap4e1* mice also identified in 2-AG the responsible of the axonal growth failure, which distinguishes neurons of patients suffering from this form of HSP. These findings open new horizons for the treatment of AP-4 deficiency syndrome (**chapter IV**). In addition, a UHPLC-TIMS-qTOF method integrated with statistical analysis and a machine learning model evidenced an alteration of plasma lipidome in severe Covid-19 patients, revealing a restricted panel of LPCs, LPC-Os and PC-O with great accuracy in discriminating severity and mortality. If measured at the time of hospitalization, the proposed lipid signature could represent an additional prognostic tool to identify high-risk patients (**chapter VI**). Finally, considering that higher sensitivity is always beneficial in mass spectrometry-based approaches and always more necessary for biomedical research, we have adapted a new nano-chromatography system, namely Evosep One, to lipidomics applications. The developed system coupled to a trapped ion mobility mass spectrometer combines the sensitivity of nano-ionization with the advantages of a high-flow rate and opens new opportunities for nano-LC in lipidomics for clinical applications (**chapter V**).

Clearly, to adopt these methods in the clinical setting, there is an urgent need of validation on a large scale, as well as deliver faster results for clinicians. Future efforts will be spent in trying to reduce analysis runtimes without compromising lipid coverage, exploiting the high acquisition speed of the current MS devices, in order to analyse larger patients' cohorts, and allow method transfer across different laboratories.

List of Papers

The thesis is based on the following papers:

- Di Pietro P., Carrizzo A., Sommella E., Oliveti M., Iacoviello L., Di Castelnuovo A., Acernese F., Damato A., De Lucia M., **Merciai F.**, Iesu P., Venturini E., Izzo R., Trimarco V., Ciccarelli M., Giugliano G., Carnevale R., Cammisotto V., Migliarino S., Virtuoso N., Strainese A., Izzo V., Campiglia P., Ciaglia E., Levkau B., Puca A.A., Vecchione C. Targeting the ASMase/S1P pathway protects from sortilin-evoked vascular damage in hypertension. *J. Clin. Investig*. **2022**. 132 (3): e146343.
- Sommella E., Carrizzo A., **Merciai F.**, Di Sarno V., Carbone D., De Lucia M., Musella S., Vecchione C., Campiglia P. Analysis of the metabolic switch induced by the spirulina peptide SP6 in high fat diet ApoE-/- mice model: A direct infusion FT-ICR-MS based approach. *J Pharm Biomed Anal*. **2021**. 20, 195: 113865.
- Davies A., Alecu J., Marvin Z., Vasilopoulou C., **Merciai F**., Jumo H., Afshar Saber W., Sahin M., Ebrahimi-Fakhari D., Borner G. AP-4-mediated axonal transport controls endocannabinoid production in neurons. *Nat. Commun.* **2022**. 13: 1058.
- Vasilopoulou C.G., **Merciai F**., Bache N., Hoerning O., Skowronek P., Geyer P.E., Sulek K., Brunner A.D., Barsch A., Mann M., Meier F. Pre-formed gradients for high-throughput and robust nanoflow lipidomics with trapped ion mobility and PASEF. *Manuscript in preparation.*
- Ciccarelli M.[†], **Merciai F.**[†], Carrizzo A., Sommella E., Di Pietro P., Caponigro V., Salviati E., Musella S., Di Sarno V., Rusciano M., Toni A., Iesu P., Izzo C., Schettino

G., Conti V., Venturini E., Vitale C., Scarpati G., Bonadies D., Rispoli A., Polverino B., Poto S., Pagliano P., Piazza O., Licastro D., Vecchione C., Campiglia P. Untargeted Lipidomics Analysis Reveals Specific Lipid Profiles in Hospitalized Covid-19 patients predictive for Severity and Mortality Outcome. *Manuscript submitted.*

List of Additional Papers

- Sommella E., Salviati E., **Merciai F**., Manfra M., Bertamino A., Gasparrini F., Novellino E., Campiglia P. Online comprehensive hydrophilic interaction chromatography ×reversed phase liquid chromatography coupled to mass spectrometry for in depth peptidomic profile of microalgae gastro-intestinal digests. *J Pharm Biomed Anal.* **2019***,* 175, 112783.
- Ostacolo C., Di Sarno V., Musella S., Ciaglia T., Vestuto V., Pepe G., **Merciai F**., Campiglia P., Gomez Monterrey I., Bertamino A. An efficient approach to aromatic aminomethylation using dichloromethane as methylene source. *Front Chem*. **2019**. 7: 568.
- Basilicata M.G., Pepe G.; Rapa S.F., **Merciai F**., Ostacolo C., Manfra M., Di Sarno V., Autore G., De Vita, D., Marzocco, S., Campiglia, P. Anti-Inflammatory and Antioxidant Properties of Dehydrated Potato-Derived Bioactive Compounds in Intestinal Cells. *Int J Mol Sci*. **2019**. 20 (23): 6087.
- Grimaldi M., Marino C., Buonocore M., Santoro A., Sommella E., **Merciai F**., Salviati E., De Rosa A., Nuzzo T., Errico F., Campiglia P., Usiello A., D'Ursi AM. Prenatal and Early Postnatal Cerebral d-Aspartate Depletion Influences l-Amino Acid Pathways, Bioenergetic processes, and Developmental Brain Metabolism. *J. Proteome Res.* **2021**. 20 (1): 727-739.
- Sarno F., Pepe G., Termolino P., Carafa V., Massaro C., **Merciai. F**, Campiglia P., Nebbioso A., Altucci L. Trifolium Repens Blocks Proliferation in Chronic Myelogenous Leukemia via the BCR-ABL/STAT5 Pathway. *Cells*. **2020**. 9 (2): 379.

- Pontieri P., Pepe G., Campiglia P., **Merciai F.**, Basilicata M.G., Smolensky D., Calcagnile M., Troisi J., Romano, R., Del Giudice F., Aletta M., Guida M., Alifano P., Del Giudice L. Comparison of Content in Phenolic Compounds and Antioxidant Capacity in Grains of White, Red, and Black Sorghum Varieties Grown in the Mediterranean Area. *ACS Food Sci. Technol*. **2021**. 1 (6): 1109-1119.

Acknowledgements

I would like to express my sincere gratitude to my tutor **Prof. Pietro Campiglia**, for his unconditionally support and for believing in me.

I'm deeply grateful to all members of *Lab. Baita* and *Lab.* 15. A special mention goes to **Prof. Eduardo Sommella** and **Prof. Giacomo Pepe** for their knowledge and experience that have been an essential support during these years, and to **Dr. Manuela Basilicata** and **Dr. Emanuela Salviati** for their priceless advice and encouragements that guided me and inspired me.

I would like to extend my sincere thanks to **Prof. Matthias Mann** for hosting me during my abroad period and to **Dr. Catherine Vasiloupolou** and to all *TimsTOF office* for their help and the nice time spent together.

I really want to thank **all my Friends**. You have the innate ability to understand me, to bear me and to support me. It is not obvious. Once again you are a fundamental part of this milestone.

Most importantly, nothing of these could have happened without my **Family**.

Dad, **Mom**, **Sis**, you are my source of inspiration and my strength.

Frida, **Sheldon**, is incredibly true that happiness starts with a wet nose and ends with a wagging tail.